



The  
University  
Of  
Sheffield.

## **Towards Base Metal Recovery from Sewage Sludge**

James P. Bezzina

Supervisor:  
Dr. Mark D. Ogden  
Co-supervisor:  
Dr. Robert Dawson

*This thesis is presented as required for the conferral of the degree:*

Doctorate of Philosophy

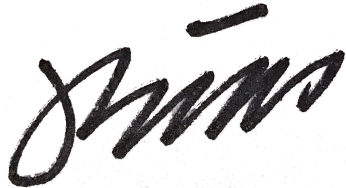
The University of Sheffield  
Department of Chemical and Biological Engineering

November 12, 2020



## **Declaration**

*I, James P. Bezzina, declare that this thesis submitted in fulfilment of the requirements for the conferral of the degree Doctorate of Philosophy, from the University of Sheffield, is wholly my own work unless otherwise referenced or acknowledged. This document has not been submitted for qualifications at any other academic institution.*

A handwritten signature in black ink, appearing to read 'James P. Bezzina', with a horizontal line above the 'P'.

**James P. Bezzina**

November 12, 2020





# Abstract

With a need for the reuse of sewage sludge as a sustainable phosphate source, removal of contaminant metallic hazards become imperative. Success in leaching metals from sewage sludge leaves open the study of removal and recovery of mobile metals from a slurry. Careful consideration of lixiviants and solution condition controls have been considered for the total removal of specific metals of interest, and the solid phase extraction of target metals has been studied extensively.

Copper, iron(II), lead and zinc extraction by C107E, TP214, MTS9100, MTS9501, MTS9301, MTS9570 were screened over the buffering regions of acetic, lactic and citric acid. With acetic acid providing the least hindrance to extraction, isotherm and kinetic characterisation determined MTS9301 as the most effective. Kinetically able to separate iron(II) and other metals (130min vs a maximum of 49min), and extracting >90% of metals without desorption or competition with a surface concentration  $2.729\text{mmol g}^{-1}$ .

Due to the large variation in sewage sludge, a resin-in-pulp was conducted utilising a modified literature surrogate. Leaching was conducted for 24h in pH 1 acetic acid and 9%  $\text{H}_2\text{O}_2$ , dissolving 33-36, 88-89 and 91-92% of copper, lead and zinc, respectively, before neutralisation and final addition of MTS9301. Elution determined that with 2mL resin 38.9, 37.9 and 53.6% recovery of copper, lead and zinc, respectively, was attained with a simple one stage extraction.

As citric acid is not only relevant to this work, but also resource recovery in general, further study was conducted into the performance of MTS9301 within citrate. It was found that optimal extraction was obtained in  $0.1\text{ mol L}^{-1}$  citrate. Total equilibrium and kinetic performance was only slightly effected for copper, lead and zinc, with the resin displaying far lower capacity for iron(II) and a secondary desorption once peak extraction was achieved.

# Acknowledgments

Firstly, many thanks are due to my supervisor, Dr. Mark D. Ogden. The guidance and support (both professionally and mentally) that you've granted has allowed for not only me to conduct this research but given me the push to get through this. To the Grantham Centre and the people within it, I not only owe you a debt for the financial support, but also for the confidence that you've supplied. The experiences and training that you have given me made this process worth it.

The life-long friends that I have made: James, Alex, Adam and Tom. Thank you. You have helped me vent from the many months (nearly years) of inactive AAS and just generally kept me sane through this all. On the topic of mental support, Mum, Dad and Tegan, although you guys are 9-11h and 16993.128km away (rough estimate), you always make time to help me through any issues I have, or just hear me complain.

Lastly, but far from the least, Laura. You've helped me go from instability to stability; there is absolutely no way that I would have stuck through this without you, without you I would have given up many times. You convinced me to stay, you encouraged me to finish, and you kept me going. Whatever is awarded to me from this is as much yours as it is mine.



# Contents

<b>Abstract</b>	<b>v</b>
<b>Acknowledgments</b>	<b>vii</b>
<b>List of Figures</b>	<b>xxvii</b>
<b>List of Tables</b>	<b>xxxiv</b>
<b>1 Introduction</b>	<b>1</b>
1.1 Phosphate . . . . .	1
1.2 Sewage Sludge . . . . .	3
1.3 Heavy Metals . . . . .	6
1.3.1 The Problem . . . . .	6
1.3.2 The Value of Metals . . . . .	10
1.4 Removal of Metals from Sewage Sludge . . . . .	12
1.4.1 Chemical and Bioleaching . . . . .	14
1.5 Acid Leached Sludge and Ion Exchange . . . . .	18
1.5.1 Lixiviants . . . . .	21
1.5.2 Ion Exchange . . . . .	25
1.6 Hypotheses . . . . .	32
1.7 Thesis Structure . . . . .	33
<b>2 General Methods and Instrumentation</b>	<b>37</b>
2.1 Materials . . . . .	37

2.2	Equipment . . . . .	37
2.3	Ion Exchange Experimental Methods . . . . .	39
2.3.1	Resin Measurement and Preconditioning . . . . .	39
2.3.2	Column Ion Exchange Experiments . . . . .	39
2.3.3	Static Ion Exchange Contacts . . . . .	43
2.4	Solution Phase Speciation Modelling . . . . .	44
2.5	Analysis . . . . .	45
2.5.1	Electrode Analysis . . . . .	45
2.5.2	Atomic Absorption Spectroscopy . . . . .	45
2.5.3	Rheology . . . . .	47
<b>3</b>	<b>Resin and Weak Acid Screening Studies</b>	<b>49</b>
3.1	Resin Screening in Citric Acid Media . . . . .	49
3.1.1	Introduction . . . . .	50
3.1.2	Experimental . . . . .	50
3.1.3	Results . . . . .	53
3.1.4	Discussion . . . . .	58
3.1.5	Conclusion . . . . .	63
3.2	Resin Screening in Weak Acid Media . . . . .	64
3.2.1	Introduction . . . . .	65
3.2.2	Materials and Methods . . . . .	65
3.2.3	Results . . . . .	68
3.2.4	Discussion . . . . .	75
3.2.5	Conclusions . . . . .	86
<b>4</b>	<b>Single Metal Isotherm Studies</b>	<b>89</b>
4.1	Introduction . . . . .	90
4.2	Methods . . . . .	90
4.3	Results . . . . .	92
4.4	Discussion . . . . .	95

<i>CONTENTS</i>	xi
4.4.1 Isotherm Modelling . . . . .	97
4.5 Conclusions . . . . .	111
<b>5 Multi-Metal Adsorption Systems</b>	<b>115</b>
5.1 Introduction . . . . .	116
5.2 Methods . . . . .	116
5.3 Results . . . . .	117
5.4 Discussion . . . . .	123
5.5 Conclusions . . . . .	152
<b>6 Acetate Resin-in-Pulp on a Simulated Sludge</b>	<b>155</b>
6.1 Introduction . . . . .	156
6.2 Experimental . . . . .	157
6.3 Results . . . . .	162
6.4 Discussion . . . . .	168
6.5 Summary . . . . .	182
<b>7 Citric Acid Adsorption System</b>	<b>185</b>
7.1 Introduction . . . . .	186
7.2 Methods . . . . .	186
7.3 Results . . . . .	187
7.4 Discussion . . . . .	190
7.5 Conclusions . . . . .	201
<b>8 Conclusive Remarks and Further Work</b>	<b>203</b>
8.1 Recycling Sewage Sludge . . . . .	203
8.2 Future Work . . . . .	213
<b>Bibliography</b>	<b>217</b>
<b>A Resin Screening: Supplementary Information</b>	<b>245</b>
A.1 Resin characteristics . . . . .	246

A.2	Separation factors . . . . .	248
A.3	Solution-phase speciation . . . . .	266
<b>B</b>	<b>Isotherm: Supplementary Information</b>	<b>273</b>
B.1	Correlation With Physical/Chemical Parameters . . . . .	280
<b>C</b>	<b>Multi-metal System Supplementary Data</b>	<b>285</b>
C.1	Multi-metal Isotherm Extraction Percentages . . . . .	285
C.2	Multi-metal Kinetic Extraction Percentages . . . . .	286
C.3	Correlation with Physical/Chemical Paramters . . . . .	288
<b>D</b>	<b>Simulated Process Supplementary Data</b>	<b>301</b>
D.1	Literary Properties of Sludge . . . . .	301
D.2	Anaerobically Digested Esholt Sludge . . . . .	303
D.3	Simulant Sludge Rheology . . . . .	305
D.4	Leaching Conditions . . . . .	308
<b>E</b>	<b>Citric Acid System Supplementary Data</b>	<b>311</b>
E.1	Citrate Concentration Dependence Data . . . . .	311
E.2	Extraction Percentages in Isotherm Data . . . . .	313
E.3	Extraction Percentages in Kinetic Data . . . . .	313



# List of Figures

1.1	Schematic representing distribution of phosphate rock reserves throughout the world as of 2019 <sup>[9]</sup> . . . . .	2
1.2	Schematic of a general waste water treatment plant, reproduced from Metcalf <i>et al.</i> <sup>[14]</sup> , including broad sludge treatment stages. . .	3
1.3	Graphical representation of the 2010 statistics for use of sewage sludge within the UK <sup>[16]</sup> . . . . .	4
1.4	A comparison of the heavy metal limits imposed on sewage sludge and those imposed upon mineral based fertilisers <sup>[23,24]</sup> . . . . .	6
1.5	Concentrations of metals in sewage sludge from different regions around the world. [1] Vriens <i>et al.</i> (2017) <sup>[33]</sup> , [2] Stevens (2009) <sup>[27]</sup> , [3] Liu <i>et al.</i> (2010) <sup>[29]</sup> , [4] Fytili and Zabaniotou (2008) <sup>[17]</sup> , [5] Hsiau and Lo (1998) <sup>[28]</sup> . . . . .	7
1.6	Graphical schematic of free water, interstitial water, surface water and intracellular water of sludge material <sup>[85]</sup> . . . . .	17
1.7	Diagram of a RIL impeller agitated multistage process. . . . .	20
1.8	Diagram of a RIP impeller agitated multistage process. . . . .	21
1.9	Eh-pH diagram of iron calculated by HYDRA/MEDUSA <sup>[104]</sup> . . . . .	22
1.10	The predominance diagrams of iron (a) and lead (b) in the presence of both sulphate and acetate, calculated by HYDRA/MEDUSA <sup>[104]</sup> . . . . .	24

1.11	General resin functionalities. A = strong acid cation exchange (SAC) (sulphonic acid), B = weak acid cation exchange (WAC) (carboxylic acid), C1 = strong base anion exchange (SBA) type I (quaternary amine), C2 = SBA type II (quaternary amine dimethylethanolamine), C3 = SBA type III (unknown), D1 = weak base anion exchange (WBA) (tertiary amine), D2 = WBA (secondary amine), D3 = WBA (primary amine), E1 = weak base chelating (WBC) (bis-picolyamine), E2 = WBC (bis-(aminomethyl)acetamide), E3 = WBC (thiourea), F1 = strong acid/chelating ion exchange (CI) (phosphonic/sulfonic acid), F2 = CI (aminophosphonic acid), F3 = CI (iminodiacetic acid), F4 = CI (amidoxime) . . . . .	29
1.12	Diagram for a simplified explanation of A - film diffusion dictated kinetics, B - pore/intra-particulate diffusion dictated kinetics and C - chemically dictated kinetics <sup>[106]</sup> . . . . .	30
2.1	Breakthrough data on the performance of a) TP214, b) MTS9100, c) MTS9570, d) MTS9301, e) MTS9501 and f) C107E for the flow through column extraction of copper, iron(II), lead and zinc (initial concentrations 100ppm; temperature 20°C; 0.5M NaCl; 0.5M acetic acid; 2ml bed volume; 2 BV/hr flowrate). . . . .	42
2.2	A simplified schematic diagram of the major components an AAS, utilised for the metals analysis throughout this thesis <sup>[127]</sup> . . . . .	46
2.3	A simplified schematic diagram of the major a Brookfield DV-E viscometer with the S64 cylindrical spindle attachment <sup>[129]</sup> . The main body of the viscometer has a cut-out drawn into the centre to display the the coiled spring used for measurement of the stress placed on each spindle. . . . .	47

3.1	Chemical structure of the functionalities of the ion exchange resins tested throughout this study (A = TP 214, B = MTS9100, C = MTS9570, D = MTS9301, E = MTS9501, F = C107E; semicircles represent the matrix). . . . .	52
3.2	Reaction schematics of the three deprotonations of citric acid. . . .	53
3.3	Extraction of metal ions by TP214 as a function of pH. Cu = ▲, Fe = ▼, Pb = ●, Zn = ■. . . . .	54
3.4	Extraction of metal ions by MTS9100 as a function of pH. Cu = ▲, Fe = ▼, Pb = ●, Zn = ■. . . . .	55
3.5	Extraction of metal ions by MTS9570 as a function of pH. Cu = ▲, Fe = ▼, Pb = ●, Zn = ■. . . . .	55
3.6	Extraction of metal ions by MTS9301 as a function of pH. Cu = ▲, Fe = ▼, Pb = ●, Zn = ■. . . . .	56
3.7	Extraction of metal ions by MTS9501 as a function of pH. Cu = ▲, Fe = ▼, Pb = ●, Zn = ■. . . . .	57
3.8	Extraction of metal ions by C107E as a function of pH. Cu = ▲, Fe = ▼, Pb = ●, Zn = ■. . . . .	58
3.9	Separation factors of copper from other metals present within solution by both TP214 and MTS9301. . . . .	59
3.10	Separation factors of iron from other metals present within solution by both MTS9570 and MTS9501. . . . .	60
3.11	Separation factors of lead from other metals present within solution by MTS9570, TP214 and MTS9301. . . . .	61
3.12	Chemical structure of the functionalities of the ion exchange resins tested throughout this study (A = TP214, B = MTS9100, C = MTS9570, D = MTS9301, E = MTS9501, F = C107E; semicircles represent the matrix). . . . .	66

3.13 The distribution of metal ions from acetic acid media by (a) TP214 and (b) MTS9100 as a function of pH at 20 °C after 24hr of contact time. . . . .	69
3.14 The distribution of metal ions from acetic acid media by (a) MTS9570 and (b) MTS9301 as a function of pH at 20 °C after 24hr of contact time. . . . .	70
3.15 The distribution of metal ions from acetic acid media by (a) MTS9501 and (b) C107E as a function of pH at 20 °C after 24hr of contact time. . . . .	70
3.16 The distribution of metal ions from lactic acid by (a) TP214 and (b) MTS9100 as a function of pH at 20 °C after 24hr of contact time. . . . .	71
3.17 The distribution of metal ions from lactic acid by (a) MTS9570, (b) MTS9301 as a function of pH at 20 °C after 24hr of contact time. . . . .	72
3.18 The distribution of metal ions from lactic acid by (a) MTS9501 and (b) C107E as a function of pH at 20 °C after 24hr of contact time. . . . .	73
3.19 The distribution of metal ions from citric acid by (a) TP214 and (b) MTS9100 as a function of pH at 20 °C after 24hr of contact time. . . . .	74
3.20 The distribution of metal ions from citric acid by (a) MTS9570 and (b) MTS9301 as a function of pH at 20 °C after 24hr of contact time. . . . .	74
3.21 The distribution coefficients of metal ions from citric acid by (a) MTS9501 and (b) C107E as a function of pH at 20 °C after 24hr of contact time. . . . .	75
3.22 TP214 separation factors of copper from iron, lead and zinc extracted from acetate, lactate and citrate media at 20 °C after 24hr of contact time. . . . .	78
3.23 MTS9570 separation factors of iron from copper, lead and zinc extracted from acetate, lactate and citrate media at 20 °C after 24hr of contact time. . . . .	80

3.24 MTS9301 separation factors of copper from iron, lead and zinc extracted from acetate, lactate and citrate media at 20 °C after 24hr of contact time. . . . .	83
3.25 MTS9501 separation factors of copper from iron, lead and zinc extracted from acetate, lactate and citrate media at 20 °C after 24hr of contact time. . . . .	84
4.1 Chemical structure of the functionalities of the ion exchange resins tested throughout this study (A = C107E, B = MTS9301, C = TP214; semicircles represent the matrix). . . . .	91
4.2 Concentration dependent extraction of copper (a), iron (b), lead (c) and zinc (d) by C107E in acetic acid media (initial concentrations 25-3000ppm; temperature 20°C; 0.5M NaCl; 0.5M acetic acid; 2ml wet settled resin; 50ml solution). The dashed lines in each figure represent the Langmuir model (described later) fitted to the data. .	93
4.3 Concentration dependent extraction of copper (a), iron (b), lead (c) and zinc (d) of MTS9301 in acetic acid media (initial concentrations 25-3000ppm; temperature 20°C; 0.5M NaCl; 0.5M acetic acid; 2ml wet settled resin; 50ml solution). The dashed lines in each figure represent the Langmuir model (described later) fitted to the data. .	94
4.4 Concentration dependent extraction of copper (a), iron (b), lead (c) and zinc (d) TP214 in acetic acid media (initial concentrations 25-3000ppm; temperature 20°C; 0.5M NaCl; 0.5M acetic acid; 2ml wet settled resin; 50ml solution). The dashed lines in each figure represent the Langmuir model (described later) fitted to the data. .	95
5.1 Concentration dependent extraction of copper (a), iron (b), lead (c) and zinc (d) by C107E in acetic acid media (initial concentration 200mmol L <sup>-1</sup> ; temperature 21°C; 0.5M NaCl; 0.5M acetic acid; 2ml wet settled resin; 20-400ml solution). . . . .	118

5.2	Time dependent extraction of copper (a), iron (b), lead (c) and zinc (d) by C107E in acetic acid media (initial concentration 200ppm; temperature 21°C; 0.5M NaCl; 0.5M acetic acid; 10ml wet settled resin; 500ml solution). . . . .	119
5.3	Concentration dependent extraction of copper (a), iron (b), lead (c) and zinc (d) of MTS9301 in acetic acid media (initial concentration 200mmol L <sup>-1</sup> ; temperature 21°C; 0.5M NaCl; 0.5M acetic acid; 2ml wet settled resin; 20-400ml solution). . . . .	120
5.4	Concentration dependent extraction of copper (a), iron (b), lead (c) and zinc (d) of MTS9301 in acetic acid media (initial concentration 200ppm; temperature 21°C; 0.5M NaCl; 0.5M acetic acid; 10ml wet settled resin; 500ml solution). . . . .	121
5.5	Concentration dependent extraction of copper (a), iron (b), lead (c) and zinc (d) TP214 in acetic acid media (initial concentration 200mmol L <sup>-1</sup> ; temperature 21°C; 0.5M NaCl; 0.5M acetic acid; 2ml wet settled resin; 20-400ml solution). . . . .	122
5.6	Concentration dependent extraction of copper (a), iron (b), lead (c) and zinc (d) of TP214 in acetic acid media (initial concentration 200ppm; temperature 21°C; 0.5M NaCl; 0.5M acetic acid; 10ml wet settled resin; 500ml solution). . . . .	123
6.1	Plotted raw data of the viscosity experiments conducted on the 5% solids content (a), 10% solids content (b) and 20% solids content simulant and the digested Esholt sewage sludge (d) (measurements taken at 20°C). . . . .	163

6.2	Percentage extraction of metal sulphides (copper, lead and zinc) from the simulant sewage sludge using acetic acid at pH 1 and hydrogen peroxide concentrations of 3% (a), 6% (b), 9% (c) and 3% (increasing the concentration to 9% after 4 hours) (d). (0.5 M acetic acid, ~500 rpm, measured values for pH, temperature and ORP are given within Table D.5, D.6, D.7 and D.8, respectively. . . . .	164
6.3	Comparison of the decrease in percentage of leached species with addition of 50% (0.5 M acetic acid, ~500 rpm, measured values for pH, temperature and ORP are given within Table D.5 conducted on the 3% H <sub>2</sub> O <sub>2</sub> leach in Figure 6.2a) and 1 mol L <sup>-1</sup> NaOH (0.5 M acetic acid, ~500 rpm, measured values for pH, temperature and ORP are given within Table D.7 conducted on the 9% H <sub>2</sub> O <sub>2</sub> leach in Figure 6.2c). . . . .	166
6.4	Solution phase percentage of each focus metal species within the leach and the RIP processes for system 1 (a) and 2 (b) (0.5 M acetic acid, ~500 rpm, measured values for pH, temperature and ORP are given within Table D.7) and D.9) for System 1 and 2, respectively. . . . .	167
6.5	Concentration of metals on the resin surface calculated by solution phase difference in the leachate slurry and by stripping for System 1 (a) and 2 (b) (1M nitric acid, 24h, 20°C. . . . .	168
6.6	Comparison between the simulant and Esholt sludge fitted Herschel-Bulkley parameters. . . . .	169
6.7	Comparison of the consistency index, K (Pa.s <sup>n</sup> ), of the simulant sewage sludge at 5, 10 and 20% moisture content, compared with the Esholt sewage sludge and literature values <sup>[213,214]</sup> . . . . .	170
6.8	Comparison of the rheological constant, n, of the simulant sewage sludge at 5, 10 and 20% moisture content, compared with the Esholt sewage sludge and literature values <sup>[213,214]</sup> . . . . .	171

6.9	Predominance diagrams of copper, iron, lead and zinc acetic acid and phosphate, generated using the combination software suite HYDRA/Medusa <sup>[104]</sup> . . . . .	172
6.10	Speciation diagram of calcium in acetate media generated using the HySS software suite <sup>[125]</sup> , stability constant data obtained from the NIST stability constant database included within the table <sup>[126]</sup> and the predominance diagram generated using the HYDRA/MEDUSA software suite <sup>[104]</sup> . . . . .	177
6.11	Speciation diagrams of calcium, copper, iron, lead and zinc citric acid and phosphate, generated using the HySS software suite <sup>[125]</sup> and stability constant data obtained from the NIST stability constant database <sup>[126]</sup> . . . . .	178
6.12	Schematic for the results of the final RIP experiment. . . . .	183
7.1	Distribution coefficients of the extraction of copper, iron(II), lead and zinc from citrate media as a function of citrate concentration (initial concentration 100ppm; temperature 21°C; 0.5M NaCl; 0.01-0.5M acetic acid; initial pH 5.75; 2mlwsr; 50ml solution; 24h). . . .	188
7.2	Concentration dependent extraction of copper (a), iron (b), lead (c) and zinc (d) by MTS9301 in citric acid media (initial concentration 200mmol L <sup>-1</sup> ; temperature 21°C; 0.5mol L <sup>-1</sup> NaCl; 0.1mol L <sup>-1</sup> citric acid; 2mlwsr; 25-400ml solution; 24h). . . . .	189
7.3	Time dependent extraction of copper (a), iron(II) (b), lead (c) and zinc (d) by MTS9301 in citric acid media (initial concentration 200ppm; temperature 21°C; 0.5mol L <sup>-1</sup> NaCl; 0.1mol L <sup>-1</sup> citric acid; 10mlwsr; 500ml solution). . . . .	190
8.1	Proportion of final routes for disposal or reuse of sewage sludge within the UK <sup>[16]</sup> . . . . .	204



8.2	Permissible limits of heavy metals within sludge intended for agricultural application and fertilisers based upon mineral phosphates <sup>[23,24,223]</sup> . . . . .	205
8.3	A comparison of the concentration of metals that constitute a deficiency in micro-nutrients <sup>[225]</sup> , concentration of metals within sludge (Cu, Zn and Mo were referenced Inglezakis, <i>et al.</i> 2014 <sup>[34]</sup> , while a lack of data required Mn and Mo to be sourced from Vriens, <i>et al.</i> 2017 <sup>[33]</sup> ), limits of metals within soils for sludge application <sup>[23]</sup> and levels that lead to toxicity within plant matter <sup>[45]</sup> . . . . .	206
8.4	A summary where the process derived throughout this thesis fits into the supplementation and replacement of mineral fertilisers. Arrows in red represent nutrients sourced from commercial fertilisers, arrows in orange represent nutrients sourced directly from digested sewage sludge and arrows in green represents the RIP process from this thesis. . . . .	209
8.5	Venn diagrams summarising the selective nature of each functionality determined from the resin screening study within acetic, lactic and citric acid media. Reproduced from Bezzina <i>et al.</i> 2019 <sup>[119]</sup> . . . . .	211
A.1	Solution speciation of Cu <sup>2+</sup> (a), Fe <sup>2+</sup> and Fe <sup>3+</sup> (b), Pb <sup>2+</sup> (c) and Zn <sup>2+</sup> (d) in acetic acid, calculated by the HySS software <sup>[125]</sup> with stability constants attained from the NIST database <sup>[126]</sup> . . . . .	267
A.2	Solution speciation of Cu <sup>2+</sup> (a), Fe <sup>2+</sup> and Fe <sup>3+</sup> (b), Pb <sup>2+</sup> (c) and Zn <sup>2+</sup> (d) in lactic acid, calculated by the HySS software (Gans, <i>et al.</i> , 2009) with stability constants attained from the NIST database (Martell, <i>et al.</i> , 2009), apart from Fe <sup>2+</sup> and Fe <sup>3+</sup> , that were gathered from Gorman and Clydesdale (1984). . . . .	269

A.3	Solution speciation of $\text{Cu}^{2+}$ (a), $\text{Fe}^{2+}$ and $\text{Fe}^{3+}$ (b), $\text{Pb}^{2+}$ (c) and $\text{Zn}^{2+}$ (d) in citric acid, calculated by the HySS software (Gans, <i>et al.</i> , 2009) with stability constants attained from the NIST database (Martell, <i>et al.</i> , 2009), apart from $\text{Cu}^{2+}$ , $\text{Fe}^{2+}$ and $\text{Fe}^{3+}$ , that were gathered from Field, <i>et al.</i> (1974). . . . .	270
B.1	Phreeqc modelling of each metal in solution at concentration ranges of 100 ppm to 3000 ppm (single metal solutions) generated in Aqion <sup>[139]</sup> ; 0.5 M NaCl; 0.5 M acetic acid; pH 4.5. . . . .	275
B.2	Predominance diagram created using the HYDRA <sup>[104]</sup> and Medusa <sup>[149]</sup> software, modelled at 25°C. . . . .	275
B.3	Speciation modelling of each metal in solution at concentration ranges of 100 ppm to 3000 ppm (single metal solutions) using the HySS software <sup>[228]</sup> ; 0.5 M acetic acid; pH 4.5. . . . .	276
B.4	Extraction % as a function of initial concentration in $\text{mol L}^{-1}$ for copper (a), iron (b), lead (c) and zinc (d) by C107E (initial concentrations 25 ppm to 3000 ppm; temperature 20 °C; 0.5 M NaCl; 0.5 M acetic acid; 2 ml wet settled resin; 50 ml solution). . . . .	277
B.5	Extraction % as a function of initial concentration in $\text{mol L}^{-1}$ for copper (a), iron (b), lead (c) and zinc (d) by MTS9301 (initial concentrations 25 ppm to 3000 ppm; temperature 20 °C; 0.5 M NaCl; 0.5 M acetic acid; 2 ml wet settled resin; 50 ml solution). . . . .	278
B.6	Extraction % as a function of initial concentration in $\text{mol L}^{-1}$ for copper (a), iron (b), lead (c) and zinc (d) by TP214 (initial concentrations 25 ppm to 3000 ppm; temperature 20 °C; 0.5 M NaCl; 0.5 M acetic acid; 2 ml wet settled resin; 50 ml solution). . . . .	279
B.7	Comparison of the Langmuir determined MTS9301 $Q_{\text{max}}$ as a function of the ionic radius of each metal. . . . .	280
B.8	Comparison of the Langmuir determined C107E $Q_{\text{max}}$ as a function of the electronegativity of each metal. . . . .	281

B.9	Comparison of the Freundlich determined C107E $b_F$ as a function of the electronegativity of each metal. . . . .	281
B.10	Comparison of the D-R determined C107E free energy of adsorption as a function of the electronegativity of each metal. . .	282
C.1	Extraction percentage of copper (a), iron (b), lead (c) and zinc (d) by C107E as a function of total number of moles in contact with in acetic acid media (initial concentration $200\text{mmol L}^{-1}$ ; temperature $21^\circ\text{C}$ ; $0.5\text{M NaCl}$ ; $0.5\text{M acetic acid}$ ; $2\text{ml wet settled resin}$ ; $20\text{-}400\text{ml solution}$ ). . . . .	286
C.2	Extraction percentage of copper (a), iron (b), lead (c) and zinc (d) by MTS9301 as a function of total number of moles in contact with in acetic acid media (initial concentration $200\text{mmol L}^{-1}$ ; temperature $21^\circ\text{C}$ ; $0.5\text{M NaCl}$ ; $0.5\text{M acetic acid}$ ; $2\text{ml wet settled resin}$ ; $20\text{-}400\text{ml solution}$ ). . . . .	287
C.3	Extraction percentage of copper (a), iron (b), lead (c) and zinc (d) by TP214 as a function of total number of moles in contact with in acetic acid media (initial concentration $200\text{mmol L}^{-1}$ ; temperature $21^\circ\text{C}$ ; $0.5\text{M NaCl}$ ; $0.5\text{M acetic acid}$ ; $2\text{ml wet settled resin}$ ; $20\text{-}400\text{ml solution}$ ). . . . .	288
C.4	Extraction percentage of copper, iron, lead and zinc by C107E as a function of time (initial concentration $200\text{ppm}$ ; temperature $21^\circ\text{C}$ ; $0.5\text{M NaCl}$ ; $0.5\text{M acetic acid}$ ; $10\text{ml wet settled resin}$ ; $500\text{ml solution}$ ). . . . .	289
C.5	Extraction percentage of copper, iron, lead and zinc by MTS9301 as a function of time (initial concentration $200\text{ppm}$ ; temperature $21^\circ\text{C}$ ; $0.5\text{M NaCl}$ ; $0.5\text{M acetic acid}$ ; $10\text{ml wet settled resin}$ ; $500\text{ml solution}$ ). . . . .	289
C.6	Extraction percentage of copper, iron, lead and zinc by TP214 as a function of time (initial concentration $200\text{ppm}$ ; temperature $21^\circ\text{C}$ ; $0.5\text{M NaCl}$ ; $0.5\text{M acetic acid}$ ; $10\text{ml wet settled resin}$ ; $500\text{ml solution}$ ). . . . .	290

- C.7 Plot of the *des* constant derived from the desorption-modified Langmuir isotherm model as a function of the IR of each metal for each resin. Figures a and b are the *des* values for C107E and MTS9301, respectively. . . . . 290
- C.8 Plot of the *des* constant derived from the desorption-modified Langmuir isotherm model as a function of the the average solution  $\Delta H$  for each metal-acetate species of each metal for each resin. Figures a and b are the *des* values for C107E and MTS9301, respectively. . . . . 291
- C.9 Plot of the *des* constant derived from the desorption-modified Langmuir isotherm model as a function of the the average solution  $\Delta S$  for each metal-acetate species of each metal for each resin. Figures a and b are the *des* values for C107E and MTS9301, respectively. . . . . 291
- C.10 Plot of the *des* constant derived from the desorption-modified Langmuir isotherm model as a function of the electronegativity of each metal for each resin. Figures a and b are the *des* values for C107E and MTS9301, respectively. . . . . 291
- C.11 Plot of the half-lives derived from the Lagergren Pseudo-First Order kinetic model as a function of the IR of each metal for each resin. Figures a and b are the half-life values for C107E and MTS9301, respectively. . . . . 292
- C.12 Plot of the half-lives derived from the Lagergren Pseudo-First Order kinetic model as a function of the average solution  $\Delta H$  for each metal-acetate species for each resin. Figures a and b are the half-life values for C107E and MTS9301, respectively. . . . . 292

- C.13 Plot of the half-lives derived from the Lagergren Pseudo-First Order kinetic model as a function of the average solution  $\Delta S$  for each metal-acetate species for each resin. Figures a and b are the half-life values for C107E and MTS9301, respectively. . . . . 292
- C.14 Plot of the half-lives derived from the Lagergren Pseudo-First Order kinetic model as a function of the electronegativity of each metal for each resin. Figures a and b are the half-life values for C107E and MTS9301, respectively. . . . . 293
- C.15 Plot of the pseudo-second order half-life and initial rate of reaction derived by the pseudo-second order kinetic model as a function of IR for each metal and each resin. Figures a and b are the values of  $t_{\frac{1}{2}}$  while c and d are the values of  $h_0$  for C107E and MTS9301, respectively. . . . . 293
- C.16 Plot of the pseudo-second order half-life and initial rate of reaction derived by the pseudo-second order kinetic model as a function of the average solution  $\Delta H$  for each metal-acetate species and each resin. Figures a and b are the values of  $t_{\frac{1}{2}}$  while c and d are the values of  $h_0$  for C107E and MTS9301, respectively. . . . . 294
- C.17 Plot of the pseudo-second order half-life and initial rate of reaction derived by the pseudo-second order kinetic model as a function of the average solution  $\Delta S$  for each metal-acetate species and each resin. Figures a and b are the values of  $t_{\frac{1}{2}}$  while c and d are the values of  $h_0$  for C107E and MTS9301, respectively. . . . . 295
- C.18 Plot of the pseudo-second order half-life and initial rate of reaction derived by the pseudo-second order kinetic model as a function of the electronegativity of each metal and each resin. Figures a and b are the values of  $t_{\frac{1}{2}}$  while c and d are the values of  $h_0$  for C107E and MTS9301, respectively. . . . . 296

C.19	Plot of the adsorption and desorption rate derived from the Elovich model as a function of the ionic radius of each metal and each resin. Figures a and b are the values of $\alpha$ while c and d are the values of $\beta$ for C107E and MTS9301, respectively. . . . .	297
C.20	Plot of the adsorption and desorption rate derived from the Elovich model as a function of the average solution $\Delta H$ for each metal-acetate species and each resin. Figures a and b are the values of $\alpha$ while c and d are the values of $\beta$ for C107E and MTS9301, respectively. . . . .	298
C.21	Plot of the adsorption and desorption rate derived from the Elovich model as a function of the average solution $\Delta S$ for each metal-acetate species and each resin. Figures a and b are the values of $\alpha$ while c and d are the values of $\beta$ for C107E and MTS9301, respectively. . . . .	299
C.22	Plot of the adsorption and desorption rate derived from the Elovich model as a function of the electronegativity of each metal and each resin. Figures a and b are the values of $\alpha$ while c and d are the values of $\beta$ for C107E and MTS9301, respectively. . . . .	300
D.1	A simplified schematic of the Esholt Wastewater Treatment Plant . . . . .	303
D.2	Analysis of the Esholtsludge . . . . .	304
E.1	Citrate acid concentration dependent extraction percentage of copper (a), iron(II) (b), lead (c) and zinc (d) by MTS9301 (initial concentration 200ppm; temperature 21°C; 0.5mol L <sup>-1</sup> NaCl; 0.01-0.5mol L <sup>-1</sup> citric acid; 2ml wet settled resin; 50ml solution; 24h). . . . .	312
E.2	Speciation of citrate, copper, iron(II), lead and zinc as a function of citric acid concentration, relative to total concentration of each species (Modelled at pH 5.75 by HySS software suite, using stability constants provided within Bezzina <i>et al.</i> (2019) <sup>[119]</sup> . . . . .	314

- E.3 Citrate acid concentration dependence of the post-contact pH for each mixed metal experiment performed (initial concentration 200ppm; temperature 21°C; 0.5mol L<sup>-1</sup> NaCl; 0.01-0.5mol L<sup>-1</sup> citric acid; 2ml wet settled resin; 50ml solution; 24h). . . . . 315
- E.4 Speciation of citrate, copper, iron(II), lead and zinc as a function of citric acid concentration, relative to total concentration of each species (Modelled at pH 5.75 by HySS software suite, using stability constants provided within Bezzina *et al.* (2019)<sup>[119]</sup>. . . . . 316
- E.5 Concentration dependent extraction percentage of copper (a), iron (b), lead (c) and zinc (d) by MTS9301 in citric acid media as a function of total mmol L<sup>-1</sup> in initial solution (initial concentration 200mmol L<sup>-1</sup>; temperature 21°C; 0.5mol L<sup>-1</sup> NaCl; 0.1mol L<sup>-1</sup> citric acid; 2ml wet settled resin; 25-400ml solution; 24h). . . . . 317
- E.6 Time dependent extraction percentage of copper (a), iron(II) (b), lead (c) and zinc (d) by MTS9301 in citric acid media (initial concentration 200ppm; temperature 21°C; 0.5mol L<sup>-1</sup> NaCl; 0.1mol L<sup>-1</sup> citric acid; 10ml wet settled resin; 500ml solution). . . . . 318





# List of Tables

1.1	Average number of sludge applications to agricultural land before soil guideline limits are breached <sup>[35]</sup> . . . . .	8
1.2	Values of specified base and rare earth metals attainable from sewage sludge. . . . .	11
1.3	Values of specified precious metals attainable from sewage sludge.	11
3.1	Physical and chemical characteristics of the resins tested throughout this study, as obtained from suppliers information data sheets (PS = polystyrene, PA = polyacrylic, DVB = divinylbenzene).	51
4.1	Variables obtained by fitting the single metal isotherm data to the non-linear Freundlich model. . . . .	98
4.2	Variables obtained by fitting the single metal isotherm data to the non-linear Langmuir model. . . . .	99
4.3	Variables obtained by fitting the single metal isotherm data to the non-linear Temkin model. . . . .	103
4.4	Variables obtained by fitting the single metal isotherm data to the non-linear D-R isotherm model. . . . .	104
5.1	Two-parameter single-metal isotherm models used within this study <sup>[151]</sup> . . . . .	124
5.2	Variables obtained by fitting the mixed metal isotherm data of C107E, MTS9301 and TP214 to the Freundlich isotherm model. .	125

5.3	Variables obtained by fitting the mixed metal isotherm data of C107E, MTS9301 and TP214 to the Langmuir isotherm model. . .	126
5.4	Variables obtained by fitting the mixed metal isotherm data of C107E, MTS9301 and TP214 to the Temkin isotherm model. . . .	127
5.5	Variables obtained by fitting the mixed metal isotherm data of C107E, MTS9301 and TP214 to D-R isotherm model. . . . .	128
5.6	Variables obtained by fitting the mixed metal concentration dependence data of C107E and MTS9301 to the desorption-modified Langmuir isotherm model. . . . .	132
5.7	Non-linear kinetic modelling data for the particle diffusion model for acetic acid media. . . . .	136
5.8	Non-linear kinetic modelling data for the film diffusion model for acetic acid media. . . . .	138
5.9	Non-linear kinetic modelling data for the Elovich model for acetic acid media. . . . .	139
5.10	Non-linear kinetic modelling data for the Lagergren model for acetic acid media. . . . .	143
5.11	Non-linear kinetic modelling data for the Pseudo-second order model for acetic acid media. . . . .	145
6.1	Composition of Miso Paste . . . . .	157
6.2	Composition of synthetic sewage sludge simulant <sup>[210]</sup> . . . . .	159
6.3	Chemical parameters utilised for determination of resin volume and contact time. . . . .	161
6.4	Solid Content and densities of the simulant sewage sludge at 5%, 10% and 20% solids content. . . . .	162
6.5	Percentage of metal in each phase from the final mass balance. .	174
6.6	$q_e$ values obtained by modelling the experimental $C_e$ values from the RIP system with the parameters obtained within Chapter 5. . .	176

6.7	Stability constant data obtained from the NIST stability constant database <sup>[126]</sup> (L=IDA functionality, H=proton, OH=hydroxyl). . . . .	179
6.8	Hypothetical costs per tonne. . . . .	181
6.9	Summarised extraction results. . . . .	183
6.10	Hypothetical costs per tonne. . . . .	183
7.1	Two-parameter single-metal isotherm models used within this study <sup>[151,152]</sup> . . . . .	192
7.2	Variables obtained by fitting the mixed metal isotherm data of MTS9301 to the two parameter isotherm models. . . . .	193
7.3	Variables obtained by fitting the mixed metal concentration dependence data of C107E to the desorption corrected Langmuir isotherm model. . . . .	196
7.4	Kinetic models used within this study. . . . .	197
7.5	Non-linear kinetic modelling data for MTS9301 within citric acid media. . . . .	199
8.1	Values of specified precious metals attainable from sewage sludge.	207
A.1	Physical and chemical characteristics of the resins tested throughout this study, as obtained from suppliers' information data sheets (PS = polystyrene, PA = polyacrylic, DVB = divinylbenzene). All are spherical beads. . . . .	247
A.2	TP214 separation factors of copper, iron, lead and zinc from acetate media at 20 °C after 24hr of contact time. . . . .	248
A.3	MTS9100 separation factors of copper, iron, lead and zinc from acetate media at 20 °C after 24hr of contact time. . . . .	249
A.4	MTS9570 separation factors of copper, iron, lead and zinc from acetate media at 20 °C after 24hr of contact time. . . . .	250
A.5	MTS9301 separation factors of copper, iron, lead and zinc from acetate media at 20 °C after 24hr of contact time. . . . .	251

A.6	MTS9501 separation factors of copper, iron, lead and zinc from acetate media at 20 °C after 24hr of contact time. . . . .	252
A.7	C107E separation factors of copper, iron, lead and zinc from acetate media at 20 °C after 24hr of contact time. . . . .	253
A.8	TP214 separation factors of copper, iron, lead and zinc from lactate media at 20 °C after 24hr of contact time. . . . .	254
A.9	MTS9100 separation factors of copper, iron, lead and zinc from lactate media at 20 °C after 24hr of contact time. . . . .	255
A.10	MTS9570 separation factors of copper, iron, lead and zinc from lactate media at 20 °C after 24hr of contact time. . . . .	256
A.11	MTS9301 separation factors of copper, iron, lead and zinc from lactate media at 20 °C after 24hr of contact time. . . . .	257
A.12	MTS9501 separation factors of copper, iron, lead and zinc from lactate media at 20 °C after 24hr of contact time. . . . .	258
A.13	C107E separation factors of copper, iron, lead and zinc from lactate media at 20 °C after 24hr of contact time. . . . .	259
A.14	TP214 separation factors of copper, iron, lead and zinc from citrate media at 20 °C after 24hr of contact time. . . . .	260
A.15	MTS9100 separation factors of copper, iron, lead and zinc from citrate media at 20 °C after 24hr of contact time. . . . .	261
A.16	MTS9570 separation factors of copper, iron, lead and zinc from citrate media at 20 °C after 24hr of contact time. . . . .	262
A.17	MTS9301 separation factors of copper, iron, lead and zinc from citrate media at 20 °C after 24hr of contact time. . . . .	263
A.18	MTS9501 separation factors of copper, iron, lead and zinc from citrate media at 20 °C after 24hr of contact time. . . . .	264
A.19	C107E separation factors of copper, iron, lead and zinc from citrate media at 20 °C after 24hr of contact time. . . . .	265

A.20 Stability constants for solid phase hydrolysis products of each metal at 0.0 M ionic strength [1]. . . . .	266
A.21 Stability constants for solution phase hydrolysis products of each metal at 0.0 M ionic strength [1]. . . . .	267
A.22 Stability constants for copper acetate species at 0.1 M ionic strength [2]. [L] = complexing acid, [M] = metal, [H] = proton, [OH] = hydroxide. . . . .	268
A.23 Stability constants for iron(II) acetate species at 3.0 M ionic strength [2]. [L] = complexing acid, [M] = metal, [H] = proton, [OH] = hydroxide. . . . .	268
A.24 Stability constants for metal acetate species at 1.0 M ionic strength [2]. [L] = complexing acid, [M] = metal, [H] = proton, [OH] = hydroxide. . . . .	268
A.25 Stability constants for metal lactate species at 1.0 M ionic strength [2]. [L] = complexing acid, [M] = metal, [H] = proton, [OH] = hydroxide.	268
A.26 Stability constants for metal lactate species at 0.1 M ionic strength [2,3]. [L] = complexing acid, [M] = metal, [H] = proton, [OH] = hydroxide. . . . .	269
A.27 Stability constants for metal citrate species at 0.1 M [2,4]. [L] = complexing acid, [M] = metal, [H] = proton, [OH] = hydroxide. . . .	270
A.28 Stability constants for lead citrate species at 1.0 M ionic strength [2]. [L] = complexing acid, [M] = metal, [H] = proton, [OH] = hydroxide. . . . .	271
A.29 Phreeqc model output for the metal oxidation states within each carboxylic acid solution. . . . .	271
B.1 Physical and chemical characteristics of the resins tested throughout this study, as obtained from suppliers information data sheets (PS = polystyrene, PA = polyacrylic, DVB = divinylbenzene). All are spherical beads. . . . .	274

B.2	Summary of the trends found by comparison of the isotherm data of C107E, MTS9301 and TP214 and the ionic radius, average $\Delta H$ of complex formation, average $\Delta S$ of complex formation and electronegativity. . . . .	280
D.1	Characteristics of digested sludges <sup>[14]</sup> . . . . .	302
D.2	Bingham Plastic Model parameters. . . . .	306
D.3	Power-Law Model parameters. . . . .	307
D.4	Herschel-Bulkley Model parameters. . . . .	308
D.5	Measured parameters of the leach consisting of 3% $H_2O_2$ . . . . .	308
D.6	Measured parameters of the leach consisting of 6% $H_2O_2$ . . . . .	309
D.7	Measured parameters of the leach consisting of 9% $H_2O_2$ , also used for system 1. . . . .	309
D.8	Measured parameters of the leach consisting of 3% $H_2O_2$ increased after $\sim 4$ h to 9%. . . . .	310
D.9	Measured parameters of the leach consisting of 9% $H_2O_2$ , also used for system 2. . . . .	310

# Chapter 1

## Introduction

### 1.1 Phosphate

As the population of the world pushes towards 10 billion (predicted to reach 9.4 to 10.1 billion by 2050<sup>[1-3]</sup>), the demand for raw materials is naturally expected to increase. This increase is, somewhat artificially enhanced by an increase in affluent class causing an increase in per capita demand<sup>[4,5]</sup>. Increased global demand for food production, particularly crop growth, has placed high levels of stress on phosphate sources; a primary macro-nutrient used within agriculture<sup>[6]</sup>.

This demand has led to the interest in an understanding of the lifetime of current phosphate reserves, which returned glum outlooks, with peak production of phosphate occurring at or before 2139 and total reserves lasting anywhere between 30 and 400 years<sup>[4,7]</sup>. The issue between supply and demand of phosphate has generated fears surrounding global food security<sup>[3]</sup>, and even sparked civil unrest in communities heavily affected. Raw phosphate minerals have since been placed on the EU critical minerals list under the umbrella term 'phosphate rock'<sup>[8]</sup>.

With imminent shortages of phosphate rock, the pressure placed upon industrial fertiliser production is paramount. This imminent shortage is only

exasperated by the disparity in distribution of phosphate, with Morocco and the Western Sahara region claiming 50 billion tonnes of global mining reserves (or  $\sim 70\%$  of the total phosphate reserves, Figure 1.1)<sup>[9]</sup>. Cumulatively, the remaining phosphate reserves account for a mere  $\sim 21$  billion tonnes, with many nations (including a large quantity of EU based nations) not having access to their own sufficient phosphate reserves, creating the potential for geopolitical tension surrounding food security<sup>[9]</sup>.

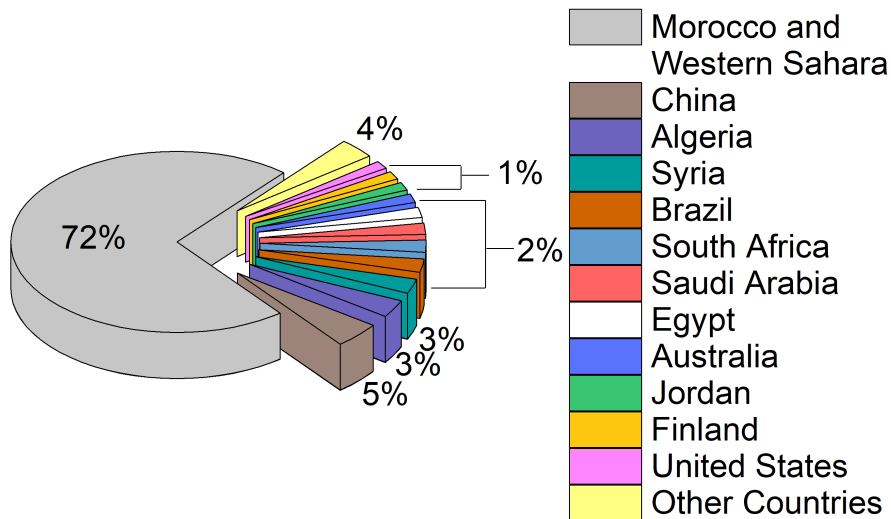


**Figure 1.1:** Schematic representing distribution of phosphate rock reserves throughout the world as of 2019<sup>[9]</sup>.

The critical nature and necessity for phosphate has led to the mining of lower grade phosphate rock, and considering phosphate forms thermodynamically stable solids, a large quantity of toxic heavy metals can be present within these sources<sup>[10–12]</sup>. The ingress of these impurities into phosphate rock generates hazards throughout the refinement process of phosphate from mineral form as well as the formation of potentially more hazardous phosphate products<sup>[13]</sup>. An ever increasing nutrient source, that is relatively underutilised, is sewage sludge.



## 1.2 Sewage Sludge

Sewage sludge is the residual solid material of the wastewater treatment process after the release of clean liquid effluent; in many cases this solid is either incinerated or discarded in landfill<sup>[14]</sup>. The screening of solids, water digestion and, perhaps the most relevant to this topic, precipitation of nutrients to prevent eutrophication of effluent release sites generates a large volume of solid material within wastewater treatment plants (Figure 1.2). This sludge is rich in nutrients, containing up to 44% of the phosphate concentration of commercially available fertilisers<sup>[15]</sup>. Why should this not be utilised in agriculture as a replacement or at least a supplement for the fertilisers obtained from phosphate rock?

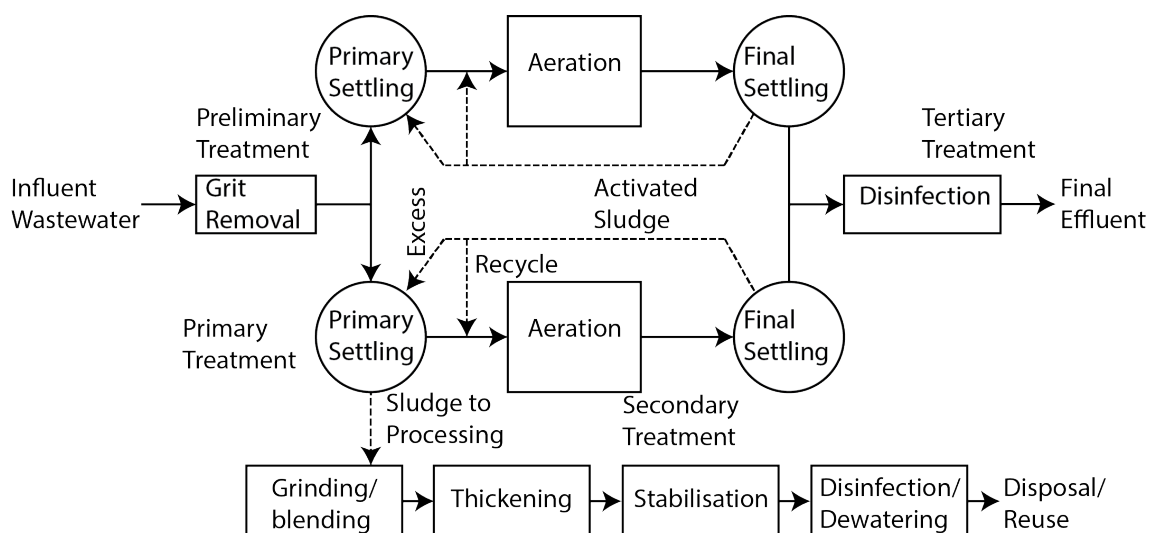


**Figure 1.2:** Schematic of a general waste water treatment plant, reproduced from Metcalf *et al.*<sup>[14]</sup>, including broad sludge treatment stages.

In the UK, specifically, there is almost an 80% utilisation of sewage sludge within agriculture (Figure 1.3)<sup>[16]</sup>. This is an excellent start, and the stabilisation and disinfection stages (followed by addition of lime and, in some cases, incineration before crop addition<sup>[17]</sup>) leave practically very little biological hazards surrounding the usage of this biosolid as a fertiliser. On top of the utilisation of sewage sludge directly, many processes have been generated for the extraction and recycling of resources from the sludge.

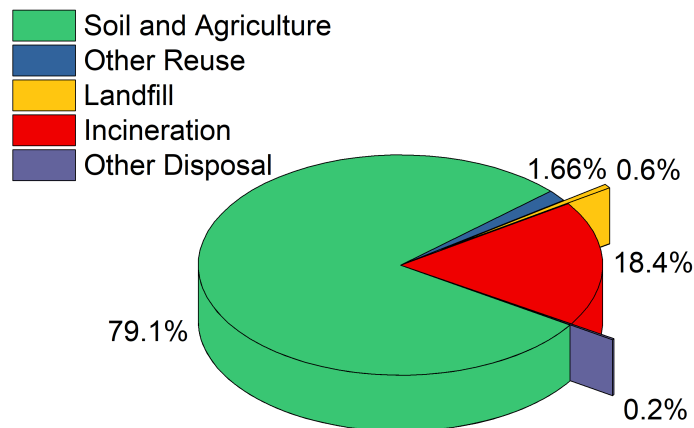
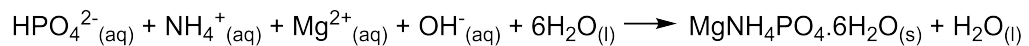


**Figure 1.3:** Graphical representation of the 2010 statistics for use of sewage sludge within the UK<sup>[16]</sup>.

One of the simplest of these processes is sources separation; the theory behind which is simple enough, separate the nutrient dense domestic waste from the bulk of municipal waste and utilise this source<sup>[15,18]</sup>. As a majority of the nutrients within wastewater exist within the liquid phase (hence the aforementioned precipitation process) this requires the installation of specially designed toilets that allow for the separation of urine and faeces, as well as household storage tanks<sup>[18]</sup>; however, this process is difficult to establish in conjunction with older communities<sup>[18]</sup>. An alternative to this process, not mutually exclusive, is the precipitation of the nutrients from urine in a biologically available form of the mineral struvite ( $\text{Mg}(\text{NH}_4)\text{PO}_4 \cdot 6\text{H}_2\text{O}$ )<sup>[19]</sup>.

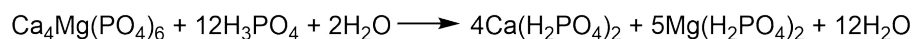
The precipitation of struvite (through the reaction in Scheme 1)<sup>[19]</sup> demonstrated nitrogen recoveries of 67-80%, with phosphate recoveries reaching 65-80%, with this process being more energy efficient than commercial fertiliser production (102MJ for 1kg of nitrogen and 2.2kg of phosphorous vs 154MJ for the same masses in commercial fertiliser). Commercially, since 1998, an advanced

water treatment plant has been in operation at the Shimane Prefecture Lake Shinji East Clean Centre (SECC) in Japan. This plant has been producing struvite at an equivalent value of £196 per tonne, with hazardous metal concentrations lower than commercial fertilizers<sup>[20]</sup>. Struvite precipitation, however, is not the only process for nutrient recovery from sewage sludge.



**Scheme 1**

Full-scale extraction of phosphate from sewage sludge ash is currently being conducted by RecoPhos<sup>[21]</sup> and SGL Carbon GmbH. This process relies on the reaction of phosphoric acid with sewage sludge ash produced from incineration (hypothetically conducted through the reaction in Schematic 2<sup>[21]</sup>), completely recovering the phosphoric acid and producing a viable and commercially available fertiliser; the RecoPhos process is currently producing 1000 tonnes of fertiliser per month. The phosphate fertiliser produced does contain elevated concentrations of the heavy metals, and while the concentrations of copper and zinc in the produced fertiliser are within the limits recommended by the German fertiliser ordinance<sup>[22]</sup>, these are still appreciable values (copper concentration in RecoPhos P38 being 663 ppm, and zinc being 1586 ppm)<sup>[21]</sup>.



**Scheme 2**

This alarming concentration of metals brings into light the negligence of all of the above mentioned processes, which is a key issue surrounding the usage of sewage as a fertiliser source - release of metals into the environment; especially true with regards to the usage of sewage sludge for agricultural purposes within the UK. Within Figure 1.4 the European limits for metals content within sewage sludge intended for use on agricultural soils<sup>[23]</sup> are compared directly against the

limit for phosphate based fertilisers<sup>[24]</sup>. This discrepancy is where many of these attempts at recycling fall short; there is a large quantity of heavy metals released into, not just crop growing agricultural land, but also the environment, and this limits the crops and time period that sewage sludge application can occur<sup>[25]</sup>. This is especially true with respect to the difference in cadmium and mercury limits, which are potentially two of the most hazardous of the limited metals<sup>[26]</sup>.

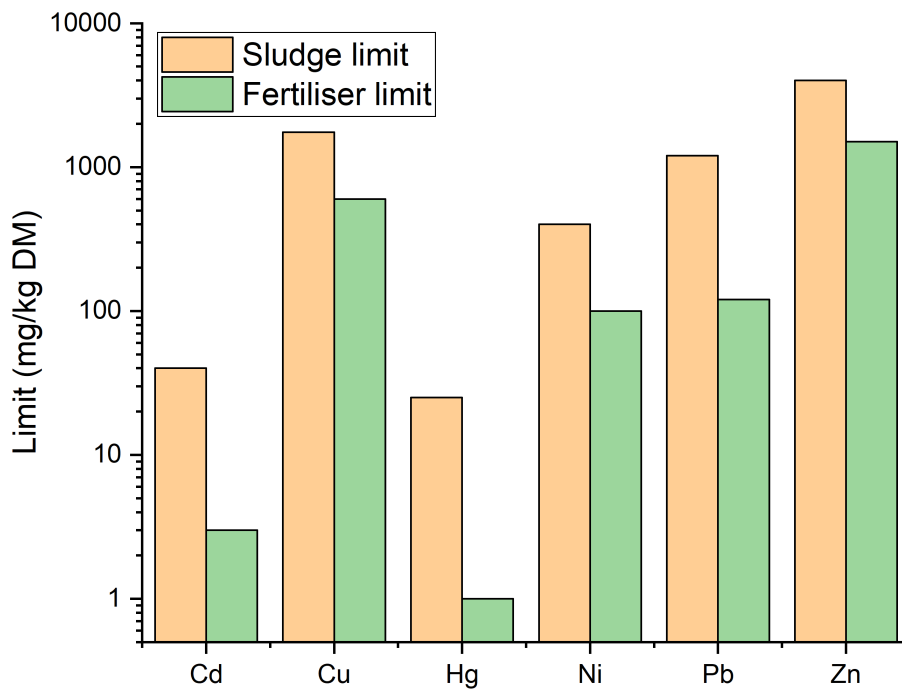


**Figure 1.4:** A comparison of the heavy metal limits imposed on sewage sludge and those imposed upon mineral based fertilisers<sup>[23,24]</sup>.

## 1.3 Heavy Metals

### 1.3.1 The Problem

Many legacy municipal wastewater treatment plant influents are a combination of multiple sources from industry to stormwater to domestic wastewater<sup>[14]</sup>; this combination of multiple sources is the main factor allowing for the ingress of multiple pollutants within wastewater<sup>[17,27-29]</sup> (Figure 1.5 displays concentrations of heavy metals from sewage sludge around the world). With the majority of

organic pollutants being dealt with through digestion, aeration or incineration<sup>[14]</sup>, the residual pollutants causing issue are heavy metals. Through sludge stabilisation processes such as digestion<sup>[14,30]</sup>, chemical precipitation<sup>[31]</sup> and wetland remediation<sup>[30,32]</sup>, these metals are removed from mobile phases, ultimately remaining within sewage sludge.

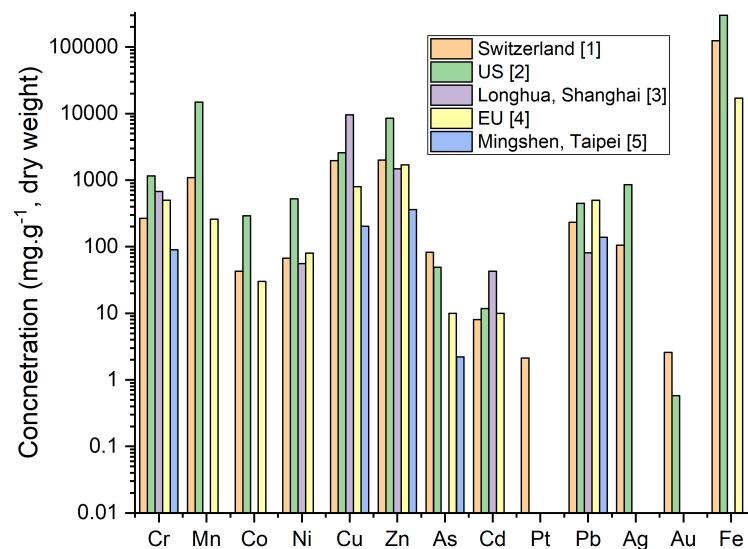


**Figure 1.5:** Concentrations of metals in sewage sludge from different regions around the world. [1] Vriens *et al.* (2017)<sup>[33]</sup>, [2] Stevens (2009)<sup>[27]</sup>, [3] Liu *et al.* (2010)<sup>[29]</sup>, [4] Fytli and Zabaniotou (2008)<sup>[17]</sup>, [5] Hsiao and Lo (1998)<sup>[28]</sup>

There are strict guidelines, within the EU and the UK, on the concentrations of metals within sludge for disposal or agricultural usage in order to minimise environmental toxicity<sup>[23,25]</sup>. Often metals within sewage sludge are within guideline limits for agricultural application; despite this, concentrations can still be alarming, with copper, lead and zinc concentrations reaching averages of 337, 124 and 1222mg kg<sup>-1</sup> in the EU, and the US reporting averages of 850, 500 and 1740mg g<sup>-1</sup> or higher<sup>[34]</sup>, all beyond the limits already imposed on commercial fertilisers (Figure 1.4)<sup>[24]</sup>. While not procuring direct legislative concern, the concentrations can lead to the accumulation of metals within soil. This, in turn, creates an indirect concern and a limitation of the total applications before soil

concentrations are of legislative concern (Table 1.1), these limits equating to between 70 and 80 years of application,<sup>[35]</sup>. An extreme accumulation in soils has been observed within historical sites of sludge amended soils, where lead concentrations were discovered to be up to 25g kg<sup>-1</sup><sup>[35]</sup>.

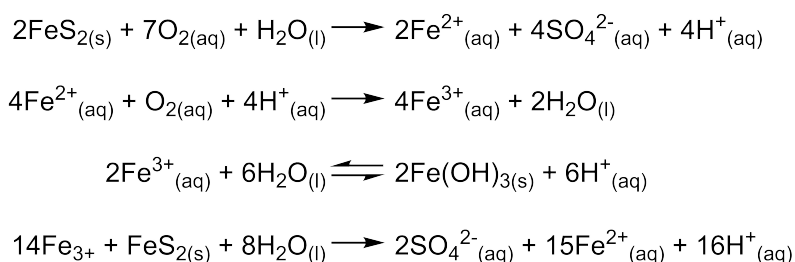
**Table 1.1:** Average number of sludge applications to agricultural land before soil guideline limits are breached<sup>[35]</sup>.

Metal	Applications
Cadmium	29
Chromium	49
Copper	31
Lead	33
Mercury	18
Nickel	37
Zinc	29

Many of these guidelines have been written with the assumption of a completely immobilised heavy metal population within sewage sludge<sup>[35]</sup>. However, depending on the treatment process and the source of the metals within sewage sludge, the speciation of these metals can differ markedly. Generally speaking the majority of metals are found within the oxidisable and residual fraction (sulphides and associated with organometallic compounds), however these metals can also be associated with reducible or exchangeable fractions (either associated with carbonates or metal oxides)<sup>[17,30,35,36]</sup>. Despite the reliance on this assumption, there is still the admission of potential mobility of metals as the pH dependence of metal mobility has led to a requirement for the treatment of sewage sludge with lime prior to addition to land, converting a majority of the previously mobile species into oxides, hydroxides and carbonates<sup>[25,35]</sup>.

With all metallic immobilisation regulations in place, it is stated that the transfer of heavy metals through any soil-plant-human/animal pathway is seen as a very

minor risk and is quite unlikely to cause harm<sup>[35]</sup>. Immobilisation, however, is not necessarily the best option for total environmental pollution, as many conditions can change, such as soil acidity and oxidation-reduction potential (ORP), leading to the mobilisation of metals. This is of concern, considering the assumption is that majority of metals within sewage sludge are associated with sulphide compounds<sup>[30]</sup>, and while these are amongst the least soluble metallic species, still maintain pathways for mobilisation throughout the environment<sup>[37]</sup>.



**Scheme 3**

Introduction of metal sulphides to agricultural soils generates concerns similar to that of acid mine drainage. Acid mine drainage is an issue associated with abandoned mine sites all across the globe and is initiated by the presence of metal sulphide in the mine, particularly pyrite<sup>[38]</sup>. The oxidation of metal sulphides generates sulphuric acid (Reaction Scheme 3), which can further push the dissolution and mobilisation of metals<sup>[38]</sup>. This is a large concern with respect to vacant mine sites, yet is overlooked in many cases when considering the usage of sewage sludge for crop fertilisation.

Therefore, while recovery of nutrients has been successful in formulation of fertiliser sources, many regions around the world are placing stricter guidelines on landfill<sup>[39]</sup>. The waste generated from these advanced wastewater treatments maintain the relatively high concentrations of heavy metals in complicated forms. Thus, if metals aren't making their way into landfill, they're being directly applied to agricultural crops. This leads to the necessity for the removal of metals from sewage sludge, and many solutions have been derived for this purpose. This,

along with a potential for added value of metals recovery, is the main reason that there will be a focus towards metals removal rather than immobilisation.

### 1.3.2 The Value of Metals

Metals, as alluded to before, are an unavoidable risk when utilising sewage sludge for agricultural purposes, but their story doesn't have to end there. Metals, themselves, are valuable. They have value both inherent value, and in low enough, controlled, concentrations they can be utilised as micro-nutrients. Here we will focus on the value of metals in both cases.

Creating a more circular economy requires seeking resources where they were previously ignored; this is especially true with respect to sewage sludge. Table 1.2 displays the base and rare earth metals of the largest concentration within sewage sludge (calculated from Vriens *et al.*<sup>[33]</sup>). A best case scenario from the extraction of these metals alone, one tonne of sewage sludge (from the selected metals) could accumulate £6.66, though the main rationale behind this extraction would be removal of toxicity. With an understanding of the extraction of base metals from sewage sludge, a process could be further derived for the extraction of precious metals, which would further exasperate the economic potential of the process.

Through various influent sources, precious metals can find their way into sewage systems. Gold and silver, for example find their way into sewage sludge in Switzerland (up to  $40\text{mg L}^{-1}$ )<sup>[33]</sup>; while the largest source of platinum group metals remains catalytic converters in the exhaust systems from cars. This latter metal influent has been the source of much recent interest in local roadside dust of the streets surrounding Sheffield<sup>[43]</sup>. The concentration of these more valuable metals (also calculated from Vriens *et al.*<sup>[33]</sup>) is included in Table 8.1.



**Table 1.2:** Values of specified base and rare earth metals attainable from sewage sludge.

Metal	Value (£.t <sup>-1</sup> )	Sludge (£.t sludge <sup>-1</sup> )	Reference
Cadmium	30539	0.24	[40]
Cerium	3139	2.68	[40]
Cobalt	25780	1.11	[41]
Copper	5190	0.30	[41]
Lead	1370	0.17	[41]
Neodinium	49091	1.01	[40]
Titanium	3696	0.86	[42]
Zinc	1860	0.29	[41]

**Table 1.3:** Values of specified precious metals attainable from sewage sludge.

Metal	Value	Sludge (£.t sludge <sup>-1</sup> )	Reference
Gold	£1923.4.t oz <sup>-1</sup>	123.80	[41]
Paladium	£1876.49.t oz <sup>-1</sup>	59.49	[41]
Platinum	£681.45.t oz <sup>-1</sup>	48.20	[41]
Rhodium	£10703.00.lb <sup>-1</sup>	237.09	[42]
Ruthenium	£215.60.lb <sup>-1</sup>	1.94	[40]
Silver	£19.32.t oz <sup>-1</sup>	65.23	[41]

The value generated by the precious metals overshadows the potential value of the more hazardous base metals by an order of magnitude, despite their small concentrations. Despite this value, the more pressing issue is the removal of toxic metals such as copper, lead and zinc, which plague the sewage sludge within the UK (especially within the incinerated sludge<sup>[44]</sup>), and are the most limiting factor towards its unrestricted use as a nutrient source<sup>[35]</sup>. Framed in another light, many metals (including copper and zinc) could be seen as beneficial to remain within sewage sludge; provided the concentrations of such metals are strictly managed and monitored.

As alluded to earlier, many of the base metals within sewage sludge, while not necessarily displaying inherent value, hold great value with regards to

soil micro-nutrients (copper, iron, manganese, molybdenum, selenium and zinc are all micro-nutrients found within sewage sludge). While the levels of copper, molybdenum and zinc can all be directly related to efficiency of crop growth, deficiencies in other nutrients, such as selenium, have more of an effect on population and livestock health<sup>[45,46]</sup>. According to The Advanced Soil Geochemical Atlas of England and Wales<sup>[47]</sup>, concentrations of copper, molybdenum, selenium and zinc are deficient across the entirety of the UK. The abundance of many of these elements within sewage sludge could definitely allow for the amendment of soils without the requirements for supplementation by secondary micro-nutrient fertilisers. This, however, requires constant and strict control of additions, as the soil concentration display narrow optimum ranges for crop growth and toxicity<sup>[45,47]</sup>.

Understanding the benefits and pitfalls of using sewage sludge to amend nutrient imbalances within soils, it becomes even clearer that utilising this sustainable source of phosphate could benefit agriculture in many ways as both a cheaper source of phosphate and a cheaper sources of micro-nutrients. This is then compounded by the value proposition of the inherent value of metals that are contained within sewage sludge. It is therefore imperative that this body of work focus on the removal of metals from sewage sludge, not just for the value sentiment, but also for the sustainability sentiment. As copper, lead and zinc are continually highlighted<sup>[35,44]</sup> as problematic metals, these will be the main focus of this extraction research, but with a proof of concept process, there is the possibility for it to be extended into precious metals in the future.

## 1.4 Removal of Metals from Sewage Sludge

Regardless of speciation, metals are contained predominantly within the solid phase of sewage sludge. This poses great difficulties with regards to the separation of metals from the sewage sludge, as you cannot physically separate

the intertwined solid-liquid mixture, and filtration of sewage sludge poses great difficulties. With regards to this, there have been multiple attempts at the removal of metals from sewage sludge, many of which have displayed, at least, laboratory level success.

In many instances, dissolved metals are removed prior to waste water treatment; this is the most efficient method for heavy metal removal as no processing is necessary. Extraction technologies such as membrane filtration<sup>[31,48]</sup> and ion exchange and adsorption<sup>[14,31]</sup> are used in initial stages of waste water treatment in order to completely remove heavy metals from the entire treatment process when concentrations are exceptionally high. This upstream processing, however would firstly require implementation of new infrastructure to well-founded technology, and secondly it would not account for the removal of metals that have already been associated with less mobile or solid phases; downstream processing of the waste would mitigate both of these issues.

Many metals within sludge can be associated with organic humic acid complexes or exchangeable forms<sup>[35]</sup>; removal of these metals from sludge can be conducted through addition of an exchanging media. Similarly to wastewater treatment, solid-phase extractants<sup>[49,50]</sup> and ionic liquids<sup>[51]</sup> have been used for the removal of metals from sewage sludge with limited success. Sludge has further been treated by subcritical water extraction<sup>[52,53]</sup> and electrokinetic remediation techniques<sup>[54–58]</sup>; the latter arriving at the most success.

Electrokinetic remediation involves passing a current through a medium (in this case sludge) between electrodes, forcing the migration of charged species towards their respective electrode, with the benefit of removal of all charged species, both cationic and anionic<sup>[57]</sup>. Depending on the speciation of metals within the sewage sludge, this method can be extremely effective, removing more than 50% of metals from anaerobically digested sludge in a study by Elicker

*et al.*<sup>[58]</sup>, with only the addition of sodium chloride as an electrolyte. However, similarly to ion exchange, this method requires the metallic fraction to favour exchangeable species, and is often required to be combined with mobilisation methods such as leaching<sup>[54–56]</sup>.

With the increasing popularity of the incineration<sup>[17]</sup> it seems fitting that this has seen research interest, as it not only deals with total mass of sludge, but is also the most thorough method for the removal of the biological hazards associated with sludge; this process removes the entire organic fraction, leaving behind not only the phosphate species, but also immobilised metals. Developments towards removal of metals from sludge have determined that with the addition of chlorinating agents (such as  $\text{MgCl}_2$  or  $\text{CaCl}_2$ ) to sludge prior to incineration can allow for the volatilisation of metals as well as an increase in the bioavailability of the phosphate within the ash<sup>[59,60]</sup>. This process is extremely effective, however it does not allow for direct recovery of metallic species and allows for volatile metallic species to be released into the atmosphere<sup>[60]</sup>, which is counter to the requirements of recovering metals for an income supplementation. Thus far, the most successful research towards the recovery of metals from sewage sludge comes in the form of bioleaching<sup>[61–65]</sup> and chemical leaching<sup>[66–72]</sup>.

### 1.4.1 Chemical and Bioleaching

The most commonly studied method for removing heavy metals from sewage sludge is the hydrometallurgical process of leaching. Leaching involves the dissolution of metallic species by addition of a leaching agent (usually an acid, a base or chelating agent) or through bacterial metabolism of iron or sulphur compounds in order to reduce solution pH. Removal of metals from sewage sludge has been stated to be possible by a combination of high acidity, oxidising environments and the presence of a complexing agent<sup>[36]</sup>.

Both chemical and bioleaching have seen success with solubilisation of metals from raw and stabilised sewage sludge and are both industrially viable processes. The majority of the sewage sludge leaching studies have been those that utilise bioleaching of metals<sup>[61–68,72,72–75]</sup>, due to the native abundance of bacteria (specifically thiobacillus) within sewage sludge<sup>[61–68,73]</sup>. With removals from the immobile phase of >90% for cadmium, copper, manganese and zinc, with 54% of chromium, 79% of nickel and 46% of lead it can be seen why so much emphasis has been placed upon this research, with the only downside being time scales of 5 d to 16 d<sup>[73]</sup>.

While less abundant, studies also show that strong mineral acids<sup>[63,70,76,77]</sup> are promising lixiviants, which is unsurprising due to the common-place application of these chemicals within industry. Mineral acids (nitric, hydrochloric and sulphuric acid) have displayed effective extraction of cadmium (59%), chromium (27%), copper (41%), manganese (83%), nickel (68%), lead (22%) and zinc (66%) under ambient conditions and a pH of just 1.5. While these values relate to a 24h leaching period, improved rates and extraction were achieved using elevated temperatures and acidities. Even phosphoric acid can be utilised as an extremely effective lixiviant (in high concentrations; >40%), with >90% extraction of arsenic, cadmium, chromium, copper and lead and >80% extraction of mercury, manganese, nickel and zinc; this process was developed with an inbuilt reconditioning phase as with the right conditions, 100% of this phosphoric acid was recovered in a small lab-scale experiment<sup>[70]</sup>.

As an alternative to strong acids, complexing agents, such as EDTA, have achieved extractions of 20-50% for copper, lead and zinc after 1 h with a concentration of only 0.05 mol L<sup>-1</sup> and no pH adjustment<sup>[78]</sup>. A combination of acidic conditions and complexation for the extraction of metals turns the attention of this work towards weak organic acids; the buffering capacity and complexing ability of these acids has proved promising within the field of leaching heavy

metals from sewage sludge<sup>[69,71,78,79]</sup>, capable of out performing strong acids at higher pH values<sup>[80]</sup>. Beginning with acetic acid, small success has been seen at relatively high pH values, with high removals of zinc, and the potential removal of copper and lead<sup>[78,81]</sup>. More promising, citric acid was capable of removing >50, 60 and 50% of copper, zinc and lead, respectively in a single stage, with lead and zinc removal reaching 100% when a higher pH was used (pH 3)<sup>[78,80,81]</sup>. Another acid to mention is oxalic acid, and while capable of removing 30, 40, 40 and 30% of nickel, copper, zinc and chromium after 1 h at pH 2<sup>[80]</sup>, with higher extractions of copper and zinc possible with longer resonance times<sup>[81]</sup>, lead oxalate is sparingly soluble in water and will therefore be ineffective.

The last to be mentioned, and perhaps most successful method for metals extraction from sewage sludge, is the usage of strong oxidising agents; for example, usage of the Fenton reagent (the addition of both iron(II) and H<sub>2</sub>O<sub>2</sub>) commonly used for the oxidation of waste waters<sup>[72,75,82,83]</sup>. This method has achieved removals of 92, 100 and 80% of zinc, lead and copper<sup>[82]</sup>, further cementing the potential for oxidants to increase extractability of heavy metals, was a study by Marchioretto (2003)<sup>[36]</sup>. Within this study, simple aeration, inclusive of high acidities, resulted in almost complete removal of copper, lead and zinc from sewage sludge (94, 100 and 100%) after 2 days. The combination of oxidative conditions and complexing lixivants create the potential for a highly effective metals recovery process.

The success of this work gives a promising outlook for the removal of heavy metals from sewage sludge. With a carefully thought out process for dissolution of immobilised metals, there lies the possibility for not only complete removal of toxic metals from the solid phase, there is also the ability to separate metals from the complicated waste stream, creating a valuable by-product. Here lies the hole in current research, while there has been success within the area of mobilisation, there has been little work done on this recovery of metals from the pregnant

leach solution (PLS) generated from the leaching process. The current state-of-art within this field is a solid-liquid separation before the filtered sludge is pH adjusted precipitating the remainder of the metals within this sludge residue<sup>[36,84]</sup>. This separation, however, comes with drawbacks; sludge contains many types of bound waters due to the porous and biological nature of the materials (free water, interstitial water, surface water and intracellular water, visually depicted within Figure 1.6), making the complete separation difficult. The quantity of water can be up to a total of 80% of the total dewatered sludge mass<sup>[14]</sup>, leading to a high moisture content in the final residue and therefore a final remaining quantity of mobile metals post separation stage; with a pH increase these metals will remain in more mobile fractions than they were before the leaching stage, negating the process as a whole.

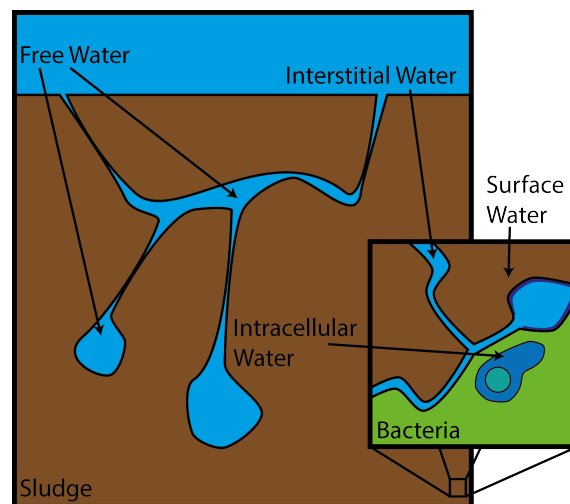


**Figure 1.6:** Graphical schematic of free water, interstitial water, surface water and intracellular water of sludge material<sup>[85]</sup>.

While the leaching of metals displays a lot of promise with regards to mobilisation and dissolution of metals from sewage sludge, the solid-liquid separation stage poses a problem. Ion exchange is often used in conjunction with other hydrometallurgical processes (such as leaching) in order to extract metals from a solid phase that contains low concentration of metals or complex organic media<sup>[86]</sup>. This combination of processes<sup>[86]</sup> could allow for the complete, or near

complete, removal of metals from sewage sludge, therefore will form the basis of this study into metals removal and recovery from sewage sludge.

## 1.5 Acid Leached Sludge and Ion Exchange

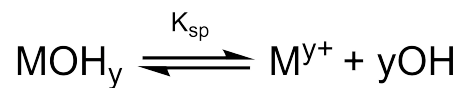
The rationale behind inclusion of ion exchange within this extractive process is simple; after the leaching stage, extraction of preferential metallic species can be conducted through either controlled precipitation, solvent extraction or ion exchange. Controlled precipitation is not an option due to the high concentration of dissolved organic matter within sludge liquid phase and solvent extraction will be ineffective at such low metal concentrations through difficulties that the low quantity of organic fraction that will be required. Due to the ability to use ion exchange resins with an infinitesimally small solid-to-liquid ratio, ion exchange quickly becomes the most beneficial for this extraction process.

The low concentration of metals within sewage sludge, however, still poses issues with regards to extraction, especially when considering the large concentration of organic matter; *in-situ* extraction processes such as reins-in-leach (RIL) and resin-in-pulp (RIP) have been used to mitigate this issue<sup>[86–92]</sup>. RIL and RIP are relatively new technologies and currently employed for previously inefficient process such as scavenging cobalt/nickel from tailings<sup>[87,88]</sup>, extraction of uranium from low grade ores<sup>[89–91]</sup> and gold recovery from carbonaceous materials<sup>[86,92]</sup>. While the solid fractions in these systems are vastly different to sewage sludge, they all possess similar qualities such as low concentrations<sup>[89,90]</sup> and solid sorbent species<sup>[86]</sup>. Hence, the direct relevance to extraction of heavy metals from sewage sludge.

RIL or RIP processes combine the leaching process parallel with solid phase extraction<sup>[91]</sup>, the useful nature of which spans beyond the negation of an intricate filtration process. Leaching within media which contains a large abundance

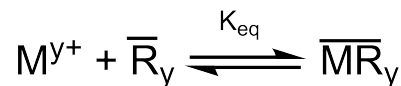


of potentially adsorbent solid particulates, such as sewage sludge<sup>[93]</sup>, may create an issue known as preg-robbing, where dissolved metallic species are simultaneously adsorbed to the surface of solid particles within the slurry; while the metallic species are then in mobile forms, the adsorbed species are removed from the PLS once filtration occurs<sup>[86]</sup>. In this instance, however, there will not only be a competition between solution and particulate surface, there will also be a competition between precipitation equilibria as well, therefore the term preg-robbing will be a blanket term used to refer to all processes that take from the leachate (described in Scheme 4).



**Scheme 4**

The theory behind both RIL and RIL technology is that, in many instances, adsorption to the surface of a resin (Scheme 5) outweighs precipitation. When this is the case (and therefore  $K_{eq} \gg K_{sp}$ ) preg-robbing has a much lower effect on the total extraction efficiency of the process. This not only allows for extraction when preg-robbing processes are involved, but it also allows for the removal of metals from low grade sources<sup>[87,88]</sup> prior to filtration where a large concentration of metals may remain in the water entrained in the filter cake.



**Scheme 5**

While both RIL and RIP processes involve the application of an ion exchange resin to a leaching slurry, the executions and use cases differ. In a RIP process, ion-exchange resin is added to the leach slurry directly (Figure 1.8), while in RIL processes the slurry is filtered prior to contact to the resin (Figure 1.7). There are advantages and disadvantages to each of these processes specifically in

relation to solids content of the slurry, biological activity of the slurry and leaching conditions.

A RIL process parallels leaching and adsorption of a metallic species; in this case unfiltered PLS slurry is pulled through a screening filter prior to contact with a resin prior to being re-introduced into the leaching vessel, depicted in Figure 1.7. This bypasses issues that may be observed with direct contact between slurry and resin; such as biological growth, pore blinding and erosion of the polymeric resin. The difficulty with filtering sludge, however, is the tendency for blinding within the filtration process<sup>[14,94]</sup>; the addition of fly-ash<sup>[95,96]</sup> or use of sand filters or a screening stage<sup>[14]</sup> could reduce resistance of the leaching slurry to filtration and reduce biological contamination<sup>[97,98]</sup>.

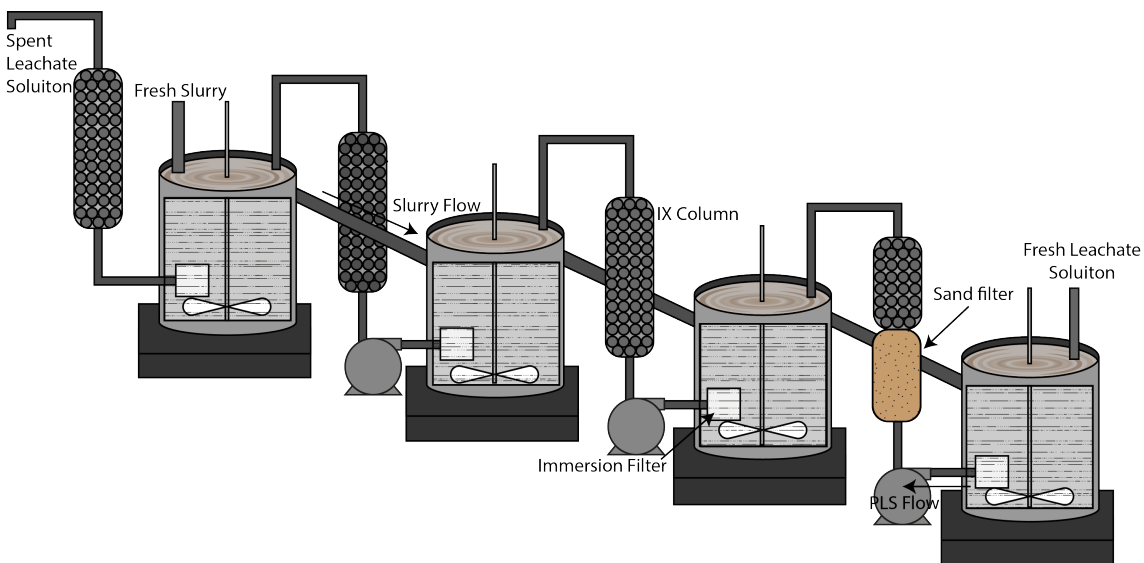


**Figure 1.7:** Diagram of a RIL impeller agitated multistage process.

While, with the addition of filter aids, a RIL process could be rendered possible, the addition fly-ash<sup>[99]</sup> or flocculants<sup>[100]</sup>, and the difficulty of filtration without these aids, creates the potential of preg-robbing of metals from the PLS prior to contact with the resin; this reliance on filtration poses a serious issue with the RIL process. A RIP process mitigates this issue (along with the difficulties in filtration as a whole) by the direct addition of resin beads to the leachate

slurry; leading to a direct competition of adsorption processes with preg-robbing processes, and negating the filtration stage entirely<sup>[89]</sup>(Figure 1.8). By using a resin with a higher particle size than the sludge, the resin beads can simply be sieved from the slurry, leading to a relatively simplistic sieving stage; low particle size of sewage sludge pre-dewatering stage being majority  $<0.01\text{ mm}$ <sup>[101]</sup> leaves the option for many commercially available ion exchange resins, as well as novel ion exchange materials. RIP can also allow for the separation of leaching and adsorption processes, creating the possibility for a temperature, pH or and ORP difference between adsorption and leaching stage<sup>[102]</sup>.

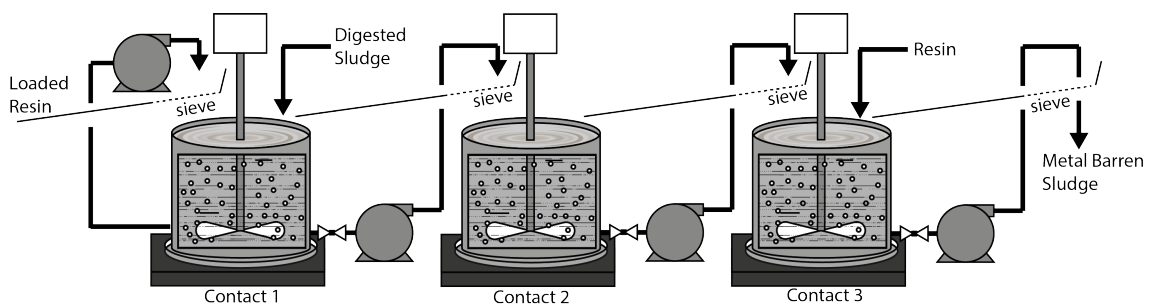


**Figure 1.8:** Diagram of a RIP impeller agitated multistage process.

### 1.5.1 Lixivants

Leaching is the process of dissolution of metals from an immobile or solid phase into a mobile or aqueous ionic phase by way of a solvent or leaching agent (lixiviant)<sup>[103]</sup>; a naturally occurring process (hence the dangers of immobile metals in agricultural soils) and one that can be kinetically enhanced by the addition of lixivants<sup>[103]</sup>. Typically speaking, and as alluded to within Section 1.4.1, strong mineral acids are most commonly used as lixivants (HCl,  $\text{H}_2\text{SO}_4$ ,  $\text{HNO}_3$ , etc.), especially sulphuric acid due to the low cost and ease of use. With respect to the complexity of sewage sludge, utilising lixivants to manipulate a factor such as pH, ORP and/or ionic strength (even by addition of a strong complexant) immobile metals can be dissolved into solution and stabilised within solution<sup>[103]</sup>.

The relationship of ORP, pH and solubility of a metal in solution is displayed within Figure 1.9, without the addition of a complexing agent. This displays a predominance diagram for iron, it describes how the speciation of iron changes as a function of both pH and ORP, between iron(II), iron(III) and the subsequent hydrolysis products and precipitation of minerals. Many of the species within Figure 1.9 are insoluble, however with the addition of acids, bases, reductants or oxidants, solution conditions can be modified in order to maximise the concentration of soluble species.

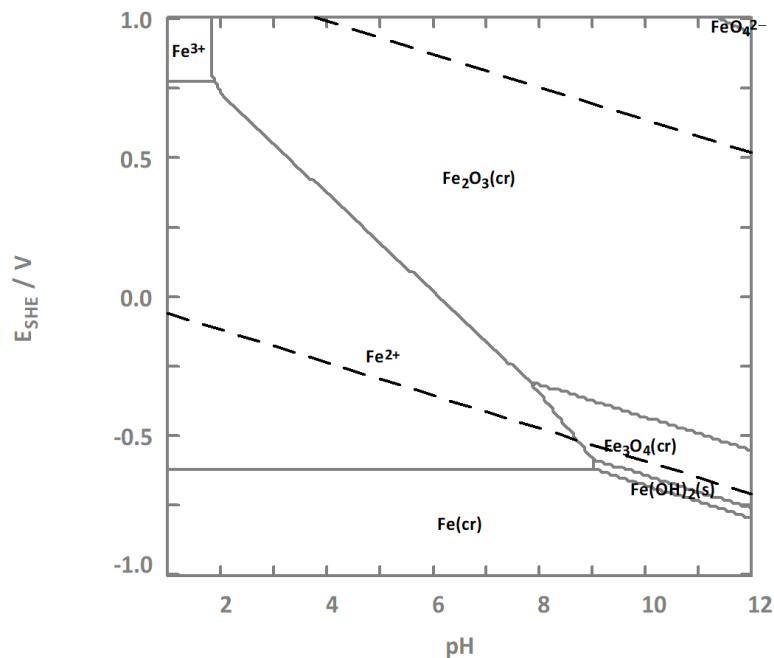
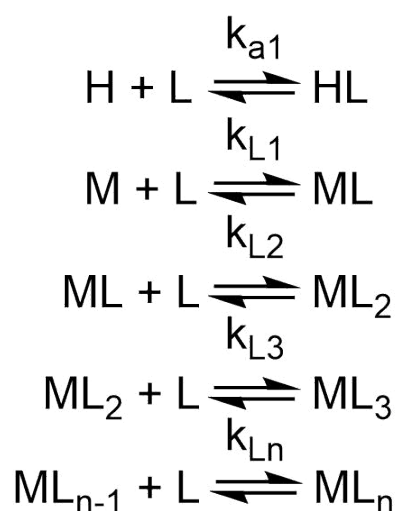


**Figure 1.9:** Eh-pH diagram of iron calculated by HYDRA/MEDUSA<sup>[104]</sup>.

With the complexity of sewage sludge, dissolution and precipitation of species in detrimental manners are inevitable; for example iron is very likely to remain in solution in concentrations higher than that of target species and lead is likely to precipitate as lead sulphate (with the oxidation of sulphide species). Complexing agents can be used in such a way that allows for the tailoring of solution pH to precipitate contaminant species and stabilise target species through the adjustment of pH in a deliberate manner; this has led to the previously discussed success of acetic and citric acid leaches within sewage sludge. This complexation

is dependent on the equilibrium between the concentration of metallic species and the corresponding complexing ligand.

The reaction depicted within Schematic 6 is a simplified version of a complexation process; in this situation, H is a proton, M is the metal within the centre of the complex and L is the complexing ligand. With a greater concentration of ligand, and therefore a greater concentration of the ligand bound metallic species, there is a tendency towards the greater formation of higher order complexing species. While ligands can be added to solution as compound, there is also an equilibrium that is formed between the binding ligand and its counter ion. The case presented in Scheme 6 is related to a weak acid and therefore the counter ion is a proton. With an increase in proton concentration (a decrease in pH) there is a decrease in concentration of available ligand, and decreasing the proton concentration leads to an increase in ligand concentration; further leading to either more or less competition between metallic species and ligand complexes, respectively.



**Scheme 6**

Utilising an equilibrium such as this, there is the possibility for stabilisation of metals within solution. Many weak organic acids are capable of behaving

as complexing agents as well as acids, effectively taking on two roles. With a lower pH there is low binding competition by  $\text{Fe}^{2+}$  over protons for the acetate anion acetate, as the pH increases,  $\text{Fe}^{2+}$  becomes more competitive for acetate binding ( $k_{a1}$  vs  $k_{L1}$  in Scheme 6). Once the propensity for formation of hydrolysis products out-competes the stability of acetate complexes, however, precipitation of iron hydrolysis products is again observed. Comparing this information to the predominance diagrams in Figures 1.9 (no complexing acid) and 1.10a (acetic acid present), it can begin to be observed how the competition between hydrolysis products and complex species leads to an increased solubility of metallic species.

As previously alluded to, the high concentrations of ions, such as iron, will make extraction of the relatively low concentrations of copper, lead and zinc extremely difficult; and weak acids can rectify this. An example can be observed with the case of the iron predominance diagram vs the lead diagram (Figure 1.10). Within this system, pH and ORP can be controlled in order to allow for a predominantly soluble species for lead, therefore rendering this species extractable within the RIP process, while simultaneously precipitating iron hydrolysis products.

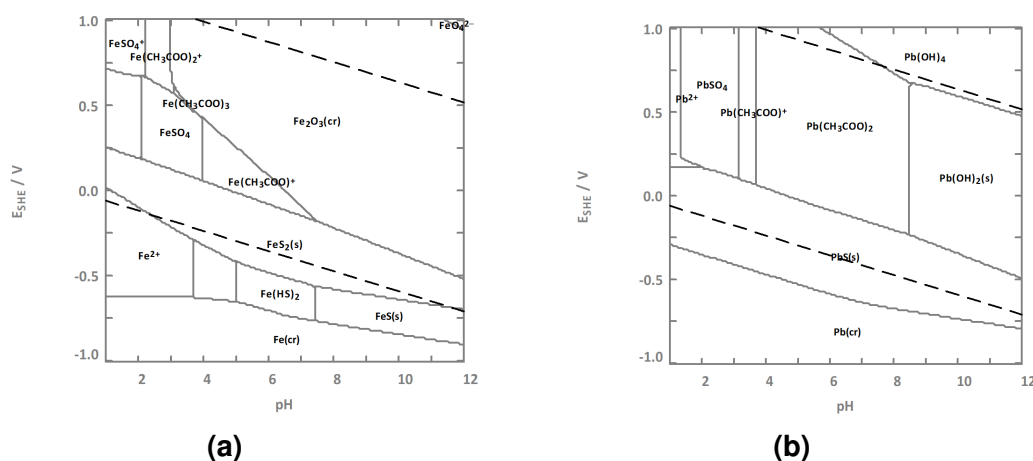


**Figure 1.10:** The predominance diagrams of iron (a) and lead (b) in the presence of both sulphate and acetate, calculated by HYDRA/MEDUSA<sup>[104]</sup>.

As weak acid leaching is currently used within research towards resource recovery, being explored in metals removals from sludge and recovery from waste

electrical and electronic equipment<sup>[105]</sup>, this field is becoming a more heavily studied area. Processes such as this show a lot of promise for less profit driven and more environmentally sensitive use cases, as the acids are generally capable of leaching at higher pH<sup>[80]</sup>. The extraction of metals from this media, however, is very understudied; due to the complexing nature of weak organic acids leading to stabilisation of metals within solution, there can be competition between extraction by ion exchange resin and stabilisation in solution phase complexes. Therefore, with reference to the hypothesised RIP process, there is a great deal of importance placed on understanding the extraction efficiency and mechanisms of ion exchange resins within complexing weak acid media.

### 1.5.2 Ion Exchange

Ion exchange extraction is a phenomenon occurring within a solution of dissolved ions where a reversible exchange of ionic groups occurs between what is in solution and an insoluble solid phase<sup>[106]</sup>, in this case an ion exchange resin. While ion exchange media can be found in many different forms, from minerals (zeolites, clays, etc.) or functional biological material (e.g. activated charcoal, functionalised loofahs, etc.), this thesis will have a distinct focus on synthetic ion exchange resins (cross-linked porous polymers functionalised with ion exchange or chelating groups). Generally, the interaction of the ion exchange functional group and the ion of interest can be explained with the following, simplified scheme:



Scheme 7

In this example of a cation exchange reaction, R<sup>-</sup> is the ion exchange functionality which is bound to a porous backbone (cross-linked polymer) of the solid resin, M<sup>+</sup> is the cationic species of interest in solution and H<sup>+</sup> is a proton,

of course the charges of species can be reversed, which would constitute an anion exchange reaction. Being an equilibrium, the extraction of the species of interest ( $M^+$ ) can be controlled by the concentration of either protons ( $H^+$  species) or hydroxyl species ( $OH^-$ ), and therefore there is a large reliance of adsorption on the solution pH. With the assumption that these adsorption processes are reversible, there is also the potential to utilise this equilibrium for recovery of the adsorbed species or regeneration of the ion exchange resin through a process known as elution.

The operational pH or the effectiveness of a functionality for a specific metal depends upon the selectivity of that functionality for the target species. A measure of the selectivity can be reported as a separation factor, which display the selectivity of a functionality for one species over another. Separation factors ( $\alpha_B^A$ ) can be calculated by:

$$\alpha_B^A = \frac{\bar{x}_A x_B}{\bar{x}_B x_A} \quad (1.1)$$

Where  $\bar{x}_A$  and  $\bar{x}_B$  are the concentration of species A and B, respectively, adsorbed to the resin, while  $x_A$  and  $x_B$  are the concentration of species remaining in solution<sup>[107]</sup>. By inclusion of charge into the equation, we arrive at Equation 1.2.

$$K_B^A = \frac{\bar{x}_A^{|z_B|} x_B^{|z_A|}}{\bar{x}_B^{|z_A|} x_A^{|z_B|}} \quad (1.2)$$

Selectivity constants can be descriptive of processes involving molality, molarity or equivalent ionic fractions both in solution or on the resin surface ( $K_B^A$ ,  $K_B^A$  or  ${}^N K_B^A$ , respectively); with equivalent charges however, each factor can be collapsed into separation factors  $((\alpha_B^A)^{|z_A|})$ <sup>[107]</sup>. Separation factors and selectivity factors for metallic species can be tailored to process specific species by exchanging the functionality of the resin<sup>[106]</sup>. The most common, commercially available ion exchange functionalities are depicted within Figure 1.11.



Broadly speaking, functional groups can be separated into five categories, these being strongly and weakly acidic, strongly and weakly basic and chelating functional groups. Strong acid cation exchange (SA) functionalities (the sulphonic acid functionality, Figure 1.11 A), are characterised by their effectiveness within extremely low pH regions and low selectivity; strongly basic anion exchange (SB) functionalities (quaternary amine functionalities, Figure 1.11 C1-3) can be conceptualised as the the pOH equivalent to SA functionalities. Weak acid (WA) (carboxylic acid functionality, Figure 1.11 B) and weak base (WB) functionalised resins (tertiary/secondary amines, Figure 1.11 D1-3) are more selective due to their higher affinities for their respective counter-ions.

Chelating functional groups (Figure 1.11 E1-F4) as the name suggests, form chelates with the adsorbent ions, allowing for a more selective extraction. These functional groups are not necessarily a separate group of functional groups as they often incorporate either WA or WB functionalities. The incorporation of multiple properties with the ability to combine multiple functionalities (sulphonic + phosphonic acid combination functionality, Figure 1.11 F1) gives a large flexibility with regards to not only selectivity of a resin functionality, but also the adsorption mechanisms and to a small extent kinetics.

As copper, lead and zinc were found, generally, to be the most common limiting factors towards sludge application<sup>[34,35,44]</sup>, these will be the focus metals. Briefly, thiol/sulphur containing groups groups<sup>[108,109]</sup>, weak acid (carboxylic acid) groups<sup>[109]</sup> and phosphorus groups<sup>[110]</sup> have shown promise as extractants of these metals. The most efficient functional groups to extract all focus metals (Pb(II), Cu(II) and Zn(II)) in a single step would potentially be complexing, nitrogen containing functional groups<sup>[109,111]</sup>, specifically an amidoxime or modified amidoxime functional group<sup>[112,113]</sup> (Figure 1.11 - F4), especially at a pH above the pKa of the functionality<sup>[114]</sup>. As well as the amidoxime functionality, other potential chelating functional groups to screen would include that of iminodiacetic

acid (IDA) functional groups (Figure 1.11 - F3) and that of other bis-picolylamine complexing groups (Figure 1.11 - E1).

IDA and bis-picolylamine functionalities (Figure 1.11 - F3 and E1, respectively) are highly selective towards copper<sup>[106,115]</sup>, however at a  $\text{pH} < 2$ , IDA groups decrease in their effective adsorption. Bis-picolylamine functionalities maintain the high affinity at low pH, with many commercial processes using the bis-picolylamine functionalities<sup>[112,115]</sup>. Both IDA and bis-picolylamine functionalities display a high affinity towards zinc as well, although not to the same extent<sup>[115]</sup>. From solutions above pH 4, commercially available aminophosphonic functionalised resins (Figure 1.11 - F2) show high selectivities towards zinc<sup>[112]</sup>. While both the IDA and aminophosphonic functionalised resins display affinities for lead in solution, research toward lead extraction has been predominantly focused towards phosphorous containing groups<sup>[110,112]</sup>.

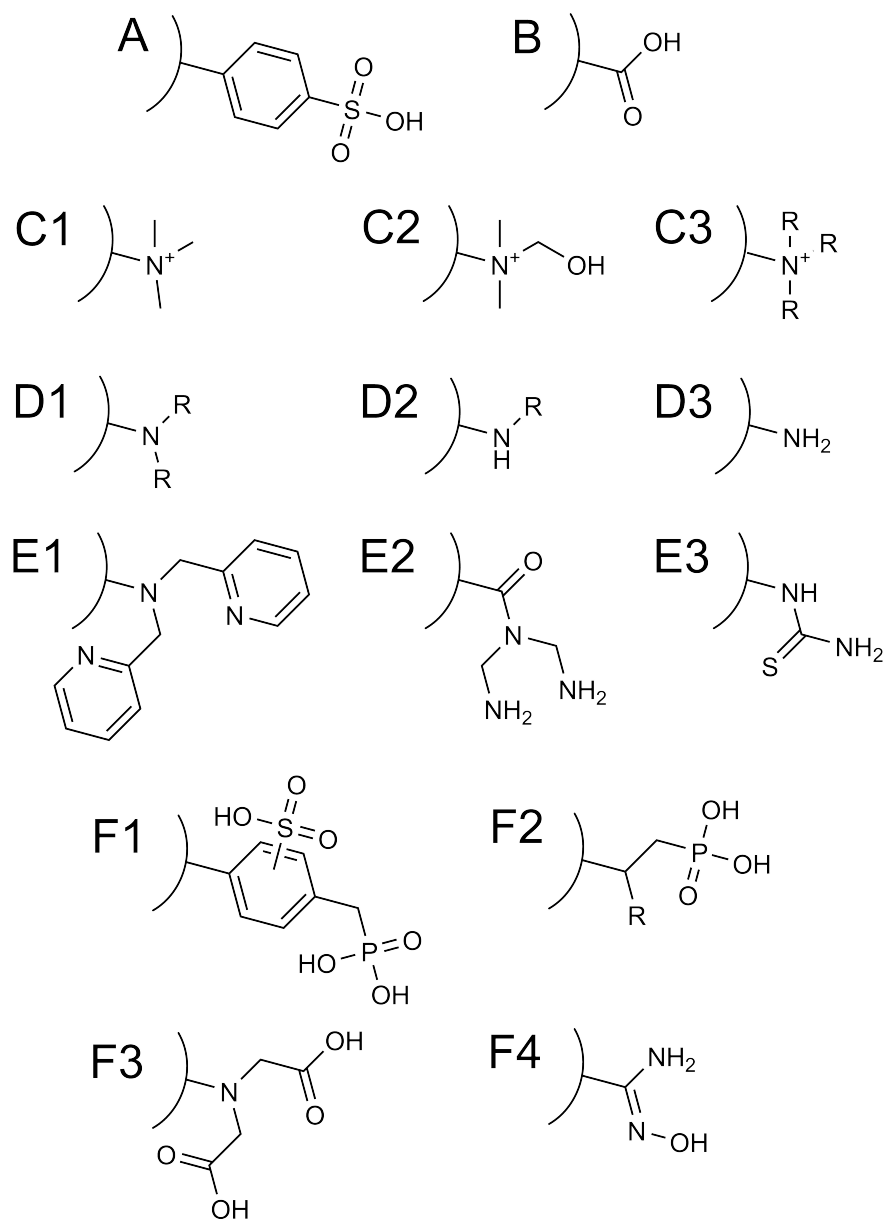


**Figure 1.11:** General resin functionalities. A = strong acid cation exchange (SAC) (sulphonic acid), B = weak acid cation exchange (WAC) (carboxylic acid), C1 = strong base anion exchange (SBA) type I (quaternary amine), C2 = SBA type II (quaternary amine dimethylethanolamine), C3 = SBA type III (unknown), D1 = weak base anion exchange (WBA) (tertiary amine), D2 = WBA (secondary amine), D3 = WBA (primary amine), E1 = weak base chelating (WBC) (bis-picolylamine), E2 = WBC (bis-(aminomethyl)acetamide), E3 = WBC (thiourea), F1 = strong acid/chelating ion exchange (CI) (phosphonic/sulfonic acid), F2 = CI (aminophosphonic acid), F3 = CI (iminodiacetic acid), F4 = CI (amidoxime)

While the functionality can contribute to the kinetics of ion exchange, the largest contributor to the kinetics of adsorption, is diffusion. Polymeric ion exchange

resin beads are porous, by nature, however the pore size (iso-, micro- or macro-porous, order of increasing size) can alter the diffusion kinetics of the adsorption process. To explain this process, Figure 1.12 is a visual representation of the kinetic limitations of ion exchange adsorption.

The limitation described by process A is known as film diffusion, where the kinetics of an adsorption process is dictated by a stagnant film layer of solution surrounding the resin's surface, creating a gradient different preventing contact to the functionality. The process B, pore or intra-particulate diffusion, is most common within iso- or micro-porous, dictated by a concentration gradient forming within the pore structure of the resin; easily mitigated by larger pore sizes and higher solution agitation. The final process for discussion will be the limitation by ion exchange between solution and ion exchange functionality, described by process C. This final process will not necessarily dictate the kinetics of the reaction, as it is often faster than diffusion kinetics, however nuances of this process can divulge information about affinities of functionalities for metals.

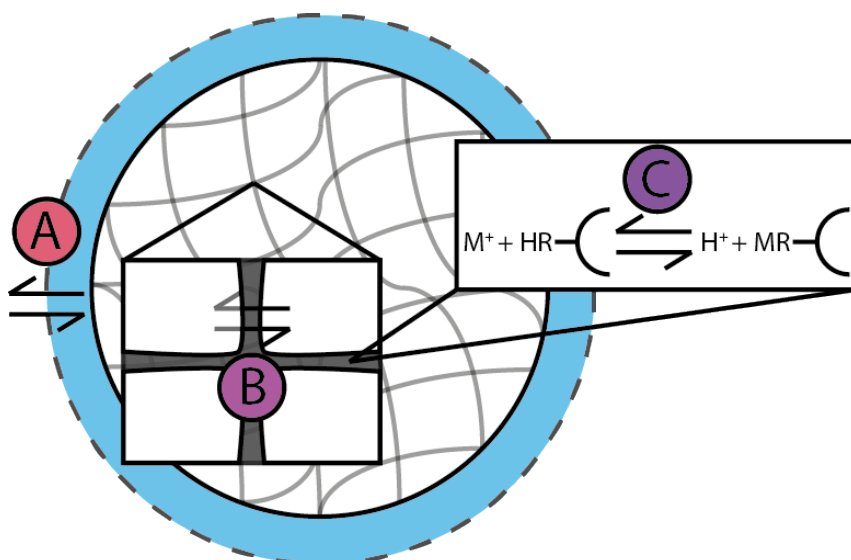


**Figure 1.12:** Diagram for a simplified explanation of A - film diffusion dictated kinetics, B - pore/intra-particulate diffusion dictated kinetics and C - chemically dictated kinetics<sup>[106]</sup>.

There have been many studies on the functionalities within Figure 1.11<sup>[112]</sup>, but there is little emphasis on the effect co-ions have on sorption capacities. The solution-phase speciation of the target ions can play a big role in multiple factors in the binding of species to a resin's surface. Depending on the complex formed, the change in the formal charge of the total species can be either deleterious or beneficial for adsorption to a specific metal causing an effect on the binding strength or mechanism between resin functionality and ionic species<sup>[106]</sup>. Therefore a characterisation of each resin is also required within the solutions in high complexant concentration.

In the case of weak acids the ion exchange equilibrium becomes a little more complicated than depicted within Scheme 7, as it also combines the equilibria outlined in Scheme 6. The extraction of the ionic species is no longer reliant on purely the competition between  $H^+/OH^-$  and the ionic species of interest, now there is also a competition between the stability of the complexes formed in solution and on the resin surface to be considered as well, with combinations of complexes and the species bound to the functionalities being involved<sup>[116,117]</sup>. These complexes can aid extraction, they can stabilise the ion in solution or they can have no effect.

Complexing species within solution can, and do, have a remarked effect on the efficiency, selectivity and overall useful nature of an ion exchange resin or functionality<sup>[118]</sup>. While typical ion exchange functional groups display high affinities towards all target metals<sup>[112]</sup>, the effect that the inclusion of a complexing buffer and subsequent alteration of speciation can have on extraction of metals has had little literature interest. The primary focus on this thesis will therefore be in gaining an understanding of the overall effect of speciation on the extraction of base metals, and the subsequent effects this can display on resin performance and whether or not this can aid in the removal of copper, lead and zinc from sewage sludge.

## 1.6 Hypotheses

Closing the phosphorous cycle by using sewage sludge as a fertilizer is a sensible option for addressing food security. Extraction of heavy metals present in sewage sludge could aid in the unrestricted use of sewage sludge as a fertilizer and potentially generate profit from the recovered metals. The overarching hypothesis to this body of work is that “utilisation of weak, complexing acids within a resin-in-pulp process could provide a method of separation and removal of metals from sewage sludge allowing for the recovery of nutrients and metals from this waste stream, overcoming deleterious effects of precipitation and hydrolysis of heavy metals as well as issues with oversaturation of the resin by contaminant ions.” With the success of metals leaching from sewage sludge, solid liquid separation stages are the current state-of-art. Inclusion of an ion exchange resin within the leachate slurry could allow for a more complete removal of metals. For this to be conducted, there are gaps within the literature that need to be addressed, those that will be addressed are as follows:

- A deficiency in the characterisation of the effect complex formation poses on ion exchange phenomena
  - This will be addressed through a screening study of resin functionalities within acetic, lactic and citric acid, inclusive of a discussion on the effect of solution phase speciation on extraction efficiency
- A lack of in-depth analysis by specific adsorption models and the mechanistic effect that weak acids can have on the adsorption of copper, iron(II), lead and zinc
  - A study on the mechanism of binding between literature sources of strong acid extraction with experimental data of extraction from weak acid media will be reported on single metal systems
  - Kinetic experiments will be conducted on unsaturated multi-metal

systems in order to determine operational parameters intended for the contact stage of the proposed RIP process

- An understanding of the effect multi-metal systems and competition pose on resin performance is lacking
  - A multi-metal isotherm model that predicts a specific system's propensity to desorb a particular species upon saturation of a species with more affinity towards the functionality will be proposed and proved against two systems
- The feasibility of a resin-in-pulp system for the extraction of metals from sewage sludge has not been previously tested.
  - A simulated process will be reported utilising acidic and oxidising conditions with a weak acid lixiviant for the extraction of copper, lead and zinc from the simulant sewage sludge. The performance of this system will be compared against the best case solid-liquid separation post-leach that has been previously reported within literature sources.

## 1.7 Thesis Structure

This thesis is presented in the alternative thesis structure, sectioned as follows:

- Chapter 2: General Methods and Instrumentation

This chapter brings a brief explanation of the experimental methods used throughout the thesis and an explanation of the analysis techniques.
- Chapter 3: Resin and weak acid screening
  - Section 3.1: Resin Screening in Citric Acid Media

This chapter presents a modified version of the paper "Extraction of Heavy Metals from Simulant Citrate Leachate of Sewage Sludge by Ion Exchange" that has been published by the Journal of Ion

Exchange on:20/09/2018. This paper describes the findings of a screening study on the performance of commercially available resins on copper, iron(II), lead and zinc extraction from citric acid media (DOI: doi.org/10.5182/jaie.29.53).

– Section 3.2: Resin Screening in Weak Acid Media

This chapter presents a modified version of the paper “Ion Exchange Removal of Cu(II), Fe(II), Pb(II) and Zn(II) from Acid Extracted Sewage Sludge - Resin Screening in Weak Acid Media” that has been published by Water Research on: 20/04/2019. The work in this paper builds upon section 3.1 by a comparison of the citric acid system with both the acetic acid and lactic acid systems, inclusive of thermodynamic solution-phase modelling (DOI: doi.org/10.1016/j.watres.2019.04.042).

• Chapter 4: Single Metal Isotherm Studies

This chapter presents a modified version of the paper “Single metal isotherm study of the ion exchange removal of Cu(II), Fe(II), Pb(II) and Zn(II) from synthetic acetic acid leachate”, has been published by the Chemical Engineering Journal on: 21/03/2020. This work further builds upon section 3.2 by producing an in-depth study on the extraction mechanism and capacity of copper, iron(II), lead and zinc from acetic acid media at pH 4.5 (DOI: 10.1016/j.cej.2020.124862).

• Chapter 5: Mutli-Metal Studies

This chapter presents a modified manuscript, intended for submission to the journal of Chemical and Engineering Data, reporting the findings of a mixed-metal isotherm and kinetics study of the extraction of copper, iron(II), lead and zinc from acetic acid media at pH 4.5 the same ion exchange resins from chapter 4. This study builds upon chapter 4 by furthering the understanding of how complexing acids may affect extraction kinetics and attempts to produce a rudimentary isotherm model to describe the



desorption processes observed with competition between metals; allowing for the determination of the initial operational parameters for conducting the bench-scale RIP process.

- Chapter 6: Simulated Acetate RIP Process

This chapter builds upon chapter 5 by presenting the final product of the acetic acid study. A simulated sewage sludge is developed from a literature source and rheologically characterised. Utilising using a low pH acetic acid leach within oxidative conditions, a RIP process is proposed and attempted.

- Chapter 7: Citric Acid Adsorption System

This chapter presents a modified manuscript, intended for submission to the Chemical Engineering Journal, reporting the findings of a mixed-metal isotherm and kinetics study of the extraction of copper, iron(II), lead and zinc from citric acid media by an IDA functionalised resin. This study builds upon chapter 3 by generating a mechanistic understanding of the extraction of these four metals from citric acid media.

- Conclusive Remarks and Future Work

This chapter summaries the findings of the thesis and responds to the initial hypotheses with a perspective on why research in this area is important to the global population. A discussion is included on the questions and possibilities of future work that has arisen upon the completion of this project. The future work has been separated into two distinct sections: the information and work required in order to further the technical readiness level of the RIP separation process; and questions that have arisen that would contribute to the fundamental understanding of ion exchange within complexing weak acid media.



# **Chapter 2**

## **General Methods and Instrumentation**

### **2.1 Materials**

Materials will vary from chapter to chapter dependent on the experiment that is conducted, materials specific to a chapter will be included in the experimental section of that chapter. Generally speaking, sodium hydroxide, sodium chloride, nitric acid and sulphuric acid have been utilised throughout the entire thesis and have been purchased from Sigma Aldrich. Nitric acid (70%) was purchased as 99.999% trace metal free as it was the dilution medium for analysis, sulphuric acid (95-97%) was purchased as analytical grade, sodium chloride was purchased as an anhydrous powder and sodium hydroxide was purchased as anhydrous pellets.

### **2.2 Equipment**

This section will list the equipment crucial to investigations throughout this thesis, as well as relevant information of each apparatus. Equipment from this list will be referred to within the specific experimental section of each chapter.

- **Orbital shaker**

The orbital shaker used for all static contact experiments within this thesis is an Incu-Shake MIDI Benchtop Shaking Incubator. This was set to 250 RPM and temperature controlled at 20 °C for each experiment, unless otherwise stated.

- **Overhead stirrer**

Agitation of leach slurries was conducted using a Stuart SS20 overhead stirrer with a four blade propeller impeller. The speed of the stirrer was maintained at between 250-500 RPM, unless otherwise stated.

- **Peristaltic Pump**

Clean PLS was pumped through packed ion exchange columns using a Watson Marlow 120U peristaltic pump. The flowrate of the solution through the packed column was calculated by pumping distilled water through a packed column for a specified amount of time before weighing the mass of water collected.

- **Fraction Collector**

The fraction collector utilised within the column experiments was a Biorad Model 2110 fraction collector. This fraction collector was fit with 10mL fraction tubes for sample collection

- **Centrifuge**

Slurry samples were centrifuged using a VWR CompactStar CS4 centrifuge fit with a 6×15mL angle rotor. All samples were centrifuged at 6500 RPM (4000 ×g) for 10min.

## 2.3 Ion Exchange Experimental Methods

### 2.3.1 Resin Measurement and Preconditioning

The resins that will be utilised throughout this body of work were either donated by Purolite International Ltd. (MTS9100, MTS9570, MTS9301, MTS9570 and C107E) or Lanxess Corporation (Lewatit Monoplus TP214). Ion exchange resin volume was measured in units of mL<sub>w</sub> (millilitres of wet settled resin), which is common practice within this field of science. Wet settled resin is measured by transferring quantities of resin (suspended within solution) into a measuring cylinder and allowing for the resin to settle upon force of gravity, this resin is then transferred to a container for contact with the target solution. This resin forms the resin bed, and the volume of the resin bed is referred to as the bedvolume.

In order to attain repeatable and reliable results, it is imperative that each resin is in the same 'form', that is the functional groups of each resin are associated with the same counter ion. This not only assures uniformity with regards to the initial resin conditions for each individual resin, but also insures that any residual materials from resin synthesis have been removed from the surface of the resin prior to contact with the PLS or slurry. Preconditioning was undertaken by contact of each resin with 10 bedvolumes of 1 M H<sub>2</sub>SO<sub>4</sub> and contacted with constant agitation at ambient temperatures (25°C) with an orbital shaker for a time period of 24h. Post-contact, acid was decanted from the resin prior to 10 cycles of washing with deionised water, or until the pH was neutralised (10 bedvolumes each wash) to ensure residual acid was removed. Once preconditioned, resins were stored under deionised water.

### 2.3.2 Column Ion Exchange Experiments

Throughout the industrial, commercial and domestic world, ion exchange resins are most commonly utilised within a flow-through column approach<sup>[106]</sup>.

While, within a static experiment, contacts are brought to an equilibrium between solution and resin, within a dynamic column experiment fresh solution is continuously pumped through an ion exchange resin that is 'packed' within a column. This forced contact with fresh PLS pushes the equilibrium, and therefore the ion exchange capacity of the resin, beyond that which would normally be observed within a reaction at equilibrium. In order to understand why many of the decisions throughout this body of work were made, especially regarding the lack of column experimentation, a brief discussion of column experiments (inclusive of preliminary data) and their pitfalls regarding sludge will be described here.

There are two possibilities for a column experiment, there is the traditional gravity fed (or downward flowing) column, which relies on either head-pressure caused by gravity or a pump to force the PLS downward through the column, however the lack of pressure caused by this directional flow can lead to 'channelling' within the column, where the PLS does not sufficiently contact all resin beads packed within the column. The 'reverse flow' technique, where the PLS is pumped counter to gravity, allows for the head pressure generated by gravity itself to create a more even contact between resin and PLS, preventing this channelling phenomena<sup>[106]</sup>. The column experiments will be conducted using the reverse flow technique.

A selection of six ion exchange resins (Lewatit TP214, Purolite MTS9100, Purolite MTS9570, Purolite MTS9301, Purolite MTS9501 and Purolite C107E) were packed with a bedvolume (BV, the volume of a resin packed within the column) of 2mL<sub>w</sub>sr (wet settled resin) within a 5mL ion exchange column, capped with Teflon frits in order to maintain constant packing pressure on the resin beads. Utilising a peristaltic pump synthetic, clean PLS was pumped through the column and aliquots of raffinate (the liquid residual waste from an extractive process) were collected for analysis in 10mL fraction tubes at predetermined time intervals by a fraction collector.

In these experiments synthetic, clean PLS was generated by dissolution of  $\text{CuCl}_2$ ,  $\text{FeCl}_2$ ,  $\text{Pb}(\text{NO}_3)_2$  and  $\text{ZnCl}_2$  (a concentration of 100ppm for each metal) into a solution of 0.5M acetic acid and 0.5M sodium chloride. This solution was then adjusted to pH 4.5 by addition of 50% NaOH, an optimal pH that was determined within Bezzina *et al.* 2019<sup>[119]</sup>. Each of the column experiments were conducted at a flow rate of 2 BV/hr for a total of 48 hours. The breakthrough data obtained for these preliminary experiments are included within Figure 2.1.

In a similar conclusion to study examining the acetic acid system<sup>[119]</sup>, ion exchange resins can be effectively utilised within this complexing media, despite the stabilisation of metals by MAce species. This becomes especially true with consideration to the column experiments, where nearly every resin is effective for the extraction of metals (an observation of a later breakthrough dictates a higher capacity)<sup>[106]</sup>; especially true for the late breakthroughs of TP214, MTS9570, MTS9301 and MTS9501, which further accentuates their industrial purposes<sup>[120–123]</sup>. Outliers from this, with regards to the specified target metals of copper, lead and zinc (for removal), are similar to the resins decided upon within Bezzina *et al.* 2019<sup>[119]</sup> and Bezzina *et al.* 2020<sup>[124]</sup>, with MTS9301 displaying high capacity for copper, lead and zinc, while also displaying a preference for these metals over iron; TP214 displaying an extraordinary affinity for copper over iron, lead and zinc, due to an apparent REDOX reaction; and, C107E, showing an unexpected<sup>[112]</sup> affinity for lead over the other metals within solution.

The ion exchange results from the breakthrough approach to ion exchange show promise for the utilisation as an extraction process for metals from a clean PLS, results that fall in-line with the theory behind a column approach. Generally speaking, in order to gain an understanding of the column performance of an ion exchange resin, there are models that can be fit that detail parameters required for scaling such a process up; and due to the commonplace nature within industry, the scale-up of such a process is simplified by turn-key solutions available. The

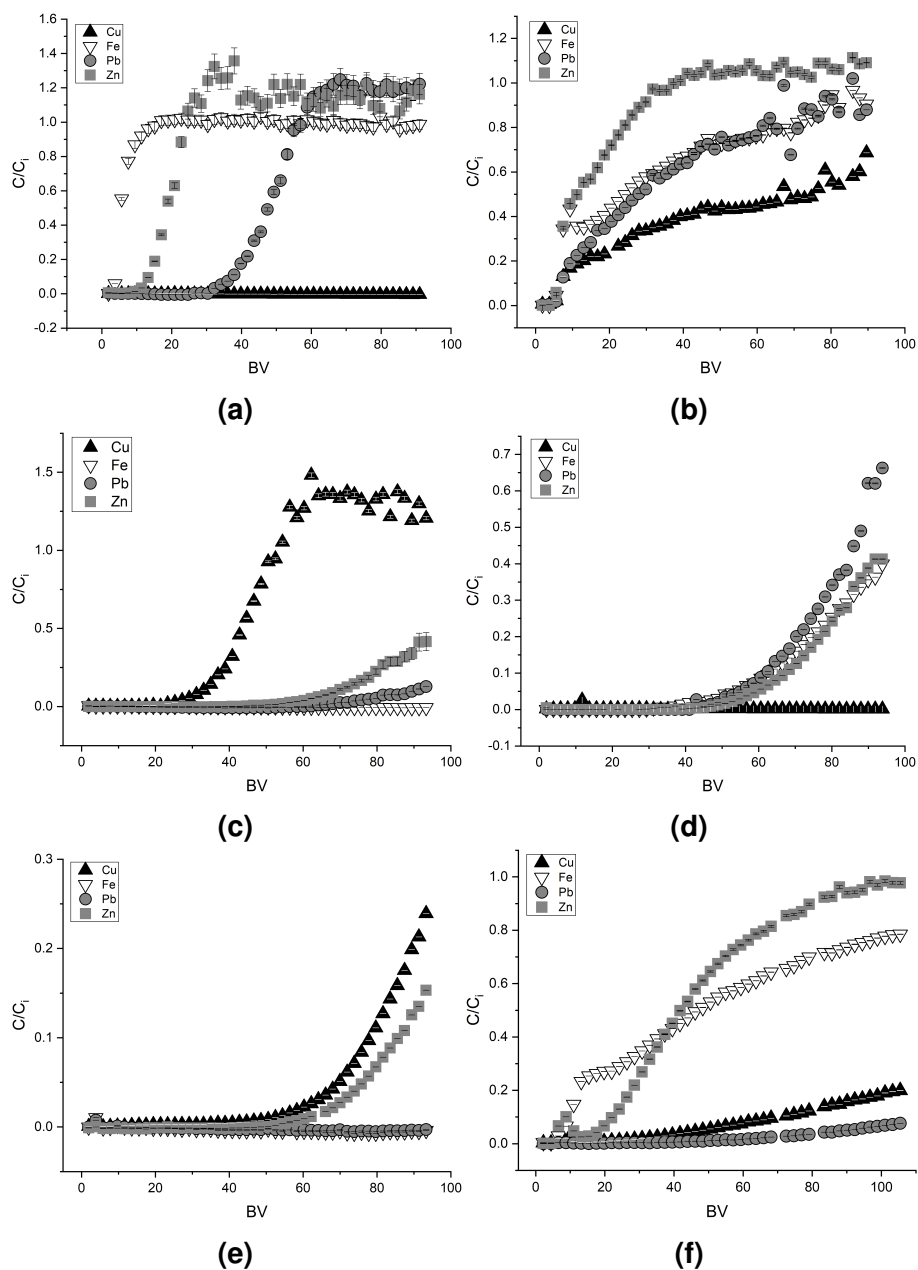


**Figure 2.1:** Breakthrough data on the performance of a) TP214, b) MTS9100, c) MTS9570, d) MTS9301, e) MTS9501 and f) C107E for the flow through column extraction of copper, iron(II), lead and zinc (initial concentrations 100ppm; temperature 20°C; 0.5M NaCl; 0.5M acetic acid; 2ml bed volume; 2 BV/hr flowrate).



reality of dealing with a slurry system with ion exchange columns is that a RIL process requires a prefiltration stage, prior to resin-solution contact. The flaws with this initially hypothesised RIL process were swiftly discovered as the filtration of, even a simulant sludge, was almost impossible even with 63 $\mu\text{m}$  sieves; it was not until a pore size of  $>100\mu\text{m}$  that there was sufficient flow through a vacuum filter.

Coupled with the difficult filtration of sludge, ion exchange columns are non-beneficial with regards to direct contact with a slurry, as pumping a slurry through a packed column (with severely limited flow rate due to the presence of resin beads) is difficult, if not an impossibility; this would lead to low flow rates and poor contact between resin beads and solution (slurry). One method of circumvention of this is to pre-filter the slurry, however as stated - one, sewage sludge is extremely difficult to filter due to organic, polymeric and colloidal material<sup>[14]</sup> and, two, the addition of a filter aid, increases the chances of pregrabbing of the leachate slurry<sup>[99,100]</sup>. As alluded to within Section 1.3, the answer to this problem is the utilisation of a RIP system, rather than RIL system, described within the introduction. As static analysis of the resin is more appropriate for the development of a RIP process<sup>[88]</sup> this will be the approach taken throughout the following research. Therefore, a more detailed discussion of the column experiments, inclusive of model fitting, will not be undertaken.

### 2.3.3 Static Ion Exchange Contacts

While there were variations on the contact conditions for each experiment in subsequent chapters, overarchingly, the experiments conducted are referred to as static experiments<sup>[106]</sup>. Static experiments involve the contact of a fixed volume of wet settled resin with a fixed volume of solution either for a known period of time or until equilibrium is observed. As with the preconditioning stage, each static experiment was agitated on an orbital shaker throughout the contact to ensure

complete dispersion of solution through the porous resin bead.

This technique will be used for the in-depth analysis of resin performance within weak acid media throughout the entirety of this thesis, altering parameters to understand their effect on adsorption and utilising this to calculate theoretical operational parameters. Individual experimental sections will describe details of each method, however, in brief: screening studies alter parameters such as pH and ionic strength in order to determine optimal conditions for operation, isotherm studies alter solution volume, resin volume or solution concentration in order to determine thermodynamic, mechanistic and equilibrium details and time dependent studies alter contact time in order to determine kinetic limitations, reaction rates and further elucidate mechanistic details.

## 2.4 Solution Phase Speciation Modelling

Solution phase speciation was calculated by the HySS software suite<sup>[125]</sup>. This modelling method requires the input of equilibrium constants of formation all species hypothetically present within solution. Equilibrium constants ( $\beta$  or K values) provide description of the strength of interaction of complexes in solutions, and are calculated as per the following, where [M] is the metallic ion in question and [L] is the complex forming ligand or anion. Stability constants of species can be calculated using the formula:

$$K = \frac{[ML_n]}{[M][L]^n} \quad (2.1)$$

Where theoretical  $\beta$  values of intricate species can be calculated, when the stepwise  $\beta$  values are known, by:

$$K_1 = \frac{[ML]}{[M][L]} \quad (2.2)$$

$$K_2 = \frac{[ML_2]}{[ML][L]} \quad (2.3)$$

$$\beta_2 = K_1 \times K_2 \quad (2.4)$$

Many of these stability constants are reported within the literature or available from the NIST Stability Constant database<sup>[126]</sup>, with a comprehensive list of hydrolysis products available within literature. Using the HySS software the theoretical speciation within solution can be visualised as a function of concentration of a specific species in solution. This can aid in the description of extraction that is observed experimentally.

## 2.5 Analysis

### 2.5.1 Electrode Analysis

pH measurements were conducted using either a double junction gel pH probe for slurry or a Ag/AgCl pH electrode for solutions. Both electrodes were calibrated by linear regression analysis of millivolt measurement of buffers at pH 2, 4, 7 and 10. ORP measurements were conducted using a double junction platinum band electrode probe. Readings were taken utilising either a Mettler Toledo FiveGo hand held metre or a Fisher Scientific accumet AE150 bench-top metre.

### 2.5.2 Atomic Absorption Spectroscopy

The metals analysis throughout all of this work was conducted by atomic absorption spectroscopy (AAS) using a Perkin Elmer Atomic Absorption Spectrometer AAnalyst 400. This equipment was run with an air-acetylene flame, and controlled using the WinLab32 software<sup>[127]</sup>. A simplistic schematic, outlining the core components of a general AAS is displayed in Figure 2.2.

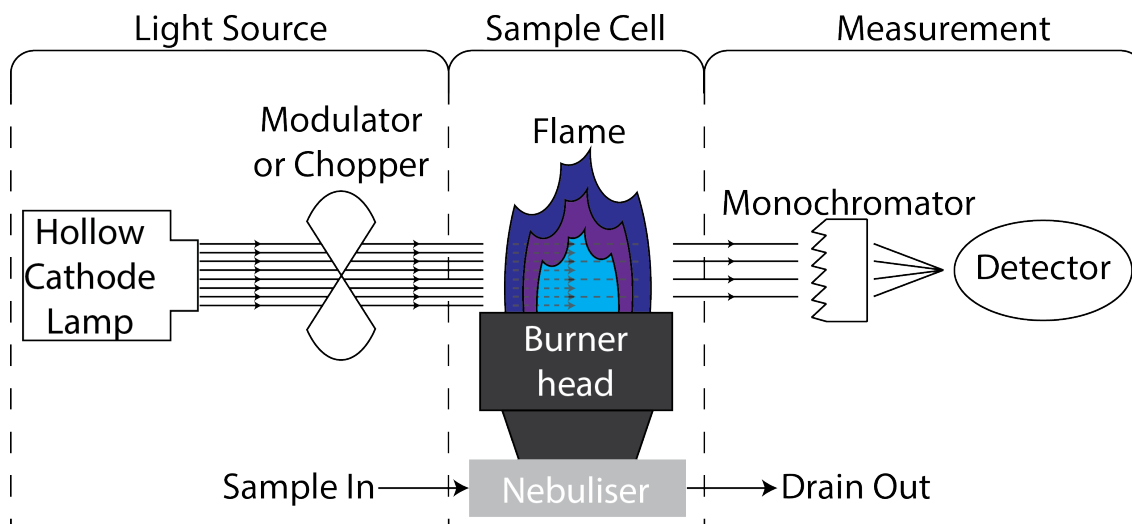


**Figure 2.2:** A simplified schematic diagram of the major components an AAS, utilised for the metals analysis throughout this thesis<sup>[127]</sup>.

AAS analysis operates under the premise that the excitation of an analyte will cause the absorbance of wavelength specific photons. Utilising this principle, the hollow cathode lamp containing an alloy of the analyte metal will produce light of a specific wavelength. This light will be modulated electronically or physically chopped to prevent interference before passing through a nebulised metallic sample. The resulting light signature will be wavelength separated and analysed by a detector before being compared to a known absorbance 'zero'<sup>[127,128]</sup>.

By analysing the difference between volume of photons into and photons out of the sample cell, there can be a measurement made of the quantity of analyte within the sample. This was calibrated against 4 standard solutions: a blank solution (1% nitric acid), and 3 different concentrations spanning the concentration range expected within the samples, generated from 1000ppm certified standard solutions. All analysed solutions were diluted within 1% nitric acid that was generated with the above stated trace metal pure nitric acid. Periodically, check standards were analysed, allowing for instrumental drift to be identified.

### 2.5.3 Rheology

The viscometer used throughout the analysis of the simulant sewage sludge was a Brookfield Digital Viscometer model DV-E<sup>[129]</sup>. All rheological measurements were conducted using either the S61 or S64 cylindrical spindles or the S62 or S63 plate spindles. A simplified diagram for this apparatus can be found in Figure 2.3.

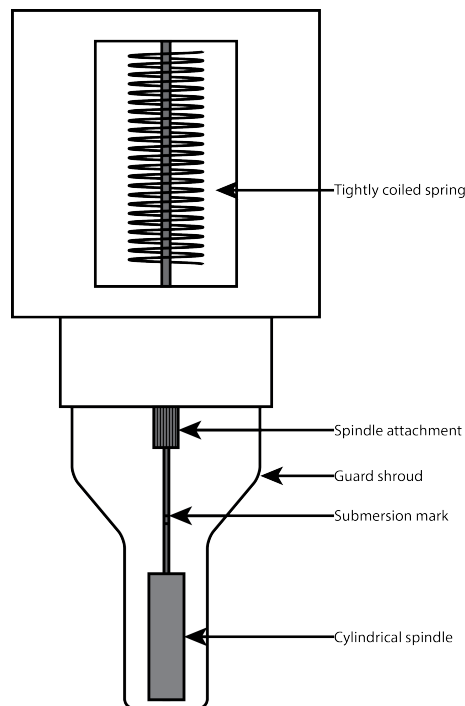


**Figure 2.3:** A simplified schematic diagram of the major a Brookfield DV-E viscometer with the S64 cylindrical spindle attachment<sup>[129]</sup>. The main body of the viscometer has a cut-out drawn into the centre to display the the coiled spring used for measurement of the stress placed on each spindle.

The DV-E viscometer measures the resistance to flow of a fluid substance. With a spindle attached to the main body of the viscometer, it is submerged within the fluid to the submersion mark. The viscometer allows for fine control of the rotational speed of the spindle which, in turn, places stress onto the tightly coiled spring within the main body. The torque placed on this spring is measured and displayed in units of centipoise (cP). By alteration of the revolution speed, and cP measurements at each speed, the rheological properties of a fluid can be characterised and fit to a model.



# Chapter 3

## Resin and Weak Acid Screening Studies

### 3.1 Resin Screening in Citric Acid Media

This chapter contains a modified version of a paper which aims to examine the copper, iron(II), lead and zinc extraction performance of the commercially available resins within citric acid media. Citric acid solutions containing 100ppm copper, iron(II), lead and zinc were contacted with TP214, MTS9100, MTS9570, MTS9301, MTS9501 and C107E. Uptake to each resin was measured as a function of pH in order to determine optimum extraction conditions and the effect solution phase complexation has on the resin extraction. This paper was accepted for publication by the Journal of Ion Exchange on 20/09/2018. DOI: [doi.org/10.5182/jaie.29.53](https://doi.org/10.5182/jaie.29.53)

#### Author Contributions:

- James P. Bezzina - Experimental work, data collection and analysis and manuscript writing
- James T. M. Amphlett - Manuscript review
- Mark D. Ogden - Principal Investigator and manuscript review

### 3.1.1 Introduction

The use of a complexing weak acid as the lixiviant can allow for the higher separation of metals by adsorption, especially when considering metallic ions that have been traditionally difficult to separate (such as rare earth elements)<sup>[118]</sup>. Currently, there is a paucity of data in the literature surrounding the adsorption of metals from weak acid media. Industrial processes tend to focus on extraction from industrial solutions of strong acid media (e.g. HCl, H<sub>2</sub>SO<sub>4</sub> and HNO<sub>3</sub>)<sup>[109,112,115,118,130,131]</sup>. This paper will focus on the extraction of problematic heavy metals (zinc, lead and copper) from buffering regions of weak organic acids utilising ion exchange resins. This paper presents the screening of multiple resins of differing functionalities and the affect pH has on the extraction of metal ions from citric acid buffered media.

### 3.1.2 Experimental

#### Reagents and stock solutions

All chemicals used were of analytical grade or higher and purchased from Sigma-Aldrich unless otherwise specified. Citric acid monohydrate and calcium chloride were purchased from Fisher Scientific. Lewatit MonoPlus TP214 was supplied by Lanxess and all other ion exchange resins were supplied by Purolite. Resin characteristics are outlined within Table 3.1 and functional groups of the resins screened are given in Fig. 3.1. Resins were preconditioned with 10 bed volumes 1 M H<sub>2</sub>SO<sub>4</sub> on an orbital shaker overnight, then washed 5 times with 10 bed volumes of deionised water, then stored in deionised water.



**Table 3.1:** Physical and chemical characteristics of the resins tested throughout this study, as obtained from suppliers information data sheets (PS = polystyrene, PA = polyacrylic, DVB = divinylbenzene).

Name	Functionality	Matrix	Ionic form as shipped	Physical form	Capacity	Size ( $\mu\text{m}$ )	Water retention (wt. %)	Specific Gravity
Lewatit MonoPlus TP214	Thiourea	PS-DVB	Free base	Spherical beads	1.0 eq/L	550	43 - 48	1.1
Purolite MTS9100	Amidoxime	PA-DVB	Free base	Spherical beads	40 g/L $\text{Cu}^{2+}$	300 - 1200	52 - 60	1.19
Purolite MTS9570	Phosphonic + sulphonic	PA-DVB	$\text{H}^+$	Spherical beads	18 g/L $\text{Fe}^{3+}$	550 - 750	55 - 70	1.19
Purolite MTS9301	Iminodiacetic	PS-DVB	$\text{Na}^+$	Spherical beads	50 g/L $\text{Cu}^{2+}$	425 - 1000	52 - 60	1.18
Purolite MTS9501	Aminophosphonic	PS-DVB	$\text{Na}^+$	Spherical beads	24 g/L $\text{Ca}^{2+}$	425 - 850	55 - 65	1.13
Purolite C107E	Carboxylic	PA-DVB	$\text{H}^+$	Spherical beads	3.6 eq/L	300 - 1600	53 - 58	1.17

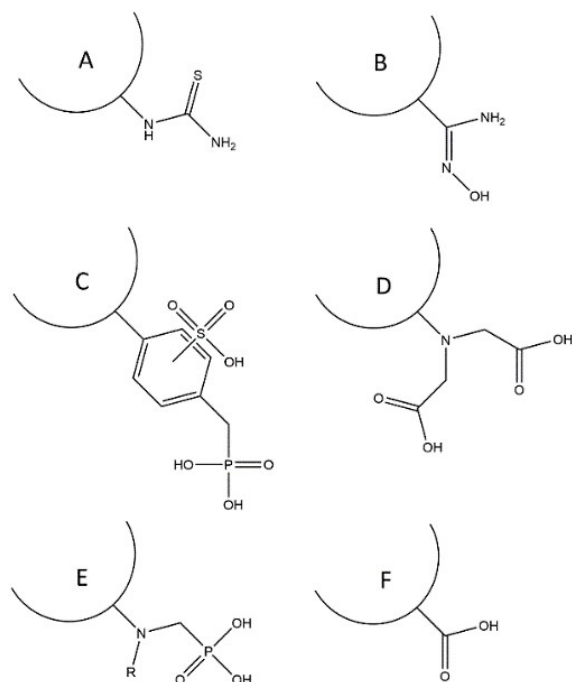


**Figure 3.1:** Chemical structure of the functionalities of the ion exchange resins tested throughout this study (A = TP 214, B = MTS9100, C = MTS9570, D = MTS9301, E = MTS9501, F = C107E; semicircles represent the matrix).

Calcium, copper, iron(II) and zinc were added by dissolution of the respective chloride salt,  $\text{Pb}^{2+}_{(\text{aq})}$  was generated using the nitrate salt due to the solubility, into deionised water (18  $\text{M}\Omega$ ). Metal concentrations were measured utilising a Perkin Elmer Atomic Absorption Spectrometer AAnalyst 400. Calibration of the instrument was performed by standard solutions diluted with 1% nitric acid.

### Batch extractions from buffered media

Pre-contact solutions were adjusted to pH 1 below  $\text{p}K_{\text{a}1}$  and pH 1 above  $\text{p}K_{\text{a}3}$  of citric acid, displayed in Fig. 3.2. Metal containing solutions (50 mL, 100 ppm  $\text{M}^{2+}$ , 0.5 M  $\text{Cl}^-$ , 0.5 M Citric acid) were contacted with resins (2 mL<sub>swr</sub> overnight with agitation by orbital shaker. Metal uptake by the resin was determined by a difference between post- and pre-contact solution concentrations. The extraction percentage (E%) was calculated using the equation:

$$E\% = \frac{C_i - C_e}{C_i} \times 100 \quad (3.1)$$

where  $C_i$  is the concentration of the solution pre-contact and  $C_e$  is the concentration of the solution at equilibrium. Measurements of pH were conducted using a Ag/AgCl reference electrode calibrated from pH 2-10 using standard buffer solutions. Error margins were calculated by triplicate measurement of the initial working solutions prior to pH adjustment.

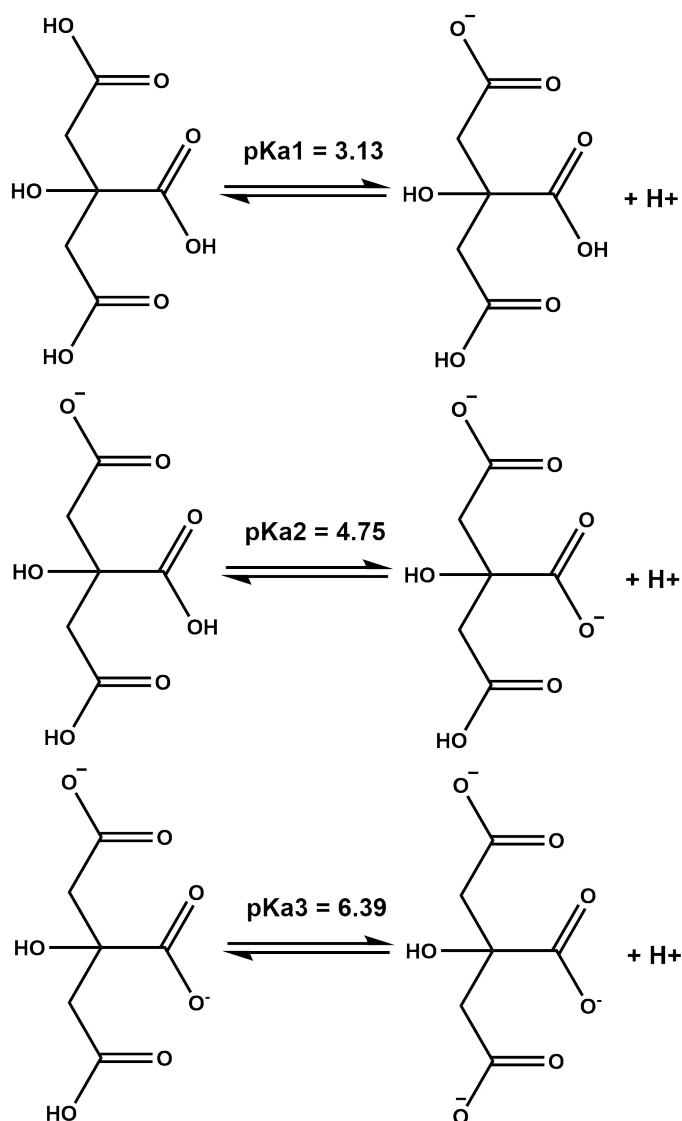
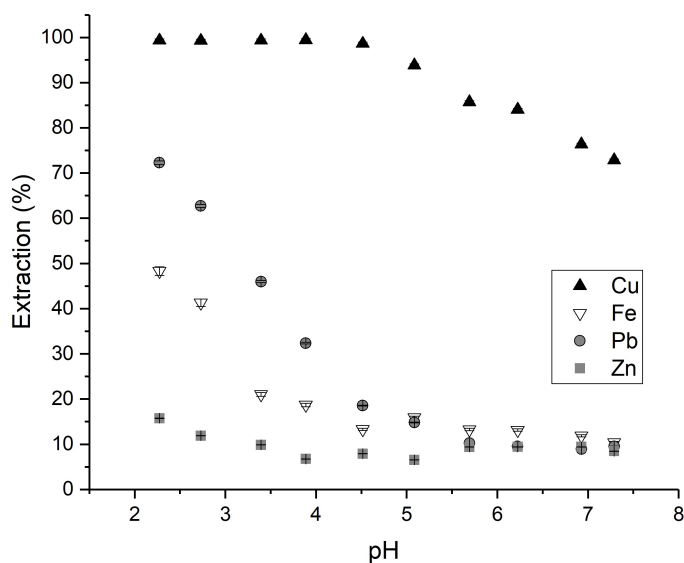


**Figure 3.2:** Reaction schematics of the three deprotonations of citric acid.

### 3.1.3 Results

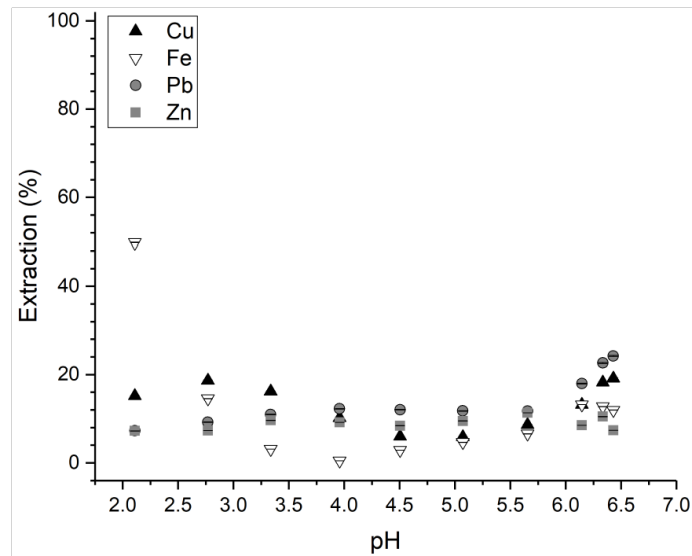
The extraction of common problematic heavy metals from solutions buffered by citric acid was measured at a pH range spanning over the buffering region of the acid. Figure 2 displays the extraction of copper, iron, lead and zinc from citric

acid solutions by TP214 (Fig. 3.3), MTS9100 (Fig. 3.4), MTS9570 (Fig. 3.5), MTS9301 (Fig. 3.6), MTS9501 (Fig. 3.7) and C107E (Fig. 3.8) as a function of pH. Generally copper or iron were observed to be extracted most effectively over the pH range studied.



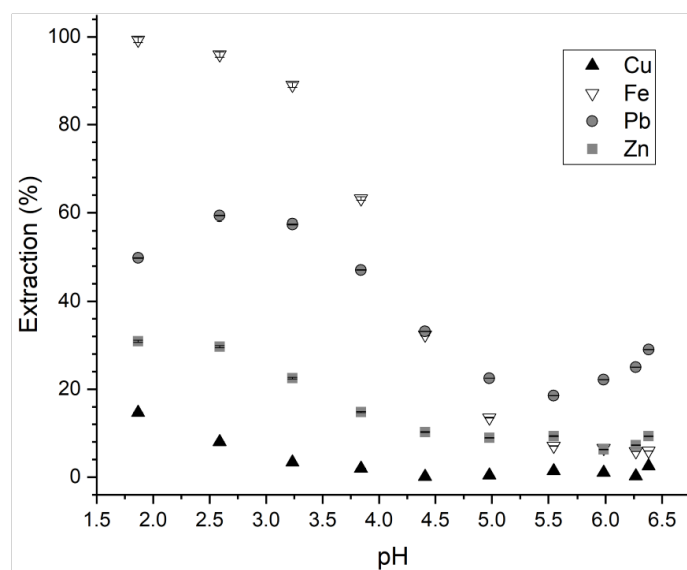
**Figure 3.3:** Extraction of metal ions by TP214 as a function of pH. Cu = ▲, Fe = ▽, Pb = ●, Zn = ■.

The extraction of metal ions from citric acid media by the thiourea functionalised resin TP214 as a function of pH is displayed in Fig. 3.3. Copper is extracted very effectively, however extraction percentage is reduced as pH increased above 4.5. Lead, iron and zinc extraction decreases with increasing pH. Throughout the pH range examined, the order of affinity of this resin may be defined as  $\text{Cu} \gg \text{Pb} > \text{Fe} > \text{Zn}$ .



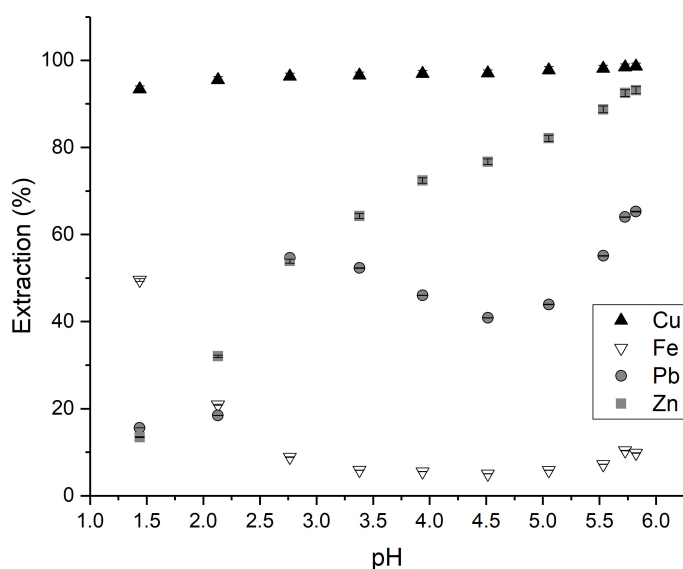
**Figure 3.4:** Extraction of metal ions by MTS9100 as a function of pH. Cu = ▲, Fe = ▽, Pb = ●, Zn = ■.

Fig. 3.4 displays the pH dependence of the extraction of  $\text{Cu}^{2+}$ ,  $\text{Fe}^{2+}$ ,  $\text{Pb}^{2+}$  and  $\text{Zn}^{2+}$  by MTS9100 from citric acid media. While at pH  $\sim 2.0$  the extraction of iron is  $\sim 50\%$ , this decreases dramatically as pH increases. Extraction remains under  $\sim 20\text{-}30\%$  for all other metals across the pH range studied. Extraction of both copper and lead increases towards a pH of 6.5, reaching  $\sim 30\%$ .



**Figure 3.5:** Extraction of metal ions by MTS9570 as a function of pH. Cu = ▲, Fe = ▽, Pb = ●, Zn = ■.

The pH dependence of the extraction of metals by MTS9570 in citrate media is displayed in Fig. 3.5. At lower pH (<3), MTS9570 displays a high affinity for iron, extracting almost 100% from solution, followed by lead, with ~60% extraction. The extraction of these metals decreases with increasing pH, however, iron, zinc and copper display a negligible extraction above pH 5.5. Conversely, lead displays an increasing trend in extraction beyond pH 5.5. At the lower pH range examined the order of affinity of metals is Fe >> Pb > Zn > Cu, with this becoming Pb >> Zn > Fe > Cu at higher pH.



**Figure 3.6:** Extraction of metal ions by MTS9301 as a function of pH. Cu = ▲, Fe = ▽, Pb = ●, Zn = ■.

Fig. 3.6 shows the extraction of metals by MTS9301 from citric acid media as a function of pH. The iminodiacetic acid functionality of MTS9301 shows a high affinity toward copper throughout the pH range studied. At lower pH, iron shows peak extraction at ~50%, this decreasing with an increase in pH, which is the opposite to that of zinc. Lead begins with a low extraction, then increases to ~55% at a pH of ~2.75, this then decreases to a trough at pH 4.5 before increasing again to ~65% at pH ~6. MTS9301 is, by far, the best extractant for zinc, with around 95% extraction towards the higher pH examined. The low pH affinity of this resin is Cu >> Fe >> Zn = Pb, which becomes Cu > Zn >> Pb

>> Fe towards the higher pH of the range tested.

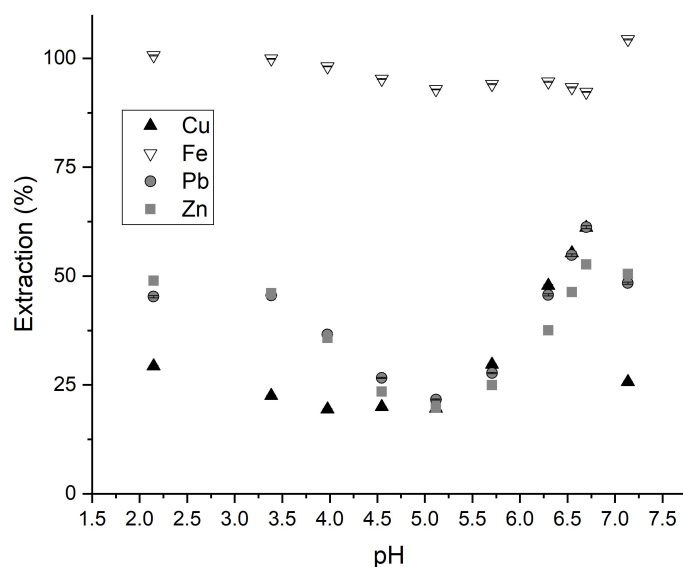


**Figure 3.7:** Extraction of metal ions by MTS9501 as a function of pH. Cu = ▲, Fe = ▽, Pb = ●, Zn = ■.

MTS9501 displays a high affinity for iron from citric acid media, as observed in the plot of metal extraction as a function of pH in Fig. 3.7. At lower pH, copper is the least extracted metal, while as pH increases lead and zinc fall in extraction to ~25% at pH ~5.0. Extraction of copper, zinc and lead is increased to ~60% at around a pH 6.5 before decreasing again at pH 7.0. The low pH order of affinity is Fe >> Zn > Pb > Cu, however as pH nears 7 this becomes Fe >> Pb = Cu > Zn.

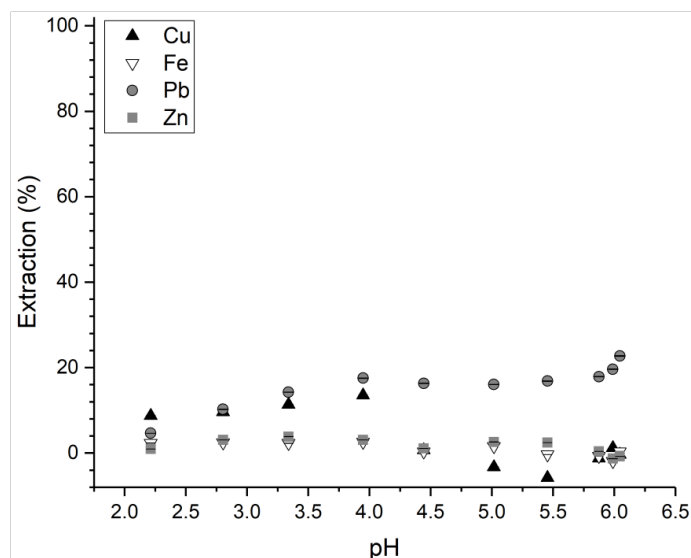


**Figure 3.8:** Extraction of metal ions by C107E as a function of pH. Cu = ▲, Fe = ▽, Pb = ●, Zn = ■.

The carboxylic acid functionalised resin, C107E, is the least effective resin tested for extraction of metals from citric acid buffered media (Fig. 3.8). Lead, in a similar fashion to that of the extraction by MTS9570, MTS9301 and MTS9501 increases in extraction until pH  $\sim$ 4.0 at what point it plateaus before beginning to increase from pH  $\sim$ 6.0. Copper initially follows the same trend, until pH  $\sim$ 4.5, where extraction decreases to a negligible amount. This resin within the pH range tested for citric acid media does not take up either zinc or iron.

### 3.1.4 Discussion

#### Extraction of copper

In the present study copper is taken up most efficiently by thiourea and iminodiacetic acid functionalities. The thiourea functionalised resin shows suppression of copper recovery above pH 5, which aligns with  $pK_{a2}$  of citric acid (pH 4.75). This decrease in copper extraction towards the higher pH studied can be explained by the higher complexation of coppercitrate between pH 5 and 6<sup>[132]</sup>, stabilising copper within solution. The iminodiacetic acid functionality binds to copper consistently across all tested pH within citric acid with a slight dip



in extraction towards lower pH. The affinity for copper by MTS9301 has also been reported elsewhere at  $\text{pH} < 2$ <sup>[130]</sup>, however within the previous studies iron is extracted in comparable amounts. The high selectivity of iminodiacetic acid functionalities for copper has also been reported by Mendes and Martins<sup>[115]</sup> as well as Edeballi and Pehlivan<sup>[109]</sup>, who also reports a high selectivity of bis-picolylamine functionalities for copper.

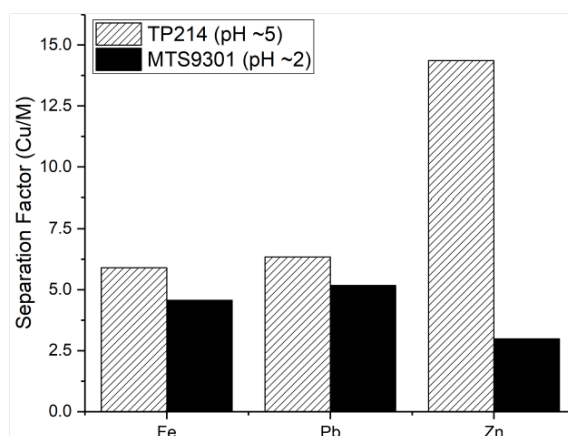


**Figure 3.9:** Separation factors of copper from other metals present within solution by both TP214 and MTS9301.

Both functionalities display similar separations from metals at their optimum pH values for copper recovery (5 and 2 respectively for TP214 and MTS9301), displayed in Fig. 3.9. Both the separation of Fe and Pb are almost identical for both MTS9301 and TP214. The rejection of Zn by TP214 is far more prominent, with a separation factor over four times that of the iminodiacetic functionalised resin.

### Extraction of iron

Both MTS9570 and MTS9501 are efficient extractors of iron, being due to both having phosphonic acid functionalities attached to the resin. (See Fig. 3.10.) Riley et al. has also reported the affinity of phosphonic acid functionalised resins towards iron<sup>[130]</sup>. This previous study, however, measured extraction in sulphuric acid media at a maximum pH of 2. The composite functionality of MTS9570 does

not compete with a dissociated citrate anion for metal binding, while the pure aminophosphonic functionalised resin, MTS9501 maintains the high iron affinity.

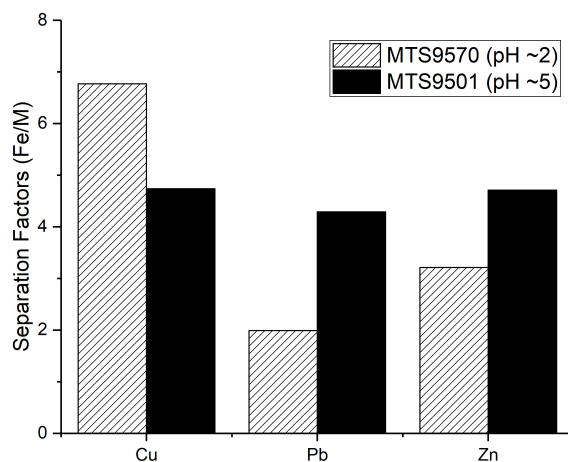


**Figure 3.10:** Separation factors of iron from other metals present within solution by both MTS9570 and MTS9501.

The highest extraction for iron over all other metals studied by MTS9570 is at a pH of  $\sim 1.75$ , which is also where the affinity of other metals is at the peak. The high extraction of iron by MTS9501 throughout all pH values screened allows for selective separation of iron as the extraction of other metals is suppressed to a maximum of  $<25\%$  at a pH of  $\sim 5$ .

### Extraction of lead

The observed general trend for lead recovery is that it is extracted less effectively than copper and iron. This being the case, however, TP214 and MTS9570 do show promising pH dependant recovery of lead. These resins show lead as the metal with the second highest extraction affinity.

While alone there may not be effective separation of lead from other metals, there is the potential to utilise resins sequentially to minimise co-extraction of iron and copper by selectively removing them from solution first. Both TP214 and MTS9570 are reported to have a peak lead extraction at pH  $\sim 2.5$ . The separation factors of lead from other metals by TP214, is much higher at this pH, while

MTS9570 maintains a high affinity for iron (represented in the separation factors presented in Fig. 3.11).

With an increased pH, MTS9570 is able to successfully reject other metals and increase extraction of lead (to a maximum of  $\sim 35\%$  extraction at pH  $\sim 6.5$ ). The iminodiacetic acid functionality is also able to extract lead to a high degree. At a pH of  $\sim 5.5$ ,  $\sim 60\%$  of the lead has been extracted, however at this same pH  $\sim 95\%$  of the copper and  $\sim 90\%$  of the zinc is extracted as well.

Octylamino pyridine ligands have been used to successfully and selectively extract lead from an aqueous succinate solution containing multiple other heavy metal contaminants<sup>[133]</sup>. This study had reported that lead extraction increases from  $\sim 20\%$  to almost 100% beyond a pH of  $\sim 8$ , which could potentially describe the increase in lead extraction towards the higher pH range examined within this study. While no entirely selective functionality was determined throughout this screening study, perhaps an aromatic nitrogen, and aliphatic chain functionality could potentially increase selectivity towards lead.

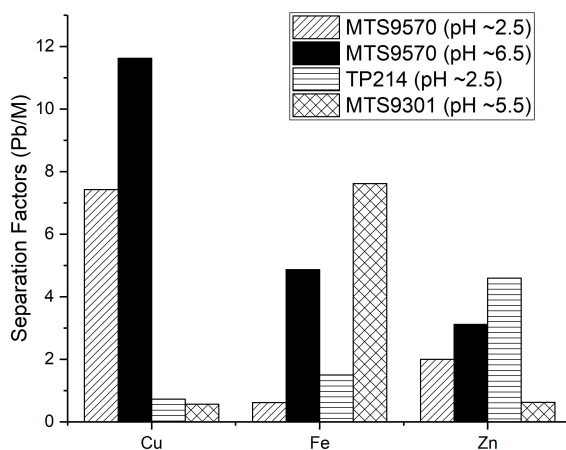


**Figure 3.11:** Separation factors of lead from other metals present within solution by MTS9570, TP214 and MTS9301.

### Extraction of zinc

Of the resins examined, only MTS9301 seems suitable for the extraction of zinc. Towards pH 6, MTS9301 reaches zinc extractions of  $\sim 90\%$ . With a lower concentration of copper within solution of citrate media, MTS9301 could be an effective extractant for zinc. While MTS9501 is the next most effective, the maximum extraction of zinc is only  $\sim 50\%$ , having far less of a recovery than iron in solution. This high affinity of zinc to iminodiacetic acid and amino/amino-acetic acid groups has been observed previously, along with the removal from a highly concentrated solution, lacking dissolved iron species<sup>[134]</sup>.

### Summary

From the results obtained it is clear that the amidoxime and the carboxylic acid functionalised resins are not well suited for extraction of the selected metals from citric acid media. While above  $pK_{a3}$  of citric acid, the extraction of lead begins to increase, beyond this point there is possibility for precipitation of the metals. Aqueous Cu, Fe, Pb and Zn citrate complexes are more stable than those formed by the functionalities on each resin, therefore recoveries are low.

At pH values below the  $pK_{a1}$  of citric acid, the extraction of lead, copper and zinc by MTS9501 decreases. These extractions then increase beyond the  $pK_{a3}$  of citric acid, suggesting a benefit to the complexation of these metals upon extraction by phosphoric acid groups. The extraction of copper, lead and zinc from solution by MTS9570 is likely due to the presence of the phosphonic functional as this behaves similarly to MTS9501.

The iminodiacetic acid functionalised resin displayed a high affinity at copper throughout lower pH values, with the selectivity for lead and zinc increasing with pH. Lead displays a higher affinity for the resin functionality as the citrate ion is deprotonated further, however there is less of an affinity as the citrate ion reaches

$pK_{a3}$ , with extraction again increasing beyond this pH.

### 3.1.5 Conclusion

A pH screening study of the extraction of metals from a simulated citric acid sewage sludge PLS utilising a selection of ion exchange functionalities has been reported. Carboxylic acid and amidoxime functionalised ion exchange resins were found inappropriate for the extraction of Cu, Fe, Pb and Zn from citrate media, across pH  $\sim$ 1.5-6.5. No resin was capable of effectively removing lead or zinc without also extracting large amounts of either copper or iron. While no singular resin functionality was found capable of extracting all of the focus metals, a combination of resins utilised in series could allow for separation of metals and valorisation of this material. The process that one could envision being created using highest concentration (within sewage sludge) and separation factors the removal of metals obtained within this study would be conducted sequentially from iron, copper, zinc then lead.

## 3.2 Resin Screening in Weak Acid Media

This chapter encompasses an altered version of a paper that examines the copper, iron(II), lead and zinc extraction performance of the commercially available resins within acetic and lactic acid system, comparing the results to the reanalysed data of the citric acid system. Following on from this previous weak acid study a screening study was conducted on the commercially available TP214 (thiourea), MTS9100 (amidoxime), MTS9570 (phosphonic/sulphonic acid), MTS9301 (iminodiacetic acid), MTS9501 (aminophosphonic acid) and C107E (carboxylic acid) resins by measuring distribution coefficients at at 10 pH points throughout the buffering region of acetic acid and lactic acid and reanalysing the data attained from citric acid. This data was compared against the thermodynamically modelled solution phase speciation in order to determine the specific effect each complex can have on the effectiveness of the functionality of each resin for the purpose of inclusion within a RIP process for the extraction of heavy metals from sewage sludge. This paper was accepted for publication by Water Research on 20/04/2019. DOI: [doi.org/10.1016/j.watres.2019.04.042](https://doi.org/10.1016/j.watres.2019.04.042)

### Author Contributions:

- James P. Bezzina - Experimental work, data collection and analysis and manuscript writing
- Laura R. Ruder - AAS analysis and manuscript review
- Robert Dawson - Manuscript review
- Mark D. Ogden - Principal Investigator and manuscript review

### 3.2.1 Introduction

Following on from the difficulty of extraction of heavy metals from citric acid media, the use of IX resins within complexing weak acid media remains sparsely understood. Ionic strength, aqueous media and pH have all been altered to optimise the extraction capabilities of IX resins<sup>[118,130,135]</sup>. Currently there is a paucity of information upon which a weak acid media extraction process can be based. The focus of this study is on the ability of complexing acid systems to alter metal ion extraction and separation characteristics of IX resins. The work presented in this chapter brings a comprehensive resin functionality screening within three different weak acid media, including an in-depth solution phase speciation analysis, for simulated leachate solutions of weak acid leached sewage sludge. The most promising resins discovered within this study will be continued through further characterisation within future research.

### 3.2.2 Materials and Methods

#### Reagents and stock solutions

The functionalities of the resins tested are given in Figure 3.12. All IX resins were supplied by Purolite, except Lewatit MonoPlus TP214, which was provided by Lanxess. Calcium chloride was purchased from Fisher Scientific, lactic acid (80%) was purchased from Scientific Laboratory Supplies and glacial acetic acid was purchased from VWR. All other chemicals were purchased from Sigma-Aldrich as analytical grade or better unless otherwise specified. All IX resins were preconditioned by treatment with 1 M H<sub>2</sub>SO<sub>4</sub> (10 bed volumes) for 24h, prior to washing with 50 bed volumes of deionised water. The characteristics of the IX resins are given in supplemental Table A.1.

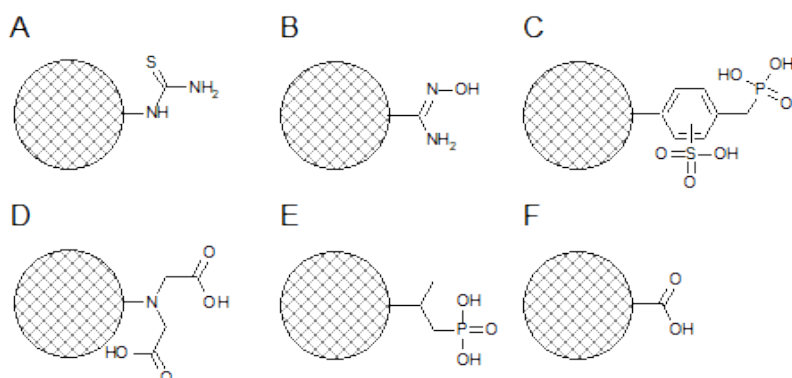


**Figure 3.12:** Chemical structure of the functionalities of the ion exchange resins tested throughout this study (A = TP214, B = MTS9100, C = MTS9570, D = MTS9301, E = MTS9501, F = C107E; semicircles represent the matrix).

### Batch extractions from buffered media

Batch extractions were carried out by contacting 2mL<sub>wsr</sub> with 50mL of mixed metal solution and agitating on an orbital shaker for 24 h at room temperature, after which samples were taken for metal concentration and pH analysis. Mixed metal solutions contained chloride salts of Ca<sup>2+</sup>, Cu<sup>2+</sup>, Fe<sup>2+</sup> and Zn<sup>2+</sup> (100ppm), in addition to Pb(NO<sub>3</sub>)<sub>2</sub> (100ppm Pb<sup>2+</sup>), NaCl (0.5M) and weak acid (0.5M, acetic acid and lactic acid). While Ca<sup>2+</sup> concentration was not analysed, a resin:solution ratio was maintained so that the total metal concentration was far below the saturation of resin functional sites. Acidity was adjusted to a range  $\pm 1$  pH unit either side of the corresponding weak acid's pK<sub>a</sub> (pH 4.76 for acetic acid and pH 3.86 for lactic acid), the approximate buffering region of the acid, using either NaOH or HCl.

Metal extraction was determined by difference using equation (1), where  $V_{aq}$  is the volume of aqueous solution,  $m$  is the mass of resin used in each experiment,  $C_i$  is the concentration of the solution pre-contact and  $C_e$  is the concentration of the solution at equilibrium.

$$K_d = \frac{C_i - C_e}{C_e} \times \frac{V_{aq}}{m} \quad (3.2)$$



Error was calculated through triplicate sampling and analysis of aqueous solutions prior to contact with exchange resins. Samples were diluted with 1% nitric acid (1:10 dilution) and metals analysis was conducted using a Perkin Elmer Atomic Absorption Spectrometer AAnalyst 400. pH measurements were conducted using a Ag/AgCl electrode, calibrated using a four-point calibration with commercially available pH calibration buffers. Citric acid data from the publication<sup>[135]</sup> has been reanalysed to produce  $K_d$  values, for comparison. This data was obtained using the exact same methodology as used for acetic acid and lactic acid, with the pH being adjusted across the three distinct  $pK_a$  values of citric acid.

### Speciation Modelling

To support understanding into the extraction mechanism of metals from weak acid leaching, speciation modelling was carried out using the HySS2008 software suite<sup>[125]</sup>. All complex stability constants attained for the modelling were sourced from the NIST database<sup>[126]</sup> where possible and all hydrolysis product stability constants were sourced from<sup>[136]</sup>. Iron-lactate stability constants were sourced from<sup>[137]</sup> and copper and iron-citrate stability constants were obtained from<sup>[138]</sup>. Tabulation of the stability constants can be found in the supplementary information (Table A.20 - A.28) with speciation diagrams (Supplementary Figures A.1, A.2 and A.3) for acetate, lactate and citrate media, respectively. Stability constants are displayed as  $\log \beta$  values, with all reported literature conditions being 25°C and consistent ionic strength.

Iron oxidation state modelling has been conducted using the Aqion software suite<sup>[139]</sup>. This modelling software is a GUI for the Phreeqc software, and the results are presented in Table A.29.

### 3.2.3 Results

#### Extraction from acetic acid media

Initially, the distribution coefficients ( $K_d$ ) of metal ions from acetic acid by all six resins were screened (Figures 3.13-3.15). While the distribution of iron onto TP214 (Fig. 3.12A) reaches  $>40$ , the high distribution value is only maintained between pH 3.97 and 4.51, outside of this region the  $K_d$  decrease to  $\leq 1$  (Figure 3.13a). Copper is extracted to  $\sim 100\%$ , with the  $K_d$  remaining between 5 and 6 throughout the entire pH range studied. Both zinc and lead maintain distribution values  $<0.5$ . Between the pH region of 3.97 and 4.51, the affinity series remains  $Fe \gg Cu > Pb > Zn$ , however outside of this region the affinity series becomes  $Cu > Fe > Pb > Zn$ .

Data for amidoxime functionalised Purolite MTS9100 (Fig. 3.12B) are shown in Figure 3.13b. Results again show a high affinity for copper from acetate media throughout the studied pH range, with the  $K_d$  increasing exponentially from  $\sim 1$  as pH increases. Zinc and lead show increasing extraction with increasing pH (although  $K_d$  remaining  $<1$ ). The  $K_d$  of iron increases exponentially to a peak of 4.2 at pH 5 before dropping to  $<1$  beyond this. The observed affinity series for MTS9100 towards the studied metals in acetic acid is  $Cu > Fe > Pb > Zn$  between pH 3.55 and 4.83 and  $\geq$  pH 5.25, with iron having the highest affinity at pH 5.06.

Figure 3.14a shows the extraction of metal ions from acetate media by MTS9570 (Fig. 3.12C). The  $K_d$  of iron increases to a peak of 14 at pH 3.75, before dropping to 8 towards the higher pH values. Lead distribution coefficients remained at  $\sim 2$  throughout the entire pH range, while zinc values continue to increase until the highest pH studied. The  $K_d$  of copper remained  $<0.3$  between the studied pH values. At pH  $\geq 3.71$  the observed affinity series is  $Fe \gg Pb > Zn > Cu$ , with  $Zn = Cu$  at pH 2.84. Figure 3.14b presents the extraction of copper, iron, lead and zinc ions from acetate media by iminodiacetic acid (IDA) MTS9301

(Fig. 3.12D) as a function of pH. This resin shows a high affinity toward copper ions, with  $K_d$  values reaching beyond 10. The IDA functionality shows moderately high affinity for the other metals studied, with the  $K_d$  of all metals  $>1$  towards higher pH values, iron peaking at  $\sim 6$  between pH 4.25 and 4.50 and zinc peaking at almost 10 at pH 5.2. At lower pH values, the resin is selective towards copper, with extraction of other metals suppressed. The affinity series at a  $\text{pH} \leq 3.62$  is  $\text{Cu} \gg \text{Zn} = \text{Pb} = \text{Fe}$ . The separation between lead, zinc and iron, changes at pH 5.32 leading to an affinity series of  $\text{Cu} \gg \text{Zn} > \text{Fe} > \text{Pb}$ . However, between pH 3.99 and 4.70 iron has more of an affinity than zinc, and at pH 5.12 lead has greater affinity than iron.

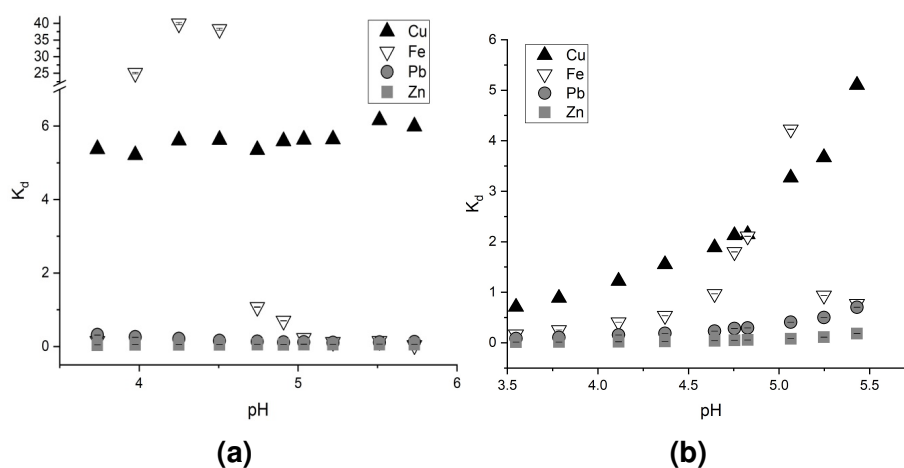


**Figure 3.13:** The distribution of metal ions from acetic acid media by (a) TP214 and (b) MTS9100 as a function of pH at 20 °C after 24hr of contact time.

Distribution coefficients of metals on the aminophosphonic acid functionalised resin MTS9501 (Fig. 3.12E) from acetate media are shown in Figure 3.15a. Copper recovery is constant from acetate media, remaining between 2 and 4. Iron is recovered very effectively from acetate media with this resin, with  $K_d$  values reaching beyond 200, however the  $K_d$  drops below 1 beyond pH 5.5. Lead and zinc affinity increases with pH, with zinc showing a higher affinity than lead for the resin. The Observed affinity at  $\text{pH} < 5.5$  is  $\text{Fe} \gg \text{Cu} \gg \text{Zn} > \text{Pb}$ , however, at the highest pH value tested (5.75) the separation of each metal decreases and the order of extraction becomes  $\text{Cu} \gg \text{Zn} > \text{Fe} > \text{Pb}$ .

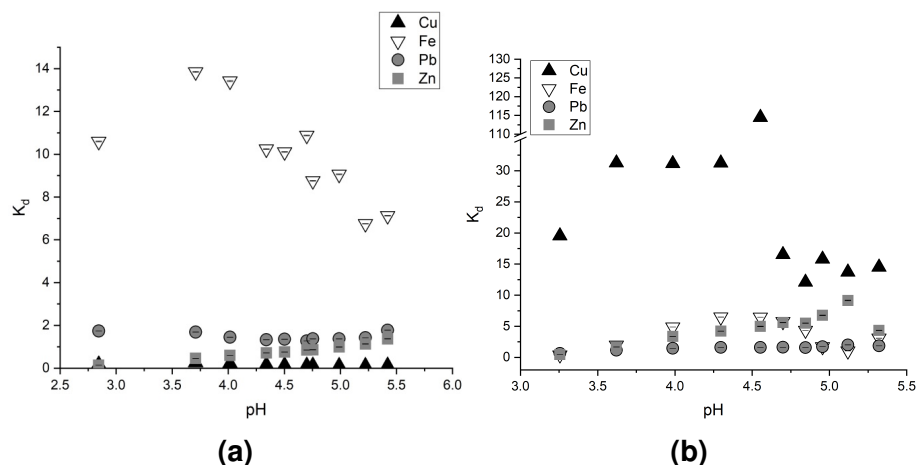


**Figure 3.14:** The distribution of metal ions from acetic acid media by (a) MTS9570 and (b) MTS9301 as a function of pH at 20 °C after 24hr of contact time.

Figure 3.15b shows the pH dependence of metal distribution onto carboxylic acid functionalised C107E (Fig. 3.12F) from an acetate media. At pH <4 in acetate media the observed affinity series for C107E is Fe >>Pb >Cu >>Zn. As pH increases, iron extraction is suppressed, whereas copper, lead and zinc  $K_d$  values increase with increasing pH. At pH ~4.5 the affinity of C107E for iron, lead and copper become roughly similar, with the affinity for zinc overtaking the affinity for iron at pH ~4.8. Above pH 4.8 the affinity of C107E for metals is in the order Cu >Pb >Zn >Fe.

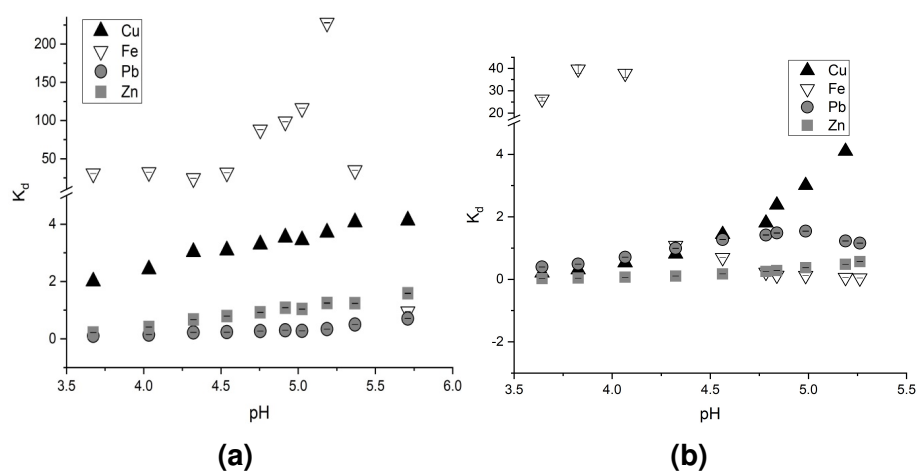


**Figure 3.15:** The distribution of metal ions from acetic acid media by (a) MTS9501 and (b) C107E as a function of pH at 20 °C after 24hr of contact time.

### Extraction from Lactic acid media

Similarly to the results from acetate media TP214 also has a high affinity for copper in lactate media (Figure 3.16a), in this case with  $K_d$  values above 50 throughout all pH values. Lead showed highest distribution at lower lactic acid pH values, with this decreasing as pH increases to around 1 at pH >4.0. Zinc and iron  $K_d$  remained below 0.05 throughout the measured pH range by TP214 in lactate media. The observed affinity series for TP214 within this media was  $\text{Cu} \gg \text{Pb} > \text{Fe} = \text{Zn}$ . MTS9100, was not as effective within lactate media (Figure 3.16b). The only metal to show  $K_d$  values >0.1 from lactate media was lead.

Observed metal extraction behaviour of MTS9570 from lactate media is similar to that observed from acetate media, with the same general trend in affinity  $\text{Fe} > \text{Pb} > \text{Zn} > \text{Cu}$  (Figure 3.17a). Iron  $K_d$  decreased as pH increased, plateauing at pH  $\sim 4.2$ . The lead  $K_d$  values increase to a maximum of 1 at pH 4.0. Copper and zinc extraction within lactate was suppressed with respect to MTS9570, as shown by the low  $K_d$  of both metals. The observed trend in affinity is  $\text{Fe} \gg \text{Pb} > \text{Zn} > \text{Cu}$ , throughout the entire pH range studied.

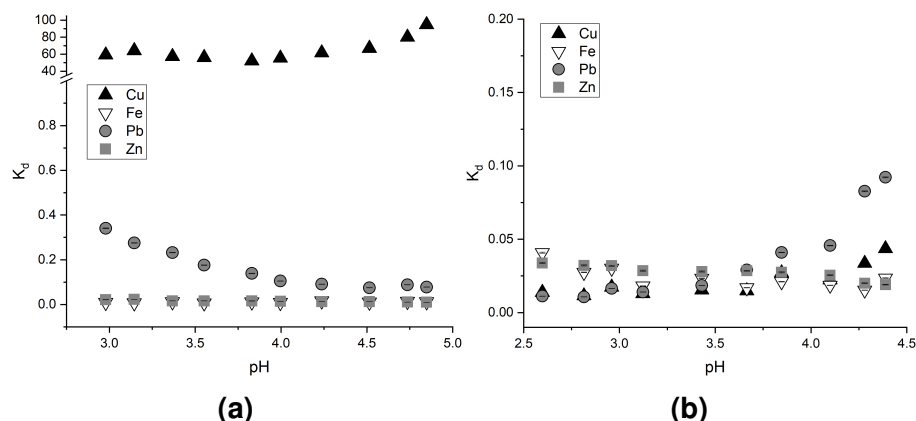


**Figure 3.16:** The distribution of metal ions from lactic acid by (a) TP214 and (b) MTS9100 as a function of pH at 20 °C after 24hr of contact time.

The lactate media displays suppression of metal uptake by MTS9301 in comparison to acetate media, with the copper reaching a  $K_d$  of  $\sim 10$ , while all

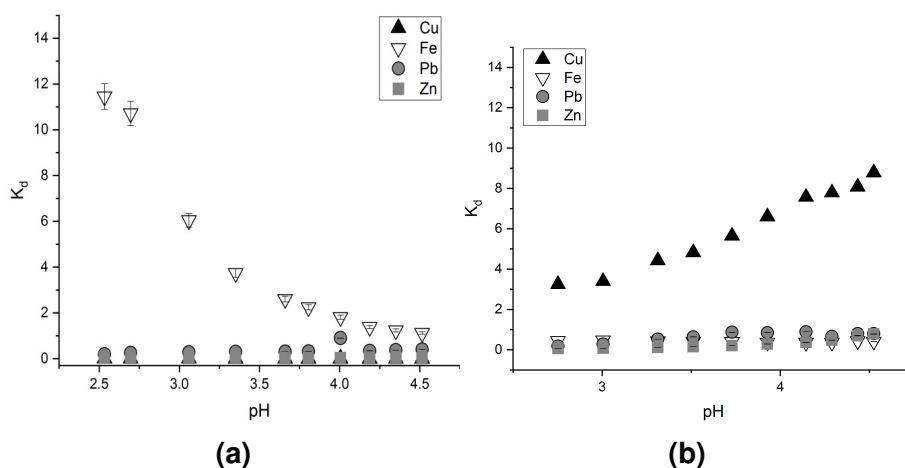


**Figure 3.17:** The distribution of metal ions from lactic acid by (a) MTS9570, (b) MTS9301 as a function of pH at 20 °C after 24hr of contact time.

other metals remain below 1 (Figure 3.17b). The  $K_d$  of lead reaches 0.89, peaking at a pH of 4.14, while zinc peaks at a pH of 4.52 with a  $K_d$  of 0.78. The  $K_d$  of iron remains at  $\sim 0.4$  throughout the entire pH range. While towards the lowest pH values studied (pH  $< 3.31$ ) the trend in affinity was  $\text{Cu} \gg \text{Fe} > \text{Pb} > \text{Zn}$ , at pH 4.52 the trend in affinity was  $\text{Cu} \gg \text{Pb} > \text{Zn} > \text{Fe}$ .

Changing weak acid medium from acetate to lactate increases selectivity of MTS9501 (Figure 3.18a). Iron  $K_d$  values remain between 25 and 50, while copper, lead and zinc remain below 1. As pH increases, copper, lead and zinc  $K_d$  values increase 0.30, 0.73 and 0.24, and an affinity series throughout the entire range studied of  $\text{Fe} \gg \text{Pb} > \text{Cu} = \text{Zn}$ . The weak acid resin, C107E, showed a high affinity and separation for lead within lactic acid media (Figure 3.18b).  $K_d$  values of lead from this media increased to 0.4, while all other metal  $K_d$  values remained below 0.02.

### Extraction from citric acid media

The pH dependence of the  $K_d$  of the metals from citric acid media, reported as extraction percentage in<sup>[135]</sup>, is displayed for each resin studied in Figures 3.19-3.21. Figure 3.19a shows the copper  $K_d$  values for TP214 within citric acid reached a maximum of 17 before decreasing past a pH of 3.88. All other metals

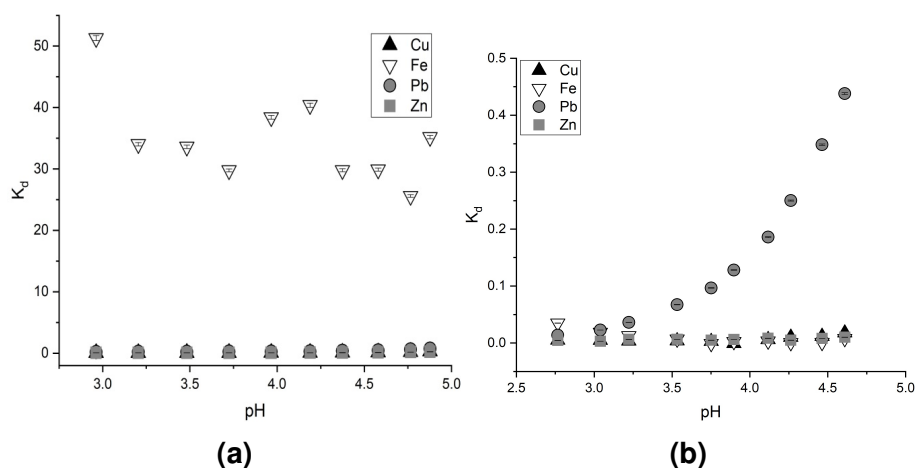


**Figure 3.18:** The distribution of metal ions from lactic acid by (a) MTS9501 and (b) C107E as a function of pH at 20 °C after 24hr of contact time.

studied show  $K_d$  values below 0.02. The affinity trend for TP214 within citrate is  $\text{Cu} \gg \text{Pb} > \text{Fe} > \text{Zn}$  at  $\text{pH} \leq 3.9$ , with lead, iron and zinc reducing the difference in extraction as pH increases. In Figure 3.19b, the plot of  $K_d$  vs pH for MTS9100 in citric acid media shows that there was no appreciable extraction of metal ions by the amidoxime functionality.

The  $K_d$  of metals extracted by MTS9570 as a function of pH within citric acid media is displayed in Figure 3.20a. The initial pH (1.8) shows the resin has a high iron affinity, after which the  $K_d$  exponentially decreases with increasing pH. Copper and zinc show little interaction with MTS9570 in citric acid, with  $K_d$  values remaining below 0.01 for copper and 0.03 for zinc. A maximum  $K_d$  of 0.1 for lead is observed at a pH of 2.5. The affinity trend for extraction of these metals from citrate media is observed to be  $\text{Fe} \gg \text{Pb} > \text{Zn} > \text{Cu}$  at  $\text{pH} \leq 3.8$ , before becoming  $\text{Pb} > \text{Zn} > \text{Fe} > \text{Cu}$  at  $\text{pH} \geq 4.4$ .

The  $K_d$  for copper extraction from citric acid media by MTS9301 (Figure 3.20b) reached a maximum of 5 from a minimum of 1, increasing with respect to pH. All other metals maintain  $K_d$  values at or below 0.1, apart from zinc, which reached a  $K_d$  of  $\sim 1$  by pH 5.8. The trend in affinity at a higher pH ( $\text{pH} \geq 4$ ) can be described as  $\text{Cu} \gg \text{Zn} > \text{Pb} > \text{Fe}$ .

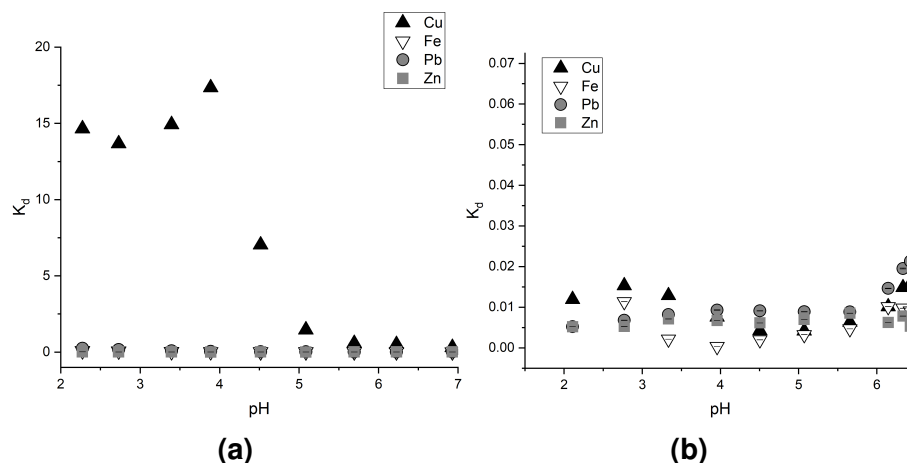


**Figure 3.19:** The distribution of metal ions from citric acid by (a) TP214 and (b) MTS9100 as a function of pH at 20 °C after 24hr of contact time.

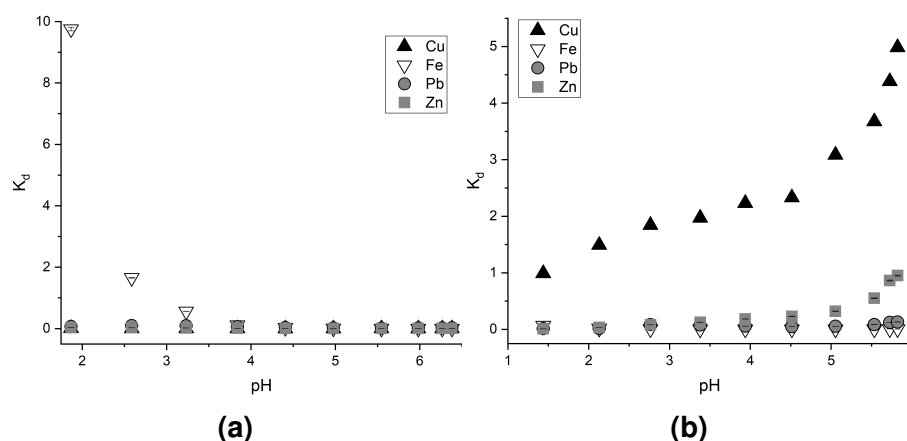


**Figure 3.20:** The distribution of metal ions from citric acid by (a) MTS9570 and (b) MTS9301 as a function of pH at 20 °C after 24hr of contact time.

Figure 3.21a displays the pH dependence of the distribution coefficients of copper, iron, lead and zinc from a citric acid media. At a lower pH there was much higher extraction of iron, with distribution coefficients beginning at 12.5 and peaking at 80, before dropping to  $<1.5$ . The higher pH values ( $\text{pH} \geq 6.7$ ) affinity trend was  $\text{Fe} > \text{Zn} = \text{Pb} = \text{Cu}$ , with separation from copper becoming more apparent as pH decreases to display a trend showing  $\text{Fe} \gg \text{Zn} = \text{Pb} > \text{Cu}$ . All other metals within this media display relatively negligible distribution coefficients ( $<0.15$ ). C107E within the citric acid media (Figure 3.21b) displayed very low distribution coefficients ( $K_d < \sim 0.02$ ), however the extraction of lead, and copper until pH 4.5, showed a relatively large separation from the other metals.



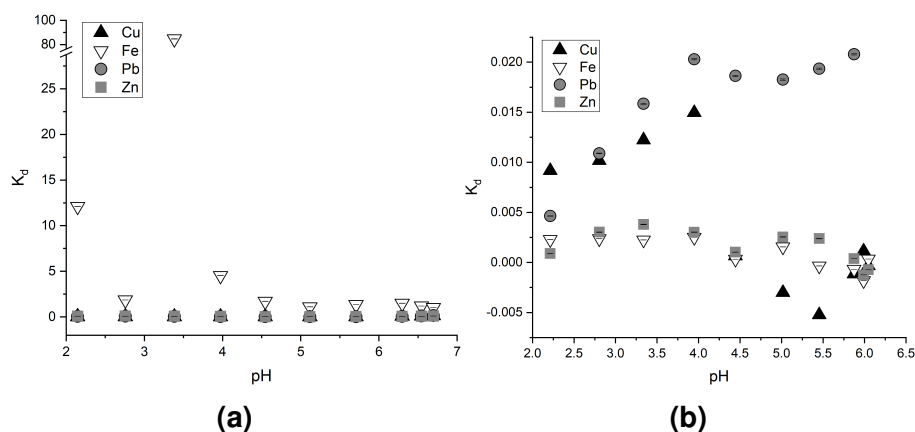
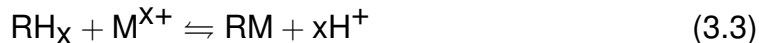


**Figure 3.21:** The distribution coefficients of metal ions from citric acid by (a) MTS9501 and (b) C107E as a function of pH at 20 °C after 24hr of contact time.

### 3.2.4 Discussion

The general IX equation for extraction of metals from solution is given by equation (2);



where a metal ( $\text{M}^{x+}$ ) is exchanged for  $X$  protons ( $\text{H}^+$ ) on the functional group ( $\text{R}$ ). A simplistic interpretation to metal uptake trends could be made by comparing solution speciation in weak acid media with the overall stability constants ( $\log\beta$ ) for a metal binding the aqueous analogue of each functional group. The caveat to this is that no consideration is given to hydrophobic matrix effects of the ion exchange resin.

As the comparison of divalent metal ions within this study includes iron(II), there is likelihood for the oxidation of iron(II) to iron(III). Modelling within studied region displays little concentration of iron(III), however there is precipitation of iron at higher pH within acetate and lactate media (Table A.29), to minimise the effect, fresh solutions were made prior to each experiment.

### Performance of TP214 in weak acid media

Thiourea functionalised TP214 has been previously used for precious metal removal and could be useful in the valorisation of some sewage sludges<sup>[120,140,141]</sup>. However, the moiety displays affinity for copper<sup>[120,142]</sup> potentially reducing effective extraction of precious metals. If complexing weak acids suppress the extraction of copper it could lead to a potential selective removal of precious metals from sewage sludge. The observed strong extraction of copper is due to the generation of copper (I) by the thiourea functional group on TP214<sup>[141–144]</sup>. The extraction is independent of speciation in acetate (Figure A.1a) and lactate media (Figure A.2a), while copper(I) displays high affinities for the thiourea group, above those of the carboxylic acid groups<sup>[126]</sup>. The observed extraction decrease, below pH 4.5, in citrate media correlates to a transition from a charge neutral CuHCit (MHL) species to a negatively charged dimer ( $M_2L_2$ ) and a hydrolysis product ( $MH_{-1}L$ ) complex of copper citrate as pH increases (Figure A.3a).

The high extraction of  $Fe^{2+}$  observed in acetate media is not recorded for lactate and citrate. Within acetic acid we see an initial uptake suppression by proton competition, followed by a transition of the iron species to  $FeAc^+$  (Figure A.1b) preventing uptake at  $pH > 4.5$ , the extraction of iron(II) at lower pH values could be explained by the observation of a thiourea complex ( $Fe(thiourea)_4Cl_2$ ) within chloride media, however little to no data exists on the stability of this complex<sup>[145]</sup>. The extraction suppression of  $Fe^{2+}$  in citrate is due to screening in solution by complexation (Figures A.3b), while the reduction of copper could be causing oxidation of iron and also leading to stabilisation by complexation in lactate media (Figure A.2b).

Lead complexation with lactate is weaker than acetate for the dominant species ( $ML^+$  and  $ML_2$ ) (Tables A.25 and A.24, respectively), explaining the higher extraction in lactate, however both decrease in extraction with increasing neutral

bis- and negative tris-complexation ( $\text{PbLac}_3^-$  being a stronger binding species than  $\text{PbAc}_3^-$ ) (Figure A.1c and A.2c, acetate and lactate, respectively). The complete suppression of extraction in citrate is due to the formation of stable multidentate complexes in solution (Figure A.3c). Zinc extraction is low within all three media. The free  $\text{Zn}^{2+}$  remains close to 10%, even towards the higher pH in acetic acid, while this is zero in lactate (Figure A.2d) and citrate (Figure A.3d), explaining the higher extraction in acetate.

The high stability of copper(I)-thiourea complexes ( $\log\beta$  of 12.3 for ML species, increasing for  $\text{ML}_2$  and  $\text{ML}_3$ ) supports the assumption of copper(II) reduction. Little to no data on iron(II)/(III) stability exists, however a comparison of copper(I) with lead and zinc suggest an affinity for low charge densities<sup>[125]</sup>, leaving copper(I) as the only species displaying higher stability bound to the surface than in solution. The separation factors of copper from other metals ( $\text{Cu } K_d/\text{M } K_d$ ) at the pH of maximum separation is displayed within Figure 3.22 (other separation factors have been tabulated in supporting information Table A.2, A.8 and A.14 for acetic, lactic and citric acid, respectively) with lactic acid providing the largest separation factors. The proposed surface redox reaction of copper is a concern regarding resin regeneration.

### **Performance of MTS9100 in weak acid media**

Within acetic acid, the amidoxime functionalised MTS9100 extraction can be assumed to be dictated by proton concentration mainly. Copper continues the increase in extraction observed from pH 2 in sulphate media<sup>[130]</sup>, with extraction at pH 2.5 being ~30%, then 75% at pH 3.5 in this study.  $\text{Fe}^{2+}$  is the only ion observably affected by speciation beyond pH 5, where a large proportion is  $\text{FeAc}^+$  in solution (Figure A.1b), relating to a decrease in extraction. There is limited information on solution phase iron-amidoxime species, alluding to a stronger binding of the carboxylic species<sup>[126]</sup>.

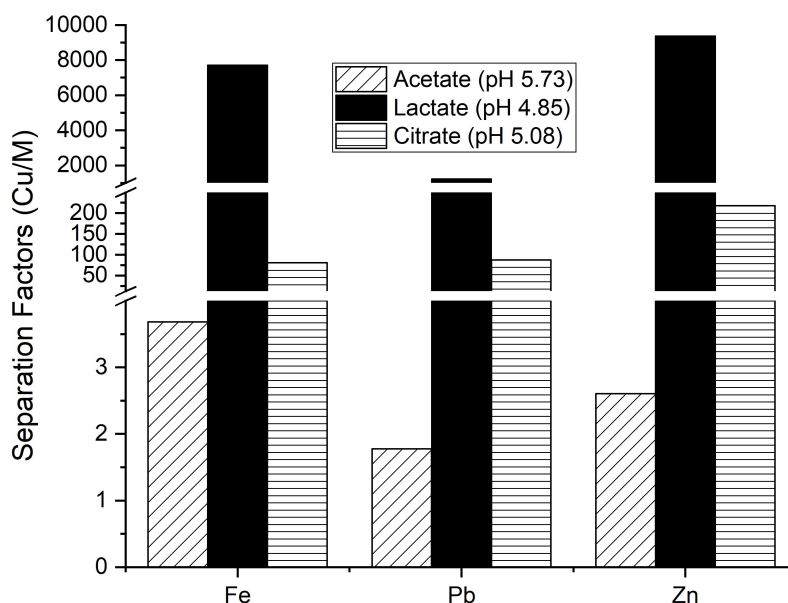


**Figure 3.22:** TP214 separation factors of copper from iron, lead and zinc extracted from acetate, lactate and citrate media at 20 °C after 24hr of contact time.

The distribution of lead and zinc increase with pH, however they do not exceed 0.7 and 0.2, respectively in all media. The extraction of all metals from lactic and citric acid by MTS9100 is greatly hindered, with these media rendering this functionality incapable of effective metals extraction. Neither metal (lead nor zinc) is effectively removed, until higher pH in the case of acetate, from any media.

### Performance of MTS9570 in weak acid media

The phosphonic/sulphonic combined functionality of MTS9570 has been proposed in previous research for the removal of ferric ions from electrolyte copper solutions<sup>[121]</sup>. This copper rejection is also demonstrated within the weak acid media, where the maximum distribution coefficient of all media was 0.25. As with other sources<sup>[130]</sup> and similarly to Diphonix<sup>TM</sup><sup>[146]</sup>, an increase in pH within acetate displayed an increase in extraction, until a peak recorded at pH ~3.75. This peak correlates to a transition between  $\text{Cu}^{2+}$  and  $\text{CuAc}^+$  before suppression by the neutral  $\text{CuAc}_2$  and negatively charged  $\text{CuAc}_3^-$  species (Figure A.1a) within solution. Within both lactic and citric acid, almost complete rejection of copper is observed.

The speciation of iron within acetate solution has no effect on the extraction (Figure A.1b), while both lactic acid and citric acid display decreasing  $K_d$  with increasing pH. In citric acid media, this relates to a transition from free iron species to negatively charged FeCit for iron(II) at pH 3 (Figure A.3b), which is when there is a perceived drop in  $K_d$ , and in lactic acid this relates to the small increase in FeLac<sup>+</sup> from free iron species (Figure A.2b), as this decrease in extraction is only ~5% (roughly the same value as the concentration of the FeLac<sup>+</sup> species).

Lead complexes with lactic acid slightly stronger than acetic acid, reducing distribution coefficients from ~2 throughout all pH ranges for acetic acid, to a maximum of 0.9 within lactic acid, where the major species is the charge neutral PbLac<sub>2</sub> (Figure A.2c). Citric acid, on the other hand, reaches a  $K_d$  of 0.1 at a pH of 2.58, decreasing as both negatively charged PbCit and PbCit<sub>2</sub><sup>4-</sup> species increase in relative concentration (Figure A.3c).

Transitioning from acetic to lactic to citric acid the maximum  $K_d$  reached for zinc is 1.37, 0.03 and 0.03, respectively. Within acetic acid, this maximum extraction is observed at the highest pH studied, when the most abundant species is that of cationic ZnAc<sup>+</sup> (Figure A.3d), however within lactate and citrate media, the transition to either a neutral ZnLac<sub>2</sub> species or ZnHCit species occurs at much lower pH values (Figure A.2d and A.3d, respectively). While sulphate media sees ~100% extraction of zinc at pH > 1<sup>[130]</sup> and the Diphonix resin sees high extraction of zinc at pH > 2 within nitric acid media<sup>[146]</sup>.

Figure 3.23 displays the maximum observed separation factors of iron from copper, lead and zinc from within acetate, lactate and citrate media. The drop in iron extraction from citrate media at the higher pH range studied becomes extremely apparent, with separation factors from all metals dropping substantially from the initially large values; especially true for copper. The

separation factors of iron from lead and zinc are less pronounced than copper (Table A.4, A.10 and A.16, for acetate, lactate and citrate media, respectively), with similarly functionalised resins displaying large extraction capability for zinc in other studies<sup>[130,146]</sup>, and the phosphonic acid group previously displaying effective extraction of lead<sup>[112,123]</sup>.

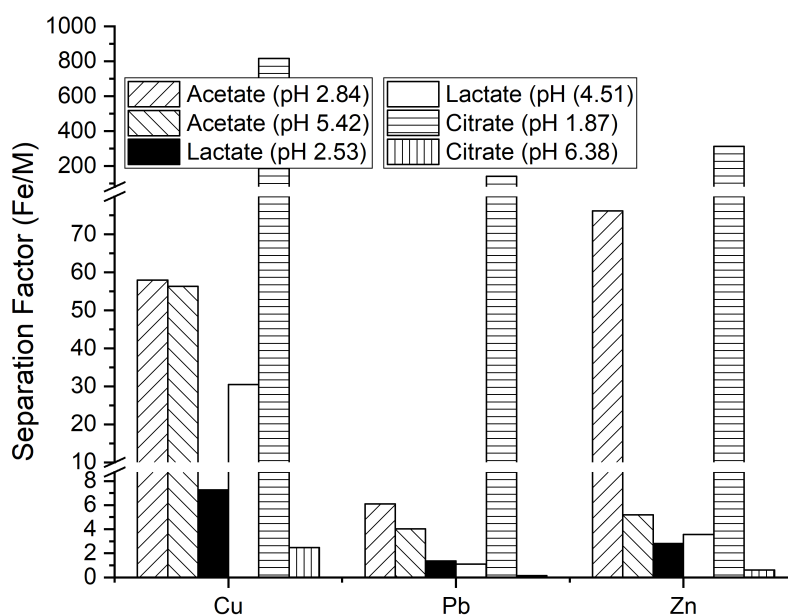


**Figure 3.23:** MTS9570 separation factors of iron from copper, lead and zinc extracted from acetate, lactate and citrate media at 20 °C after 24hr of contact time.

### Performance of MTS9301 in weak acid media

IDA functionalised resins are generally efficient at the extraction of copper, and can also show high affinity toward zinc<sup>[109,122,130,147]</sup>. This functionality could have had the potential to extract high concentrations of copper and zinc that are common within modern sewage treatment plants<sup>[17]</sup>. In accordance with the high affinity of the IDA resin for copper, the  $ML_2$  stability constant trend follows 4 coordinate Z/IR with  $Cu^{2+} > Zn^{2+} > Fe^{2+} > Pb^{2+}$ , with all of the focus IDA-metal stability constants outcompeting predicted carboxylic acid complexes (Tables A.22, A.25 and A.27)<sup>[126]</sup>.

Copper extraction within acetate media maintains  $K_d$  values between 30 and 10, (one outlier at  $\sim 110$ , or an extraction difference of 0.2%), lactic and citric acid media increases from relatively low  $K_d$  values ( $\sim 2$  and 1, respectively) to  $\sim 9$  and 5, respectively. Literature sources show that the extraction of copper by this functionality is generally hindered by competition between copper and protons, which is often found to dramatically reduce extraction after pH 1 [109,122,147], therefore the increase in copper extraction, irrespective of the neutral and anionic solution phase species, is likely due to the lower competition of protons.

Within lactate the extraction of iron remains consistent throughout all pH values, as does the solution speciation (Figure A.2b). The acetate behaviour can be rationalised by a decrease in the competition between iron in solution and protons to a peak extraction at pH 4.5, before a transition between  $\text{Fe}^{2+}$  and  $\text{FeAc}^+$  (Figure A.1b) suppressing extraction, alluding to a bidentate binding mechanism ( $\text{ML}_2 \gg \text{ML}$ ). In both acetate and lactate media, the extraction of iron(II) was  $>85\%$ , showing a similarly high affinity for iron as within strong acid media, with high proton concentration being detrimental to extraction [130,147]. This high affinity is not observed within citric acid, where the  $K_d$  decreases from a low 0.06 to 0.007 as the speciation transitions to 100% iron citrate complexes (Figure A.3b).

Lead reaches a maximum by pH  $\sim 3.25$  in acetate and lactate media, with extraction irrespective of the speciation (Figures A.1c, and A.2c, respectively), a similar pH to that observed by an iminodiacetic acid and carboxylic acid co-functionalised resin [122]. Citrate media, however, shows a peak at pH  $\sim 3$  leading to extraction suppression, corresponding to a peak in anionic  $\text{PbCit}^-$  concentration (Figure A.3b), before extraction again increases beyond the studied region, with an increase in anionic  $\text{Pb}_2\text{Cit}_2^{2-}$  abundance (Figure A.3c).

Acetic acid sees maximum zinc extraction by pH  $\sim 4$ , with 98-99% extraction ( $K_d$  of  $\sim 3.5 - \sim 9$ ), similar to Chelex 100 in nitrate media [147]. Within either acetic

acid or lactic acid, zinc extraction seems to be irrespective of speciation changes (Figures A.1d and A.2d, respectively), with the aqueous IDA-zinc complexes being more stable<sup>[126]</sup>. The formation of  $\text{ZnLac}_2$  and  $\text{ZnLac}_3^-$  complexes reduces the recorded distribution coefficients from  $\sim 5$  at pH 4.5 in acetate media to  $\sim 0.8$  in lactate media (translating to a decrease from 99% to 92% extraction). In citric acid zinc maintains a  $\text{ZnHCit}$  complex (Figure A.1d), further suppressing the extraction of zinc, to  $\sim 0.2$  at pH  $\sim 4.5$  and a maximum of  $\sim 1$  at pH 5.8, where the anionic  $\text{ZnCit}_2^{4-}$  species becomes apparent.

At higher pH ( $>2$ ), the iminodiacetic acid functionality is known to be a great extractor of metals, it is one of the best chelating resins for the extraction of copper and lead from waste water streams<sup>[112,130]</sup>. The selectivity of this resin towards copper becomes apparent when looking at the separation factors for citric acid (Table A.17), in comparison to those of lactate and acetate media (Table A.11 and A.5, respectively), where the resin is far less selective (Figure 3.24). From all media, this resin is shown to be the most selective towards the target metals (copper, lead and zinc) over iron, from lactate and citrate media. Of all the resins tested, this was, overall, the most effective at extraction of metals from solution, maintaining relatively high extraction of all metals from solution from all media tested.

### **Performance of MTS9501 in weak acid media**

The aminophosphonic acid functionalised MTS9501 has been shown to have a high affinity for iron(III) towards a  $\text{H}^+$  concentration through to  $\sim 4\text{M}$ <sup>[130]</sup>, while towards higher pH values, the aminophosphonic acid functional group has a high affinity for all of the focus metals in this study (copper, iron, lead and zinc)<sup>[112]</sup>. Despite this experimental data, there is little information for iron(II)/(III) or lead complexes, however, the high stability constants of aqueous copper and zinc complexes allude to extraction of both hard and soft species<sup>[126]</sup>.



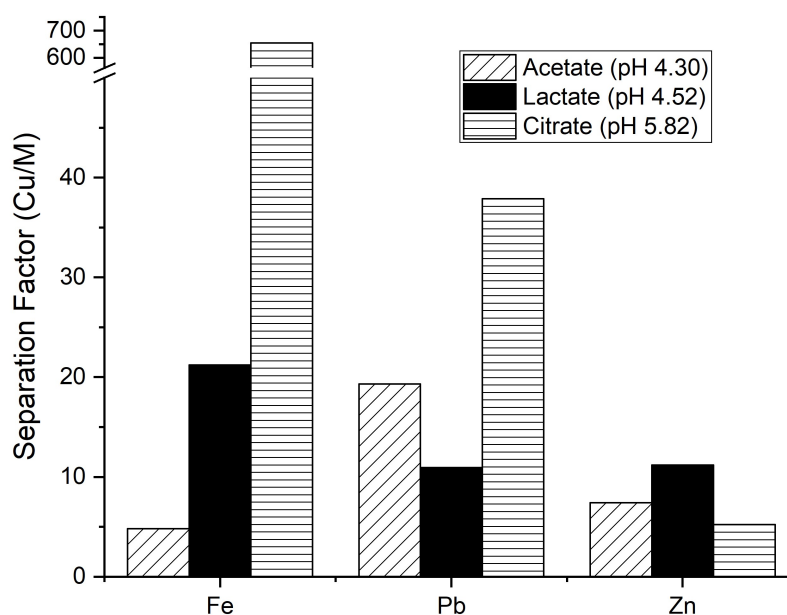


**Figure 3.24:** MTS9301 separation factors of copper from iron, lead and zinc extracted from acetate, lactate and citrate media at 20 °C after 24hr of contact time.

The separation factors (Figure 3.25, Table A.6, A.12 and A.18, for acetate, lactate and citrate, respectively) show that the MTS9501 has a high selectivity for iron. Neither lactate media nor acetate media are a substantial hindrance of the extraction of iron by this functionality. The citrate media, however, was able to reduce the  $K_d$  values to  $<12.5$  (still relatively high), with an outlier at pH 3.4 of 85, with these values decreasing to remain at  $\sim 1$  towards the higher studied pH range, which still translates to an extraction of  $>90\%$ . The extraction efficiency of iron(III) by the industrial equivalent Duolite ES 467 has been shown to decrease beyond pH 2<sup>[123]</sup>, which is contrary to what is observed with iron(II) in this study. However, the use of complexing species within this study could be, to a certain extent, preventing hydrolysis of the iron, and therefore preventing precipitation.

$>99\%$  of copper is removed from solution by the MTS9501 resin functionality within acetate media, displaying  $K_d$  values between 2 and 4, with the extraction increasing with pH. The extraction of copper from lactate media however, is hindered to produce  $K_d$  values  $<0.5$  (the presence of neutral  $\text{CuLac}_2$  or anionic  $\text{CuLac}_3^-$  assumed to be the major contributing factor), while within citrate media

the extraction is restricted even more with a maximum  $K_d$  of 0.13 (with either neutral  $\text{CuHCit}$  or anionic  $\text{Cu}_2\text{Cit}_2^{2-}$  and  $\text{CuOHCit}^{2-}$  stabilising copper in solution). While remaining low, the copper recovery within lactate media increases with an increasing pH, this increase in extraction with a decrease in proton competition has also been observed within strong acid media<sup>[130,148]</sup>, which is similar case to lead and zinc. While the complexation with the acid has hindered extraction of metals by the aminophosphonic functionality, the competition for binding sites between metals and protons has remained one of the driving factors in removal of metals from solution.

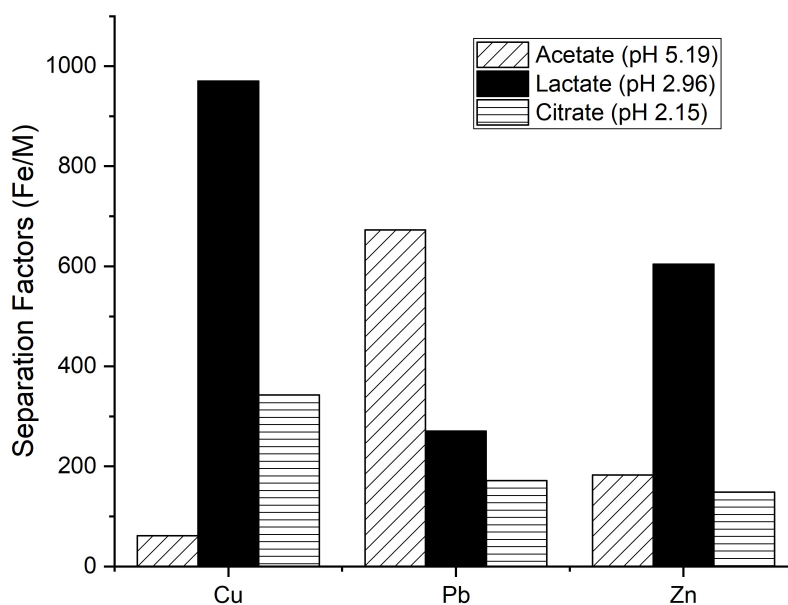


**Figure 3.25:** MTS9501 separation factors of copper from iron, lead and zinc extracted from acetate, lactate and citrate media at 20 °C after 24hr of contact time.

### Performance of C107E in weak acid media

The weak acid resin functionality is a similar structure to the complexing acids, and therefore is assumed to have similar affinities towards the metals. This similarity should allow for a tailored approach to the extraction of the metals, manipulating pH either side of both resin functionality and weak acid species in order to gain the desired extraction. The binding affinity of copper, lead and zinc for the weak acid functionality seem to be higher than for the solution phase

acetate, as their extraction increases beyond the approximate  $pK_a$  of the weak acid resin (assumed to be similar to formic acid, 3.75). While small values, and therefore a very speculative statement, the extraction of copper from citric acid is dictated highly by the complexation (Figure A.3a) in a similar fashion to the thiourea based resin, with the extraction dropping substantially in conjunction with the speciation change of solution phase copper.

Within acetic acid, changing the pH seems to allow for either the selective extraction or rejection of iron, by shifting the pH either side of the acetate  $pK_a$ , this could possibly be due to the higher presence of the  $FeAc^+$  species beyond a pH of 4; in this case, the decrease in concentration is observed beyond the pH where  $Fe^{2+}$  complexes with acetate (Figure A.1b). This is also contrary to what had been observed for ferric ions within a similar media where no  $Fe^{3+}$  had been taken up by the weak acid resin throughout the same pH range<sup>[118]</sup>.

Within lactic acid, all metals are stabilised within the solution, apart from lead, potentially due to the higher ionic radius; allowing the  $Pb^{2+}$  ions to interact with more functional groups on the resin surface. This stabilisation leads to large separation factors for lead from copper, iron and zinc for this media, exceeding 50 (Table A.13). If lead were to be the target metal, a higher pH within lactate media would allow for very selective extraction (assuming low concentrations of metals unstudied).

Linking the functional group to formic acid, once again, the stability constants of these metals with this functional group are relatively low when compared to the largest constants of the other resins<sup>[126]</sup>. The available data shows increasing stability constants with increasing ionic radii (with the exception of copper as the strongest bound species)<sup>[126]</sup>, with zinc displaying the least stable complex of the studied metals. Within both acetate and lactate media, the metals are bound in similar fashion to both the functional group and the complexing acid, as the

singular carboxylic acid unit is present in both. The lactic acid moieties have far higher binding strength than the acetic acid moieties possibly due to a conjugation effect between the  $\beta$  hydroxy group and lactate being a stronger binding ligand, this effect must not be present within the functional groups bound to the resin surface, leaving lactic acid as a far stronger binding species. Again, citric acid being a stronger binding agent than lactic acid (due to the three protonation sites), it has been observed to restrict extraction by this functionality even more than lactic acid.

### 3.2.5 Conclusions

The removal of metals from simulated weak acid sewage sludge leachates have been studied, with promising results. The complexing nature of carboxylic weak acids stabilise metal ions in solutions generating broader functional pH regions for metal extraction. Depending on the metals present in solution, a variety of different combinations of acids and resin functionalities could be used for selective separation processes. While lactate complexes are more stable in solution than acetate, neither of these ligands compared to the stability of citrate complexes. The increased stability in solution could render extraction processes more expensive, as more solid phase extraction stages would be required for removal of the target metals. TP214 has a high affinity for copper, as well as iron in acetate media, and must be taken out prior to a precious metals recovery stage. The amidoxime functionalised resin MTS9100 is rendered ineffective in lactate and citrate media. MTS9570 maintained a high affinity for iron within all media, while decreasing extraction efficiency of copper, lead and zinc within lactate and citrate media. The phosphonic acid functionalised resin MTS9501 is extremely efficient at extracting copper and iron in acetate media, while only iron extraction is maintained in lactate, lead extraction displays little response to the change of buffer. The weak acid functionalised resin selectivity for lead was significantly increased within lactic acid media, with speciation dependent extraction in acetate

media. The MTS9301 IDA functionalised resin displayed the best performance for metals in all media. This resin was especially effective at the removal of metals from an acetic acid media, with high separation of copper. Further investigation is required to understand the kinetics, as well as capacity of the MTS9301 resin within these weak acid systems.



# Chapter 4

## Single Metal Isotherm Studies

This chapter aims to determine the mechanism of extraction and capacity of copper, iron(II), lead and zinc as a continuation of the resin screening study (Section 3.2). An isotherm study was conducted on C107E, MTS9301 and TP214 within acetic acid at pH 4.5. The data was fit to the common two-parameter isotherm models: Langmuir, Freundlich, Temkin and Dubinin-Radushkevich. Mechanistic details and capacities determined by each model has been compared to literature values of analogous strong acid systems, and a review of each model, inclusive of the details each model can provide has been conducted. This will allow for the further characterisation of the behaviour of each resin within a clean simulated sewage sludge acetic acid PLS prior to the increase in complexity of the system. This paper was accepted for publication by Chemical Engineering Journal on 21/03/2020. DOI: 10.1016/j.cej.2020.124862

### Author Contributions:

- James P. Bezzina - Experimental work, data collection and analysis and manuscript writing
- Thomas Robshaw - Manuscript review and model assistance
- Robert Dawson - Manuscript review
- Mark D. Ogden - Principal Investigator and manuscript review

## 4.1 Introduction

The work presented in this chapter follows on from the previous work by attempting to understand the chemistry governing the reported ion exchange behaviour; through isotherm loading experiments within the presence of the complex-forming acetic acid, and as an understanding of resin capacity is required to determine the number of stages required within a completed RIP process, this study is imperative<sup>[89]</sup>. The novelty of this research is derived from a new understanding of the competition between functionality and complexing weak acid, departing from the generally studied strong mineral acid media (HCl, HNO<sub>3</sub> and H<sub>2</sub>SO<sub>4</sub>)<sup>[112]</sup>; adding to the body of literature an analysis of the effect the complexing nature of acetic acid can have on resin capacity and thermodynamic behaviours. This work is, in part, towards the understanding of ion exchange processes proposed for a technique for the removal of base metals from sewage sludge for recycling of both heavy metals and the phosphate within sewage sludge.

## 4.2 Methods

### Reagents and stock solutions

All chemicals used were of analytical grade or higher and purchased from Sigma-Aldrich apart from glacial acetic acid, which was purchased from VWR. MTS9301 (iminodiacetic acid functionality) and C107E (carboxylic acid functionality) were supplied by Purolite, and Lewatit MonoPlus TP214 (thiourea functionality), which was supplied by Lanxess (Table B.1, Figure 4.1). Ion exchange resins were preconditioned to the protonated form by 24hr contact with 1 M H<sub>2</sub>SO<sub>4</sub> (10 bed volumes) prior to washing with 50 bed volumes of deionised water, then stored under deionised water.



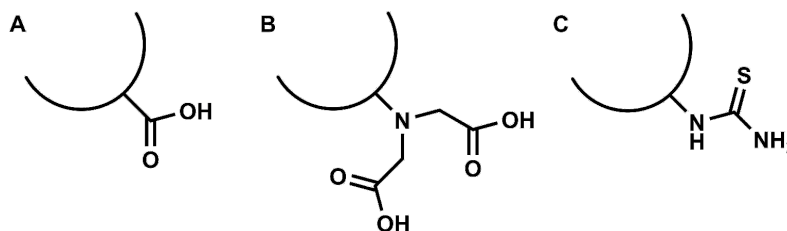


**Figure 4.1:** Chemical structure of the functionalities of the ion exchange resins tested throughout this study (A = C107E, B = MTS9301, C = TP214; semicircles represent the matrix).

## Isotherm Loading Studies

Single metal contacts were conducted by contacting 2mLwsr with 50mL of solution. Experiments were left for 24h to reach equilibrium on an orbital shaker (250 rpm) at 20°C. Single-metal solutions were made up, with concentrations from 50-3000ppm with either the chloride salt of copper, iron(II) and zinc or lead nitrate. Each solution was made to 0.5M acetic acid and 0.5M NaCl in order to lower the impact of varying ionic strength and then adjusted to pH 4.5 using NaOH due to performances within the previous study and the proximity to acetic acid's  $pK_a$ , allowing for dissociation of the acetic acid and complexation of the acetate species. All samples were diluted in 1% nitric acid and analysed using AAS (Perkin Elmer Atomic Absorption Spectrometer), experimental error was calculated as two standard deviations of triplicate measurement of each pre-contact solution. All pH measurements were conducted using a commercially available Ag/AgCl electrode, calibrated using a four-point calibration.

## Speciation Modelling

PHREEQC calculations were conducted using the Aqion interface for PHREEQC modelling software<sup>[139]</sup>. Each model was generated as a single metal and metals were entered into the models as chloride salts. All PHREEQC models had a NaCl concentration of 0.5M, an acetic acid concentration of 0.5M, with an open CO<sub>2</sub> system calculated at 298K. The data generated by this modelling is presented within Figure B.1.

Predominance diagrams were generated using a combination of the HYDRA<sup>[104]</sup> and MEDUSA<sup>[149]</sup> software packages, being a database of logK data (at 25°C) and software to create diagrams, respectively. The data obtained using this software is presented in Figure B.2. To determine effect of metal concentration on solution phase speciation, speciation modelling was carried out using the HySS2008 software suite<sup>[125]</sup>. Speciation was modelled at a metal concentration of 50-3000ppm, with the resultant speciation diagrams displayed in Figure B.3. All complex stability constants attained for the modelling were sourced from Bezzina, et al. (2019)<sup>[119]</sup>.

## 4.3 Results

### C107E

Plots of collected isotherm data for the extraction of  $\text{Cu}^{2+}$ ,  $\text{Fe}^{2+}$ ,  $\text{Pb}^{2+}$  and  $\text{Zn}^{2+}$  from acetic acid solutions using C107E are displayed in Figure 4.2. The initial slope of the isotherm for each metal is extremely gradual, bar  $\text{Fe}^{2+}$ .  $\text{Pb}^{2+}$  and  $\text{Zn}^{2+}$  were not seen to reach their experimental maximum loading capacities ( $q_{max}$ ) under the experimental conditions, whereas  $\text{Cu}^{2+}$  and  $\text{Fe}^{2+}$  were. The experimentally observed  $q_{max}$  values for  $\text{Cu}^{2+}$  and  $\text{Fe}^{2+}$  were 0.004 and 0.002mol g<sup>-1</sup>, respectively.

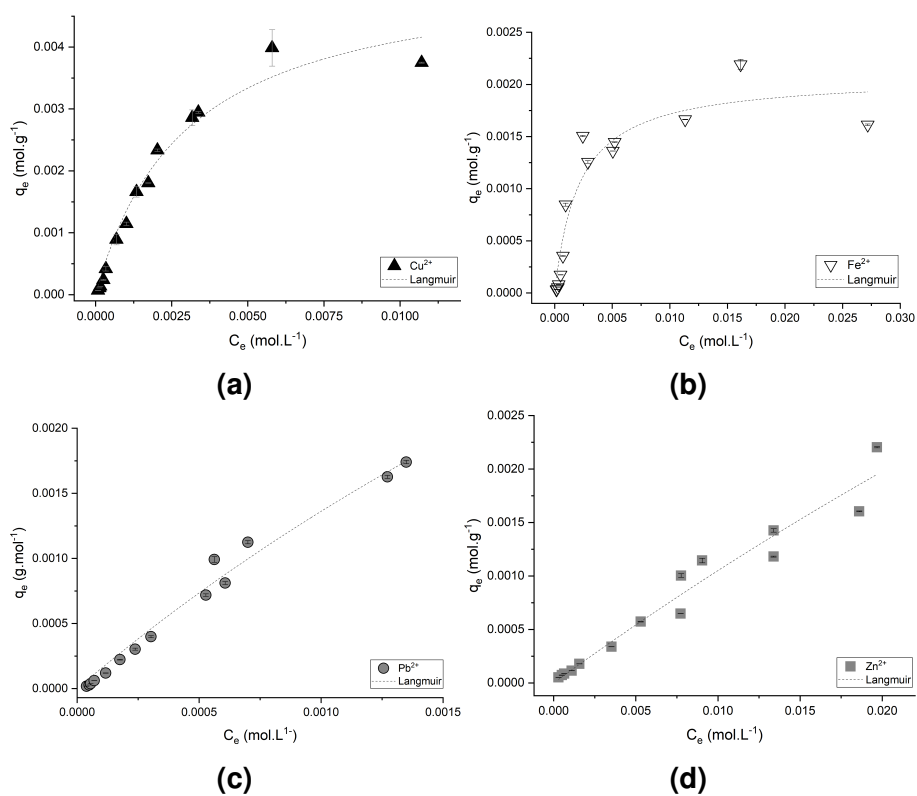


**Figure 4.2:** Concentration dependent extraction of copper (a), iron (b), lead (c) and zinc (d) by C107E in acetic acid media (initial concentrations 25-3000ppm; temperature 20°C; 0.5M NaCl; 0.5M acetic acid; 2ml wet settled resin; 50ml solution). The dashed lines in each figure represent the Langmuir model (described later) fitted to the data.

## MTS9301

Plots of collected isotherm data for the extraction of  $\text{Cu}^{2+}$ ,  $\text{Fe}^{2+}$ ,  $\text{Pb}^{2+}$  and  $\text{Zn}^{2+}$  from acetic acid solutions using MTS9301 are displayed in Figure 4.3. The initial slopes for each metal are much steeper than those observed for C107E, with lead displaying a much less sharp initial slope than the other metals. In this case, both copper and zinc reach an adsorption of  $\sim 0.004 \text{ mol g}^{-1}$ , however copper reaches this with an equilibrium solution concentration of  $\sim 0.002 \text{ M}$ , whereas zinc saturates the resin at a  $C_e$  five times higher at  $\sim 0.010 \text{ M}$ . Experimentally, both lead and iron(II) reach a similar experimental maximum, both reaching  $\sim 0.002 \text{ mol g}^{-1}$ , however iron(II) reaches this with a much lower equilibrium solution concentration, and the sorption of lead seems to continue to increase beyond the range of the isotherm.

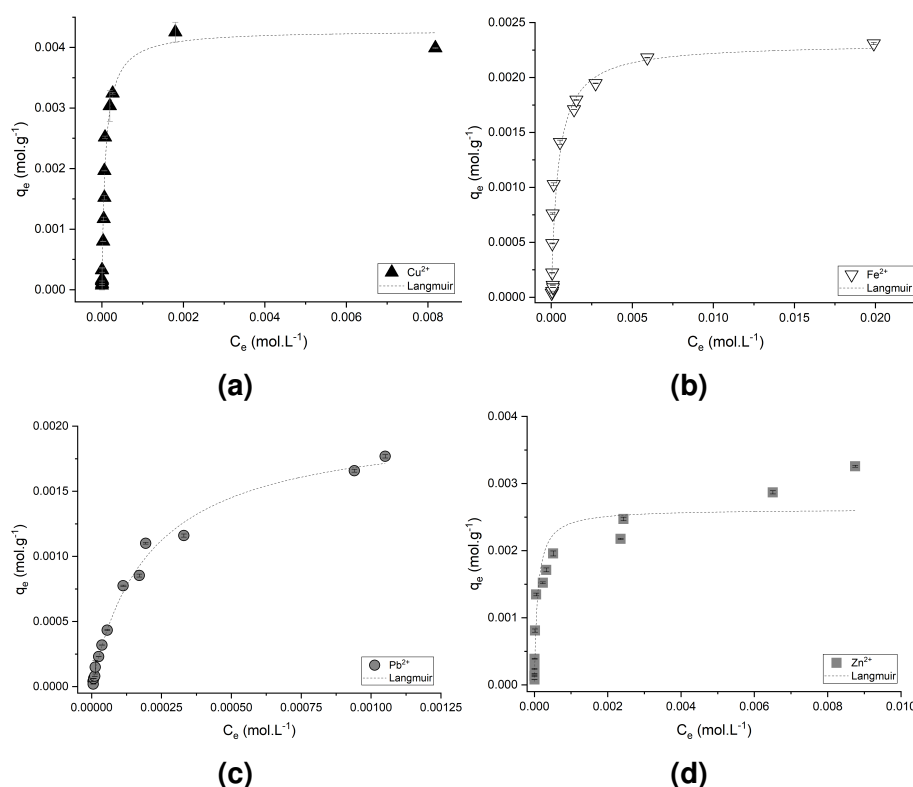


**Figure 4.3:** Concentration dependent extraction of copper (a), iron (b), lead (c) and zinc (d) of MTS9301 in acetic acid media (initial concentrations 25-3000ppm; temperature  $20^\circ\text{C}$ ;  $0.5 \text{ M NaCl}$ ;  $0.5 \text{ M acetic acid}$ ;  $2 \text{ ml wet settled resin}$ ;  $50 \text{ ml solution}$ ). The dashed lines in each figure represent the Langmuir model (described later) fitted to the data.

## TP214

Figure 4.4 displays the single metal isotherms of the adsorption of copper, iron(II), lead and zinc to the surface of the thiourea based TP214 resin. In this case copper displays the largest experimental maximum adsorption, with  $\sim 0.002 \text{ mol g}^{-1}$ , while all other metals remain  $< 0.001 \text{ mol g}^{-1}$ . This high maximum is also accompanied by a more definite plateau, while iron(II), lead and zinc maximums are reached either more gradually, or seemingly not at all.

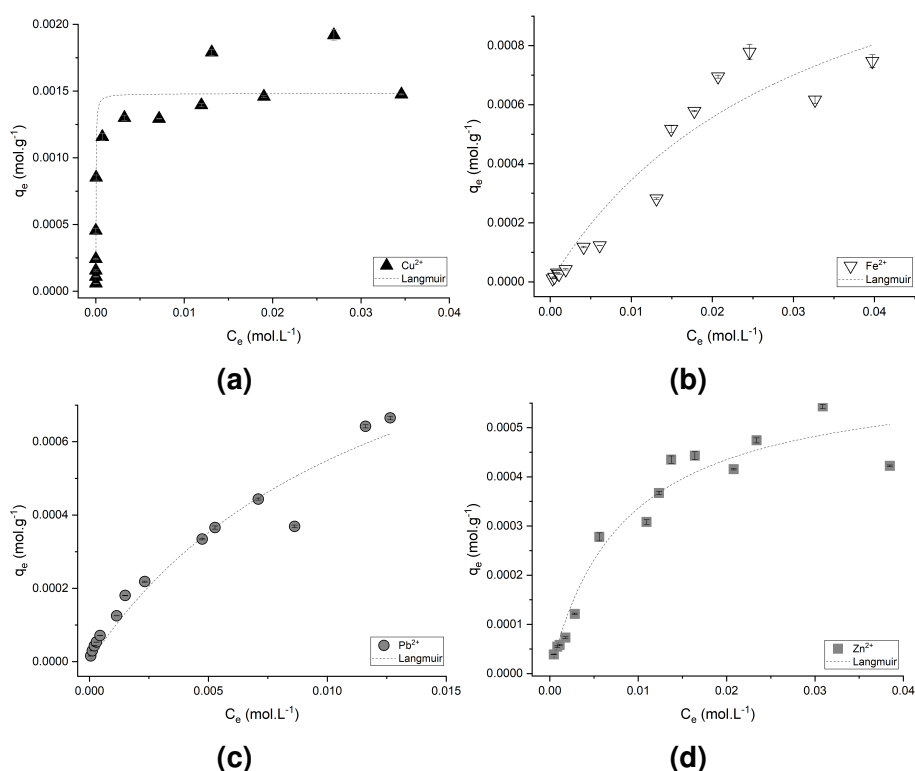


**Figure 4.4:** Concentration dependent extraction of copper (a), iron (b), lead (c) and zinc (d) TP214 in acetic acid media (initial concentrations 25-3000ppm; temperature  $20^\circ\text{C}$ ; 0.5M NaCl; 0.5M acetic acid; 2ml wet settled resin; 50ml solution). The dashed lines in each figure represent the Langmuir model (described later) fitted to the data.

## 4.4 Discussion

In all instances, excessive weak acid has been used in order to determine the effect, if any, that the presence of the complex forming acetate anion has on isotherm performance on each resin. The initial slopes of the isotherms for

the carboxylic acid (WA) functionality are extremely gentle, alluding to a weaker interaction between this carboxylic acid functionality and the metallic ions. This becomes of interest due to the similarity between the functionality on the resin and the complexing acetate in solution, creating a competitive equilibrium between the two species. While this is prevalent for the extraction of iron(II), which displays a steep initial slope of the isotherm before a plateau, copper begins to show binding hindrance, while zinc displays behaviour that leads to the assumption of solution stabilisation. Due to solubility restraints regarding lead, saturation was not observed. The behaviour of zinc counters what would be assumed by the low stability constants of zinc acetate species ( $\log\beta$  of 1.79, 2.80 and 3.30 for  $\text{CuAc}^+$ ,  $\text{CuAc}_2$  and  $\text{CuAc}_3^-$ , respectively vs 0.87 and 1 for  $\text{ZnAc}^+$  and  $\text{ZnAc}_2$ , respectively)<sup>[119]</sup>, as the weak acid functionality has a decreasing affinity for protons towards high pH values, which coincides with its capacity for zinc<sup>[150]</sup>.

Contrarily, the initially weak interaction is not observed towards the iminodiacetic acid (IDA) functionality, most likely due to the high strength of the chelation or bidentate binding mechanism between these metals and the functionality. Lead, however does not show such strong adsorption, leading to the assumption of weaker interactions; creating a hypothesis of a different mechanism due to the high ionic radius of lead preventing the chelation. The adsorption isotherms of lead, zinc and iron(II) for the thiourea functionality display the same hindrance seen for the adsorption of lead and zinc to the WA functionality. This is assumed to be due to the weak interactions (inability for ion exchange mechanisms) towards the thiourea functionality, which is further justified by the extremely low experimental  $q_e$  values. The copper isotherm for the thiourea functionality, on the other hand, displays a steep initial slope, indicating extremely strong interaction. This supports the previous observation of a redox reaction between copper and thiourea<sup>[119]</sup>.

### 4.4.1 Isotherm Modelling

This section will describe models used to analyse data related to the extraction capacities and thermodynamic properties of extraction for adsorbents. In each instance, there are the values  $C_e$  (equilibrium solution concentration in M) and  $q_e$  (equilibrium concentration of adsorbed species in  $\text{mol g}^{-1}$ ),  $T$  is the temperature in Kelvin and  $R$  is the universal gas constant ( $\text{J} \cdot \text{K}^{-1} \cdot \text{mol}^{-1}$ )<sup>[151]</sup>. The models that will be utilised for the data analysis within this study will be the commonly used two parameter models, the Freundlich, Langmuir, Temkin and Dubinin-Radushkevich isotherms<sup>[152]</sup>. In all cases, the best fit was determined by the  $r^2$  value of the fit, and confidence intervals were obtained by the square root of the covariance matrix of each model.

### Homogeneity of Binding

This section will cover the use of the Freundlich and Langmuir models in describing the heterogeneous or homogeneous nature of adsorption with descriptions of capacities and intensity of binding. The Langmuir describes a monolayer adsorption process, with interactions purely between the adsorption species and adsorbent, with no co-extraction and generally more intense binding, while the Freundlich model can be used to describe a system where adsorption includes co-extraction of species and weaker interactions<sup>[152]</sup>. The Freundlich model describes systems displaying a decrease in energy with increasing binding, a relationship that is exponential<sup>[151]</sup>. This model is given by:

$$q_e = a_F C_e^{b_F} \quad (4.1)$$

where  $a_F$  and  $b_F$  are the Freundlich isotherm constants. The value  $a_F$  represents adsorption capacity<sup>[153–155]</sup> or relative adsorption capacity<sup>[152,156–161]</sup>. The parameter  $b_F$  is either given as the degree of heterogeneity<sup>[152,154,156]</sup> or intensity of adsorption<sup>[153,157–160]</sup>. When  $b_F = 0$  the reaction is irreversible, when

$0 < b_F < 1$  there is favourable adsorption and when  $b_F > 1$  there is unfavourable or cooperative adsorption<sup>[154,158]</sup>; in this capacity the more 'intense' the binding mechanism, the more homogeneous the binding surface, with less intense processes leading to heterogeneous binding<sup>[152]</sup>.

**Table 4.1:** Variables obtained by fitting the single metal isotherm data to the non-linear Freundlich model.

Resin	Values	Copper	Iron(II)	Lead	Zinc
C107E	$a_F$	$0.05 \pm 0.02$	$0.008 \pm 0.003$	$0.8 \pm 0.3$	$0.07 \pm 0.03$
	$b_F$	$0.51 \pm 0.06$	$0.37 \pm 0.07$	$0.92 \pm 0.06$	$0.93 \pm 0.01$
	$r^2$	0.905	0.776	0.979	0.956
MTS9301	$a_F$	$0.015 \pm 0.005$	$0.007 \pm 0.003$	$0.05 \pm 0.01$	$0.010 \pm 0.002$
	$b_F$	$0.23 \pm 0.04$	$0.28 \pm 0.05$	$0.47 \pm 0.04$	$0.24 \pm 0.02$
	$r^2$	0.768	0.781	0.958	0.941
TP214	$a_F$	$0.0031 \pm 0.0004$	$0.008 \pm 0.004$	$0.012 \pm 0.003$	$0.0025 \pm 0.0007$
	$b_F$	$0.17 \pm 0.03$	$0.7 \pm 0.1$	$0.67 \pm 0.06$	$0.46 \pm 0.07$
	$r^2$	0.893	0.896	0.970	0.888

The variables obtained by the fitting of the isotherm data to the Freundlich model are displayed in Table 4.1. The interactions of lead and zinc with the WA functionality displays very reasonable fits to this model ( $r^2$  of 0.979 and 0.956, respectively), with copper displaying a tentative fit ( $r^2$  of 0.905), however the fit to iron(II) was poor, with an  $r^2$  of 0.776. With the very poor fit of iron(II) in mind, the intensities of adsorption generate the trend of  $Zn > Pb > Cu$ . The Freundlich isotherm fit to the experimental data for the IDA functionality isotherms displayed poor correlation to both copper and iron(II), while lead and zinc found reasonable fits to this model ( $r^2$  values of 0.958 and 0.941, respectively), with zinc displaying a higher intensity of binding than lead. The adsorption of lead to the thiourea functionality displays a reasonable fit to this model ( $r^2$  of 0.970), no other metals fit the model, with  $r^2$  values  $< 0.9$ .



The Langmuir model, unlike the Freundlich model, does follow Henry's law as concentration decreases<sup>[151]</sup>, i.e. while at high concentrations it predicts constant adsorption. This model is capable of describing monolayer sorption mechanisms, and is given by:

$$q_e = \frac{q_m a_L C_e}{1 + a_L C_e} \quad (4.2)$$

In this instance  $a_L$  is the Langmuir isotherm constant ( $L \cdot \text{mol}^{-1}$ ), related to the sorption energy (equilibrium constant for the sorption of the species) and  $q_m$  is the monolayer capacity of the sorbent ( $\text{mol g}^{-1}$ )<sup>[152]</sup>.

**Table 4.2:** Variables obtained by fitting the single metal isotherm data to the non-linear Langmuir model.

Resin	Values	Copper	Iron(II)	Lead	Zinc
C107E	$a_L$	340±60	500±100	170±90	10±10
	$q_m$	0.005±0.001	0.0021±0.0008	0.009±0.004	0.02±0.03
	$r^2$	0.976	0.915	0.983	0.955
MTS9301	$a_L$	11000±2000	2400±600	4800±400	11000±5000
	$q_m$	0.0043±0.0007	0.0023±0.0008	0.0021±0.0002	0.003±0.001
	$r^2$	0.975	0.928	0.992	0.909
TP214	$a_L$	50000±20000	30±20	80±30	120±30
	$q_m$	0.001±0.001	0.0014±0.0008	0.0012±0.0005	0.0006±0.0002
	$r^2$	0.890	0.922	0.955	0.952

The Langmuir fits to the isotherm data of the adsorption of copper, lead and zinc to the WA functionality (Table 4.2) display reasonable fits ( $r^2 > 0.95$ ), with iron(II) displaying a slightly more tentative fit of 0.915. The calculated theoretical maximum adsorbance calculated by the Langmuir model for the WA functionality dictates that zinc displays the highest capacity, with  $0.02 \text{ mol g}^{-1}$ , however the high error, along with weak interaction, removes any credibility to this value, regardless of the  $r^2$ . The capacity trend then follows  $\text{Pb} > \text{Cu} > \text{Fe}$ , with lead showing  $0.009 \text{ mol g}^{-1}$ . The Langmuir isotherm fits the data obtained by the IDA

functionality isotherm experiments quite well, all metals return  $r^2$  values  $>0.9$ , with lead and copper returning values  $>0.97$ . The maximum sorption capacities follow a trend of  $\text{Cu} > \text{Zn} > \text{Fe} > \text{Pb}$ , with copper's theoretical sorption capacity being  $0.0043 \text{ mol g}^{-1}$ . Neither the Langmuir nor Freundlich model was capable of fitting the copper adsorption isotherm data for the thiourea functionality, with lead and zinc being reasonably described and iron(II) showing a tentative relationship.

Copper displays more homogeneous binding behaviour for both the WA and IDA functionalities, deriving theoretical  $q_m$  values closely related to experimental values and poor fits to the Freundlich model. This leads to the assumption that the binding mechanism of both of these resins follows a monolayer coverage with uniform binding energies and a more traditional equilibrium adsorption<sup>[154]</sup>; while similar to literature descriptions of copper adsorption reactions in strong acid media<sup>[150,162–166]</sup>, there is a much lower (although described by a tentative fit) binding intensity for the adsorption of copper towards the carboxylic acid functionality in within this study, emphasising a competition between carboxylic acid functionality and solution phase acetate. Overall, both IDA and WA functionalities have the highest capacity for the adsorption of copper from the resins studied (both within error margins of each other), while thiourea lagged behind in capacity; however, this is taken from an experimental observation as the thiourea functionality data was a poor fit ( $r^2 < 0.9$ ), although this could be due to the degree of scatter within the experimental data

Iron(II) displays a poor fit to Freundlich towards all functionalities, with the Langmuir providing a better description. Further alluding to monolayer adsorption processes, the Langmuir model was able to predict the maximum loading capacity for both the WA and IDA functionality, however due to the lack of saturation, the values obtained by the fitting of the TP214 isotherms were difficult to compare with certainty. Similarly, to the case of copper, the WA and IDA functionalities displayed the highest capacity for iron(II), with thiourea remaining fairly low

despite high  $K_d$  values towards lower concentrations<sup>[119]</sup> and high capacities described in previous studies<sup>[153,167]</sup>. Modelling of the thiourea resin isotherm with the iron(II) system poses a challenge due to the possibility of oxidation and iron(III) precipitation; while oxidation is not modelled (Figure B.1b) within a closed system, introduction of thiourea functionality and agitation of solution potentially allows for the precipitation of  $\text{Fe}_2\text{O}_3$  through an alteration in solution oxidation-reduction potential (as alluded to in the predominance diagram in Figure B.2).

Lead displays a reasonable fit to the Freundlich and Langmuir isotherm (this is true for all three resins), with little deviation from literature capacities ( $0.923^{[168]}$ ,  $1.27^{[169]}$ ,  $0.912\text{mol g}^{-1}[170]$  for WA, IDA and thiourea functionalities, respectively). The WA functionality isotherm data, displays a similar fit to both models with a low sorption intensity and the allusion to heterogeneous binding. IDA displayed behaviour better fit to the monolayer sorption model with a binding intensity indicative of more homogeneous behaviour. The thiourea functionality displays a low binding intensity (although higher than the WA functionality), leading to the assumption of a homogeneous binding mechanism. The heterogeneous nature being alluding to a speciation dependent binding (with  $\text{PbAc}^+$ ,  $\text{PbAc}_2$  and  $\text{PbAc}_3^-$  present in solution), and similar functionalities describing more homogeneous behaviour<sup>[150,162,166,169–173]</sup>.

Zinc displays interesting adsorption behaviour, with little adsorption to the WA resin, a closer fit to Freundlich for IDA functionality and a bias towards Langmuir behaviour for the thiourea functionalised resin. Within both WA and thiourea isotherm experiments, saturation was not reached due to complex competition leading to low equilibrium adsorption at this pH ( $K_d$  values for such systems have previously been reported as 0.174 for the WA functionality and 0.053 for TP214)<sup>[119]</sup>; therefore, comparison of experimental and modelled capacities is not possible. The maximum capacity determined by the Langmuir fitting of the IDA functionality data is closer to the experimentally observed maximum,

with the largest experimental value being  $\sim 0.003 \text{ mol g}^{-1}$ , this coupled with the low stability constants of each zinc-acetate complex leads to the assumption of homogeneous binding.

## Sorption Energies and Interaction

The D-R isotherm model (and the Temkin to a much lesser extent) can be used to determine the energy associated with adsorption. From this, the adsorption process (physisorption, ion exchange or chemisorption) can be determined and therefore, to a small extent, the reversibility of the reaction as well as the potential selectivity of a functional group for one ion over another. The Temkin model describes systems that are heterogeneous in binding nature, similar to that of the Freundlich model<sup>[174]</sup>, however with a linear, not exponential decrease in energy<sup>[151,175]</sup>. This isotherm is given by:

$$q_e = \frac{RT}{b_T} \ln(a_T C_e) \quad (4.3)$$

where  $R$  is the gas constant,  $T$  is the temperature of the experiment,  $b_T$  is the Temkin isotherm constant relating to the heat of sorption ( $\text{J mol}^{-1}$ )<sup>[176]</sup> and  $a_T$  is the Temkin equilibrium sorption isotherm constant ( $\text{L mol}^{-1}$ ) relating to the maximum adsorption capacity<sup>[177]</sup>. As with many of isotherm models this model was devised for predicting gas-solid equilibrium isotherms, however in this case is often a poor descriptor of liquid-solid adsorption<sup>[152]</sup>, not only this but the Temkin isotherm is assumed to only fit within a small region of the isotherm (ignoring high and low values of concentrations)<sup>[154,158]</sup>; therefore, this model is often ill equipped to describe a system effectively and will be used as supplemental to the D-R isotherm.

The Temkin model is unable to describe the data obtained for the adsorption of iron(II), lead and zinc to the WA functionality, with copper displaying the tentative

**Table 4.3:** Variables obtained by fitting the single metal isotherm data to the non-linear Temkin model.

Resin	Values	Copper	Iron(II)	Lead	Zinc
C107E	$b_t$	2800±200	5900±600	5500±600	5900±900
	$a_t$	7000±1000	5000±1000	15000±3000	1600±500
	$r^2$	0.922	0.842	0.859	0.787
MTS9301	$b_t$	4300±400	6100±600	7600±500	7100±300
	$a_t$	$4\pm 1 \times 10^5$	$3\pm 1 \times 10^4$	$12\pm 2 \times 10^4$	$5\pm 1 \times 10^5$
	$r^2$	0.911	0.908	0.953	0.980
TP214	$b_t$	1700±100	1500±200	2200±300	2100±200
	$a_t$	$3\pm 2 \times 10^6$	1300±500	7000±3000	1700±400
	$r^2$	0.925	0.813	0.825	0.924

$r^2$  of 0.922 (Table 4.3), with a binding energy of  $2.8\pm 0.2\text{kJ mol}^{-1}$ . This model displays reasonable fits to the sorption of lead and zinc to IDA, as both display the most heterogeneous behaviour towards this functionality, with  $r^2$  values of 0.953 and 0.980, with copper and iron(II) having more tentative fits. The tentative trend of sorption energies obtained therefore follows  $\text{Cu} < \text{Fe} < \text{Zn} < \text{Pb}$ . The Temkin model returned tentative fits to both copper and zinc isotherms ( $r^2$  0.914 and 0.931, respectively) with binding energies of  $1.7\pm 0.1$  and  $2.1\pm 0.2\text{kJ mol}^{-1}$ , respectively, while both iron(II) and lead returned poor fits with this model ( $r^2$  0.831 and 0.847, respectively).

The Dubinin-Radushkevich (D-R) isotherm is used to determine the binding energy of a specific sorption process, allowing characterisation of the adsorption mechanism<sup>[151,152]</sup>. This isotherm is described by:

$$q_e = q_D \exp\left(-B_D \left(RT \ln\left(1 + \frac{1}{C_e}\right)\right)^2\right) \quad (4.4)$$

where  $q_D$  is the capacity ( $\text{mol g}^{-1}$ )<sup>[154,158,178]</sup>,  $R$  is the gas constant and  $T$  is the temperature at which the experiment is conducted. The constant  $B_D$  related to the free energy of adsorption,  $E$  ( $\text{kJ mol}^{-1}$ )<sup>[151,161]</sup>, of the sorbate species to the

surface of the resin. This can be calculated using:

$$E = \frac{1}{\sqrt{2B_D}} \quad (4.5)$$

Using this calculation, assumptions can be made of the binding mechanism of the adsorption. If  $E$  is  $< 8 \text{ kJ mol}^{-1}$  the binding mechanism is assumed to be physical (physisorption),  $8 \text{ kJ mol}^{-1} < E < 16 \text{ kJ mol}^{-1}$  it is assumed to be ion exchange and if  $E$  is  $> 16 \text{ kJ mol}^{-1}$  then the adsorption mechanism can be assumed to be chemical (chemisorption)<sup>[117,164]</sup>.

**Table 4.4:** Variables obtained by fitting the single metal isotherm data to the non-linear D-R isotherm model.

Resin	Values	Copper	Iron(II)	Lead	Zinc
C107E	$q_D$	$0.011 \pm 0.002$	$0.0034 \pm 0.0006$	$0.027 \pm 0.005$	$0.009 \pm 0.002$
	$B_D$	$7.0 \pm 0.7 \times 10^{-9}$	$6 \pm 1 \times 10^{-8}$	$1.02 \pm 0.06 \times 10^{-8}$	$1.6 \pm 0.2 \times 10^{-8}$
	$E$	$8.4 \pm 4$	$9.4 \pm 0.8$	$7.0 \pm 0.2$	$5.5 \pm 0.3$
	$r^2$	0.943	0.842	0.985	0.953
MTS9301	$q_D$	$0.007 \pm 0.001$	$0.0039 \pm 0.0005$	$0.0067 \pm 0.0007$	$0.0044 \pm 0.0003$
	$B_D$	$2.5 \pm 0.4 \times 10^{-9}$	$3.7 \pm 0.6 \times 10^{-9}$	$4.5 \pm 0.3 \times 10^{-9}$	$2.5 \pm 0.2 \times 10^{-9}$
	$E$	$14 \pm 1$	$11.6 \pm 0.9$	$10.5 \pm 0.3$	$14.0 \pm 0.6$
	$r^2$	0.852	0.853	0.977	0.965
TP214	$q_D$	$0.0019 \pm 0.0001$	$0.0020 \pm 0.0004$	$0.0020 \pm 0.0003$	$0.0009 \pm 0.0001$
	$B_D$	$1.8 \pm 0.3 \times 10^{-9}$	$1.4 \pm 0.2 \times 10^{-8}$	$1.0 \pm 0.1 \times 10^{-8}$	$8 \pm 1 \times 10^{-9}$
	$E$	$17 \pm 1$	$6.0 \pm 0.5$	$7.1 \pm 0.4$	$7.8 \pm 0.5$
	$r^2$	0.919	0.918	0.961	0.928

For copper, lead and zinc, the D-R model fits quite well to the WA data (Table 4.4), as these metals return  $r^2$  values of 0.943, 0.985 and 0.953, respectively, however iron(II) returns a low value of 0.842, therefore the values obtained are more tentative. The free energies of adsorption for metals on the surface of this resin follow a different trend, with the derived values following the trend  $\text{Fe} > \text{Cu} > \text{Pb} > \text{Zn}$ , opposite to that of the Temkin values (with the omission of the

extremely tentative iron(II) value), which is to be expected if the Temkin energies relate to the energy required for binding. The isotherm data of lead and zinc adsorption to IDA was adequately described by the D-R isotherm, with both iron(II) and copper showing far less correspondence to the model ( $r^2 \sim 0.85$ ), leading to the tentative trend in energies of adsorption of  $\text{Cu} > \text{Zn} > \text{Fe} > \text{Pb}$ . The thiourea functionality isotherm data for all metals returned a fit to the D-R model with  $r^2$  values  $> 0.91$ . The free energies of adsorption of this resin displayed a different trend, with iron(II), lead and zinc displaying free energies within similar regions (6, 7.1 and  $7.8 \text{ kJ mol}^{-1}$ , respectively), while copper returned an energy of  $17 \text{ kJ mol}^{-1}$ .

Copper displays an ion exchange mechanism for the adsorption to both IDA (while tentative, it agrees with literatures values<sup>[164,165]</sup>) and WA functionality ( $14 \pm 1$  and  $8.4 \pm 0.4 \text{ kJ mol}^{-1}$ ). The free energy is tentatively much larger for MTS9301, rationalised by a bidentate binding mechanism theorised by this resin, forming much more stable chelation complex, while increasing the entropy of the system, from the potential release of not only acetate ions but also two protons from the IDA functionality; agreeing with a lack of interference of the acetate species to copper extraction by IDA. The WA functionality does not produce energy values that agree with literature sources, which allude to strong ion-exchange extraction mechanisms ( $\sim 15 \text{ kJ mol}^{-1}$ )<sup>[165]</sup>, whereas in this study the competition between WA functionality and solution-phase acetate reduced binding energy to  $8.4 \pm 0.4 \text{ kJ mol}^{-1}$ . The Temkin binding energy for copper to the WA functionality is much lower than that of IDA, due to a greater extent of ligand transfer when adsorbed by the IDA functionalised resin.

The argument for a redox reaction between copper and thiourea can be further justified by the calculation of high sorption free energies ( $17 \text{ kJ mol}^{-1}$ ), alluding to a chemisorption process, with the better fit to the Temkin isotherm (over Langmuir and Freundlich) alluding to a heterogeneous binding mechanism, supported

by the multitude of species formed by the redox reaction between aqueous thiourea and copper(II)<sup>[144,179]</sup>. Studies within strong acid media (but low ionic strength) do not display trends describing a similar redox process (free energy of  $5.28\text{kJ mol}^{-1}$ <sup>[173,180]</sup>). However, thiourea has been previously observed to out compete the binding of copper with solution phase citrate and lactate complexes, having a high affinity for this ion over iron(II), lead and zinc<sup>[119]</sup>, alluding to high ionic strengths facilitating the reaction.

The poor fits of the WA and IDA functionality data to the D-R isotherm for iron(II) leads to tentative assignments of the mechanisms as ion exchange. With respect to the thiourea isotherm, the low oxidation-reduction potential required for oxidation and precipitation at this pH throughout the isotherm concentration range leads to the assumption of  $\text{Fe}_2\text{O}_3$  formation (Figure B.2). Due to the high concentration of iron within sewage sludge being deleterious to the adsorption of other species, this precipitation is beneficial for the removal of the other metals.

Lead returned a free energy value closer to physisorption ( $7\text{ kJ mol}^{-1}$ ) for the carboxylic acid functionalised resin, despite the ability of this resin to extract lead selectively from other complexing media<sup>[119]</sup>. The competition of lead-acetate complexes (being 25%  $\text{PbAc}^+$ , 50%  $\text{PbAc}_2$  and 25%  $\text{PbAc}_3^-$ ) and the WA functionality led to a free energy of binding value higher than that of strong acid media values ( $3.5\text{kJ mol}^{-1}$ )<sup>[172]</sup>. The much higher free energy reported for IDA functionality is potentially due to the diacetic acid functionality creating a bidentate ion exchange process, breaking the acetate complexation, which can be supported by the Temkin binding energy, which is high, relative to the other metals studied. Thiourea functionality displays physisorption binding energies towards lead, again concurrent with the lack of exchangeable ions; interestingly, higher energy than that of literature values<sup>[173]</sup>.



Zinc still displays far lower free energy of adsorption and binding energy towards the WA resin, which could be explained by the extremely low stability constants of zinc to carboxylic acid complexes<sup>[119]</sup>, with a ligand transfer between the carboxylic acid groups on the resin surface and solution phase acetate. The free energy of adsorption related to the sorption to the IDA functionality implies a strong ion exchange interaction, most likely to do with the chelating effect of this functionality, allowing for the interaction between the nitrogen atom as well as both carboxylic acid functionalities. Thiourea functionality displays physisorption towards this metal through both free energy of adsorption, with the lowest overall capacity calculated. Weak Van der Waals forces are the most likely present, supported by the low Temkin binding energy calculated.

### **Correlation of Physical and Chemical Parameters to Modelled Values**

Summaries of the comparisons of values derived by isotherms to the ionic radii, the average  $\Delta H$  and  $\Delta S$  of metal-acetate complex formation and electronegativity are included in Table B.2, with the important findings displays in Figures B.7-B.10 in order to generate tentative correlations between ionic properties and isotherm values. With the exception of zinc, the WA functionality seems to have the trend of increasing capacity with electronegativity (Figure B.8), intensity of binding and energy of binding however display a tentative decreasing trend towards increasing electronegativity (Figures B.9 and B.10). This is understandable, as this functionality relies purely upon the attraction to a negative charge for extraction, and the behaviour of zinc corresponds to the extremely low stability constants of zinc acetate complexes<sup>[119]</sup>.

The  $q_{max}$  of the IDA functionality for metals depends, exponentially, on the ionic radius of the metal observed; the smaller the ionic radius, the higher the capacity (Figure B.7). The rationale for this is the chelating nature of the resin. This trend

is again observed, linearly, when comparing the intensities of binding; leading to the assumption that the equilibrium for this resin is dictated entirely by ionic radii. The thiourea functionality results could be skewed due to the redox reaction that occurs between thiourea and copper(II).

## Capacities and Resin Performance

While mechanisms of binding and specific interactions of resins with a species is fundamentally interesting; in order to gauge the relative performance of a resin within the conditions specified, each system will be required to be compared to other similar ion exchange systems. This section will focus on such a comparison, using either the derived Langmuir or D-R capacities (dependent on which was best-fitting). Within this section, all values of capacity will be converted from  $\text{mol g}^{-1}$  to  $\text{mg g}^{-1}$  for comparison with the literature. These can be used as justification for the choice and usage of a resin within the proposed resin-in-pulp system.

The carboxylic acid and IDA functionalised resin displayed monolayer ion exchange mechanisms towards copper(II), their capacities are  $320 \pm 60 \text{ mg g}^{-1}$  and  $273 \pm 40 \text{ mg g}^{-1}$ , respectively, both being within error of one another; both resins displaying capacities well beyond that of the bispicolylamine functionalised M4195 (although recorded at pH 2)<sup>[181]</sup>, which is an effective copper(II) extractor at low pH values<sup>[112]</sup>. For the extraction of copper(II) from solution, the IDA functionality is more prevalent within the literature among the commercially available<sup>[163,164,166,182]</sup> (which include S930<sup>[164]</sup> and S930+<sup>[182]</sup>, predecessors to the MTS9300 and MTS9301 resins) and novel adsorbents<sup>[169,183,184]</sup>. However, the extraction within this study is higher than many literature values double that of S930<sup>[164]</sup> and double that of the manufacturer's specifications, giving rise to the suggestion that two  $\text{Cu}^{2+}$  ions bind to one IDA functionality. Comparable literature capacities have been achieved with the weak acid functionalised resin NDMC

(novel) and C106 (Purolite), at  $239.9$  and  $236.7 \text{ mg} \cdot \text{g}^{-1}$ , respectively<sup>[165]</sup>, with these values within error of the MTS9301 and C107E data from this study (C107E being comparable to C106, though being described as a 'potable water grade' resin by the manufacturer data sheet).

Interestingly, the C106 resin displayed a free energy of copper adsorption almost double that of C107E ( $15.04 \text{ kJ mol}^{-1}$  vs  $8.4 \pm 0.4 \text{ kJ mol}^{-1}$ ), with the NDMC resin, C106 and IRC748 having free energy of adsorption  $>1 \text{ kJ mol}^{-1}$ <sup>[166]</sup> higher than that of MTS9301 within acetic acid media; assumed to be due to the stabilisation of the acetate complexes within solution. This alludes to the reason for the decrease in capacities of the resins. The thiourea functionalised resin, with a speculated redox reaction adsorption mechanism has the lowest capacity of all three with a D-R isotherm capacity of  $121 \pm 6 \text{ mg g}^{-1}$ , which is comparable to many modified silica and chitosan adsorbents<sup>[173,176,180,185]</sup>. The difference lies with the large free energy value  $17 \text{ kJ mol}^{-1}$ , especially when considering the other thiourea functionalised adsorbents<sup>[173,180]</sup>. While the stronger adsorption of TP214 would be preferential for extraction from a sewage sludge pulp (due to the preg-robbing from sewage sludge organic matter<sup>[93]</sup>), the far superior capacity and the higher likelihood of regeneration of the MTS9301 resin makes it a better choice.

Extraction of iron(II) was low for these resins, with all three functionalities displaying lower affinities for iron(II) than all other metals. While this would not be favourable with respect to the other metals, the low affinity for iron(II) is a positive attribute for the resins to have in order to eliminate competition; as iron is of low value and has no agricultural restrictions<sup>[34]</sup>, it is not necessarily advantageous to remove from the sludge. If iron(III) were to remain in solution, however, there would be a tendency for thiourea functionalities to maintain a higher capacity for this species, over iron(II); as a study conducted on functionalised chitosan displayed a  $71.9 \text{ mg g}^{-1}$  capacity for iron(III) compared to a  $48.3 \text{ mg g}^{-1}$

capacity for iron(II), however this was synthesised with an iron(III) template<sup>[153]</sup>, with unmodified chitosan having higher capacity for iron(II) at  $51.81 \text{ mg g}^{-1}$ <sup>[167]</sup>. This could also, however, be explained by the potential for precipitation of  $\text{Fe}_2\text{O}_3$  (Figure B.2).

The calculated capacities of C107E and TP214 for lead were unreliable, due to the under-saturation, and the potentially heterogeneous mechanisms. The extrapolation required for C107E and TP214 devalues calculated values for capacities, leaving the only reliable capacity being that of MTS9301 returning a capacity of  $\sim 400 \text{ mg} \cdot \text{g}^{-1}$ . The high capacity of MTS9301 for lead within this study unperturbed by the acetate complexes, being on par with commercial and novel macroporous alternatives<sup>[150,162,166,169–172]</sup>, and outperforming cheap, alternative sorbents (activated carbon, inorganic sorbents and biomass materials<sup>[186–188]</sup>).

At the pH that these experiments were conducted at, zinc did not display high distribution coefficients towards the C107E resin<sup>[119]</sup>, due to this low equilibrium it was difficult to convincingly predict maximum capacities for zinc to the surface of the resin, as a maximum value was not reached. Therefore, the highest maximum value calculated for zinc was via D-R isotherm, calculated at  $600 \pm 100 \text{ mg g}^{-1}$ . However, again, due to the poor  $K_d$  values obtained, these capacities are unreasonable to assume as correct. MTS9301, on the other hand displays capacities that are reasonable at  $200 \pm 70 \text{ mg g}^{-1}$  assuming homogeneous binding (Langmuir behaviour), also displaying double the milliequivalent capacity of the manufacturer specifications, alluding to the binding of two  $\text{Zn}^{2+}$  ions to each IDA functional group. Both of these resins display, experimentally, a higher capacity for zinc than the thiourea functionalised resin, which was reported to have a monolayer capacity of only  $40 \pm 10 \text{ mg g}^{-1}$ . Interestingly, the thiourea functionality was found to display the highest capacity from the literature, with the IDA functionalised IRC748 displaying only  $19.7 \text{ mg} \cdot \text{g}^{-1}$ <sup>[163]</sup>, but a novel thiourea functionalised adsorbent displaying a capacity well beyond that of this study with

226.32 mg · g<sup>-1</sup> (although at pH 7)<sup>[189]</sup>, also out-competing studies conducted on strong acid functionalised resins, with capacities of ~40mg g<sup>-1</sup> to 70mg g<sup>-1</sup><sup>[117,190]</sup>.

Interestingly, while the acetate moiety does affect the performance of each resin, it is not necessarily deleterious to the entire performance of each resin. The carboxylic acid functionalised C107E is effective at the removal of lead from solution, with saturation not reached within this study, whether there are kinetic limitations with this extraction or not will need further research. TP214 displays an extremely strong affinity for copper, while lacking in capacity for all other metals. The strength of binding between the thiourea functionalised resin and copper, apparent towards much lower pH values, generates the possibility of a highly selective process for the removal of copper from a sludge high in copper concentration with potential for high returns. Overall, however, the most effective extractant was MTS9301, with reasonably high free energies of binding and high capacities. The capacity for lead wasn't as high as for C107E, but on par with literature sources. Within the resin-in-pulp process, each of these resins could be utilised for their own purpose, depending on the contaminant metals, and whether the focus is extraction of value from metals or from phosphate nutrients.

## 4.5 Conclusions

Single metal isotherm analysis of C107E, MTS9301 and TP214 has been conducted for copper, iron(II), lead and zinc. This is, in part, work towards the removal of metals from sewage sludge by resin-in-pulp. Consideration of the effect of acetate complexation on performance and mechanism has been discussed.

Copper was found to undergo a homogeneous binding mechanism to the surface of C107E and MTS9301, both having free energies of adsorption (calculated by the D-R isotherm, however with a poor fit to the MTS9301 data)

relating to ion exchange mechanisms; the acetate media hindering the weak acid resin performance. TP214, displayed a free energy of adsorption relating to chemisorption, higher than the other metals studied, further alluding to a proposed redox reaction. The C107E and MTS9301 resins both displayed capacities for copper that were similar to those reported in literature sorbents, while TP214 lagged behind in performance (while maintaining a large free energy).

While there is a possibility for iron(II) to oxidise and precipitate, it was assumed throughout the study that iron(II) would likely remain the dominant species in solution at this pH. This species still, however, displayed poor performance throughout. While this metal had the lowest reported capacities, extraction of this metal is not a required feature of the selected resin, therefore advantageous to the proposed system resin-in-pulp system.

For all resins studied within this body of work, lead was observed to display the most heterogeneous binding to the resin surfaces because of the variety of complex species in solution. The capacity of MTS9301 for lead was similar to that described by literature, while saturation was not attained by either C107E or TP214, due to competition between adsorption and acetate complexation. In both cases, this competition increased the reported D-R free energy of adsorption relative to strong acid media.

For C107E and TP214, zinc loading was not observed to reach saturation, assumed to be hindered by acetate media due to weak interactions with functional groups. C107E and MTS9301 both returned relatively close fits to Langmuir and Freundlich models, returning values relative to high homogeneity. The most reliable capacity value returned from the monolayer sorption model was that of MTS9301 which is comparable to the higher literature values, while TP214 was found to perform poorer than literature thiourea studies.

Of the resins studied within this body of work, MTS9301 was the best overall performer. The selectivity of thiourea for copper (and the strong interactions between), warrants further inspection, while C107E displayed a higher capacity for lead and had similar performance for copper, however poor performance with regards to zinc. The complexing nature of MTS9301 has given this resin a strong recommendation in the selection of a resin within the resin-in-pulp system.





# Chapter 5

## Multi-Metal Adsorption Systems

### Summary

This chapter will report the multi-metal isotherm and kinetics of Cu, Fe(II), Pb and Zn adsorption to C107E, MTS9301, TP214 from acetate media to understand the effect of a complex multi-metal system on resin performance. Mixed metal isotherm data was fit to common two parameter isotherm models, while also being fit to a Langmuir model proposed to be modified for desorption/competition, and kinetic data has been fit to common two parameter kinetic models. C107E showed fast kinetics for the adsorption of lead, above that which the trend in ionic radii had predicted (half-life of  $26 \pm 3$  min), with all other metals lagging behind (half-lives  $> 90$  min), while displaying the least desorption for both copper and lead. MTS9301 resin displayed different behaviour for lead, as well, displaying behaviour similar to that of C107E (half-life of  $25 \pm 5$  min). MTS9301 displayed high levels of desorption beyond a point of saturation by copper ions, however also showed the smallest half-lives towards all metals. C107E and MTS9301 showed far slower half-lives for iron(II) than the other three metals in solution. TP214 proved reasonably effective for the removal of copper, while rejecting all other metals as determined by the poor uptake observed with both the mixed metal isotherm study and the rejection after 20-60 min.

## 5.1 Introduction

Complicated multi-metal isotherms are rare within literature, with very little explanation of the effect that saturation can have on resin capacity for specific metals or competition dependent desorption. With the leaching of metals from sewage sludge leading to varying concentrations of a multitude of metals, these are issues that will be reported within a complicated synthetic PLS. Kinetic parameters can also be diffusion dependent, and therefore are also likely to be hindered by a RIP process with a high solids content and adsorbent species content such as sludge. This study will be used to understand the multi-metal behaviour with isotherm studies, with an attempt at modelling competitive adsorption-desorption processes as well as including a thorough investigation of the kinetically limiting factors created by the acetate complexes in multi-metal systems and the most common adsorption kinetic models, as a continuation of the work conducted within Chapter 4. This study will be utilised in order to determine the parameters surrounding the ion exchange resin required for initial studies into the RIP process for the extraction of heavy metals from sewage sludge.

## 5.2 Methods

### Reagents and analysis

All chemicals used were of analytical grade or higher and purchased from Sigma-Aldrich apart from glacial acetic acid, which was purchased from VWR. MTS9301 and C107E were supplied by Purolite, and Lewatit MonoPlus TP214, which was supplied by Lanxess. All ion exchange resins were preconditioned by 24 hour contact with 1M H<sub>2</sub>SO<sub>4</sub> (10 bed volumes) prior to washing with 50 bed volumes of deionised water. Analysis was conducted via AAS, as described within Chapter 2.

## Extraction Isotherms of Metals from Acetic Acid Media

Isotherms were undertaken to understand the capacity of MTS9301, C107E and TP214 for  $\text{Cu}^{2+}$ ,  $\text{Fe}^{2+}$ ,  $\text{Pb}^{2+}$  and  $\text{Zn}^{2+}$ . Due to the large influence of equilibria on the values obtained, and therefore influence that molar ratios will have on each adsorption reaction, equimolar solutions were generated. Solutions were made up as mixed metal solutions of 200mM each metal. Each solution was made to 0.5M acetic acid and 0.5M NaCl and then adjusted to pH 4.5 using NaOH. Volumes of 20-400mL of solution was then contacted with 2mLwsr of the ion exchange resin and agitated for 24h on an orbital shaker.

## Extraction Kinetics of Metals from Acetic Acid Media

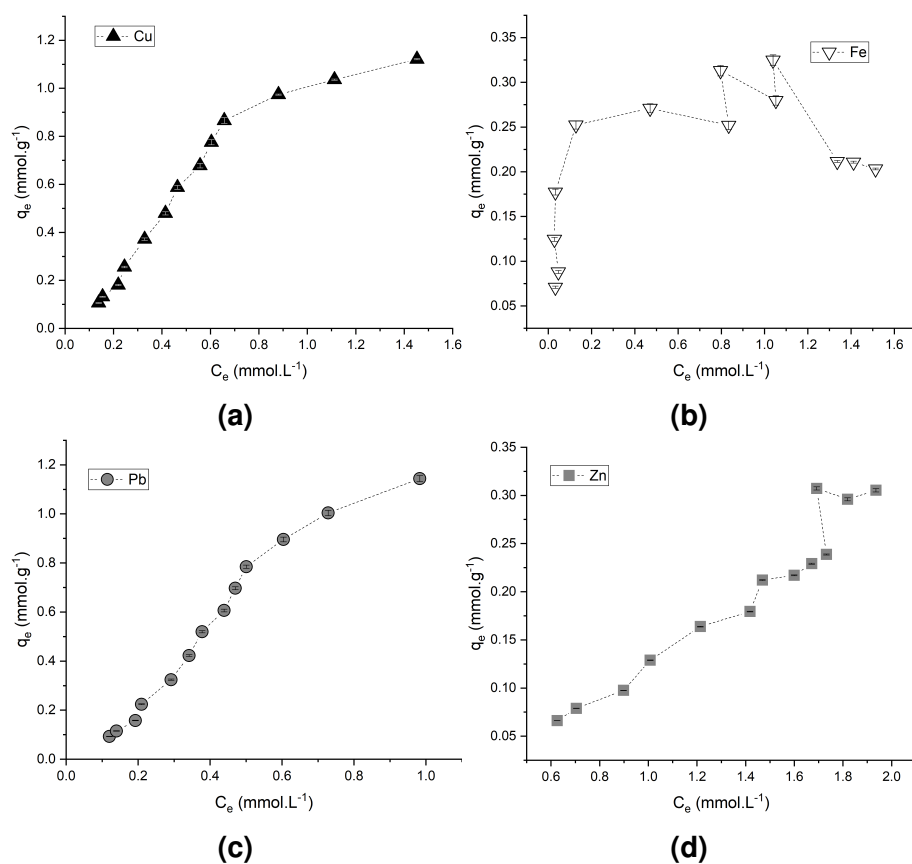
Kinetic experiments were undertaken for MTS9301, C107E and TP214, in order to gain an understanding of the mechanism and kinetic behaviour of each resin. Solutions for kinetic experiments were generated by creating mixed metal solutions of 200ppm  $\text{Cu}^{2+}$ ,  $\text{Fe}^{2+}$ ,  $\text{Pb}^{2+}$  and  $\text{Zn}^{2+}$ . Each solution was made to 0.5M acetic acid and 0.5M NaCl, then adjusted to pH 4.5 using NaOH. A 500mL volume of solution was contacted with 10mLwsr over a 24h period of agitation on an orbital shaker, with ten 1mL samples taken between 0 and 24h.

## 5.3 Results

### C107E

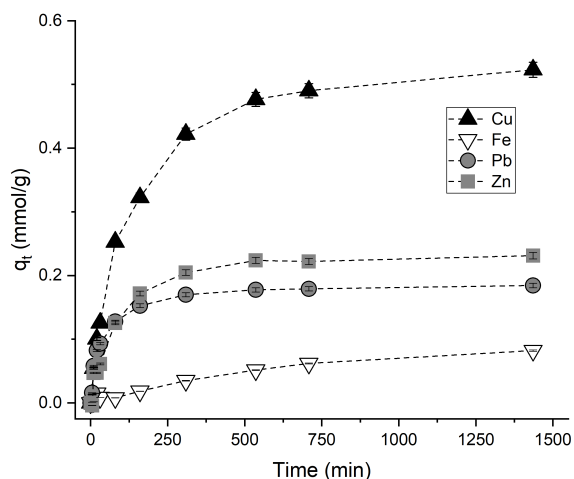
The C107E mixed metal isotherm is shown in Figure 5.1 with copper, iron(II), lead and zinc (Figures 5.1a-5.1d). The extractions of copper, lead and zinc display weak interactions, with gentle initial slopes, however, copper and lead reach an experimentally observed maximum of  $\sim 1.1 \text{mmol g}^{-1}$  (lead not reaching saturation), while zinc reaches  $\sim 0.3 \text{mmol g}^{-1}$  without displaying typical saturation. Iron(II), unlike the other three, displays a step initial adsorption isotherm, with a

low maximum capacity of  $\sim 0.3 \text{ mmol g}^{-1}$  and low levels of observable desorption and a large degree of scatter.



**Figure 5.1:** Concentration dependent extraction of copper (a), iron (b), lead (c) and zinc (d) by C107E in acetic acid media (initial concentration  $200 \text{ mmol L}^{-1}$ ; temperature  $21^\circ\text{C}$ ;  $0.5 \text{ M NaCl}$ ;  $0.5 \text{ M acetic acid}$ ;  $2 \text{ ml}$  wet settled resin;  $20\text{-}400 \text{ ml}$  solution).

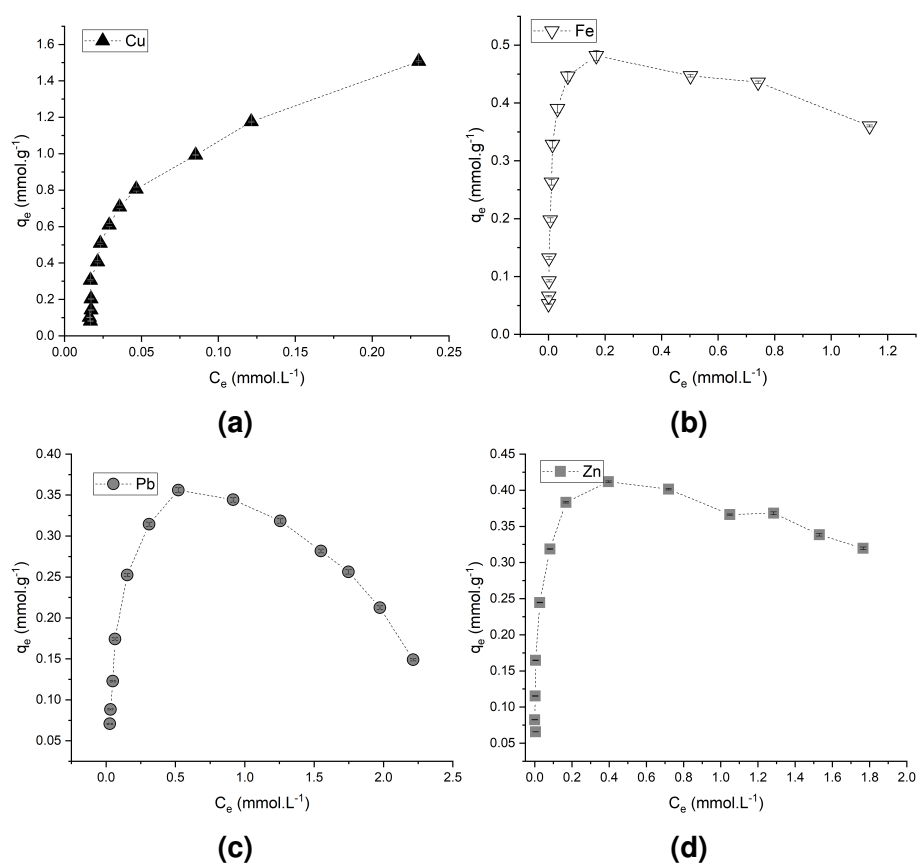
The C107E kinetics are displayed (metal adsorbed as a function of time) in Figure 5.2. The adsorption of copper and iron to the carboxylic functionality is perceptibly slower than that of zinc and lead, with equilibrium reached at  $>750 \text{ min}$ , while both lead and zinc were able to reach an equilibrium at  $>500 \text{ min}$ . Again, C107E displays stronger adsorption interactions towards copper and lead than zinc and iron (Figure C.4).



**Figure 5.2:** Time dependent extraction of copper (a), iron (b), lead (c) and zinc (d) by C107E in acetic acid media (initial concentration 200ppm; temperature 21°C; 0.5M NaCl; 0.5M acetic acid; 10ml wet settled resin; 500ml solution).

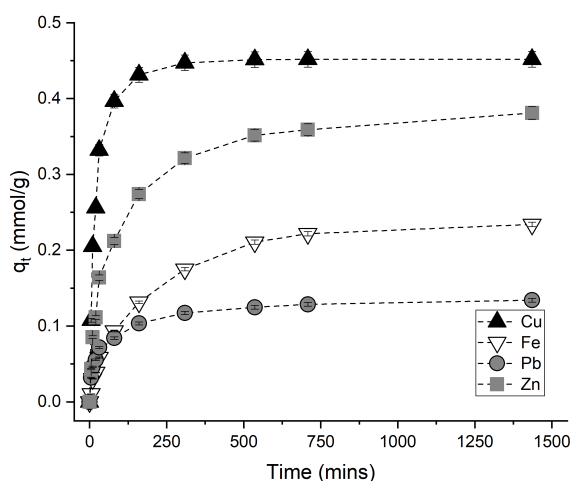
### MTS9301

Figure 5.3 displays the plots of the mixed metal isotherm data of copper, iron(II), lead and zinc. Copper is extracted to  $\sim 1.6 \text{ mmol g}^{-1}$ , with a rapid increase in the  $q_e$  to  $C_e$  ratio occurring until  $\sim 0.5 \text{ mmol g}^{-1}$  where it begins to display a lower gradient. Iron(II), lead and zinc display a peak of metal on the resin's surface before displaying desorption. Iron(II) adsorption peaks at  $q_e \sim 0.5 \text{ mmol g}^{-1}$  at  $C_e \sim 0.2 \text{ mmol g}^{-1}$ , while lead and zinc peak at  $\sim 0.4 \text{ mmol g}^{-1}$ .



**Figure 5.3:** Concentration dependent extraction of copper (a), iron (b), lead (c) and zinc (d) of MTS9301 in acetic acid media (initial concentration 200mmol L<sup>-1</sup>; temperature 21°C; 0.5M NaCl; 0.5M acetic acid; 2ml wet settled resin; 20-400ml solution).

The MTS9301 performance as a function of time is reported in Figure 5.4. The equilibrium of copper adsorption to the MTS9301 resin occurs first, out of the four metal ions, this rapid equilibrium is reached <250min. Iron(II), zinc and lead are all much slower to reach equilibrium at >500min. In this instance, the resin displays a similar affinity to all species, with these values equating to  $\geq 90\%$  extraction by the end of the 24h contact (Figure C.5).



**Figure 5.4:** Concentration dependent extraction of copper (a), iron (b), lead (c) and zinc (d) of MTS9301 in acetic acid media (initial concentration 200ppm; temperature 21°C; 0.5M NaCl; 0.5M acetic acid; 10ml wet settled resin; 500ml solution).

## TP214

The mixed metal adsorption isotherms for copper, iron(II), lead and zinc onto TP214 are displayed in Figure 5.5). Copper displays a maximum experimental adsorption capacity of  $\sim 1.125 \text{ mmol g}^{-1}$ , slowly increasing beyond the limit of this study. Iron(II), lead and zinc show poor extraction, however, with the adsorption maximum of lead being an order of magnitude lower than copper, and two orders of magnitude lower for iron(II) and zinc.

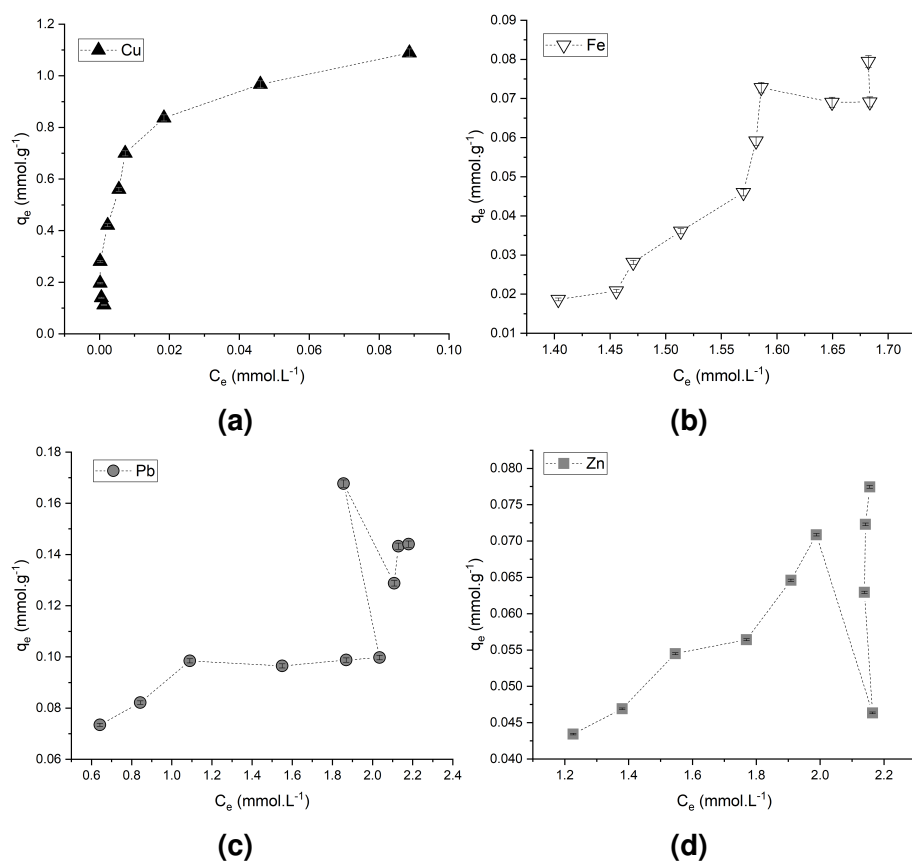


**Figure 5.5:** Concentration dependent extraction of copper (a), iron (b), lead (c) and zinc (d) TP214 in acetic acid media (initial concentration 200mmol L<sup>-1</sup>; temperature 21°C; 0.5M NaCl; 0.5M acetic acid; 2ml wet settled resin; 20-400ml solution).



The results of the TP214 kinetic study are presented in Figure 5.6. This displays, once again, high affinity for the copper ions from solution, with equilibrium being reached between 500 and 750min. Iron(II) is not uptaken within this media, as it remains at a low concentration on the surface of the resin. Both lead and zinc begin with a high extraction rate, before reducing in uptake past 100min, and drifting back into solution.

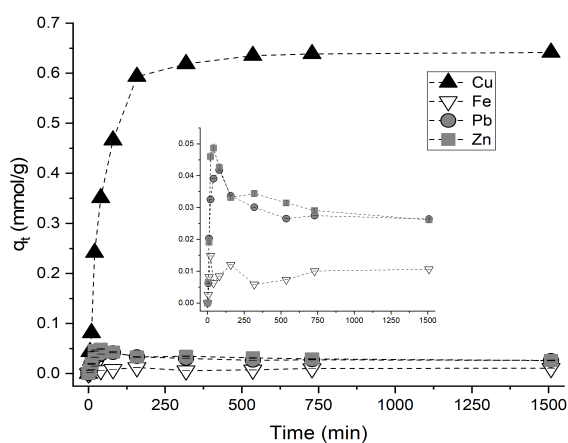


**Figure 5.6:** Concentration dependent extraction of copper (a), iron (b), lead (c) and zinc (d) of TP214 in acetic acid media (initial concentration 200ppm; temperature 21°C; 0.5M NaCl; 0.5M acetic acid; 10ml wet settled resin; 500ml solution).

## 5.4 Discussion

### Mixed Metal Isotherms

Copper and lead display the highest observed capacities with respect to C107E (both reaching  $\sim 1.2 \text{ mmol g}^{-1}$ ). Both of these metal seemingly display two distinct regions, most likely where metal-proton exchange transitions to metal-metal exchange or coextraction of the copper and lead metallic species, hindering capacity. While iron(II) displays an adsorption maximum similar to that of zinc, before plateauing with a large level of scattering within the data. In contrast MTS9301 displays a clear affinity for copper above all other metals, with each other metal being desorbed for further copper adsorption, creating a

second, more linear adsorption profile for copper. Similarly to MTS9301, TP214 displays an obvious preference to copper, however the deleterious nature of this adsorption is emphasised by the negligible adsorption of all other species.

### Comparison to Single Metal Isotherms

The multi-metal isotherm systems will be fit to the Freundlich, Langmuir, Temkin and Dubinin-Radushkevitch (D-R) models. The majority of isotherm models have been generated to describe the adsorption of a singular gaseous species to the surface of a solid adsorbent, therefore they quite often pose difficulty when fit to solution-phase systems; a difficulty that is further compounded by the co-existence of multiple solution-phase species competing for the resin surface. This becomes especially prominent towards saturation of the resin where the binding mechanisms change. The models given in Table 5.1 briefly outline the models that will be used for comparison of the multi-metal isotherm data to the single metal isotherm data from the previous chapter (Chapter 4).

**Table 5.1:** Two-parameter single-metal isotherm models used within this study<sup>[151]</sup>.

Name	Model
Freundlich	$q_e = a_F C_e^{b_F}$
Langmuir	$q_e = \frac{q_m a_L C_e}{1 + a_L C_e}$
Temkin	$q_e = \frac{RT}{b_t} \ln(a_t C_e)$
D-R	$q_e = q_D \exp\left(-B_D \left(RT \ln\left(1 + \frac{1}{C_e}\right)\right)^2\right)$

Briefly, the Freundlich isotherm determines the heterogeneity of the binding of a species to the resin surface, giving the parameters  $a_F$  (relative sorption capacity) and  $b_F$  (intensity of binding). The Langmuir model describes a system undergoing monolayer sorption, determining the monolayer sorption capacity,  $q_m$  ( $\text{mol g}^{-1}$ ) and the Langmuir isotherm constant,  $a_L$  ( $\text{L mol}^{-1}$ ). The Temkin isotherm is capable of describing the binding energy of a heterogeneous system within

a restricted capacity, where the Temkin constant  $b_t$  ( $\text{J mol}^{-1}$ ) is related to the heat of sorption, with  $a_t$  being the Temkin isotherm constant. The D-R isotherm is capable of determining the resin capacity ( $q_D$ ,  $\text{mol g}^{-1}$ ) as well as the D-R constant,  $B_D$ , which is related to the free energy of binding,  $E$  ( $\text{kJ mol}^{-1}$ ) by<sup>[151]</sup>:

$$E = \frac{1}{\sqrt{2B_D}} \quad (5.1)$$

**Table 5.2:** Variables obtained by fitting the mixed metal isotherm data of C107E, MTS9301 and TP214 to the Freundlich isotherm model.

Resin	Values	Copper	Iron(II)	Lead	Zinc
C107E	$a_F$	$0.2 \pm 0.1$	–	$1.1 \pm 0.7$	$2 \pm 2$
	$b_F$	$0.75 \pm 0.08$	–	$0.98 \pm 0.09$	$1.4 \pm 0.1$
	$r^2$	0.947	0.497	0.944	0.942
MTS9301	$a_F$	$0.3 \pm 0.2$	$19 \pm 6 \times 10^{-4}$	–	–
	$b_F$	$0.60 \pm 0.07$	$0.18 \pm 0.03$	–	–
	$r^2$	0.874	0.808	0.330	0.721
MTS9301 Altered	$a_F$	–	$0.006 \pm 0.002$	$0.011 \pm 0.005$	$0.003 \pm 0.002$
	$b_F$	–	$0.28 \pm 0.03$	$0.44 \pm 0.05$	$0.26 \pm 0.05$
	$r^2$	–	0.929	0.949	0.876
TP214	$a_F$	$0.017 \pm 0.007$	$76 \pm 6 \times 10^{15}$	–	–
	$b_F$	$0.29 \pm 0.04$	$7 \pm 1$	–	–
	$r^2$	0.904	0.856	0.532	0.477

The values obtained by fitting the Freundlich model are displayed in Table 5.2. Overall, the C107E Freundlich isotherm fits reasonably well to this data, with iron(II) being the only metal attaining a  $r^2$  value  $< 0.9$  (copper, lead and zinc being 0.947, 0.944 and 0.942, respectively). The relative capacities calculated by this model display the best performance by lead ( $1.1 \pm 0.7$ ) with copper following with  $0.2 \pm 0.1$ , while the value for zinc is meaningless with respect to error. Due to the eventual reduction of metal uptake, the models were also fit to data sets for MTS9301 that were altered so that experimental  $q_e$  is equal to the experimental  $q_{max}$ , for the sake of comparison. The altered data sets for lead and iron(II)

display the best fits to this model ( $r^2$  of 0.949 and 0.929, respectively), with the whole dataset for copper and the altered data set for zinc returning  $r^2$  values of  $<0.9$ . The tentative lowest sorption intensity determined was that of copper ( $0.60\pm 0.07$  and also the highest relative capacity, tentatively), followed by lead with  $0.44\pm 0.05$  and then zinc (again, tentative) and iron(II) with 0.26 and 0.28, respectively. The deleterious nature of the binding of copper(II) to the thiourea functionality has led to an inability of this resin to adsorb any other metal, returning an  $r^2$  of 0.904 for copper (iron(II) being the only other metal with a tentative  $r^2$ , displaying extremely low binding intensity), however with a low relative capacity compared to C107E and MTS9301, and a much higher binding intensity.

**Table 5.3:** Variables obtained by fitting the mixed metal isotherm data of C107E, MTS9301 and TP214 to the Langmuir isotherm model.

Resin	Values	Copper	Iron(II)	Lead	Zinc
C107E	$a_L$	$600\pm 200$	–	$100\pm 200$	–
	$q_m$	$0.0027\pm 0.0006$	–	$0.01\pm 0.01$	–
	$r^2$	0.947	0.639	0.949	0.888
MTS9301	$a_L$	$9\pm 3\times 10^3$	$16\pm 3\times 10^4$	–	$10\pm 3\times 10^4$
	$q_m$	$22\pm 3\times 10^{-4}$	$47\pm 2\times 10^{-5}$	–	$37\pm 2\times 10^{-5}$
	$r^2$	0.919	0.971	0.600	0.885
MTS9301	$a_L$	–	$13\pm 2\times 10^4$	$8700\pm 900$	$8\pm 3\times 10^4$
Altered	$q_m$	–	$49\pm 2\times 10^{-5}$	$43\pm 2\times 10^{-5}$	$40\pm 1\times 10^{-5}$
	$r^2$	–	0.971	0.992	0.878
TP214	$a_L$	$22\pm 7\times 10^5$		–	–
	$q_m$	$11\pm 1\times 10^{-4}$	–	–	–
	$r^2$	0.906	0.241	0.523	0.482

In a similar fashion to the Freundlich isotherm, the Langmuir displays reasonable fits for the adsorption to C107E of both copper and lead ( $r^2$  of 0.947 and 0.949, respectively) (Table 5.3). Due to the low capacity and interactions between this functionality and iron(II) and zinc (observed within the single metal system<sup>[124]</sup>), the values of this fit become meaningless. Lead then displays a

capacity an order of magnitude higher than that of copper, however with lead errors leaving meaningless values ( $0.01 \pm 0.01$  and  $0.0027 \pm 0.0006 \text{ mol g}^{-1}$ , for lead and copper, respectively). The Langmuir model fits the MTS9301 isotherm data for copper and the altered data for iron(II) and lead reasonably well ( $r^2$  0.919, 0.972 and 0.992, respectively), while failing to describe zinc data ( $r^2 < 0.9$ ). The modelled  $q_m$  for copper is  $0.0022 \pm 0.0003 \text{ mol g}^{-1}$ , with the altered data sets following the tentative trend  $\text{Fe} > \text{Pb} > \text{Zn}$  and a tentative trend of  $\text{Pb} < \text{Cu} \ll \text{Zn} \ll \text{Fe}$  for the values of  $a_L$ . TP214 isotherm data, again, fails to describe all data apart from copper; returning the  $q_m$  of copper as  $0.0011 \pm 0.0001 \text{ mol g}^{-1}$ , and a value for  $a_L$  much higher than all other values returned within this study.

**Table 5.4:** Variables obtained by fitting the mixed metal isotherm data of C107E, MTS9301 and TP214 to the Temkin isotherm model.

Resin	Values	Copper	Iron(II)	Lead	Zinc
C107E	$b_t$	$5200 \pm 300$	–	$4600 \pm 300$	$12000 \pm 1000$
	$a_t$	$7600 \pm 500$	–	$7700 \pm 600$	$1900 \pm 200$
	$r^2$	0.973	0.540	0.952	0.895
MTS9301	$b_t$	$4900 \pm 300$	$50000 \pm 7000$	–	–
	$a_t$	$94000 \pm 8000$	$3 \pm 2 \times 10^7$	–	–
	$r^2$	0.959	0.841	0.397	0.396
MTS9301 Altered	$b_t$	–	$46000 \pm 8000$	$25000 \pm 900$	–
	$a_t$	–	$2 \pm 2 \times 10^7$	$80000 \pm 6000$	–
	$r^2$	–	0.819	0.994	0.297
TP214	$b_t$	$16000 \pm 2000$	$7200 \pm 900$	–	–
	$a_t$	$10 \pm 6 \times 10^7$	$34 \pm 4 \times 10^{-5}$	–	–
	$r^2$	0.868	0.898	0.523	0.487

The Temkin model displays the best fits for C107E adsorption copper and lead, with  $r^2$  0.973 and 0.952, respectively while zinc displays a tentative fit ( $r^2$  0.895) and iron(II) is not described at all (Table 5.4); the tentative trend in binding energy values following  $\text{Pb} > \text{Cu} \gg \text{Zn}$ . This model fits the data for MTS9301 is again, unable to fit the data for iron(II) or zinc (altered datasets), with copper and the

altered lead dataset fitting reasonably well ( $r^2$  0.959 and 0.994, respectively). Lead adsorption returned a much higher binding energy than copper, far more pronounced than what was observed within a single metal system<sup>[124]</sup>. This model fits the copper TP214 data poorly ( $r^2$  0.868) better describing the data for iron(III), however still tentative ( $r^2$  0.898).

**Table 5.5:** Variables obtained by fitting the mixed metal isotherm data of C107E, MTS9301 and TP214 to D-R isotherm model.

Resin	Values	Copper	Iron(II)	Lead	Zinc
C107E	$q_D$	$0.011 \pm 0.003$	–	$0.028 \pm 0.008$	$0.019 \pm 0.009$
	$B_D$	$84 \pm 8 \times 10^{-10}$	–	$106 \pm 8 \times 10^{-12}$	$17 \pm 2 \times 10^{-9}$
	Energy	$7700 \pm 400$	–	$6900 \pm 300$	$5400 \pm 300$
	$r^2$	0.936	0.528	0.957	0.940
MTS9301	$q_D$	$0.015 \pm 0.004$	$8 \pm 1 \times 10^{-4}$	–	–
	$B_D$	$52 \pm 6 \times 10^{-10}$	$15 \pm 2 \times 10^{-10}$	–	–
	Energy	$9800 \pm 600$	$19 \pm 2 \times 10^3$	–	–
	$r^2$	0.890	0.861	0.381	0.768
MTS9301 Altered	$q_D$	–	$14 \pm 2 \times 10^{-4}$	$16 \pm 3 \times 10^{-4}$	$10 \pm 2 \times 10^{-4}$
	$B_D$	–	$21 \pm 2 \times 10^{-10}$	$41 \pm 4 \times 10^{-10}$	$22 \pm 4 \times 10^{-11}$
	Energy	–	$15000 \pm 800$	$11000 \pm 600$	$15000 \pm 1000$
	$r^2$	–	0.950	0.964	0.892
TP214	$q_D$	$34 \pm 7 \times 10^{-4}$	$2 \pm 8 \times 10^5$	–	–
	$B_D$	$20 \pm 3 \times 10^{-10}$	$9 \pm 1 \times 10^{-8}$	–	–
	Energy	$16 \pm 1 \times 10^3$	$2400 \pm 200$	–	–
	$r^2$	0.915	0.858	0.530	0.480

The D-R isotherm fits well to the adsorption of copper, lead and zinc to C107E ( $r^2$  of 0.936, 0.957 and 0.940), while fitting poorly to iron(II) (Table 5.5). In a similar fashion to the Langmuir isotherm C107E displays the highest capacity for lead, then showing capacities for Zn > Cu, with free energies of binding displaying returning the trend Cu > Pb > Zn. For MTS9301, the D-R model fits reasonably well to the altered data sets of iron(II) and lead, with both copper and zinc displaying  $r^2$  of  $\sim 0.89$ ; while the  $q_D$  values being a reasonable estimate for

copper experimental adsorption maximum, this value was a far over estimation for iron(II), lead and zinc. The free energies of adsorption return iron(II) and zinc as the strongest binding species to this functionality, followed by lead then copper. This model again only fit tentatively to copper, with iron(II)  $r^2$  being  $<0.9$  and the iron(II) capacity being nonsensical; the capacity for copper is returned as  $0.0034 \pm 0.0007 \text{ mol g}^{-1}$ , which is beyond that recorded, however the free energy of adsorption is a reasonable value ( $16 \pm 1 \text{ kJ mol}^{-1}$ ).

The intensity of binding of copper to C107E was much lower than that observed in the single metal system, at 0.76 (versus 0.51)<sup>[124]</sup>, leading to the assumption of competition causing a more heterogeneous binding mechanism; this is observable in the experimental data, with the almost two stage adsorption isotherm profile. The weaker binding intensity is then reflected within the D-R isotherm, with energies of binding within the multi-metal system being  $0.7 \text{ kJ mol}^{-1}$  lower than they are within the single metal system ( $7.7 \pm 0.4 \text{ kJ mol}^{-1}$  vs  $8.4 \pm 0.4 \text{ kJ mol}^{-1}$ ); this comparison is again compounded by the large difference in Temkin binding energies ( $5.2 \pm 0.3 \text{ kJ mol}^{-1}$  vs  $2.8 \pm 0.2 \text{ kJ mol}^{-1}$ ), better describing the later metal-metal exchange lending to its ability to describe heterogeneous mechanisms<sup>[124]</sup>. The adsorption of copper to MTS9301 displays a more intense binding mechanism than C107E, at  $0.60 \pm 0.07$ , however, is ill-described by the Freundlich model in this instance.

The more heterogeneous binding reported for multi-metal MTS9301 copper adsorption (although tentative) could be explained by the metal-metal exchange as opposed to proton-metal exchange as saturation increases, and again, although tentative, is evidenced by the decrease in binding energy with comparison to the single metal system ( $9.8 \pm 0.6 \text{ kJ mol}^{-1}$  vs  $14 \pm 1 \text{ kJ mol}^{-1}$ <sup>[124]</sup>). With respect to TP214, the intensity for both mixed metal and single metal isotherms is large (0.29 and 0.17, respectively, however fitting slightly better within a mixed metal system), again alluding the irreversible redox reaction. This is

further justified by the large energy of binding that remains, with  $16 \pm 1 \text{ kJ mol}^{-1}$  remaining close to an energy related to chemisorption. For both C107E and MTS9301, the multi-metal capacity of copper was seen to decrease ( $5 \pm 1$  to  $2.7 \pm 0.6 \text{ mmol g}^{-1}$  and  $4.3 \pm 0.7$  to  $2.2 \pm 0.3 \text{ mmol g}^{-1}$ , respectively). TP214 displayed a seemingly increased capacity with comparison of the D-R isotherm capacities ( $1.9 \pm 0.1$  to  $3.4 \pm 0.7 \text{ mmol g}^{-1}$ ), however this is inclusive of a large extrapolation, and the multi-metal Langmuir capacity is much closer to the value obtained without competitive sorption.

The multi-metal isotherm results for the adsorption of iron(II) to C107E fit neither Freundlich nor Langmuir (potentially due to the scatter in data), however adsorption to MTS9301 does display a better fit towards the Langmuir model. This species displays highly homogeneous binding towards the MTS9301 iminodiacetic acid functionality within a mixed metal system, although, the capacity is decreased severely due to desorption and competition with copper towards higher volumes ( $0.47 \pm 0.02 \text{ mmol g}^{-1}$  vs  $2.3 \pm 0.8 \text{ mmol L}^{-1}$  in the single metal system (Chapter 4)). The poor performance of the TP214 resin is attributed to the deleterious nature of the copper binding, and is therefore excluded from the remaining isotherm discussion.

The adsorption of lead to C107E displays a reasonable fit to both Langmuir and Freundlich adsorption models, however the binding intensity is extremely low (0.98), leading to the assumption of heterogeneous adsorption. This heterogeneity is also observed within the single metal system, both displaying low free energies of adsorption, close to that indicative of physisorption. Similarly to the copper system, the binding of lead to C107E also displays two distinct adsorption curves within the adsorption profile, seemingly a 'before and after' competition between metals for binding sites, supporting this higher level of heterogeneity in the adsorption intensity. While the multi-metal data for the adsorption of lead to MTS9301 does display a better fit to the Langmuir model,



the intensity of binding returned by the Freundlich model suggests a more heterogeneous binding mechanism (more so than the single metal system). The free energies of single and multi-metal fits display overlapping errors ( $\sim 11 \text{ kJ mol}^{-1}$ ), however the reduced dataset reveals a much lower capacity than the single metal capacity for lead in the presence of copper competition ( $0.43 \pm 0.02 \text{ mmol g}^{-1}$  vs  $2.1 \pm 0.2 \text{ mmol g}^{-1}$ ).

Within this study, the adsorption of zinc to C107E was poorly modelled due to its low interaction with the functionality, also observed within the single metal system<sup>[124]</sup>. Again, zinc adsorption to MTS9301 was poorly modelled ( $r^2 < 0.9$ ), however from what information was attained: binding intensity was similar between the multi-metal and single metal systems, however the multi-metal system displays a severely hindered monolayer capacity ( $3 \pm 1$  for the single metal system vs  $0.40 \pm 0.04 \text{ mmol L}^{-1}$  for the multi-metal system). The energies of binding determined by fitting the zinc adsorption to both C107E and MTS9301 (altered datasets) returned free energies of binding within error for both the single and multi-metal systems.

### **Multimetal Modelling**

Due to the competitive nature of the binding of metals to each resin surface, lower capacities and, in the case of MTS9301, desorption is observed. Not one of the above single metal isotherm models are capable of predicting the level of desorption/competition observed in the multi-metal system. There have been multiple attempts to model these interactions in the past for two metals or more<sup>[191–193]</sup>, however there are a few difficulties with the modelling of these systems, especially considering the level of saturation and desorption observed in this study. With the use of an extended Langmuir<sup>[193]</sup> it is possible to fit and obtain data from multi-metal isotherms with infinite species, however this model does not predict a system that displays high levels of desorption, relying on initial

fits to single metal isotherm models.

Modification of the Langmuir model in order to describe the desorption phenomena observed within this study, can give insight into the operational  $q_{max}$  of the resin for each metal. Due to the parabolic nature of a saturated multi-metal isotherm, it is possible to add a parameter to describe this trend. The desorption of one metal in place of another metal will be attempted to be described by the inclusion of such a parameter, with:

$$q_e = \frac{q_m a_L C_e}{1 + a_L C_e} - des C_e^{des} \quad (5.2)$$

where  $des$  is an arbitrary parameter describing the concentration dependent extent of desorption. While this does not take into account interactions of specific metals, it is able to model a system with high competition between species and a large affinity for one species over many other. The inclusion of a secondary parameter could allow for a better fit to each dataset, however the more parameters included within a function, the more difficulty there is in the assigning meaning to the parameter, therefore going forward this desorption-modified Langmuir will be used to describe metallic capacities.

**Table 5.6:** Variables obtained by fitting the mixed metal concentration dependence data of C107E and MTS9301 to the desorption-modified Langmuir isotherm model.

Resin	Values	Copper	Iron(II)	Lead	Zinc
C107E	$a_L$	$1700 \pm 500$	$12000 \pm 5000$	$1000 \pm 300$	–
	$q_m$	$21 \pm 1 \times 10^{-4}$	$40 \pm 6 \times 10^{-5}$	$30 \pm 5 \times 10^{-4}$	–
	$des$	$0.0003 \pm 0.0001$	$1.39 \pm 0.07$	$27 \pm 8 \times 10^{-5}$	–
	$r^2$	0.983	0.790	0.982	0.936
MTS9301	$a_L$	$6 \pm 3 \times 10^4$	$13 \pm 2 \times 10^4$	$6600 \pm 600$	$26 \pm 6 \times 10^4$
	$q_m$	$28 \pm 6 \times 10^{-4}$	$49 \pm 3 \times 10^{-5}$	$51 \pm 2 \times 10^{-5}$	$41 \pm 3 \times 10^{-5}$
	$des$	$0.0012 \pm 0.0007$	$1.4 \pm 0.1$	$1.37 \pm 0.01$	$1.6 \pm 0.1$
	$r^2$	0.965	0.976	0.990	0.912

Due to the negligible adsorption shown by iron(II), lead and zinc, this model was not used to describe the data for TP214, with the fits of this proposed model for all metals to both C107E and MTS9301 being reported in Table 5.6. The isotherm data of C107E adsorption for copper and lead fit well to the desorption modified Langmuir isotherm ( $r^2$  values of 0.999 and 0.987, respectively), however due to high scatter in the iron(II) adsorption data and low interactions between this functionality and zinc, these data were not reasonably described by the model (returning poor  $r^2$  values or high errors). MTS9301 data, on the other hand, displayed more positive results when fit to the desorption-modified Langmuir model, with all complete data sets being adequately described and the  $r^2$  of each being improved relative to the Langmuir model (returning  $r^2$  values of 0.965, 0.976, 0.990 and 0.912 for copper, iron(II), lead and zinc, respectively).

The  $q_m$  for copper adsorption to C107E calculated by the desorption-modified Langmuir model are more realistic than those determined by the normal Langmuir model, however involve extrapolation. In the case of the adsorption of copper by MTS9301, the  $q_m$  value involved further extrapolation than the normal Langmuir model ( $2.8 \pm 0.8$  vs  $2.2 \pm 0.3 \text{ mmol g}^{-1}$ ), the desorption-modified Langmuir being closer to the single metal value ( $4.3 \pm 0.7 \text{ mmol g}^{-1}$ ). In both cases, there is an observable increase in adsorbed species beyond the scope of the study, with each adsorption profile displaying almost a 'two-stage' adsorption process; this process includes an initial exchange between proton-metal species, then there is a distinct transition to a metal-metal exchange as the surface of the resin is saturated with less selective species. With the low desorption constants obtained by copper ( $\text{des} \ll 1$ ) it can be assumed that in both cases copper is not observed to undergo desorption; while C107E also displays negligible desorption towards lead, copper is the only species with negligible desorption towards MTS9301.

The poor fit for C107E adsorption of iron(II) to the desorption-modified Langmuir model, assumed to be due to the large amount of scatter towards the

higher volumes, leaves any discussion very tentative and therefore will not be considered further. Fitting to the MTS9301 iron(II) isotherm, however provides a very reasonable fit, and provides an excellent prediction of the experimental  $q_m$  ( $0.482 \pm 0.009 \text{ mmol L}^{-1}$ ) with a calculated  $q_m$  of  $0.49 \pm 0.03 \text{ mmol g}^{-1}$ . This gives a desorption constant of  $1.4 \pm 0.1$ , which is three orders of magnitude higher than copper, giving a numerical value to the level of competition/desorption observed between iron(II) and the other metals.

Following on from this, the capacity of C107E for lead within the mixed metal system predicted by the desorption-modified Langmuir model is far extrapolated from experimental data, while also displaying a far higher capacity than the single metal data; however in both cases, typical saturation is not reached, and therefore the experimental capacity is not determined. C107E does display a high affinity for lead, while even though there is nothing particularly outstanding with regards to the free energy of adsorption, this metal displayed the lowest desorption constant. The adsorption to MTS9301, however, did display observable desorption, falling within error of iron(II) and less than zinc ( $1.4 \pm 0.1$  for iron(II) vs  $1.37 \pm 0.01$  for lead and  $1.6 \pm 0.1$  for zinc). The lead  $q_m$  predicted by this model ( $0.51 \pm 0.02 \text{ mmol g}^{-1}$ ) is outside error margins of the experimentally observed ( $0.356 \pm 0.003 \text{ mmol L}^{-1}$ ).

Similarly to iron(II), the data for the adsorption of zinc to C107E did not return meaningful results, due to weak interactions<sup>[124]</sup>. Zinc adsorption to MTS9301 returns a great fit to this model, with a modelled  $q_m$  within error of the experimentally observed value ( $0.320 \pm 0.002$ , experimental, vs  $0.41 \pm 0.03 \text{ mmol g}^{-1}$ , modelled). Zinc, however, displays the highest level of desorption from this resin, with a desorption constant of  $1.6 \pm 0.1$ , leaving it to be the most likely to be hindered by competition between other species, such as calcium or iron, both of which are in high abundance within sewage sludge<sup>[194]</sup>. For both zinc and lead, the high levels of desorption from MTS9301 seem to be

due to the small  $\Delta S$  values of the acetate complex formation with regards to those of copper (Figure C.9b).

While this model was capable of describing those species that were desorbed from a functionality, it was less capable of modelling the change in mechanism that occurs due a shift from metal-proton exchange to metal-metal exchange, as observed in the case of the isotherm of copper and lead for C107E or copper for MTS9301. On top of this, the molar ratio of each metallic species in solution will have a large effect on the overall values obtained as this is very reliant on equilibrium. In summary, this model was able to describe the data obtained in this specific experiment and is very situational, however comparison of similar experimental conditions could make the information viable.

## **Kinetics**

The kinetic data obtained displays typical extraction kinetic trend for both C107E and MTS9301, in both cases an equilibrium adsorption is reached, with MTS9301 displaying much faster kinetics than C107E. Whether this difference is due to the affinity of each resin to the metals or the similarity of the C107E functionality to the buffering acids will be discussed throughout this section. TP214, however, rejects all other metals in favour of copper beyond  $\sim 10$ min. This is hypothesised to be due to the redox reaction that has been observed in previous studies, and will be discussed as to whether it is kinetically beneficial or not.

## **Diffusion Limiting Steps**

The first rate limiting step to consider, and perhaps the easiest to visualise, is the diffusion limiting step. The diffusion kinetics of adsorption of a species to a resin can be limited by particle diffusion, where a species is limited by a concentration gradient formed within the bead or limited by the diffusion through

a Nernst film later that surrounds the resin's surface. To determine the most likely situation, two models (aptly named particle- or pore-diffusion model and film-diffusion model) have been devised in order to describe the system.

Particle, intra-particulate or pore diffusion, involves kinetic limitation by the formation of a concentration gradient within the resin bead. This gradient can be dictated by multiple factors such as pore size, resin structure, backbone composition and functionality/co-ion interactions. The particle or pore diffusion model describes adsorption kinetics limited by this diffusion of species within the particulate pores<sup>[195–197]</sup>, described by:

$$q_t = k_{PD}t^{\frac{1}{2}} + C \quad (5.3)$$

Where  $k_{PD}$  ( $\text{mmol.g}^{-1}.\text{min}^{-\frac{1}{2}}$ ) and  $C$  is a constant related to the boundary layer thickness<sup>[197]</sup>; the larger the value of  $C$ , the greater the boundary layer effect<sup>[198]</sup>.

**Table 5.7:** Non-linear kinetic modelling data for the particle diffusion model for acetic acid media.

ResinI	Value	Copper	Iron	Lead	Zinc
C107E	$K_{PD}$	$16 \pm 2 \times 10^{-3}$	$23 \pm 1 \times 10^{-4}$	$48 \pm 9 \times 10^{-7}$	$7 \pm 1 \times 10^{-3}$
	$C$	$0.04 \pm 0.03$	$-0.004 \pm 0.002$	$5 \pm 2 \times 10^{-5}$	$0.03 \pm 0.02$
	$r^2$	0.883	0.968	0.741	0.824
MTS9301	$K_{PD}$	–	$71 \pm 7 \times 10^{-4}$	$11.9 \pm 0.6 \times 10^{-5}$	$0.001 \pm 0.002$
	$C$	–	$0.02 \pm 0.01$	$4 \pm 1 \times 10^{-5}$	$0.07 \pm 0.03$
	$r^2$	0.589	0.916	0.792	0.840
TP214	$K_{PD}$	–	–	–	–
	$C$	–	–	–	–
	$r^2$	0.685	0.151	0.094	0.046

Efficient agitation of solution and large pore size can prevent the formation of concentration gradients, the surface of a resin bead will maintain a stagnant

film, especially considering the charged nature of ion exchange resins. This film prevents direct contact of fresh solution, generating a one dimensional diffusion process in order for contact to be made between the adsorbate and adsorbent. Diffusion through this layer is purely determined by concentration gradient between the stagnant film and the bulk solution<sup>[195]</sup>. The film diffusion model describes adsorption kinetics dictated by diffusion of species through a liquid film at this particle-solution interface (Nernst diffusion layer)<sup>[195,196]</sup>. It can be described by:

$$\log(1 - F(t)) = -\frac{k_{FD}t}{2.303} \quad (5.4)$$

where  $k_{FD}$  is the film diffusion kinetic constant  $F(t)$  is the fraction of adsorbed species at time  $t$  to the equilibrium adsorbed species ( $q_e$ , mol.g<sup>-1</sup>), determined by:

$$F_t = \frac{q_t}{q_e} \quad (5.5)$$

By substituting equation (5.4) into equation (5.5), this equation can be rearranged in order to make  $q_t$  the subject, creating the equation:

$$q_t = q_e(1 - e^{k_{FD}t/2.303}) \quad (5.6)$$

The fits of the C107E kinetic data to the particle diffusion model were fairly poor overall (Table 5.7), with copper, lead and zinc producing  $r^2$  values of <0.89, while iron(II) achieved a reasonable  $r^2$  of 0.968; with the film diffusion kinetic model (Table 5.8) describing the kinetic trend of all metals better. The macroporous structure of the resin bead is the assumed cause for the alluded film diffusion mechanism, as there are no particle kinetic bottle-necks in the adsorption process. This is supported by the film-diffusion calculated  $q_e$  values of each metal being reasonable estimations (within error or 10%) of the experimental values. The reaction rate trend, derived by this model, follows Pb > Zn > Cu > Fe.

**Table 5.8:** Non-linear kinetic modelling data for the film diffusion model for acetic acid media.

Resin	Value	Copper	Iron	Lead	Zinc
C107E	$q_e$ exp	$0.52 \pm 0.01$	$0.082 \pm 0.001$	$0.184 \pm 0.003$	$0.23 \pm 0.005$
	$K_{FD}$	$18 \pm 2 \times 10^{-3}$	$35 \pm 7 \times 10^{-4}$	$60 \pm 9 \times 10^{-3}$	$23 \pm 2 \times 10^{-3}$
	$q_e$	$0.49 \pm 0.01$	$0.092 \pm 0.001$	$0.171 \pm 0.006$	$0.223 \pm 0.006$
	$r^2$	0.989	0.977	0.965	0.987
MTS9301	$q_e$ exp	$0.45 \pm 0.01$	$0.234 \pm 0.003$	$0.134 \pm 0.002$	$0.381 \pm 0.008$
	$K_{FD}$	$113 \pm 9 \times 10^{-3}$	$14 \pm 2 \times 10^{-3}$	$7 \pm 1 \times 10^{-2}$	$35 \pm 6 \times 10^{-3}$
	$q_e$	$0.439 \pm 0.008$	$0.223 \pm 0.008$	$0.119 \pm 0.006$	$0.34 \pm 0.01$
	$r^2$	0.986	0.983	0.918	0.958
TP214	$q_e$ exp	$0.641 \pm 0.003$	$106 \pm 3 \times 10^{-4}$	$264 \pm 3 \times 10^{-4}$	$261 \pm 7 \times 10^{-4}$
	$K_{FD}$	$43 \pm 4 \times 10^{-3}$	–	–	$0.3 \pm 0.1$
	$q_e$	$0.631 \pm 0.01$	–	–	$94 \pm 8 \times 10^{-3}$
	$r^2$	0.990	0.542	0.783	0.691

Similarly to C107E, MTS9301 displays poor fits to the particle diffusion model (copper, lead and zinc  $r^2 < 0.9$ ), with iron(II) displaying a slightly better fit than the other metals; again with all metals fitting much better to the film diffusion model, with the  $r^2$  of lead falling behind the other metals. Again, this model generates good estimates (within error or 10%) of the experimental  $q_e$  values. The MTS9301 resin displays a reaction rate trend of  $\text{Cu} > \text{Pb} > \text{Zn} > \text{Fe}$ . TP214 only returned fitted data for the copper(II) ion, and again this ion follows a film-diffusion limited kinetic profile. The macroporous nature of the TP214 resin matrix lowers the possibility of a concentration gradient/limitation by a concentration gradient. The assumed covalently binding nature of this ion to the thiourea functionality is further alluded to by the low kinetic hindrance generated by the Nernst film layer.

## Desorption

Within adsorption processes solution phase complexation, adsorption equilibrium and competitive species can all effect the reaction rate. The Elovich model can model systems such as this by its ability to describe a system where



chemical adsorption is observed on a heterogeneous surface, or by its ability to describe an ion exchange interaction with both adsorption and desorption occurring in parallel<sup>[199]</sup>. The equation for this model is as follows<sup>[200]</sup>:

$$q_t = \frac{1}{\beta} \ln\left(t + \frac{1}{\alpha\beta}\right) + \frac{1}{\beta} \ln \frac{1}{\alpha\beta} \quad (5.7)$$

In this model,  $\beta$  is the desorption constant ( $\text{g mol}^{-1}$ ) and the parameter  $\alpha$  is the initial sorption rate of the reaction ( $\text{mol/gmin}$ )<sup>[201]</sup>. This analysis of desorption processes will be extremely relevant with the discussion of this buffered system.

**Table 5.9:** Non-linear kinetic modelling data for the Elovich model for acetic acid media.

Resin	Value	Copper	Iron	Lead	Zinc
C107E	$\alpha$	$9 \pm 2 \times 10^{-3}$	$1.8 \pm 0.3$	$18 \pm 7 \times 10^{-3}$	$6 \pm 2 \times 10^{-3}$
	$\beta$	$8.3 \pm 0.6$	$23 \pm 5$	$33 \pm 3$	$20 \pm 2$
	$r^2$	0.986	0.975	0.965	0.963
MTS9301	$\alpha$	$0.2 \pm 0.2$	$34 \pm 5 \times 10^{-4}$	$19 \pm 3 \times 10^{-3}$	$18 \pm 3 \times 10^{-3}$
	$\beta$	$17 \pm 2$	$18 \pm 1$	$51 \pm 2$	$14.6 \pm 0.8$
	$r^2$	0.930	0.991	0.992	0.989
TP214	$\alpha$	$0.04 \pm 0.02$	–	–	–
	$\beta$	$8 \pm 1$	–	–	–
	$r^2$	0.920	0.384	0.461	0.374

Using the Elovich equation to describe the kinetic data obtained from the C107E experiment, copper, iron(II), lead and zinc reach a  $r^2 > 0.96$  (Table 5.9). Copper, lead and zinc show the highest rates of adsorption with this model, with iron(II) falling behind by an order of magnitude, displaying the trend  $\text{Pb} > \text{Cu} > \text{Zn} \gg \text{Fe}$ . The trend in rates of desorption, however, does not reflect this adsorption rate trend, with zinc and iron(II) achieving higher rates than copper, creating the series  $\text{Pb} \gg \text{Fe} > \text{Zn} > \text{Cu}$ .

MTS9301 kinetics returned reasonable fits to the Elovich model ( $r^2 \sim 0.99$ ) for iron(II), lead and zinc, however displaying more tentative fits to copper (Table 5.9). The initial rate of adsorption recorded is, in general, much higher than that of C107E, leading to a rate trend of  $\text{Cu} \gg \text{Pb} = \text{Zn} \gg \text{Fe}$ . The constant  $\beta$  displays a trend of  $\text{Pb} \gg \text{Fe} > \text{Cu} > \text{Zn}$ , countering the relatively high adsorption rate of lead. Again, fitting the TP214 kinetic data to the Elovich model generated extremely poor fits to all metals, apart from copper. While the initial rate of copper adsorption is lower than that of MTS9301, it has a much lower rate of desorption, which may contribute to an overall fast adsorption rate. C107E on the other hand, shows a similar desorption rate, with a much slower initial rate of adsorption.

The adsorption of copper to MTS9301 displays the same desorption constant as iron(II) with this constant being lower than lead, however higher than that of zinc. C107E returned the least desorption with respect to all resins studied, while also returning the lowest binding energy,  $8.4 \pm 0.4 \text{ kJ mol}^{-1}$  (physisorption/ion exchange) and lowest binding intensity. MTS9301, while displaying the highest desorption constant for copper, also displays the (tentative) highest initial rate of adsorption ( $0.2 \pm 0.2 \text{ mmol/g min}$ ) and also a free energy adsorption energy of  $14 \pm 1 \text{ kJ mol}^{-1}$  (in an unsaturated situation) and a much higher binding intensity (Chapter 4); far beyond that of the C107E resin. The high intensity of adsorption and binding energy could be causing the high initial rate of adsorption, while the  $\text{CuAc}_3^-$  (a species becoming more prominent in solution at this pH), however, is much more stable than the  $\text{CuAc}_2$  ( $\log \beta$  3.30 vs 2.80) leading to the assumption of the potential for a second slower adsorption process by the second species.

Rates of desorption for the theorised redox reaction of copper to TP214 were much lower than the previous two resins, returning a binding energy of  $17 \pm 1 \text{ kJ mol}^{-1}$  (chemisorption) and a binding intensity of 0.17, being the closest of all systems studied of all metals to being irreversible (Chapter 4). The extraction of copper by TP214 seems to not only be a reduction reaction for the copper(II)

species, but it also seems to be deleterious for the thiourea functionality. Beyond a time of  $\sim 150$  min the extraction of all metals other than copper is severely hindered. This level of selectivity of copper over iron(II), lead and zinc is not represented by either the intensity of binding or the adsorption energies returned from the isotherm models, therefore these metals will not be considered with respect to TP214.

The desorption of iron(II) from the carboxylic acid functionality is higher than that of the desorption from the iminodiacetic acid functionality, despite the much lower initial rate. This can be rationalised by the chelating nature of the iminodiacetic acid functionality, also supported by the higher intensity and binding energy returned from the isotherm models<sup>[124]</sup>. The lack of data and low stability constant for the ferrous acetate complex<sup>[126]</sup> lead to the assumption of low interactions between carboxylic acid functionalities and iron(II).

The stability constant for  $\text{PbAc}_2$  is quite large in comparison to the  $\text{PbAc}^+$  constant<sup>[126]</sup>, leading to an assumption of a weaker interaction between lead and a singular carboxylic acid functionality. Lead, however, displays a trend counter to this assumption, with a lower desorption (although still high) for the carboxylic acid functionality over the iminodiacetic acid functionality, both displaying similar rates of adsorption. The ionic radii of lead is a hindrance when it comes to the iminodiacetic acid, as the two charges have limited mobility, this could lead to a higher stability as acetate complexes in solution, therefore leading to the higher desorption constant. The weak interaction between lead and the carboxylic acid functionality (Chapter 4), due to the low effective charge, coupled with the high stability of the  $\text{PbAc}_2$  species over  $\text{PbAc}^+$  are the speculative cause for desorption after initial spikes in reaction kinetics.

Zinc displays the lowest desorption constant for MTS9301 of all the metals, with  $14.6 \pm 0.8 \text{ g mol}^{-1}$ , and an initial rate similar to that of lead. As the adsorption

of metals by the MTS9301 functional group is dependent of the ionic radii, giving zinc similar properties to copper, which is consistent with the binding energies and intensities (Chapter 4). The desorption constant calculated for zinc towards C107E is similar to that of iron(II).

### Rate Orders

Using the previous factors as supplementary information, the adsorption mechanisms can be classified into a rate order and performance (half-life and rates) can be determined. A first order reaction rate is a description of a reaction reliant on the concentration of a singular species; with the assumption of the excess of all other species, this can be fit to other reactions, creating a pseudo-first order kinetic reaction. The Lagergren pseudo-first order model is derived from the fundamental first-order kinetic law in order to describe liquid-solid adsorption reactions<sup>[202]</sup>, where the value of ' $k_1 q_e - q_t$ ' is non-representative the number of binding sites<sup>[203]</sup>. The Lagergren first-order law can be described as<sup>[201]</sup>:

$$q_t = q_e(1 - e^{-k_1 t}) \quad (5.8)$$

In this instance  $q_e$  is the equilibrium concentration of ion on the resin surface ( $\text{mmol g}^{-1}$ ) and ' $k_1$ ' ( $\text{sec}^{-1}$ ) is the pseudo-first order rate coefficient of this specific reaction<sup>[203]</sup>. Utilising this, the pseudo-first order half-life can be determined:

$$\frac{0.693}{k_1} \quad (5.9)$$

**Table 5.10:** Non-linear kinetic modelling data for the Lagergren model for acetic acid media.

Resin	Value	Copper	Iron	Lead	Zinc
C107E	$q_e$ exp	$0.52 \pm 0.01$	$0.082 \pm 0.001$	$0.184 \pm 0.003$	$0.23 \pm 0.005$
	$q_e$ mod	$0.49 \pm 0.01$	$0.092 \pm 0.009$	$0.171 \pm 0.006$	$0.223 \pm 0.006$
	$k_{1st}'$	$79 \pm 8 \times 10^{-4}$	$15 \pm 3 \times 10^{-4}$	$26 \pm 4 \times 10^{-3}$	$10 \pm 1 \times 10^{-3}$
	$t_{1/2}$	$88 \pm 9$	$450 \pm 80$	$27 \pm 4$	$68 \pm 7$
	$r^2$	0.989	0.977	0.965	0.987
MTS9301	$q_e$ exp	$0.45 \pm 0.01$	$0.234 \pm 0.003$	$0.134 \pm 0.002$	$0.381 \pm 0.008$
	$q_e$ mod	$0.439 \pm 0.008$	$0.223 \pm 0.008$	$0.119 \pm 0.006$	$0.35 \pm 0.01$
	$k_{1st}'$	$49 \pm 4 \times 10^{-3}$	$62 \pm 7 \times 10^{-4}$	$30 \pm 6 \times 10^{-3}$	$15 \pm 3 \times 10^{-3}$
	$t_{1/2}$	$14 \pm 1$	$110 \pm 10$	$23 \pm 5$	$46 \pm 8$
	$r^2$	0.986	0.983	0.918	0.958
TP214	$q_e$ exp	$0.641 \pm 0.003$	$106 \pm 3 \times 10^{-4}$	$263 \pm 3 \times 10^{-4}$	$261 \pm 7 \times 10^{-4}$
	$q_e$ mod	$0.631 \pm 0.01$	–	–	–
	$k_{1st}'$	$19 \pm 2 \times 10^{-3}$	–	–	–
	$t_{1/2}$	$37 \pm 3$	–	–	–
	$r^2$	0.990	0.542	0.783	0.691

Fitting the Lagergren kinetic model to the C107E data displayed  $r^2$  values of 0.989, 0.977, 0.965 and 0.987 for copper, iron(II), lead and zinc, respectively (Table 5.10); however, only copper and zinc display predicted  $q_e$  values within experimental error, while lead is within 10% of the experimental value, iron(II) is outside this margin and this displays a half-life trend of  $Pb < Zn < Cu \ll Fe$ . The Lagergren model for the kinetic data associated with MTS9301 produced reasonable fits for copper, iron(II) and zinc ( $r^2 > 0.95$ ) with a poorer fit for the lead data at  $r^2$  0.918, with the predicted  $q_e$  values being within error for copper, iron(II) and lead, while the predicted value for zinc is only within 10% of the experimental value. The MTS9301 trend for the Lagergren half-lives predicted by the Lagergren model is  $Cu < Pb < Zn \ll Fe$ , with the copper adsorption to TP214 half-life being only  $14 \pm 1$  minutes. Similarly to all other cases, copper is the only data described by the model, with error margins of the modelled  $q_e$  value encompassing the experimental value.

As the first-order rate law was a model describing a reaction limited by one species, a second-order reaction is limited by two species, and is therefore more complicated. While, in theory, a reaction may only have two reactants and therefore the concentration of these two reactants may be assumed to control a reaction's kinetics, in reality both products and reactants effect the equilibrium of a reaction as well as other side-reactions occurring within a complex system. In this case the order of reaction is difficult to understand, and therefore assuming a negligible influence of other reactions within a system allows for the calculation of a pseudo-second order reaction to be modelled.

The Ho pseudo-second order model<sup>[201,203]</sup>, an adsorption modified derivation of the second order rate law, can be described by:

$$q_t = \frac{q_e^2 k_{2nd} t}{1 + q_e k_{2nd} t} \quad (5.10)$$

where  $q_e$  is the sorption at equilibrium and  $k_{2nd}$  is the pseudo-second order rate constant ( $\text{g.mol}^{-1}.\text{min}^{-1}$ ). From the parameters acquired by the fitting of this model, it is also possible to attain the initial rate of reaction ( $h_0$ ) and the half-life of the reaction with the equations (5.11) and (5.12), respectively.

$$h_0 = k_{2nd}q_e^2 \quad (5.11)$$

$$\frac{1}{k_{2nd}q_e} \quad (5.12)$$

**Table 5.11:** Non-linear kinetic modelling data for the Pseudo-second order model for acetic acid media.

Resin	Value	Copper	Iron	Lead	Zinc
C107E	$q_e$ exp	0.52±0.01	0.082±0.001	0.184±0.003	0.23±0.005
	$q_e$ mod	0.562±0.008	0.13±0.02	0.185±0.004	0.251±0.008
	$k_{2nd}$ '	16±1×10 <sup>-3</sup>	9±3×10 <sup>-4</sup>	0.184±0.2	50±8×10 <sup>-3</sup>
	$t_{1/2}$	105±6	800±400	29±3	80±10
	$h_0$	54±4×10 <sup>-7</sup>	16±7×10 <sup>-8</sup>	63±7×10 <sup>-7</sup>	32±5×10 <sup>-7</sup>
	$r^2$	0.998	0.976	0.991	0.989
MTS9301	$q_e$ exp	0.45±0.01	0.234±0.003	0.134±0.002	0.381±0.008
	$q_e$ mod	0.464±0.005	0.257±0.007	0.128±0.004	0.380±0.009
	$k_{2nd}$ '	0.153±0.009	0.029±0.003	0.31±0.06	0.054±0.007
	$t_{1/2}$	14.1±0.9	133±17	25±5	49±6
	$h_0$	32±2×10 <sup>-3</sup>	1.9±0.2	52±9×10 <sup>-4</sup>	8±1×10 <sup>-3</sup>
	$r^2$	0.997	0.994	0.973	0.990
TP214	$q_e$ exp	0.641±0.003	106±3×10 <sup>-4</sup>	264±3×10 <sup>-4</sup>	261±7×10 <sup>-4</sup>
	$q_e$ mod	0.69±0.02	–	–	–
	$k_{2nd}$ '	0.035±0.006	–	–	–
	$t_{1/2}$	41±7	–	–	–
	$h_0$	17±3×10 <sup>-3</sup>	–	–	–
	$r^2$	0.983	0.476	0.677	0.572

For the adsorption of copper and lead to C107E, the pseudo-second order model displayed better  $r^2$  values than the Lagergren model, while iron(II) and

zinc fit slightly better to the Lagergren (Table 5.11 and 5.10, respectively) with corresponding  $q_e$  predictions reinforcing this. The calculated half-lives of the pseudo-2nd order model are larger than the Lagergren model, however displaying the same trend, with the initial rates displaying the trend  $Pb > Cu > Zn >> Fe$ . The pseudo-2nd order modelling of the MTS9301 kinetic data returned returned  $r^2$  values of  $>0.99$  for copper, iron(II) and zinc, and 0.973 for lead, with predicted  $q_e$  values falling within error apart from iron(II) which was deviated by  $<10\%$ . The half-lives were similar to that of the Lagergren fits, with initial rates of reaction, however, show a trend of  $Cu > Zn > Pb > Fe$ , with the zinc and lead positions being swapped. Fitting of the TP214 kinetic data for copper to the pseudo-2nd order model resulted in a similar fit to the Lagergren model with a predicted copper  $q_e$  within  $\sim 10\%$  to the experimental value.

For both C107E and MTS9301 copper shows the best fit to the pseudo-second order model, with the TP214 kinetics fitting better to the Lagergren model. For the carboxylic acid functionalised resin, the  $q_e$  derived by the pseudo-first order model describes the experimental  $q_e$  better, both values overlapping in error values. The low desorption predicted by the Elovich model for copper adsorption fits into an assumption of pseudo-first order activity, the higher stability of copper within solution and weaker surface interactions however, potentially lead to a pseudo-saturation of copper; with the solution phase equilibrium feeding the surface equilibrium, an equilibrium reliant on surface saturation driving decomplexation of copper is created, explaining the slow kinetics.

MTS9301 is overall described best by the pseudo-second order model. Not only is the  $r^2$  higher for this model, the  $q_e$  derived by the model is a much better descriptor (within error) of the experimental  $q_e$ . The high binding energy and the high intensity of binding<sup>[124]</sup>, coupled with the relatively low desorption constant, allude to a high dependence on both solution phase copper concentration as well as functionality saturation, without this kinetic hindrance observed by C107E.



Thiourea kinetic data fits slightly better to the pseudo-first order model, with this model also describing the experimental  $q_e$  better. The strength of interaction between copper and thiourea and the deleterious nature of the copper(II) metal to the thiourea functionality potentially leads to a saturation of functionality by copper(II) ions in solution creating a pseudo-first order environment. Again, this deleterious nature leads to an impossibility to describe iron(II), lead or zinc with respect to TP214.

The kinetic data for the adsorption of iron(II) to C107E fits to both the pseudo-first and pseudo-second order models, and the pseudo-first order model is better at describing the experimental  $q_e$ . The high level of desorption of this species leads to the assumption that the concentration of iron(II) within solution potentially saturated the resin sites, as, of all metals, this displayed the lowest capacity<sup>[124]</sup> creating a pseudo-first order process, reliant purely on the functionality. MTS9301 displays a much better fit to the pseudo-second order reaction model, however again, the pseudo-first order reaction model was a better predictor of the experimental  $q_e$ ; potentially due to low interaction between acetate and ferrous ions.

The kinetics of the adsorption of lead to C107E fits best to the pseudo-second order rate model, with this model also being the best descriptor of the experimental  $q_e$  value. This process has a low adsorption intensity, low binding energy<sup>[124]</sup> and a high desorption constant, however it also displays the highest capacity for this functionality. Therefore the understuration in solution in this case could cause pseudo-second order reaction mechanism, despite the high stability of the lead acetate complexes. MTS9301 fits best to the pseudo-second order rate model, with both models describing the experimental  $q_e$  within error. This coincides with the reasonable intensity of adsorption and binding energy, all supporting a pseudo-second order mechanism.

The kinetic data obtained for the adsorption of zinc to the surface of C107E was better described by the pseudo-first order model. While zinc displays low levels of desorption (the lowest observed for this resin), it also displays low adsorption intensities and a physisorption binding energy<sup>[124]</sup>. The similarities between the functionality and the media, coupled with the weak interaction of zinc with carboxylic acids leads to this equilibrium being assumed as the rate controlling step. Conversely, MTS9301 displays a clear pseudo-second order rate controlled reaction, with both the  $r^2$  and the predicted  $q_e$  favouring this model. The high intensity of adsorption, high binding energy<sup>[124]</sup> and low desorption of this support this hypothesis.

### **Comparison of Physical and Chemical Characteristics to Modelled Parameters**

Overall, the ionic radius seemed to define the half-lives of the process for both C107E and MTS9301, as is plotted out in Figures C.7-C.18. There is a linear trend between the half-lives obtained for C107E (both pseudo-first and second order), with the omission of iron(II), while there is an obvious linear trend between the half-lives (both pseudo-first and pseudo-second order) for MTS9301, with the omission of lead. The deviation of iron(II) from the observed trend is potentially due to an oxidation of iron(II) at this pH, leading to some of the species having a much higher ionic radius and therefore displaying different mechanisms.

Kinetic limitations contrast the limitations determined by isotherm analysis, as these display a correlation to thermodynamic parameters (Figure C.9). C107E does not show any trend with regards to isotherm modelled parameters and physical parameters, however due to the lack of interaction between this functionality and iron(II), this is unsurprising. MTS9301, on the other hand, displays a tentatively linear trend between the proposed desorption constant and average  $\Delta S$  of the solution phase complexes, in a similar manner to the

correlation between decreasing average  $\Delta S$  of the solution phase complexes and decreasing  $q_m$  in the single metal system.

The initial adsorption rate of C107E seems to also follow this trend of reliance on ionic radius, however, in this case, it seems that lead is the metal that displays a different trend (Figure C.15c). Comparing this value against either the average  $\Delta H$  of solution phase complexation or electronegativity, a linear trend arises (again with the omission of iron). This leads to an assumption of electronegativity and the heat of complex formation driving the initial rate of reaction, causing a rate limiting step through an activation energy of the breakage of metal-acetate complexes. The inclusion of iron(II) in this case is an outlier due to the potential for oxidation.

The rate of desorption, for C107E, described by the Elovich model seems to be reliant on ionic radius, with the adsorption rate (according to the Elovich model) also being related to ionic radius, with the omission of lead which seems to run counter to the trend. When comparing these values to electronegativity, however, iron(II) is in disagreement with the adsorption rate trend, while copper is in disagreement with the desorption rate trend. The low desorption of copper can be explained by the high energy of adsorption<sup>[124]</sup>, while iron(II) displayed higher adsorption energies than copper in this instance, the fit to the model used was far worse.

MTS9301 displays an increase in half-life from copper through to iron(II) which displays linear correlation to ionic radius, which can be explained by a hindrance to the formation of the chelate on the resin surface. Lead, however, displays a half-life much lower than what would be expected which leads to the assumption of a different binding mechanism. The similar half-life to the carboxylic acid functionality creates the possibility of similar mechanisms between the two resins, not chelation binding. This is also amplified by the low energies of binding

determined from the isotherm studies<sup>[124]</sup>. Ionic radii and electronegativity appear to be determining factors of the Elovich desorption constant.

## Overall Resin Comparison and Performance

While, academically and mechanistically, the modelling thermodynamic and kinetic experiments can be useful for many of the pre-described factors, functionally they're most useful for determination of capacities, competition and half-lives and rates in order to determine operational parameters. Here these parameters will be discussed with respect to how each modelled mechanism will affect them. This will be used to place each resin in the perspective of the aforementioned resin-in-pulp process.

The slower half-lives of copper, iron(II) and zinc adsorption to C107E are potentially due to the similarities between the functional group and the media, creating a rate-limiting step; however lead does not display this limitation, returning a half-life similar for the adsorption from solution to both C107E and MTS9301, which are similar to IRC748<sup>[166]</sup>. C107E displays a high affinity for both lead and copper, with neither metals displaying observable levels of competitive desorption within the mixed metal isotherm, and relatively high capacities (not dissimilar to that of the capacities observed within the single metal systems); however, neither reaching saturation within the current study, and while capacities were seemingly high, the extraction percentages decreased dramatically with higher volumes of solution added (Figure C.1). With respect to iron(II) and zinc, however this resin displays poor performance; with the interaction between the functionality and zinc being hindered by the presence of solution phase acetate, and the lower extraction percentages are beneficial in the case of iron, zinc extraction is seen as a requirement for the resin-in-pulp system.

MTS9301 was the better kinetic performer, with regards to copper, iron(II) and zinc, being equal to C107E for lead. Copper is the only species observed to show no obvious desorption through competition within the mixed metal isotherm, with this trend for high affinity following into the kinetics as the high rate of adsorption by MTS9301 in the acetic acid media is similar to that of the iminodiacetic acid functionalised IRC748<sup>[166]</sup>. The same commercial product (previously called S930+, currently MTS9301), displays a much faster rate of adsorption within sulphate media at pH 4 (displaying a pseudo-second order half-life of 3.6min) and showing a poor fit to the pseudo-first order rate model<sup>[182]</sup>, leading to the assumption of a kinetically hindered adsorption process by the addition of complexing buffers. This kinetic hindrance is not observed for lead, with respect to the IDA functionalised IRC748<sup>[166]</sup>.

With all other species being desorbed with the saturation of copper on the surface of this resin, the calculation of the desorption-modified Langmuir model leads to a competition trend of  $\text{Cu} \gg \text{Pb} = \text{Fe} > \text{Zn}$ . This differs from that observed within the screening process<sup>[119]</sup>, however is similar to that observed when comparing percentage extractions, where we see the drop in extraction first by zinc then iron(II) and finally lead (Figure C.2), even though only slight differences are observed. C107E and MTS9301 kinetics are similar for lead, and are similar to IRC748 (IDA functionality)<sup>[166]</sup>, this similarity between the carboxylic acid and IDA resin of this study leads to the assumption of a different binding mechanism for the adsorption of lead to MTS9301, compared to the other three metals, caused by the higher ionic radius, preventing chelation; further alluded to by the similarly high levels of Elovichian desorption returned for both resins. Zinc, while displaying higher desorption and a lower capacity within the MTS9301 mixed metal isotherm than iron(II), also shows a remarkably lower adsorption half-life, with the pseudo-second order half-life of iron(II) being almost ten times that of copper, five times that of lead and nearly three times that of zinc leading the a

high possibility of kinetic separation in the instance of high iron concentrations.

Of all three resins, TP214 was poorest performer overall, as it was unable to extract any metal apart from copper, and the kinetics were slower than that of the macroporous MTS9301. The thiourea functionalised resin displays a half-life of its assumed redox reaction of  $35 \pm 3$  min, while the chelating mechanism of MTS9301 displays a half-life of less than half this value of  $14.1 \pm 0.9$  min; completely rejecting uptake of all other metallic species in solution. This deleterious copper adsorption detracts from the potential effectiveness of the thiourea functionality for removal of, not only iron<sup>[153,167,204]</sup>, but also lead<sup>[170,186,205]</sup>. Near 100% extraction of copper is maintained throughout the entire concentration range studied, however extraction above 75% is not achieved for any other metal, with this decreasing dramatically towards high abundance of copper, leading to declaration of inefficiency for this resin.

MTS9301 is the most effective extractant of all three resins due to kinetics as well interactions with metals, especially considering the ability to maintain high extraction % of copper lead and zinc in the initial volumes of solution (Figure C.2). Maintaining >90% extraction of each metal (without competition) 2mL wet settled resin would be capable of extracting a total of 0.729mmol metal from solution. At this point, the resin is assumed to be at capacity, with a total surface concentration of  $2.729 \pm 0.007$  mmol g<sup>-1</sup>

## 5.5 Conclusions

Mixed metal isotherms become difficult to model as the level of competition and saturation increased, due to either the desorption of metals or the transition from proton-metal exchange to metal-metal exchange with adsorption. A model that predicts the level of desorption within a specific system has been formulated, however there is little data in which to compare. The model is capable of

predicting experimental capacities of desorbed species relatively well, however the lack of saturation within the species that were not desorbed created difficult situations to predict. C107E displayed overall lowest levels of desorption for copper and lead, with saturation not reached for either species and both displaying more heterogeneous behaviour than the single metal systems due to saturation. MTS9301 displayed no desorption of copper although decreased capacities, and metals behaved in similar fashion to single metal isotherm counterparts prior to saturation.

Mechanistic details have been elucidated alluding to differences between moieties of varying ionic radius and effective ionic charge. In the majority of instances (apart from iron(II) on C107E and adsorption processes to TP214), kinetic differences can be explained by ionic radii, with an increase in this factor hindering the kinetics of both C107E and MTS9301; with the exception of lead which is assumed to undergo a similar adsorption mechanism for both the IDA and carboxylic acid functionality. Desorption can also be explained by ionic radii, initial reaction rates, however, seem to be more dictated by either change in enthalpy (C107E) or change in entropy (MTS9301).

Overall, the copper, iron(II) and zinc kinetics were hindered towards the carboxylic acid functionality, however lead did not display this same hindrance. Zinc and iron(II) were poorly competitive for the adsorption to the surface of C107E, with copper and lead not reaching saturation, however displaying a two-stage adsorption profile as proton exchange becomes metal exchange and the adsorption mechanism changes. This was again observed for copper in the case of MTS9301, which also displayed a high desorption of lead, iron(II) and zinc as saturation become more apparent; the kinetics of this resin being relatively unhindered by the acetate species and comparable to that reported for strong acid media. TP214 did not display kinetics for copper adsorption that were particularly fast in comparison to MTS9301, nor did it display higher capacities either; this

poor kinetic performance was in conjunction with negligent extraction of all other metals studied, therefore decreasing the applicability of the resin in relation to this study.

C107E does display the largest separation of iron(II) from the other metals and high capacities for each metal, however the kinetics are relatively slow, and while it would display usefulness within a system plagued with copper and lead, the ineffective nature towards zinc is concerning. TP214 is ineffective at the extraction of any species apart from copper, therefore it does not find a use here. The inclusion of strongly complexing organic acids (e.g. humic acid) leads to the possibility of this resin to remove copper in such situation.

In an equilibrium and a kinetic sense, MTS9301 was the best overall performing resin. The capacity may be hindered with saturation of copper, however provided resin volume is increased to compensate for this, this resin would be an effective adsorbent. With the large concentration of iron within sewage sludge, and the potential for a kinetic separation of any remaining dissolved iron at this pH, MTS9301 will be the best resin of the three within the RIP system.



## **Chapter 6**

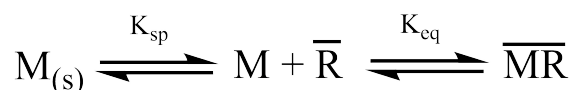
# **Acetate Resin-in-Pulp on a Simulated Sludge**

### **Summary**

This chapter will focus on the performance of MTS9301 within a simulated acetic acid RIP process for the extraction of copper, lead and zinc. Within this part a simulated sewage sludge was formulated, characterised and compared against sewage sludge collected from Esholt Wastewater Treatment Plant and doped with copper, lead and zinc prior to a leaching stage. This simulated leachate slurry was subjected to the hypothesised RIP system for which the ion exchange process has been characterised throughout this thesis. This attained total maximum recoveries of 38.9, 37.9 and 53.6% of copper, lead and zinc, respectively, which was concluded by a preliminary economic evaluation of materials cost vs output, determining that, in its current state, the process is not economically viable; however further optimisation could potentially lead to both economical and environmental viability of the process.

## 6.1 Introduction

Rehashing the current state-of-knowledge discussed within Chapter 1, the separation of metals from sewage sludge requires a solid-liquid separation stage in order to remove the PLS from a leachate slurry; this assumes a maximum fraction of metals are removed from the sewage sludge<sup>[84]</sup>. While leaching does convert a large fraction of metallic species from immobile to mobile phases, due to the retention of water within sludge solids<sup>[14]</sup>, up to 80% of the metals contained within the leach slurry remain in the sludge. What is of more concern is that these metals will no longer be in the less mobile sulphide fraction<sup>[36]</sup>, but will generally be precipitated by an increase in pH and therefore remain within more mobile forms such as hydrolysis products.



**Scheme 8**

The negation of a solid-liquid separation process prior to contact with the adsorption material has been theorised to increase the removal of metals entrained within bound waters<sup>[91]</sup>. Briefly summarising the points brought to light in Section 1.5, as a sewage sludge leach slurry will contain a high concentration of adsorbent organic material<sup>[86]</sup>, pre-robbing will be of a high concern. By introduction of an ion exchange resin RIP systems can circumvent this by removing solution phase metals ( $K_{eq}$  in Scheme 8) within the leachate slurry, causing a shift in the equilibrium of the multitude of pre-robbing processes ( $K_{sp}$ ) and further extraction of metals. This section will utilise the knowledge that has already been attained within the previous sections on the MTS9301 resin system and its performance within an acetate media, and attempt to understand how the incorporation into a simplified RIP system will affect the resin performance. As competition between metals was observed within the previous chapter, the

addition of solids and competing ions within a slurry will further complicate the ability for an understanding of the system.

## 6.2 Experimental

### Materials

All chemicals used were of analytical grade or higher and supplied by Sigma-Aldrich unless otherwise specified. High activity instant dry yeast (Mauripan), psyllium husks (Bulk Powders: Pure Series), rapeseed oil (by Sainsburys), organic miso paste (Yutaka), microcrystalline cellulose (Redwells Premium Supplements) and super soft pure white toilet paper (by Sainsburys) were purchased from Sainsburys (UK). Miso paste ingredients: water, soybeans (28%), rice, salt (a summary of the composition is included within Table 6.1). Metals analysis was conducted via AAS as described in Chapter 2.

**Table 6.1:** Composition of Miso Paste

Component	g/100 g
Fat (saturated)	5.8 (1)
Carbohydrates (sugars)	20 (12)
Protein	7
Salt	10.9

Digested sewage sludge was obtained from the Esholt Wastewater Treatment Plant near Bradford, UK (Yorkshire Water Ltd.). A schematic of this wastewater treatment plant (inclusive of sampling point) and an analysis of metals composition of this digested sludge cake is included within Figures D.1 and D.2, respectively. For a brief description, this plant has a maximum throughput of 82 tonnes of dry solids per day by a BioThelys™ thermal hydrolysis plant (supplied by Veolia Water Technologies), treated by thermal hydrolysis pretreatment (165°C

and 6bar for 20min), before being fed into an anaerobic digester (mesophilic anaerobic digestion over 11 days).

### **Sludge Simulant Generation**

Until this point in the study, a clean PLS has been generated for the study of ion exchange resins in weak acid media. While generating the most realistic scenario, utilising digested sewage sludge would be beneficial, the quantities required in order to measure actual fluctuations in metal concentrations would be extraordinary, creating further issues concerning biological hazards involved in handling such large volumes of digested sewage sludge. This hazard, coupled with the potential plant-to-plant variation in real sewage sludge<sup>[206]</sup>, leads to the requirement for a repeatable, safe surrogate. Therefore, this study will utilise a simulant sewage sludge to investigate the effectiveness of MTS9301 within a simulated RIP system in order to mitigate these issues.

With repeatability as a major concern, currently, a standard reference material for domestic sewage sludge (SRM 2781) is available from the National Institute of Standard Technology (NIST), however the price of this material is quite high (\$759.00 for 40 g). The quantities of material for all experimentation throughout this body of work create a necessity for a much cheaper alternative determined from the literature<sup>[207–209]</sup>. Radford *et al.* developed a simulant sludge utilising kaolin and top soil, in order to improve desludging pumps, emptying waste pits; there were found to be difficulties with this simulant, however, due to the variations in kaolin from region to region<sup>[207]</sup>. A study by Wignarajah *et al.*<sup>[209]</sup> produced multiple faecal matter simulants that were developed specifically for research into waste processing technologies on spacecraft, comprised, primarily, of household food items.

As part of the Bill and Melinda Gates foundation - 'Water, Sanitation & Hygiene: Reinvent the Toilet Challenge' the Pollution Research Group of University

of KwaZulu-Natal<sup>[207,209,210]</sup> have produced an extensive report on multiple simulants, all being modifications on the simulants developed by Wignarajah *et al.*<sup>[209]</sup>. From this report, a simulant was produced that was used for projects undertaken by research institutions, universities and companies around that world in order to improve the sustainability sanitation. This simulant was developed to mimic a range of faecal matter properties, most importantly density, solids content, rheology and particle size. Due to the extensive testing undertaken, cost-effective nature and similarity to organic waste, this sludge has been formulated and characterised within the for utilisation within this study.

The simulant sewage sludge was generated to the solids content composition depicted within Table 6.2. In this case peanut oil was substituted with vegetable oil, this was to negate any potential issues regarding allergies as there are a multitude of lab uses both temporary and more permanent. Deionised water was added to the simulant in order to generate the desired water content and in order to guarantee a homogeneous mixture, were stirred using the overhead stirrer (Chapter 2) for 24h.

**Table 6.2:** Composition of synthetic sewage sludge simulant<sup>[210]</sup>

Component	Dry Weight %
Yeast	32.49
Psyllium husk	10.84
Oil	17.31
Miso	10.84
PEG400	12.14
CaHPO <sub>4</sub>	10.84
Cellulose (cotton linters:tissue paper 50:50)	5.53

Viscosity measurement was conducted using a Brookfield Digital Viscometer model DV-E (Chapter 2) in triplicate, using the disc spindles S62 and S63 and the cylindrical spindles S61 and S64 depending on the torque of the viscometer. Viscosity measurements were carried out at either 5%, 10% or 20% dry weight

of the simulant, determining the effect of water content on viscosity. Drying of the sample for moisture content analysis was conducted by drying between 5 and 10g of wet sludge for three days at 70 °C. Density was calculated by measuring the volume of the wet sludge previous to drying of the sample.

### **Leaching**

Leaching for the RIP experiments was conducted on the previously described simulant sewage sludge, spiked with 100ppm each of copper, lead and zinc sulphide. Sulphides were chosen due to being the most difficult of the three leachable species (acid soluble, reducible and oxidisable)<sup>[103]</sup>. After mixing for 1h to allow for adequate diffusion of metal sulphides, acetic acid was added to a concentration of 0.5M and the pH was decreased to pH 1. Hydrogen peroxide was added to a concentration of between 3-9% and the leach was conducted for 24h. All leaches were conducted within a 250mL plastic jar, stirred by an overhead stirrer (described in Chapter 2).

The pH and ORP were measured throughout the sampling periods, and pH was adjusted after sampling when required. After a 24h period, the pH was neutralised to pH 4.5 by either addition of 50% or 1 mol L<sup>-1</sup> sodium hydroxide in order to conduct the RIP studies. Sludge samples were analysed for density, solids and centrifuged (Chapter 2) for metals concentration analysis.

### **Resin-In-Pulp**

RIP experiments were conducted by addition of a precalculated volume of wet settled resin to the neutralised leached slurry. Ion exchange parameters utilised were those derived within previous chapters, summarised within Table 6.3.

**Table 6.3:** Chemical parameters utilised for determination of resin volume and contact time.

	Copper	Lead	Zinc
[Total potential ppm]	100	100	100
[Total potential mM]	1.8	0.48	1.5
Mixed metal capacity mmol g <sup>-1</sup>	2.8±0.6	0.51±0.02	0.41±0.03
Total mmol at >90% per 1 mL	1.91	0.365	0.61
>90% extraction mmol mL <sup>-1</sup>	0.305±0.004	0.356±0.003	0.2448±0.0006
Extraction half-life min	14.1±0.9	25±5	49±6

The resin bedvolumes within the RIP systems were calculated with the assumption of 100% dissolution of metals. The total number of mmol removable from solution prior to a reduction in resin efficiency for lead <90% is 0.365mmol mL<sup>-1</sup>wsr, however the total number of mmol within solution after the leach is conducted (again, assuming 100% efficiency) is 0.57mmol. Therefore, these preliminary tests will study a system (system 1, 1mLwsr) where the resin surface is saturated and a system (system 2, 2mLwsr) where the resin is in excess. In order to make sure that extraction is maximised, 6 half-lives of the limiting species will be used in order gain an assumed <5% of the leached zinc within solution. As zinc was the limiting species, with a half-life of 49min, the total resin contact time will be 5h.

### Resin Stripping

Concentration of metal on the surface of the resin was determined by stripping of the resin bed post contact with the slurry. Resin was stripped by contact with 50mL 1mol L<sup>-1</sup> nitric acid. Prior to stripping resin was separated from slurry by decanting and then washed multiple times in order to ensure as little contamination by simulated slurry.

## Solution Analysis

Slurry samples for metals analysis were centrifuged for 10min at 6000RPM. The supernatant of each centrifuged sample and clean eluent sample was then diluted as described in Chapter 2 for metals analysis via AAS. Measurements of pH and ORP were *in-situ* on the slurry utilising double-junction pH and ORP electrodes as described in Chapter 2.

## 6.3 Results

### Moisture/Solids Content and Density

Table 6.4 displays the moisture and densities of the simulant sewage sludges generated for this study. As would be expected, the density increased with the solids content of the simulant sludge. The digested sludge from Esholt waste water treatment plant had a solids content of 3.792%, with a density of  $1.017 \pm 0.007 \text{ g.mL}^{-1}$ , matching both solids and density closest to that of the 5% solids simulant.

**Table 6.4:** Solid Content and densities of the simulant sewage sludge at 5%, 10% and 20% solids content.

	Total Solids (%)	Density ( $\text{g ml}^{-1}$ )
5% water	$4.682 \pm 0.002$	$1.03 \pm 0.01$
10% water	$11.87 \pm 0.01$	$1.05 \pm 0.01$
20% water	$19.65 \pm 0.07$	$1.088 \pm 0.004$
Esholt Sludge	$3.792 \pm 0.005$	$1.017 \pm 0.007$

### Viscosity

The viscosity measurements taken on the simulant sludge ((a), (b) and (c)) and the digested sludge from the Esholt plant (d) is included within Figure 6.1. Each measurement displays a shear thinning trend (as the stress decreases as



stirring rate increases). Both 5% and 10% moisture content simulants display less prominent shear thinning nature. The 5% simulant reaches  $0.020 \pm 0.004 \text{ Pa}$ , similar to that of the digested sludge ( $0.0233 \pm 0.0003 \text{ Pa}$ ), with 10 and 20% reaching beyond this with  $0.069 \pm 0.002 \text{ Pa}$  and  $0.287 \pm 0.005 \text{ Pa}$ , respectively.

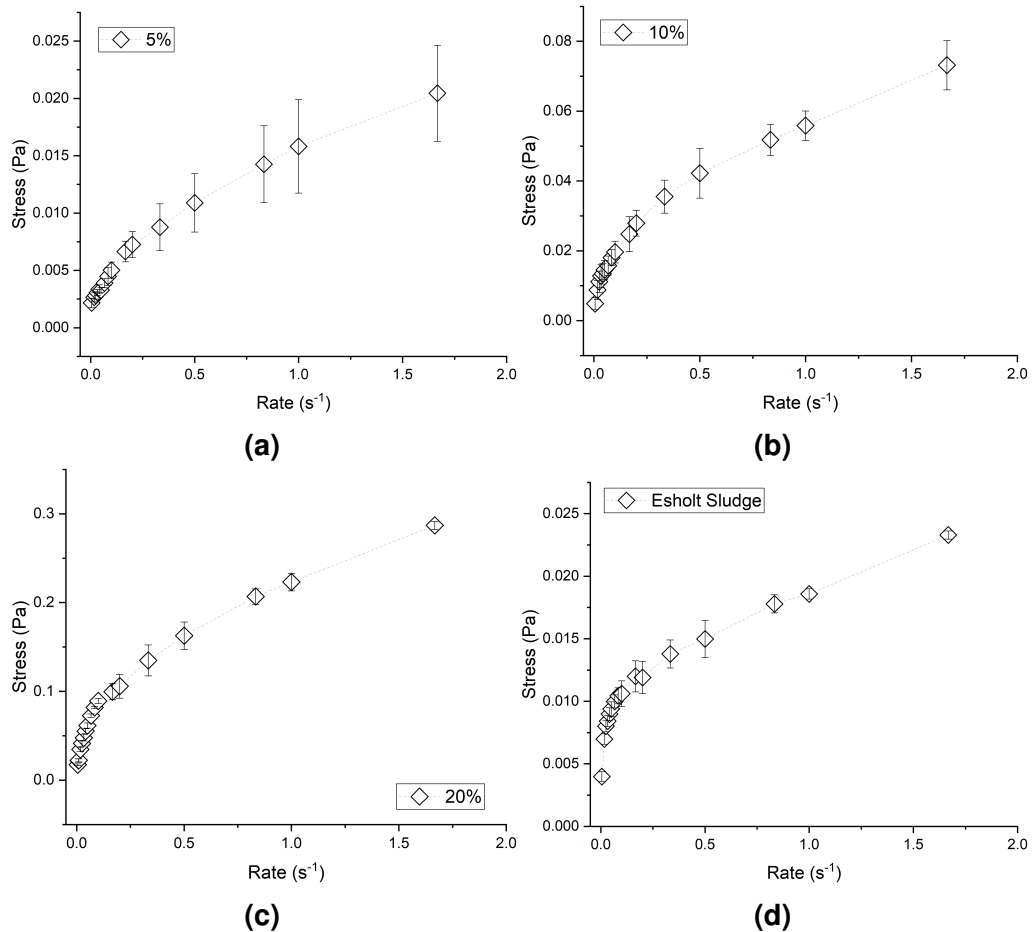


**Figure 6.1:** Plotted raw data of the viscosity experiments conducted on the 5% solids content (a), 10% solids content (b) and 20% solids content simulant and the digested Esholt sewage sludge (d) (measurements taken at 20°C).

## Leaching

Four instances of the leaching of the simulant sewage sludge have been conducted, in each each the concentration of hydrogen peroxide had been incrementally increased in order to aid in metal oxidation/dissolution. The data obtained by these experiments are presented within Figure 6.2. The leach involving the addition of 3% hydrogen peroxide is displayed within Figure 6.2a. This displays almost instantaneous dissolution of lead sulphide with addition of

$\text{H}_2\text{O}_2$ , while zinc dissolution plateaus after  $\sim 4$ -5 hours; both reaching leached fractions of 93 and 94% after 24h, respectively. Copper, on the other hand, does not reach such high extractions, with a maximum of 22% extraction, and this continuing slowly throughout the entire 24h experiment. Increasing the  $\text{H}_2\text{O}_2$  addition to a total concentration of 6% gives instant dissolution of lead sulphide, with a peak zinc dissolution being observed at  $\sim 5$ h and copper dissolution occurring slowly and to a lesser extent (Figure 6.2b). After a 24h period, the extractions were 30, 95 and 90% for copper, lead and zinc, respectively.

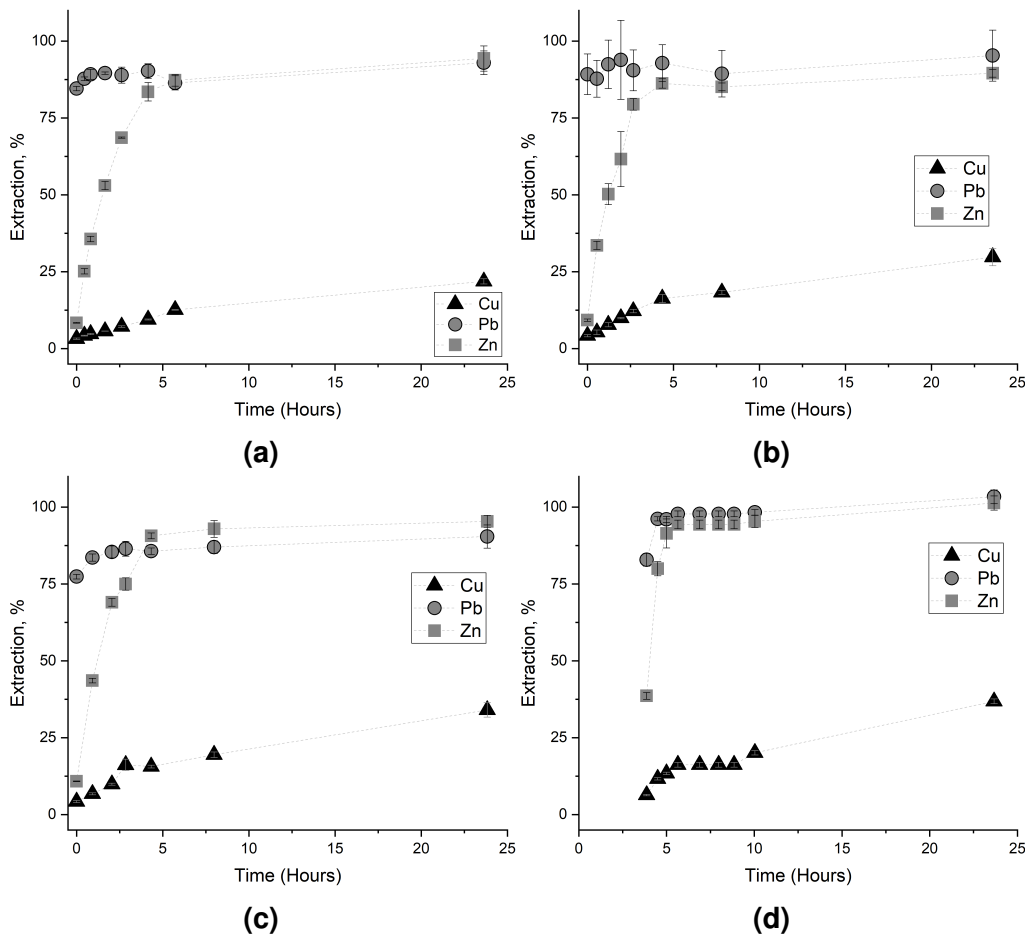


**Figure 6.2:** Percentage extraction of metal sulphides (copper, lead and zinc) from the simulant sewage sludge using acetic acid at pH 1 and hydrogen peroxide concentrations of 3% (a), 6% (b), 9% (c) and 3% (increasing the concentration to 9% after 4 hours) (d). (0.5 M acetic acid,  $\sim 500$  rpm, measured values for pH, temperature and ORP are given within Table D.5, D.6, D.7 and D.8, respectively).

With a hydrogen peroxide concentration of 9%, we see slightly more dissolution of copper (Figure 6.2c). While there is no visually observable increase in the extraction trend of copper, the overall leached fraction after 24h is 36%, making it the best case so far. Again, both lead and zinc are leached rapidly, with zinc reaching a plateau at ~5h once more; achieving extractions of 89 and 91%, respectively. The final leach conducted is a two stage leach, where the initial concentration of  $H_2O_2$  was 3%, before this concentration was increased to 9% in an attempt to further leach copper sulphide from the slurry, the resultant leaching profile is displayed within Figure 6.2d. The initial data point at ~4h is previous to the second addition of  $H_2O_2$ , returning extractions of 6, 83 and 39% for copper, lead and zinc, respectively. After the second addition of  $H_2O_2$ , there is a remarked increase in sulphide dissolution, with all metals showing a sudden increase in dissolved species; especially lead and zinc which quickly reach complete dissolution. Again, copper displays slower leaching kinetics, reaching only 37% after 24h.

With neutralisation by either 50% or 1M NaOH, the fraction of mobile species in Figure 6.3 is reached. Copper showed the least decrease in mobile fraction, while lead and zinc were far more pronounced within both neutralisation experiments. As 1M NaOH led to far less precipitation of both lead and zinc, this was be the neutralisation stage utilised for the RIP system.

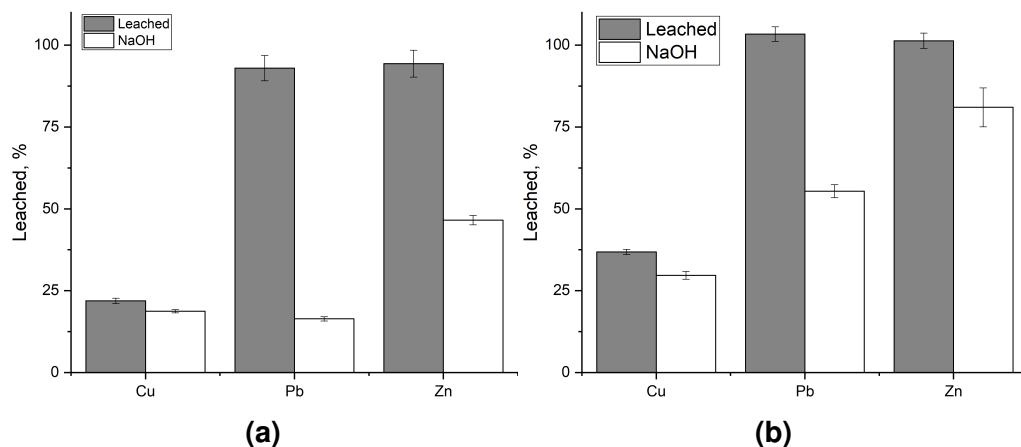


**Figure 6.3:** Comparison of the decrease in percentage of leached species with addition of 50% (0.5 M acetic acid,  $\sim 500$  rpm, measured values for pH, temperature and ORP are given within Table D.5 conducted on the 3%  $\text{H}_2\text{O}_2$  leach in Figure 6.2a) and  $1\text{ mol L}^{-1}$  NaOH (0.5 M acetic acid,  $\sim 500$  rpm, measured values for pH, temperature and ORP are given within Table D.7 conducted on the 9%  $\text{H}_2\text{O}_2$  leach in Figure 6.2c).

## Resin-In-Pulp

The solution phase fraction of each metal at each stage of the RIP process (from leaching process to post RIP) for System 1 and System 2 are displayed in Figure 6.4. In both cases, relatively similar leach extractions were attained; 33 (Cu), 88 (Pb) and 92% (Zn) vs 36 (Cu), 89 (Pb) and 91% (Zn) leached fractions for System 1 and System 2, respectively. Both cases follow similar trends observed within the leaching section and the leach was conducted to  $\sim 24\text{h}$ .

Neutralisation from pH of 1 to a pH of 4.5 decreases the dissolved % of metals. Within system 1 (Figure 6.4a) the increase in pH decreased from 33, 88 and 92% to 25, 46 and 75% dissolution of copper, lead and zinc, respectively. System 2 decreased in dissolved species from 36, 89 and 91% to 29, 49 and 74% dissolution of copper, lead and zinc, respectively, after the pH was increased.

After contact with the resin, the solution phase concentration of each metal had decreased by a small extent. With the addition of 1 mL wsr, solution phase concentration of zinc displayed the largest decrease, with a drop from 59 ppm to

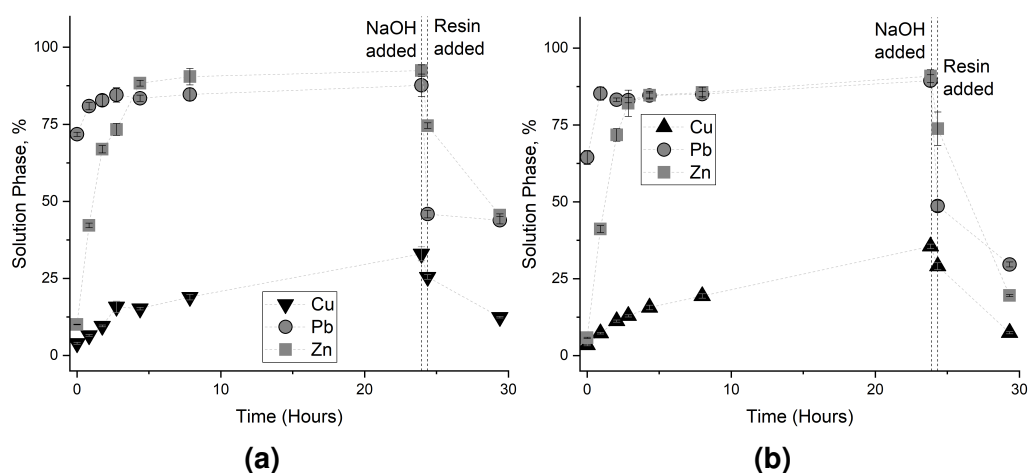


**Figure 6.4:** Solution phase percentage of each focus metal species within the leach and the RIP processes for system 1 (a) and 2 (b) (0.5 M acetic acid, ~500 rpm, measured values for pH, temperature and ORP are given within Table D.7) and D.9) for System 1 and 2, respectively.

36ppm, this was followed by copper with a decrease from 22 to 11ppm and lead removal being nearly negligible, decreasing from 38 to 37ppm. The decrease in dissolved metallic species within the system that utilised 2mLwsr (Figure 6.4b) is much more pronounced, with copper showing a decrease of 24 to 8ppm, lead a decrease from 36 to 27ppm and zinc a decrease from 61 to 20ppm.

The concentration of metals on the resin's surface ( $\text{mg g}^{-1}$ ) resin obtained by stripping each resin with 1M nitric acid compared to the concentration on the resin's surface ( $\text{mg g}^{-1}$ ) resin determined by difference between before and after contacts is displayed in Figure 6.5a and 6.5b for system 1 and 2, respectively. In both cases more metals were stripped from the surface of the resin than were calculated to be extracted by difference between before and after contact with the slurry. The concentration of metals on the surface of the resin is generally higher for system 1 than for system 2, with low concentrations estimated by solution phase differences. The difference between resin concentration difference calculated for zinc displayed the most variation between the two volumes of resin, with lead also showing a difference, however copper shows a similar variance.

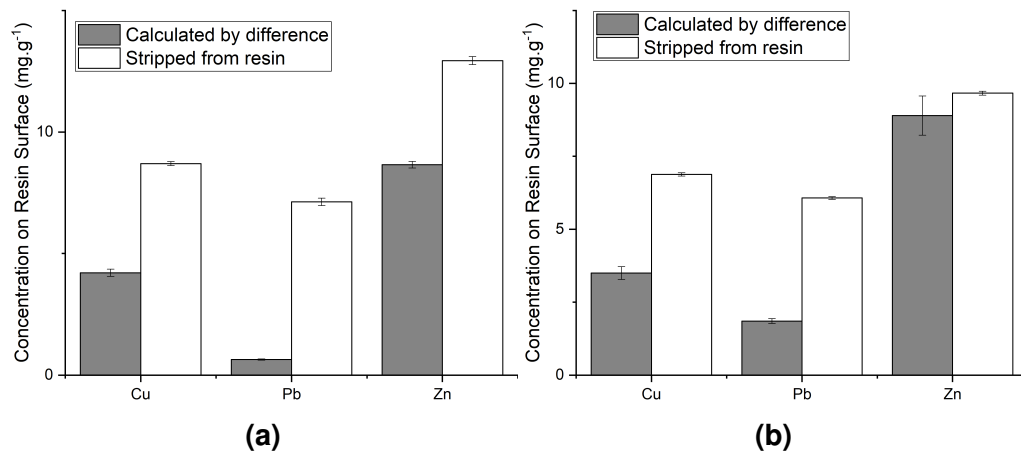


**Figure 6.5:** Concentration of metals on the resin surface calculated by solution phase difference in the leachate slurry and by stripping for System 1 (a) and 2 (b) (1M nitric acid, 24h, 20°C).

## 6.4 Discussion

### Rheology

As there is a marked variation in, not only sludge characteristics and complexity, but also measurement techniques<sup>[206]</sup>, the main deciding factor for a viability of the sludge will be that of a comparison between the simulant and real sludge utilising the rheological equipment at the disposal of the current author. Descriptions of rheological models, fitting of the rheological data to the models and the physical characteristics of sewage sludge is contained within Tables D.1 - D.4. The best results for both the simulant sewage sludge and the anaerobically digested Esholt sludge were attained by fitting the rheological data with the Herschel-Bulkley Model, this led to a very close comparison of both slurries (Figure 6.6). Fitting this model leads to the calculation of negligible yield stress from any of the simulants or the actual sludge, compressing the function into the Power-Law.

While sludge has been fit to both the Plastic Power-Law and Herschel-Bulkley model, it is most commonly fit to the power-law model<sup>[209,211-214]</sup>, and since both the simulant and Esholt sludges not only obtained reasonable fits to this model (Table D.3), but also obtained negligible yield stress within the Herschel-Bulkley fitting (Table D.4), this model will be used to compare to literature sources of sludge

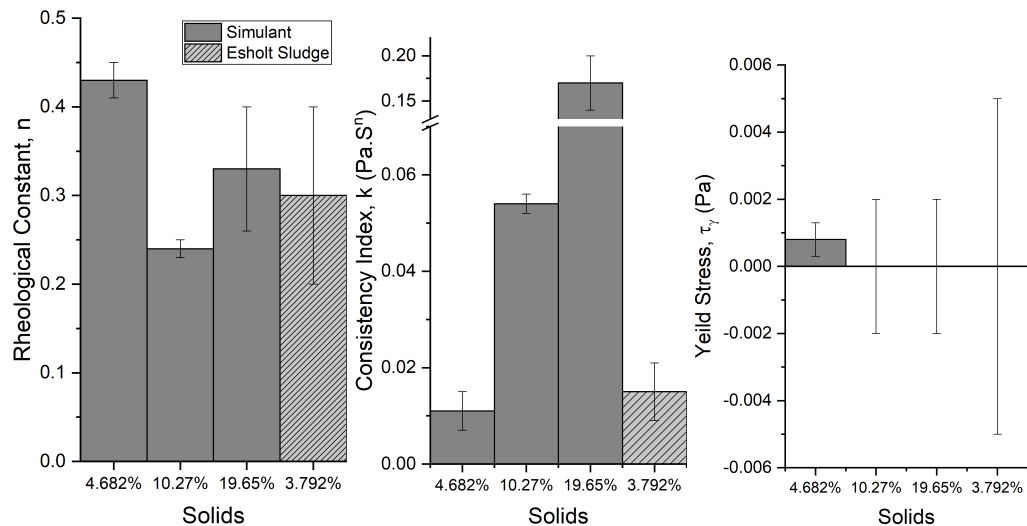


**Figure 6.6:** Comparison between the simulant and Esholt sludge fitted Herschel-Bulkley parameters.

rheology. Two sources were chosen for comparison for either the rheological method used being similar in nature to that of this study<sup>[214]</sup> or the display of variation from sludge to sludge measured by the same rheological method<sup>[213,214]</sup>. This pseudo-plastic behaviour is consistent with other sources of information that fit the sewage sludge to the power law model, and is compared to many of the literature results in Figures 6.7 and 6.8.

The consistency index of sewage sludge varies widely, from  $<0.025 \text{ Pa.s}^n$  for sludges from Bari West and Esholt, to  $>3$  for similar solids content sludges from Bari East<sup>[213]</sup>. The 5% solids content simulant<sup>[213]</sup> sludge consistency index displays behaviour similar to that of the Esholt sludge, both with similar solids contents of  $\sim 5\%$ . The values reported for anaerobically digested sludge from Chapultepec<sup>[214]</sup> are also similar to the simulant with a similar solids content (both roughly 10% solids).

The sludge rheological constants display much less scatter than the consistency index. Majority of the digested sludge measurements obtained  $n$  values of  $\sim 0.3 < n < 0.5$ , while the sample from Esholt is lower and both Monopoli and Bari East<sup>[213]</sup> are well beyond this region, although the solids content of

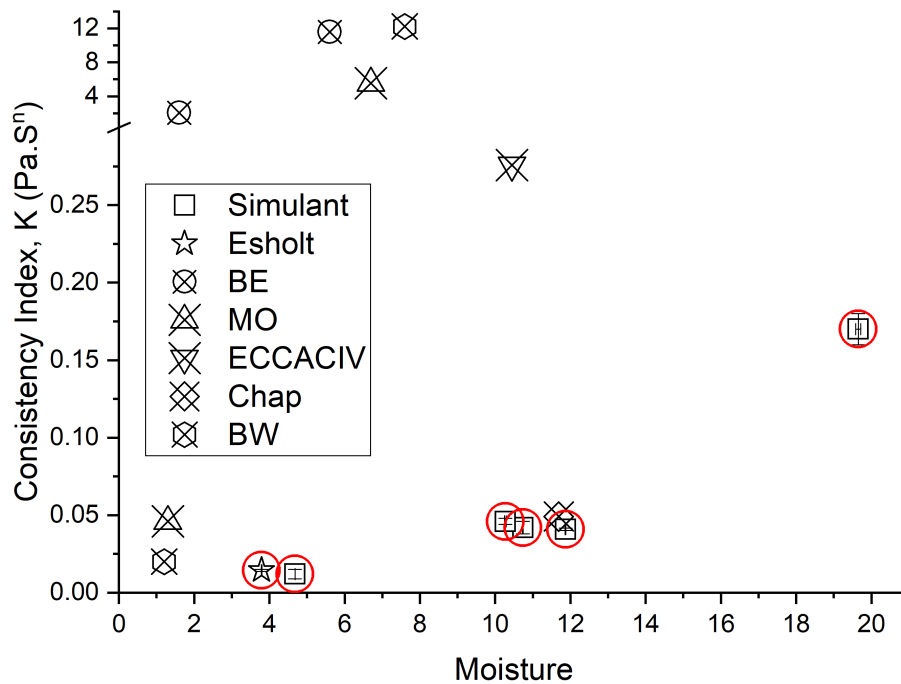


**Figure 6.7:** Comparison of the consistency index,  $K$  (Pa.s<sup>n</sup>), of the simulant sewage sludge at 5, 10 and 20% moisture content, compared with the Esholt sewage sludge and literature values<sup>[213,214]</sup>.

the last two samples are <2% solids. The simulant rheology constant displays consistency regardless of solids content, and while this is not necessarily the same as real sludges, it does fall within the large scatter of literature values.

## Leaching

With leaching of metals from real sewage sludge proven possible by acidic and oxidative leaching within the literature<sup>[36,72,75,82,83]</sup>, inclusive of the use of acetic acid<sup>[81]</sup>, this discussion will be solely for the purpose of proving the concept of this RIP system and not for the determination of operational parameters of an actual leaching process. As H<sub>2</sub>O<sub>2</sub> concentration increases there is a large increase in rate and percentage of leached copper as well as zinc, and in each case, lead is almost instantaneous. The addition of H<sub>2</sub>O<sub>2</sub> after zinc and lead dissolution does not effect the total percentage of extracted copper, therefore for simplicity 9% H<sub>2</sub>O<sub>2</sub> will be used for the leaching stage. Within the short time frame, this leach performed better than pure sulphuric acid leaches, however as discussed before, the precipitation of lead sulphate would be deleterious to



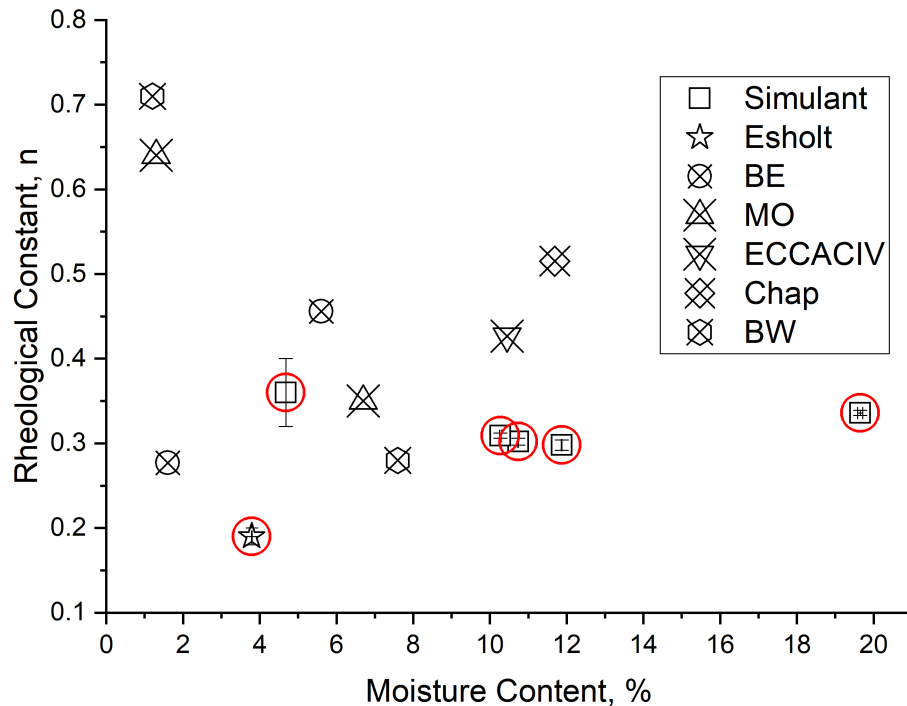


**Figure 6.8:** Comparison of the rheological constant,  $n$ , of the simulant sewage sludge at 5, 10 and 20% moisture content, compared with the Esholt sewage sludge and literature values<sup>[213,214]</sup>.

this process<sup>[63,70,76,77]</sup>; the system also outperformed both acetic and citric acid leaches (with the exception of copper being leached to 50% by the citric acid system after numerous days)<sup>[78,80,81]</sup>. While there was success with comparisons to purely acidic leaches, the addition of stronger oxidising agents, or longer time periods, has proven to increase metals dissolution<sup>[36,72,75,82,83]</sup>.

Despite the complexing nature of acetic acid, the neutralisation stage led to the precipitation of previously dissolved species. The most dramatic effect being caused by neutralisation by 50% NaOH, assumed to be due to the occurrence of localised regions where the pH of the slurry is much higher than the bulk, prior to effective diffusion. There was, however a remarked decrease in leached fraction upon neutralisation by both 50% and 1M NaOH.

In order to discuss this, Figure 6.9 reports predominance diagrams of copper (a), iron (b), lead (c) and zinc (d), in a system containing all four metallic species, as well as phosphate and acetate species. Neutralisation led to a decrease

in dissolved lead species, most likely due to the modelled formation of lead phosphate (Figure 6.9c). Due to the addition of iron for the removal of phosphate during the treatment of wastewater<sup>[14]</sup>, there is most likely a predominance of iron phosphate over calcium phosphate (as was added directly to this simulant). As iron phosphate is far less soluble than many other species, there is a high likelihood that, either this will be the preferentially precipitated species, or there will be little to no solution phase phosphate generated throughout the leaching stage.

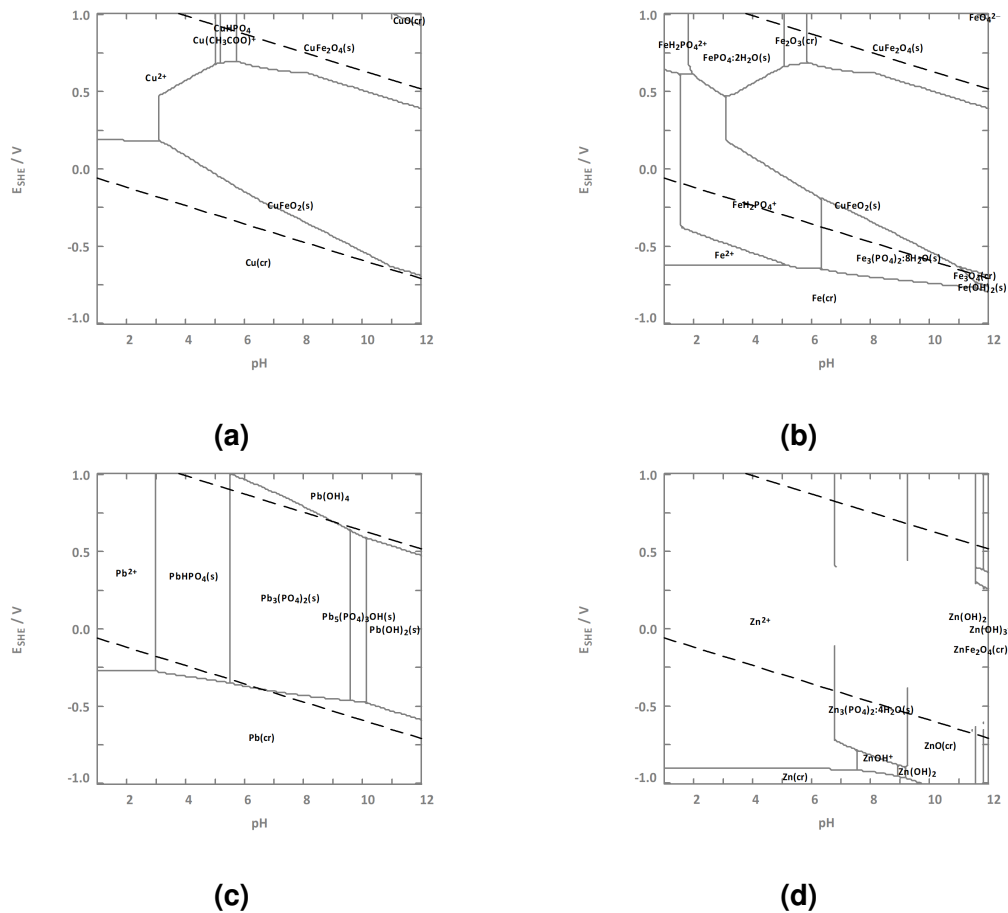


**Figure 6.9:** Predominance diagrams of copper, iron, lead and zinc acetic acid and phosphate, generated using the combination software suite HYDRA/Medusa<sup>[104]</sup>.

An issue that arises with the inclusion of higher iron concentration is the precipitation of cuprous ferrite species (Figure 6.9a). Copper is not only one of the higher concentration species in sludge, it is also the highest value species

of those studied throughout this thesis, and therefore the most attractive for recovery<sup>[41]</sup>. Due to this, there is the necessity for a fine control of both pH and ORP, as there is a small window where the predominant copper species will be that of the soluble copper acetate, rather than the precipitated  $\text{CuFeO}_2$  species. At pH 4.5 (in the presence of acetic acid) with an ORP below  $\sim 500\text{mV}$ , the predominant copper species would be  $\text{CuFeO}_2$  as a solid species, however above this ORP, copper will exist as either  $\text{Cu}^{2+}$  or copper-acetate species (Figure 6.9a). While  $\sim 50\%$  of the leached lead remained in solution after an increase in pH, this is not modelled to be the case, as lead phosphate is extremely insoluble, and acetate is not a strong enough complexant to compete, unlike with sulphate. Both of these issues, however, can be rectified with the control of both pH and ORP in order to precipitated iron as both haematite and iron phosphate species.

As was initially discussed, the aim of this section was not to characterise a realistic leaching scenario, as leaching of sewage sludge is not novel and this is an extremely simplified system, therefore development of a leaching process that could be called comparable is of little merit. What is important, however, is that there are mobilised metals within the slurry so that the viability of the increase in pH and extraction via a RIP system can be determined. The focus therefore is not on this as a definitive leaching study, but more of a preparation stage for the ultimate goal of removal of mobilised metallic species from a sewage sludge leach slurry.

### **Resin-In-Pulp**

The mass balances of the unoptimised process of both System 1 and 2 are included within Table 6.5. Within both systems, recoveries of the metals calculated by a difference in solution phase species is fairly low; 13 (Cu), 2 (Pb) and 29% (Zn) for System 1 and 22 (Cu), 19 (Pb) and 54% (Zn) for System 2. Analysis of the data obtained by elution of the resin, however, describes a

much more effective process in both instances (27 (Cu), 23 (Pb) and 43% (Zn) recovery within System 1 and 22 (Cu), 38 (Pb) and 54% (Zn) recovery within System 2). This leads a maximum mobile phase removal of 109, 42 and 59% for copper, lead and zinc, respectively (calculated by mass); such high disparities (and such large solution phase removal of copper) leads to the assumption that there are beneficial dissolution processes occurring, by either dissolution from a solid phase compound or desorption from organic matter, as was the original hypothesis for the RIP system.

**Table 6.5:** Percentage of metal in each phase from the final mass balance.

	Copper	Lead	Zinc
	1mL		
Remainder in Solid, %	61±2	34±1	11.1±0.2
Solution phase, %	12.4±0.5	44±2	45.5±0.9
Recovery, %	27.0±0.2	22.6±0.5	43.4±0.6
Removal from solution, %	76±3	24±0.9	43.6±0.9
	2mL		
Remainder in Solid, %	52±3	25±1	22±2
Solution phase, %	9.3±0.6	37±2	24±2
Recovery, %	38.9±0.3	37.9±0.3	53.6±0.4
Removal from solution, %	109±7	42±2	59±4

With respect to the saturation limits calculated within Chapter 5, there is a theoretical resin saturation in system 1 and a theoretical excess of resin within system 2; referring to the mobile phase fraction of each metal after the neutralisation stage ( $0.23 \pm 0.01 \text{mM}$  and  $0.27 \pm 0.02 \text{mM}$  for System 1 and 2, respectively) neither system was in saturation at the time of resin contact. With this taken into account, the total resin saturation by leached species of each system is 55 and 31% for system 1 and 2, respectively. The increase in the volume of added resin increased the recoveries of metal by the resin, as would be assumed with the over saturation levels calculated, it is also assumed that

saturation of the resin is achieved due to the contact for 6 half-lives of zinc. Contrary to both assumptions, and the resin saturation, >90% of solution phase metals for each species was not extracted.

Due to the discrepancy between the values obtained from a clean metal system in comparison with this RIP system, experimental values were integrated into the desorption-modified Langmuir, Langmuir isotherm models in order to determine competition limitations and pseudo-first order and pseudo-second order models in order to determine kinetic limitations. While the fitting to the isotherm models is fairly straight forward (substitute in the  $C_e$ ,  $\text{mmol L}^{-1}$ , into the models with the fitted variables), fitting to the kinetic models required determination of a potential  $q_e$  values as equilibrium was not technically reached (>98.4% had occurred, according to half-lives). Therefore, in order to do this, the percentage completion of reaction was calculated for each species according to the half-life, and this was then used to determine a theoretical experimental  $q_e$ . Utilising this to compare performance of the RIP system with a clean multi-metal system we gain the values reported within Table 6.6.

**Table 6.6:**  $q_e$  values obtained by modelling the experimental  $C_e$  values from the RIP system with the parameters obtained within Chapter 5.

	Copper	Lead	Zinc
	1mL ( $\text{mg g}^{-1}$ )		
Experimental $q_e$	0.137±0.001	0.0344±0.0007	0.198±0.003
Desorption Langmuir $q_e$	1.5	0.27	0.41
Langmuir $q_e$	1.3	0.26	0.39
Pseudo-1st order $q_e$	0.14	0.034	0.20
Pseudo-2nd order $q_e$	0.12	0.026	0.15
	2mL ( $\text{mg g}^{-1}$ )		
Experimental $q_e$	0.11±0.04	0.029±0.006	0.15±0.09
Desorption Langmuir $q_e$	1.4	0.24	0.40
Langmuir $q_e$	1.1	0.23	0.38
Pseudo-1st order $q_e$	0.09	0.021	0.11
Pseudo-2nd order $q_e$	0.11	0.029	0.15

The modelled  $q_e$  values obtained by fitting both the desorption-modified Langmuir and Langmuir model overestimate the experimental values by an order of magnitude for both copper and lead, displaying a better estimate of the zinc equilibrium capacity, at 2-3 times the experimental  $q_e$  ( $\text{mmol g}^{-1}$ ). In contrast to this result, however, fitting the models to the pseudo-first and pseudo-second order kinetic models produces  $q_t$  values that are remarkably close to the experimental values. From this it can be determined that the kinetics of extraction are not necessarily the limiting factor in this instance, the limiting factor is the saturation of the resin.

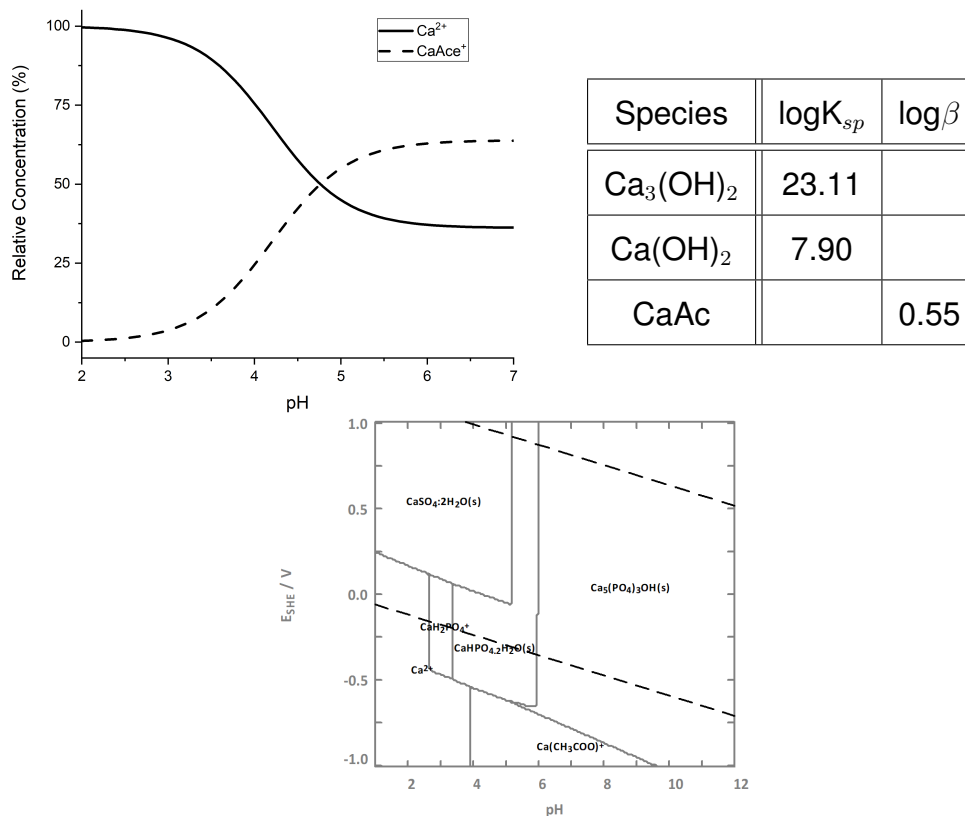


**Figure 6.10:** Speciation diagram of calcium in acetate media generated using the HySS software suite<sup>[125]</sup>, stability constant data obtained from the NIST stability constant database included within the table<sup>[126]</sup> and the predominance diagram generated using the HYDRA/MEDUSA software suite<sup>[104]</sup>.

This is potentially due to a competition with calcium, as  $\text{CaHPO}_4$  is soluble in this media (determined by the solubility data displayed within Figure 6.10), leading to an extremely high concentration of free calcium ions. The binding of acetate to calcium in comparison to other metals within this system is a fairly weak interaction (displaying 50%  $\text{Ca}^{2+}$  and  $\text{CaAc}$  at  $\text{pH} \sim 4.5$ , with  $\text{CaAc}$  displaying a low stability constant of 0.55) and calcium is in high excess of the other metals ( $\sim 8000\text{ppm}$  vs  $200\text{ppm}$ ). While this could seem to be mitigated by the use of iron phosphate within the simulant, and not  $\text{CaHPO}_4$ , high concentrations of calcium are still prevalent within sewage sludge due to pH control via lime/limestone<sup>[14]</sup>. The precipitation of gypsum with sulphate concentrations could lead to a hindrance to the adsorption, however the weakly binding acetate species is still capable of stabilising a percentage of calcium in the solution phase.

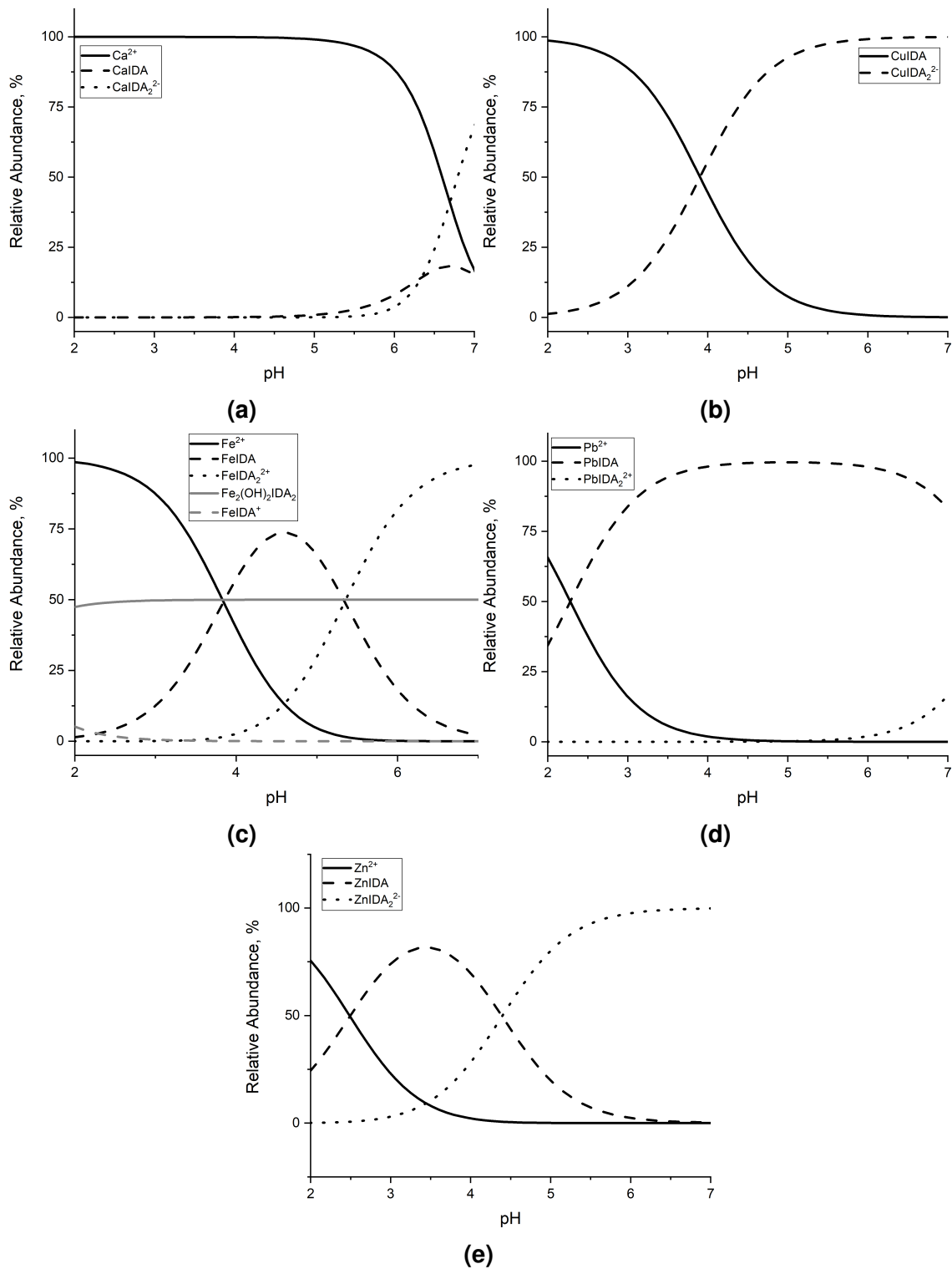


**Figure 6.11:** Speciation diagrams of calcium, copper, iron, lead and zinc citric acid and phosphate, generated using the HySS software suite<sup>[125]</sup> and stability constant data obtained from the NIST stability constant database<sup>[126]</sup>.

In order to potentially discuss the competition between calcium and the other metallic species for IDA binding, the speciation of each metal in contact with



aqueous IDA ligand is displayed in Figure 6.11, with stability constants reported in Table 6.7. Copper, iron(III), lead and zinc maintain IDA complexes throughout the entirety of the pH region modelled, with lead maintaining 100% PbIDA from pH  $\sim$ 4 to  $\sim$ 6, copper and zinc transitioning between mono- and bis- complexes and iron(III) forming bis-complexes from pH  $>$ 2. Iron(II) doesn't display appreciable interaction with IDA in solution until pH  $>$ 3 where it becomes Fe(II)IDA, then Fe(II)IDA<sub>2</sub>. Calcium was not modelled to interact with the IDA functionality until pH  $>$ 5. While this alludes to an out-competition of calcium by other solution phase metallic ions, the abundance of calcium within solution forces the equilibrium towards calcium-IDA complexes on the resin's surface. A buffering acid that creates stronger complexes with the calcium ion, could prevent this out-competition, however, therefore citric acid, due to its stronger stronger complexing ability, may be able to mitigate this issue.

**Table 6.7:** Stability constant data obtained from the NIST stability constant database<sup>[126]</sup> (L=IDA functionality, H=proton, OH=hydroxyl).

Species	log $\beta$	Species	log $\beta$	Species	log $\beta$	Species	log $\beta$
HL	9.34	CuL <sub>2</sub>	16.3	Fe(III)L <sub>2</sub>	9.42	PbL <sub>2</sub>	9.3
HL <sub>2</sub>	2.62	CuHL	2.3	Fe(III)HL	2.7	PbHL	3.84
HL <sub>3</sub>	1.77	CuOHL	8.5	Fe(III)OHL	3.17	PbOHL	-2
CaL	2.6	Fe(II)L	5.8	Fe(III)HL <sub>2</sub>	3	ZnL	7.15
CaL <sub>2</sub>	5.9	Fe(II)L <sub>2</sub>	10.1	Fe(II) <sub>2</sub> (OH) <sub>2</sub> L <sub>2</sub>	22.4	ZnL <sub>2</sub>	12.4
CuL	10.56	Fe(III)L	10.7	PbL	7.36		

## Viability of the process

Comparing the total metal recovery to the removal of metals by solid-liquid separations reveals somewhat of a success to this process at this early stage of its development. Solid-liquid separations of sewage sludge generally generate a dewatered sludge of up to 80% moisture content<sup>[14]</sup>, assuming that mobile species are distributed equally, this will result in a similar percentage removal

of metal. As mobile species of the dewatered sludge will be immobilised by precipitation by hydrolysis<sup>[36]</sup>, the metallic species are rendered more mobile (and therefore more hazardous) than prior to the leaching process. With the RIP process, while there were low recoveries, controlling solution phase calcium or increasing volume of resin could allow for higher recoveries, not only this but the recovered species are completely removed from the slurry.

Bearing in mind that this process has not been optimised, and the input chemicals were chosen with regards to what would be most effective at a laboratory scale, we can use the recovery of metals to calculated metallic value extracted on top of the potential phosphate recovery price, and then compare these results with the input cost of the chemicals required, Table 6.10 is then generated (it needs to be noted that this does not include chemical consumption for resin regeneration or elution). From the chemical inputs, the first change that could be made without much alteration of the process is the exchange of nitric acid for sulphuric acid, these acids are incomparable with regards to price (<£200 per tonne for 98% sulphuric acid and ~£400 per tonne for 68% nitric acid<sup>[215]</sup>), the diprotic nature of sulphuric acid and higher concentrations would also lend to a higher economic efficiency. The second, and most obvious however most difficult to substitute is the hydrogen peroxide (£303 per 25L<sup>[216]</sup>); the price of this is extremely high due to the energy required to generate the solution and stabilise the gaseous molecule within solution. One option for the replacement of this chemical is the installation of an ozone generation station, and costing between £5000 and 10000 would be more economically favourable within 10 tonnes of sewage sludge. The last cost-saving measure would be the reuse of of the resin, depending on the price of this and the most cost-efficient elution conditions this could also be a contributing factor for reducing overall cost, as MTS9301 (or the S930/S930+ legacy equivalents) have the potential to be regenerated and reused, however the limited studies in this area, especially when considering biofouling of

the resin within the sludge media, this is an area that needs to be considered.

**Table 6.8:** Hypothetical costs per tonne.

Input	System 1 (£.t <sup>-1</sup> )			System 2 (£.t <sup>-1</sup> )		
MTS9301	102			204		
Glacial Acetic Acid	104			104		
70% Nitric acid	187			187		
30% Hydrogen peroxide	1116			1116		
50% NaOH	70			70		
Total Expenditure	1578			1680		
Metals	Cu	Pb	Zn	Cu	Pb	Zn
Metal Income	0.08	0.04	0.12	0.12	0.06	0.16
Phosphate Income	1.57			1.57		
Gross Income	0.24			0.34		
Net Income	-1576.19			-1678.09		

## 6.5 Summary

Summarising the analysis conducted on the simulant, the simulant faecal matter produced by the Pollution Research Group of University of KwaZulu-Natal<sup>[210]</sup> can be diluted to similar moisture contents as sewage sludge and maintain a rheology similar to that of sewage sludge. The variation from sludge to sludge is so much that this lands within the scatter of data available within the literature, therefore deciding on either a pump or stirrer in a scaled up, simulated system should arrive similar values to that of working with sewage sludge. This should also translate into a correct dispersion of the ion exchange resin throughout the sewage sludge for diffusion kinetics to remain similar from real to simulated RIP experiments.

A schematic description of the RIP experiment conducted is depicted within Figure 6.12, summarising the experiment and the results obtained (Table 6.9). With the addition of acetic acid, nitric acid and hydrogen peroxide to the simulant sewage sludge, a 24h leach led to dissolution of 33, 88 and 92% of the copper, lead and zinc, respectively (for system 1) and 36, 89 and 91% of the copper, lead and zinc, respectively (for system 2). With a decrease in dissolved species resulting from the increase in slurry pH prior to the addition of the MTS9301 ion exchange resin, system 1 attained a recovery of 27 (copper), 23 (lead) and 43% (zinc) and system 2 attained 39 (copper), 38 (lead) and 54% (zinc), eluted from the resin. High removals from solution were recorded, however these were skewed due to equilibrium shifts and redissolution either from adsorbed species, hydrolysis or phosphate precipitation. All of these factors lead to a successful extraction from acetic acid media.

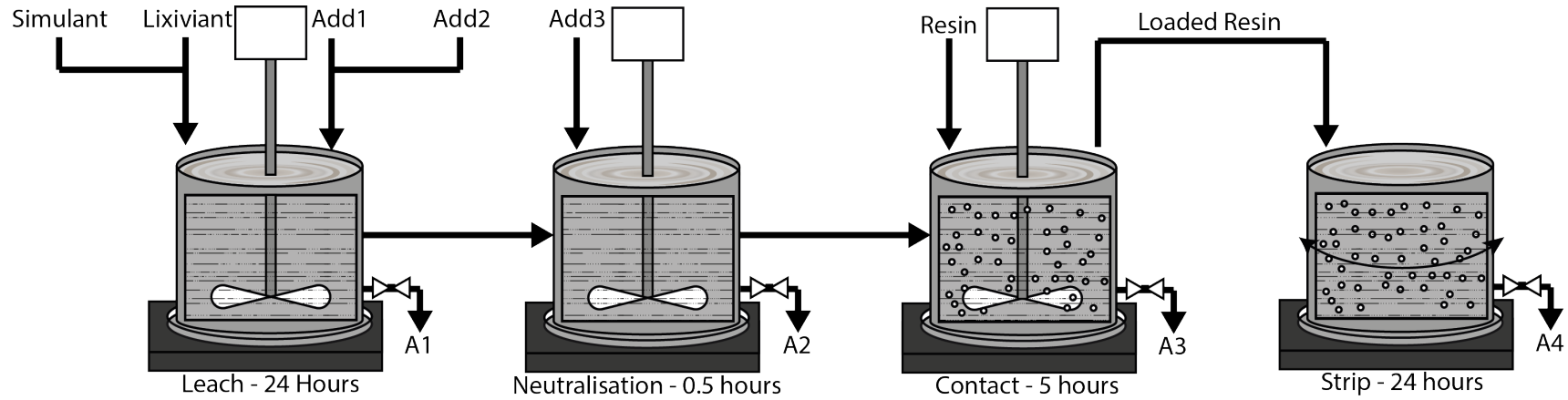


Figure 6.12: Schematic for the results of the final RIP experiment.

Table 6.9: Summarised extraction results.

	System 1			System 2		
Resin	MTS9301 (1mL)			MTS9301 (2mL)		
Lixiviant	Acetic acid (0.5M)			Acetic acid (0.5M)		
Add 1	70% nitric acid (pH 1)			70% nitric acid (pH 1)		
Add 2	Hydrogen peroxide (9%)			Hydrogen peroxide (9%)		
Add 3	1M NaOH (pH 4.5)			1M NaOH (pH 4.5)		
Metals	Cu	Pb	Zn	Cu	Pb	Zn
A1	33%	88%	92%	36%	89%	91%
A2	25%	46%	75%	29%	49%	74%
A3	12%	44%	45%	9%	37%	24%
A4	27%	23%	43%	39%	38%	54%

Table 6.10: Hypothetical costs per tonne.

Input	System 1 (£.t <sup>-1</sup> )			System 2 (£.t <sup>-1</sup> )		
MTS9301	102			204		
Glacial Acetic Acid	104			104		
70% Nitric acid	187			187		
30% Hydrogen peroxide	1116			1116		
50% NaOH	70			70		
Total Expenditure	1578			1680		
Metals	Cu	Pb	Zn	Cu	Pb	Zn
A4	0.08	0.04	0.12	0.12	0.06	0.16
A3 (Phosphate)	1.57			1.57		
Gross Income	0.24			0.34		
Net Income	-1576.19			-1678.09		

While the overall extractions of this process managed to return values comparable, with the potential for out-competing, the solid-liquid separation with a single stage process, the overall cost of this process far outweighs the income that could be generated by sales of the materials extracted within this study. While optimisation of the process and replacement of the most expensive components (nitric acid and hydrogen peroxide) could potentially lead to a much more economically viable process, the easiest way to increase the economic gain would be to broaden the efforts of extraction from toxic base metals to include valuable platinum group metals<sup>[33,194]</sup>. There is also, however, the volatility of phosphate prices to keep in mind<sup>[217]</sup>, due to the dwindling nature and disproportionate control of reserves (Chapter 1). While this exact process may not be conceivably profitable at the time of writing this thesis, the future nature of phosphate supply may not be so certain, and this invaluable resource may be harvested in this manner.

# Chapter 7

## Citric Acid Adsorption System

### Summary

This chapter will focus on the removal of copper, iron(II), lead and zinc from a simulated citric acid sewage sludge leachate by commercially available MTS9301 ion exchange resin, determining the effect of citrate concentration, metal abundance and time. Solution phase speciation was predicted by HySS. Isotherm data obtained was fit to Freundlich, Langmuir, Temkin and Dubinin-Radushkevitch isotherm models and the previously proposed desorption modified Langmuir model, while kinetic data was fit to the Particle and Film-diffusion, Elovich, Lagergren and Pseudo-second order models. Copper displayed the highest capacity within this media ( $1.79 \pm 0.06 \text{ mmol g}^{-1}$ ), while lead and zinc displayed capacities a fraction of this ( $0.50 \pm 0.01$  and  $0.391 \pm 0.007 \text{ mmol g}^{-1}$ , respectively). Copper displayed the fastest binding mechanism with a half-life of  $12.7 \pm 0.7 \text{ min}$ , while zinc and lead displayed half-lives of  $31 \pm 2$  and  $32 \pm 4 \text{ min}$ , respectively. Iron(II) displayed a lack of affinity for MTS9301 within citrate media, desorbing from the resin surface as an equilibrium was met with the other metals. Generally, citric acid, while being an excellent stabilisation agent for mobile metals, can be utilised in order to allow for effective and selective extraction.

## 7.1 Introduction

With competition hindering extraction within the acetate system, this chapter will attempt to characterise the stronger complexing citrate system with respect to the IDA functionalised MTS9301. This study will also include a multi-metal isotherm and kinetic exploration of the citrate-IDA system, accompanied by speciation modelling of the solution conditions. This study will not only add into a body of work contributing to the development of a RIP process for the removal of heavy metals from sewage sludge, but also has implications in contribution to the extraction of value from waste electronic equipment and other citric acid hydrometallurgical processes<sup>[218]</sup>.

## 7.2 Methods

### Reagents and Analysis

All chemicals used were of analytical grade or higher and purchased from Sigma-Aldrich. Metal solutions were generated by adding chloride salts of each metal apart from lead that was added as a nitrate. MTS9301, supplied by Purolite, was preconditioned by 24 hour contact with 1 M H<sub>2</sub>SO<sub>4</sub> (10 bed volumes) prior to washing with 50 bed volumes of deionised water. Analysis was conducted by AAS, as described in Chapter 2.

### Citric Acid Concentration Dependence

Reliance on citric acid concentration on the extraction efficiency of MTS9301 was conducted by alteration of citric acid concentration. Solutions were made to a concentration of 100ppm each of copper, iron(II), lead and zinc, 0.5mol L<sup>-1</sup> sodium chloride and citric acid concentrations of 0.01, 0.05, 0.1, 0.25 and 0.5mol L<sup>-1</sup>. The pH of each solution was adjusted to pH 5.75 by addition of sodium hydroxide. A



50mL aliquot of each solution was contacted with 2mLwsr, and equilibrated for 48h at 20°C (agitated at 250 rpm, as described in Chapter 2).

### **Extraction Isotherms**

Isotherms were undertaken to understand the capacity of MTS9301 for copper, iron(II), lead and zinc within citric acid media. Due to the large influence of equilibria on the values obtained, and therefore influence that molar ratios will have on each adsorption reaction, equimolar solutions were generated. Solutions were made up as mixed metal solutions at 200 mmol L<sup>-1</sup> of each metal. Each solution was made to a concentration of citric acid media determined within this study and 0.5 M NaCl and then adjusted to pH 4.5 using NaOH. Isotherms were conducted by contacting 2mLwsr with volumes of mixed-metal solution ranging from 25-400mL. Contacts were allowed to reach equilibrium for 48h, agitated on an orbital shaker (250 rpm) at 20°C.

### **Extraction Kinetics**

Kinetic analysis of the extraction of copper, iron(II), lead and zinc by MTS9301 from citric acid media was attempted contacting 10mLwsr with 500mL and agitated (250 rpm) at 20°C. Solutions were made to a concentration of 200ppm of each metal, with a NaCl concentration of 0.5mol L<sup>-1</sup> and a citric acid concentration determined within this study. Contacts were conducted over a 48h period, taking 1mL samples at set time periods between 0 and 48h.

## **7.3 Results**

### **Citric Acid Concentration Dependence**

Figure 7.1 displays the distribution coefficients of the extraction of copper, iron(II), lead and zinc from citrate media as a function of citrate concentration.

This displays a distinct increase in copper extraction with decreasing citrate concentration, as  $k_d$  values increased from 3 to 16 by  $0.01\text{mol L}^{-1}$  citrate. A similar increase was observed with iron(II), however occurring at much lower concentrations, with a  $k_d$  of almost zero until  $0.01\text{mol L}^{-1}$  citric acid, then an increase to  $\sim 2.5$ . Both zinc and lead display increase in  $k_d$  values with decreasing citrate concentrations, however remain higher than iron(II); which is then counteracted by a citrate concentration of  $0.01\text{mol L}^{-1}$  as the extraction of both species decreases dramatically.

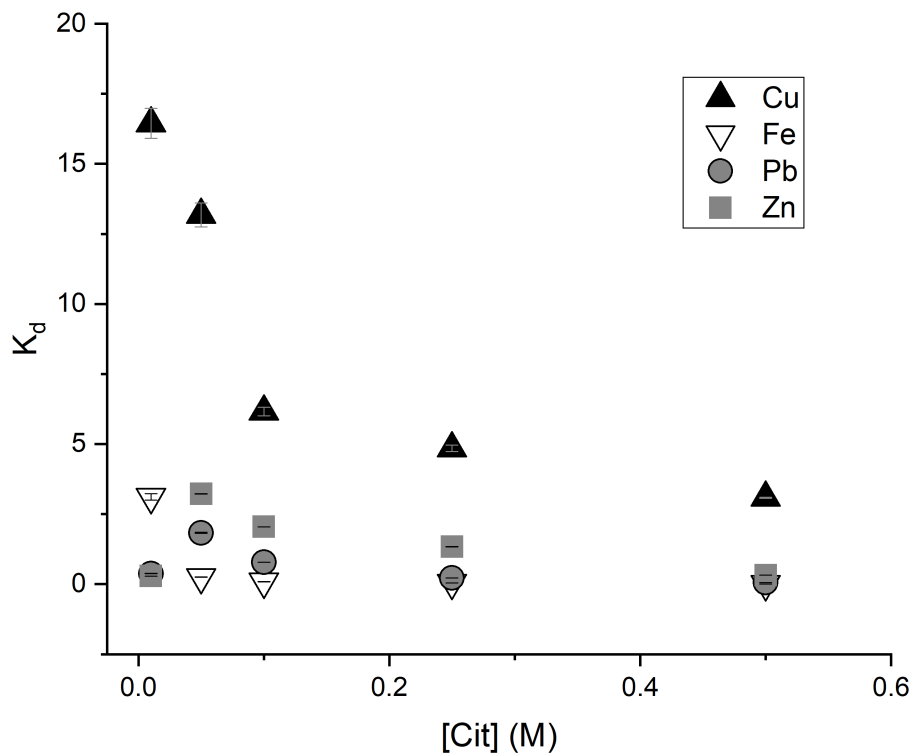


**Figure 7.1:** Distribution coefficients of the extraction of copper, iron(II), lead and zinc from citrate media as a function of citrate concentration (initial concentration 100ppm; temperature  $21^\circ\text{C}$ ;  $0.5\text{M NaCl}$ ;  $0.01\text{-}0.5\text{M}$  acetic acid; initial pH 5.75; 2mlwsr; 50ml solution; 24h).

## Mixed Metal Isotherms

Mixed metal isotherms of copper, iron(II), lead and zinc are displayed in Figures 7.2 (a), (b), (c) and (d). Copper is extracted to  $\sim 1.6\text{mmol g}^{-1}$ , displaying a steep increase in  $q_e$  until a  $C_e$  of  $\sim 0.2\text{mmol L}^{-1}$ , where the gradient increase is more linear. Both zinc and lead display substantial levels of desorption as the volume

of solution in contact with the resin is increased, for both species, this occurs at a  $C_e$  of 1-1.25  $\text{mmol L}^{-1}$ . The extraction of iron displays a decrease until 1.5  $\text{mmol L}^{-1}$  before a rapid increase in extraction at a  $C_e$  of 1.75  $\text{mmol L}^{-1}$ , then following a similar decrease trend from  $\sim 2.0 \text{mmol L}^{-1}$ .

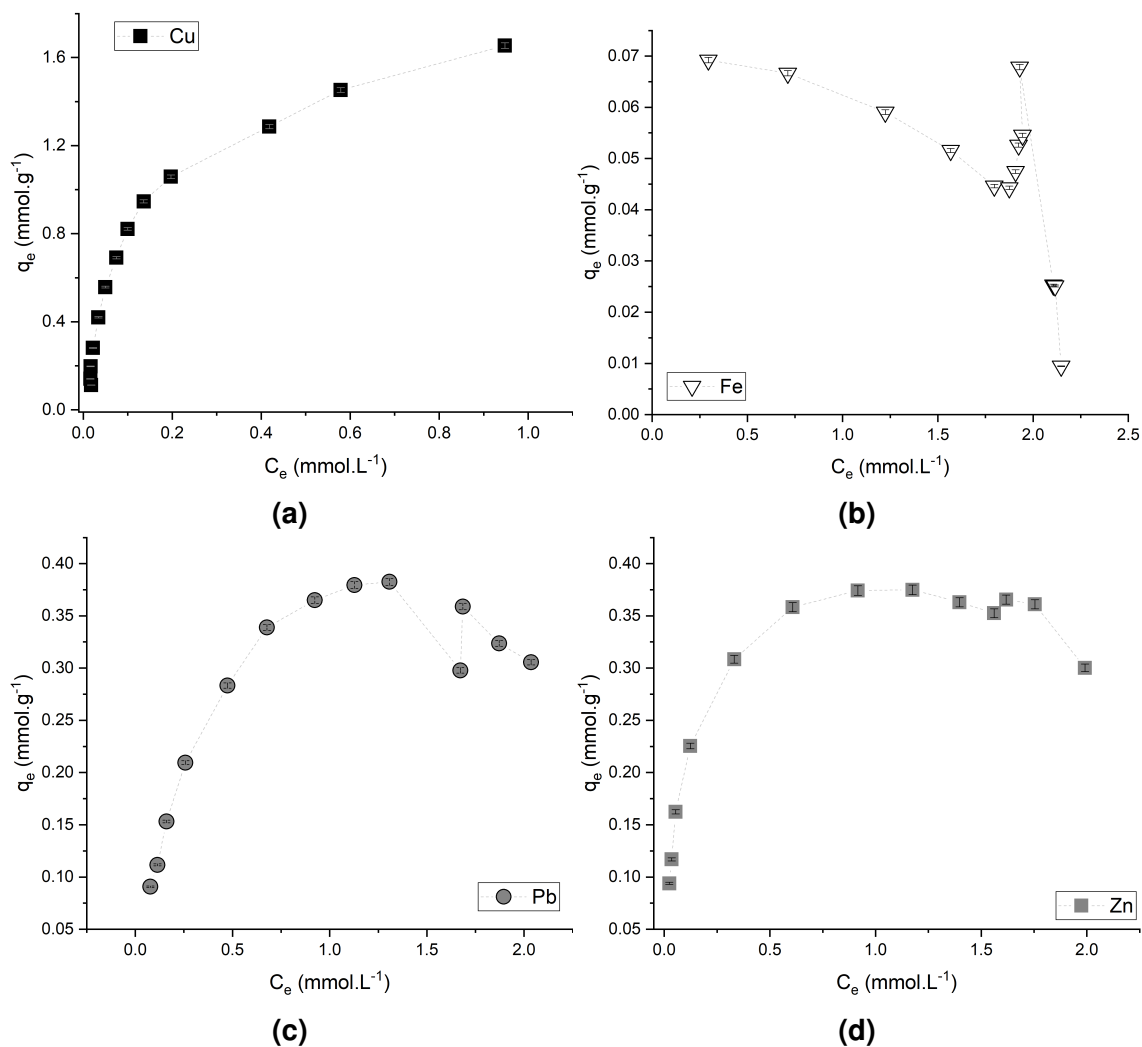


**Figure 7.2:** Concentration dependent extraction of copper (a), iron (b), lead (c) and zinc (d) by MTS9301 in citric acid media (initial concentration  $200 \text{mmol L}^{-1}$ ; temperature  $21^\circ\text{C}$ ;  $0.5 \text{mol L}^{-1}$  NaCl;  $0.1 \text{mol L}^{-1}$  citric acid; 2mlwsr; 25-400ml solution; 24h).

## Kinetics

The time dependent extraction performance of MTS9301 in citric acid is reported in Figure 7.3. Copper is the first species to attain equilibrium, at  $<250 \text{min}$ . Zinc and lead reach equilibrium after copper at  $<700 \text{min}$ , with iron

reaching a peak adsorption at  $\sim 500$ min before being desorbed from the resin back into solution. Equilibrium concentrations on the resin surface allude to the highest affinity for copper, with lead and zinc being similar, and iron(II) displaying a much lower affinity.

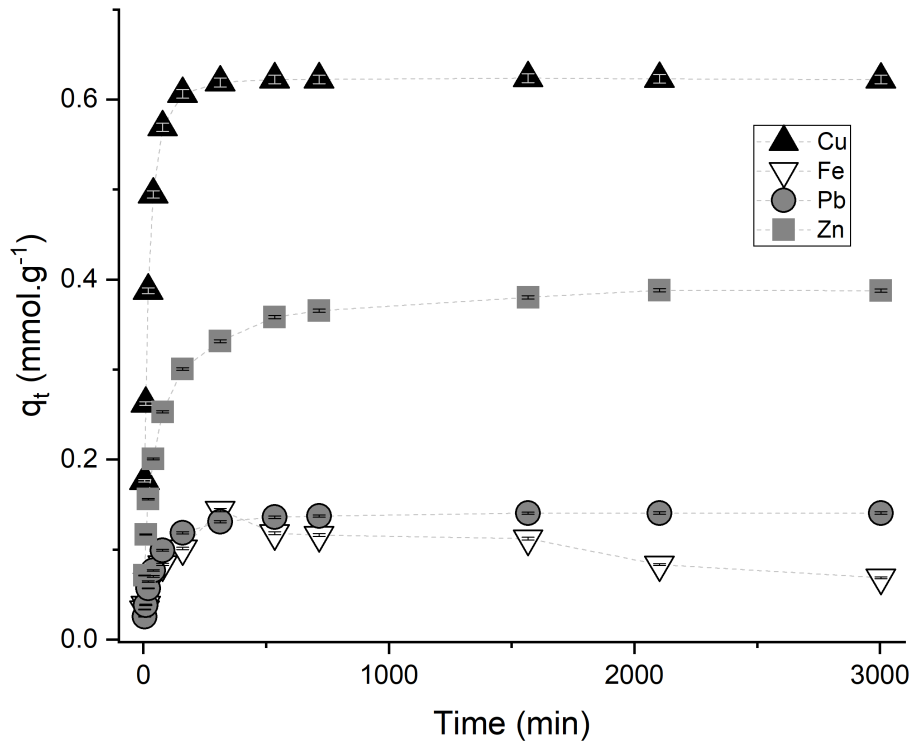


**Figure 7.3:** Time dependent extraction of copper (a), iron(II) (b), lead (c) and zinc (d) by MTS9301 in citric acid media (initial concentration 200ppm; temperature 21°C;  $0.5\text{mol L}^{-1}$  NaCl;  $0.1\text{mol L}^{-1}$  citric acid; 10mlwsr; 500ml solution).

## 7.4 Discussion

### Citric Acid Concentration Dependence

With decreasing concentration of citric acid, there is a clear increase in extraction of most metals. This is most obvious with both copper and iron(II), with copper  $k_d$  increasing from 3 to 16 and extractions of iron(II) extraction increasing to 98% from 6% (with citrate decreasing from 0.5 to 0.01M, Figures 7.1 and E.1). This trend is contradicted by lead and zinc at  $0.01\text{mol L}^{-1}$  which both display sharp decrease in extraction. This phenomenon is due to two potential factors.

The first explanation for both trends is the complex stability constants for lead and zinc being higher than that of iron(II) for citric acid, forcing iron(II) out of complexes (Figure E.2). The total molar concentration of metals within solution is  $0.0054\text{mol L}^{-1}$  (100ppm of each metal, vs  $0.01\text{mol L}^{-1}$  citric acid) leaves the total concentration of free citrate almost saturated (<50% remaining in solution), leading to lower complexation of iron(II) and higher competition for both lead and zinc from the remaining citrate complexes.

The sudden decrease at  $0.01\text{mol L}^{-1}$  citrate can also be hypothesised to be due to the exchange of metals for protons on the metals surface. The logarithmic relationship between protons and metals led to a large decrease in pH (pH 5.75 to  $\sim 2.5$ , Figure E.3), leading to a final proton concentration of  $\sim 0.0032\text{mol L}^{-1} \text{H}^+$ . The citric acid concentration of 0.01, will display a far lower buffering capacity, especially considering the exchange for  $0.0054\text{mol L}^{-1}$  divalent metals, as well as any proton-sodium exchange. The decrease in pH pushes the system into a far less favourable pH region for the extraction of both lead and zinc, where mono-citrate complexes out-compete for the IDA functionality<sup>[119]</sup>.

### Mixed Metal Isotherms

Four common two parameter isotherm models that will be used for description of the data obtained within this study are the Freundlich, Langmuir, Temkin and Dubinin-Radushkevitch (D-R) models. While these models are generally used for modelling singular metal systems, there is still merit that can be obtained by fitting them to regions of a multi-metal isotherm that do not incur either competition or desorption. These models are included within Table 7.1.

The Freundlich isotherm can be used to describe the heterogeneity of a binding species (determining relative sorption capacities,  $a_F$  and intensity of binding/heterogeneity,  $b_F$ ), and the Langmuir model describes a system

**Table 7.1:** Two-parameter single-metal isotherm models used within this study<sup>[151,152]</sup>.

Name	Model
Freundlich	$q_e = a_F C_e^{b_F}$
Langmuir	$q_e = \frac{q_{max} a_L C_e}{1 + a_L C_e}$
Temkin	$q_e = \frac{RT}{b_T} \ln(a_T C_e)$
D-R	$q_e = q_D \exp(-B_D (RT \ln(1 + \frac{1}{C_e}))^2)$

undergoing monolayer sorption (determining the monolayer sorption capacity,  $q_{max}$  ( $\text{mol g}^{-1}$ ) and the Langmuir isotherm constant,  $a_L$  ( $\text{L mol}^{-1}$ )). The energy related to sorption can be determined by the Temkin isotherm ( $b_T$  ( $\text{J mol}^{-1}$ ) is related to the heat of sorption and  $a_T$  is the Temkin isotherm constant), and D-R isotherm, which is also capable of determining the resin capacity ( $q_D$ ,  $\text{mol g}^{-1}$ ). The D-R free energy of adsorption,  $E$  ( $\text{kJ mol}^{-1}$ ), is then determined using  $B_D$ <sup>[151,152]</sup>, by:

$$E = \frac{1}{\sqrt{2B_D}} \quad (7.1)$$

The fits of the multi-metal isotherm data to each previously described models the data reported in Table 7.2, displaying the data for both the entire dataset of each metal and that of an altered data set, where the model is fit to the point where experimental  $q_e$  is equal to experimental  $q_{max}$ . Copper fits to the Temkin model with the highest  $r^2$  value (0.997), then the Langmuir model (0.988); both Freundlich and D-R models then fit with an  $r^2$  of 0.940 and 0.961. Due to the scatter in the data and the poor performance, iron(II) was not able to be fit to any of the models. While zinc attained an  $r^2$  of 0.955 when fit to the Langmuir model, the altered datasets provided much better fits to all models, with the poorest fit to the Freundlich model. The altered dataset of lead was capable of being fit with  $r^2$  of  $>0.95$  better.

Within the citric acid system, the intensities of binding of both copper and lead are similar, leading to an assumption of slightly heterogeneous binding

**Table 7.2:** Variables obtained by fitting the mixed metal isotherm data of MTS9301 to the two parameter isotherm models.

Model	Values	Copper	Iron(II)	Lead	Zinc
Unaltered Dataset					
Freundlich	$a_F$	$0.03 \pm 0.01$	–	$0.0023 \pm 0.001$	$0.0015 \pm 0.0004$
	$b_F$	$0.42 \pm 0.04$	–	$0.29 \pm 0.07$	$0.22 \pm 0.04$
	$r^2$	0.940	0.312	0.735	0.828
Langmuir	$a_L$	$7900 \pm 700$	–	$5000 \pm 1000$	$14000 \pm 2000$
	$q_m$	$1.79 \pm 0.06$	–	$0.40 \pm 0.02$	$0.38 \pm 0.01$
	$r^2$	0.988	0.000	0.878	0.955
Temkin	$b_t$	$6800 \pm 100$	–	$31000 \pm 4000$	$41000 \pm 4000$
	$a_t$	$92000 \pm 4000$	–	$5 \pm 3 \times 10^4$	$3 \pm 1 \times 10^5$
	$r^2$	0.997	-0.005	0.815	0.893
D-R	$q_D$	$5.7 \pm 0.7$	–	$0.8 \pm 0.2$	$0.66 \pm 0.08$
	$B_D$	$4.0 \pm 0.3 \times 10^{-9}$	–	$3.2 \pm 0.7 \times 10^{-9}$	$2.3 \pm 0.4 \times 10^{-9}$
	Energy	$11200 \pm 400$	–	$12000 \pm 1000$	$15000 \pm 1000$
	$r^2$	0.961	0.301	0.772	0.865
Altered Dataset					
Freundlich	$a_F$	–	–	$0.009 \pm 0.003$	$0.0021 \pm 0.0006$
	$b_F$	–	–	$0.46 \pm 0.04$	$0.26 \pm 0.04$
	$r^2$	–	–	0.964	0.909
Langmuir	$a_L$	–	–	$2800 \pm 200$	$12000 \pm 1000$
	$q_m$	–	–	$0.50 \pm 0.01$	$0.391 \pm 0.007$
	$r^2$	–	–	0.997	0.990
Temkin	$b_t$	–	–	$2200 \pm 700$	$36 \pm 3 \times 10^7$
	$a_t$	–	–	$26000 \pm 2000$	$19 \pm 6 \times 10^4$
	$r^2$	–	–	0.992	0.963
D-R	$q_D$	–	–	$1.5 \pm 0.2$	$0.77 \pm 0.08$
	$B_D$	–	–	$4.8 \pm 0.4 \times 10^{-9}$	$2.6 \pm 3 \times 10^{-10}$
	Energy	–	–	$10200 \pm 400$	$13800 \pm 800$
	$r^2$	–	–	0.977	0.937

for both species. The heterogeneity was much less apparent within the zinc system ( $b_F$  value of 0.26, accompanied with a much lower fit correlation). The extremely homogeneous nature of zinc can be explained by the overwhelming majority complexation of  $ZnHCit$  within solution (Figure E.2), while lead displays a combination of mono- and bis-citrate complexes, relating to the more heterogeneous intensity of binding; similar, in both cases, to what is observed within the single and multi-metal acetate systems. Copper, while it displays a majority  $CuOHCit^{-2}$  speciation, also displays slightly heterogeneous binding towards this functionality within the acetate system (Chapter 5); hypothesised to be due to a transition from proton-metal exchange to metal-metal exchange on the IDA functional groups of MTS9301, which would also be assumed to be the case in this situation, being more pronounced than within the acetate system with a much better description obtained by the Freundlich model (Chapter 5).

The low level of heterogeneity displayed in each of these fits is emphasised by the excellent fits observed for the Langmuir, monolayer model. Copper displays the highest monolayer capacity, by far, at  $1.79\text{mmol g}^{-1}$ , with lead and zinc displaying lesser capacities at  $0.50\pm 0.1$  and  $0.391\pm 0.0007\text{mmol L}^{-1}$ , respectively, all displaying reasonable estimates of the experimental data (copper and zinc being within error and lead being within 20% of experimental value), also being comparable capacities observed in the absence of complexing agents<sup>[163,172]</sup>. This is a similar observation to that of the acetate system, where copper has a much higher affinity towards the IDA functionality than the other metals; which is not perturbed by the presence of  $0.1\text{mol L}^{-1}$  citrate, a similar statement can be made for all metals, apart from iron(II) (Chapter 5).

The free energy of adsorption for copper, lead and zinc are all reasonably close with energies relating to ion exchange mechanism energies. In this instance, there are variances between the acetate and citrate systems, with a trend of  $Zn > Cu > Pb$ , while in the acetate system copper returns the lowest free energy of



binding (Chapter 5). This is same trend is observed with reference to the Temkin binding energies, with a larger variation between zinc and copper, however there is an inability to fit the Temkin isotherm to the acetate data. The observed trend is hypothesised to be due to the neutral charge on the ZnHCit complex, opposed to the negative charge on the copper complex (Figure E.2), leading the copper complex to be attracted to the IDA functionality through a  $\delta$ -positive caused by the doubly protonated IDA functionality at this pH. In the citrate system 100% of copper is found in  $\text{CuOHCit}^{2-}$  complexes and 100% of copper is in  $\text{CuIDA}_2^{2-}$  (at pH5.75). In contrast, not only do acetate complexes display lower stability constants (citrate out-competing the mono-, bis- and tris- acetate complexes), the lower pH dictates the higher abundance of CuIDA, and therefore a stronger, less heterogeneous binding mechanism<sup>[119]</sup>; although, the mechanism change (proton-metal to metal-metal exchange) was less pronounced in the citric acid system, playing another factor into the variation between systems. The lower binding energies of lead, are assumed to be caused by the lack of chelation within the IDA complex of the lead metal due to the large ionic radius of this ion.

While the models designed for systems containing singular metals fit well to each of these systems, either altered datasets or not, this is no description of processes governed by competition/desorption. This process has attempted to be described previously with the model:

$$q_e = \frac{q_{max} a_L C_e}{1 + a_L C_e} - des C_e^{des} \quad (7.2)$$

which is an alteration of the Langmuir model, where  $q_{max}$  and  $a_L$  are the adsorption maximum ( $\text{mol g}^{-1}$ ) and Langmuir equilibrium constant ( $\text{L mol}^{-1}$ ), respectively. This model then proposes an extra constant,  $des$ , that accounts for desorption (Chapter 5). While this model found difficulty in describing systems where there was a transition from proton-metal exchange to metal-metal exchange, it was able to describe a system that displayed desorption/competition

where saturations was reached, and give numerical value to the level of desorption occurred, allowing comparison between metals that showed a reduction in  $q_e$ .

**Table 7.3:** Variables obtained by fitting the mixed metal concentration dependence data of C107E to the desorption corrected Langmuir isotherm model.

Model	Values	Copper	Iron(II)	Lead	Zinc
Desorption	$a_L$	$9000 \pm 1000$	–	$1500 \pm 400$	$10000 \pm 1000$
Langmuir	$q_m$	$1.81 \pm 0.06$	–	$0.8 \pm 0.1$	$0.44 \pm 0.02$
	Des	$6 \pm 6 \times 10^{-5}$	–	$1.35 \pm 0.05$	$1.58 \pm 0.05$
	$r^2$	0.989	0.542	0.977	0.980

Table 7.3 displays the parameters acquired from fitting the desorption-modified Langmuir model to the isotherm data obtained within this study. Overall, this model was capable of fitting the unaltered data better than the single metal isotherm models were capable of doing, with  $r^2$  values of 0.989, 0.977 and 0.980 for copper, lead and zinc, respectively. While both copper and zinc displayed reasonable estimations of the experimental  $q_{max}$ , the estimation of lead was almost double of the experimental value. The Langmuir equilibrium constants remained similar between the two models.

It is observable from the isotherm profiles that copper displays very little, if any, desorption, which is then emphasised by the negligible desorption constant of  $6 \pm 6 \times 10^{-5}$ . Lead and zinc reported desorption values relative to that observable within this study, with lead displaying lower desorption than zinc. Both lead and zinc decrease in adsorption sharply until  $\sim 25\%$ , however the decrease in extraction is observed to be sharper in the case of zinc, than lead, with lead reaching  $\sim 25\%$  at total concentration of  $\sim 0.0005$  moles and zinc at closer to 0.0004 moles.

In a similar manner to the acetate system, using the same resin, there was a desorption trend of Zn>Pb>>Cu. The high affinity of copper for this functionality is again displayed through its out-competition of lead and zinc within another media (Chapter 5). The stability of zinc within solution by the formation of ZnHCit complexes, however has led to a higher level of desorption. In order for >90% extraction of all three metals, total molar concentration of metals cannot breach 0.1mmol, as opposed to the 0.729mmol within the acetate system. In the face of this, however, there is a much lower interference by iron(II), and due to the high concentration of iron within sewage sludge, potentially negating issues concerning iron saturation.

## Kinetics

The adsorption kinetics will be fit to the particle diffusion, film diffusion, Elovich, Lagergren and pseudo-second order kinetic models in order to describe and compare the kinetic limitations of each metal. These models can help in the determination of diffusion limitations, description of reverse reaction processes and operational parameters. The kinetic models in Table 7.4 give a brief outline of the models that will be used for description of the MTS9301 kinetics within citric acid media, in each case  $q_e$  is the equilibrium concentration of the respective metal on the resin's surface ( $\text{mmol g}^{-1}$ ).

**Table 7.4:** Kinetic models used within this study.

Name	Model
Particle Diffusion	$q_t = k_{PD}t^{\frac{1}{2}} + C$
Film Diffusion	$q_t = q_e(1 - e^{-k_{FD}t/2.303})$
Elovich	$q_t = \frac{1}{\beta} \ln(t + \frac{1}{\alpha\beta}) + \frac{1}{\beta} \ln \frac{1}{\alpha\beta}$
Pseudo-First Order	$q_t = q_e(1 - e^{-k_1t})$
Pseudo-Second Order	$q_t = \frac{q_e^2 kt}{1 + q_e kt}$

The particle and film diffusion models describe kinetics that are dictated by either diffusion through the particle or a stagnant concentration gradient at the particle-solution interface. In this case,  $k_{PD}$  and  $k_{FD}$  are the particle and film diffusion rate constants, respectively, with  $C$  begin the boundary layer thickness<sup>[195]</sup>. The Elovich model is capable of describing heterogeneous binding where both forward and reverse reactions are described; with  $\beta$  as the desorption constant ( $\text{g mol}^{-1}$ ) and  $\alpha$  as the initial sorption rate of the reaction ( $\text{mol/gmin}$ )<sup>[201,219]</sup>.

The pseudo-first and pseudo-second order rate models are capable of determining stoichiometric factors of reaction kinetics, however, using these operational parameters such as the initial rate and reaction half-lives can be calculated<sup>[201,203]</sup>. With a fit to the Lagergren pseudo-first order kinetic model, the half-life of an adsorption process can be calculated by:

$$\frac{0.693}{k_1} \quad (7.3)$$

where  $k_1$  is the pseudo-first order rate constant. From the parameters then acquired through the pseudo-second order model, the initial rate of reaction ( $h_0$ ) and the half-life of the reaction<sup>[203,220]</sup>, respectively with the following equations (where  $k_{2nd}$  is the pseudo-second order rate constant):

$$h_0 = k_{2nd}q_e^2 \quad (7.4)$$

$$\frac{1}{k_{2nd}q_e} \quad (7.5)$$

The variables obtained by fitting the kinetic data of the adsorption of copper, iron(II), lead and zinc from citric acid media by MTS9301 are displayed in Table 7.5. Neither copper, lead nor zinc was able to reasonably fit to the particle

**Table 7.5:** Non-linear kinetic modelling data for MTS9301 within citric acid media.

Model	Value	Copper	Iron	Lead	Zinc
Experiment	$q_e$	$622 \pm 5 \times 10^{-3}$	$144 \pm 2 \times 10^{-3}$	$141 \pm 1 \times 10^{-3}$	$388 \pm 2 \times 10^{-3}$
Particle	$K_{PD}$	–	–	–	$5 \pm 1 \times 10^{-3}$
Diffusion	C	–	–	–	$0.17 \pm 0.03$
	$r^2$	0.442	0.113	0.629	0.708
Film	$K_{FD}$	$117 \pm 7 \times 10^{-3}$	–	$51 \pm 6 \times 10^{-3}$	$49 \pm 8 \times 10^{-3}$
Diffusion	$q_e$	$613 \pm 8 \times 10^{-3}$	–	$135 \pm 3 \times 10^{-3}$	$36 \pm 1 \times 10^{-2}$
	$r^2$	0.982	0.641	0.963	0.922
Elovich	$\alpha$	$1 \pm 1$	–	$2 \pm 1 \times 10^{-2}$	$6 \pm 2 \times 10^{-2}$
	$\beta$	$15 \pm 3$	–	$52 \pm 5$	$19 \pm 1$
	$r^2$	0.789	0.411	0.922	0.962
Lagergren	$q_e$	$613 \pm 8 \times 10^{-3}$	–	$135 \pm 3 \times 10^{-3}$	$36 \pm 1 \times 10^{-2}$
	$k_{1st}$	$51 \pm 3 \times 10^{-3}$	–	$22 \pm 3 \times 10^{-3}$	$21 \pm 4 \times 10^{-3}$
	$t_{1/2}$	$13.7 \pm 0.9$	–	$32 \pm 4$	$32 \pm 6$
	$r^2$	0.982	0.641	0.963	0.922
Pseudo-2nd	$q_e$	$638 \pm 5 \times 10^{-3}$	–	$143 \pm 1 \times 10^{-3}$	$380 \pm 7 \times 10^{-3}$
Order	$k_{2nd}$	$51 \pm 3 \times 10^{-3}$	–	$23 \pm 1 \times 10^{-2}$	$82 \pm 9 \times 10^{-3}$
	$t_{1/2}$	$12.7 \pm 0.7$	–	$31 \pm 2$	$32 \pm 4$
	$h_0$	$50 \pm 3 \times 10^{-3}$	–	$46 \pm 3 \times 10^{-4}$	$12 \pm 1 \times 10^{-3}$
	$r^2$	0.994	0.653	0.996	0.983

diffusion model, instead all display reasonable correlation coefficients when described by the film diffusion model. The Elovich model fits reasonably to both lead and zinc, however copper was not described in a reliable manner. Both Lagergren and pseudo-second order models fit to this data with quite reliable correlation coefficients ( $r^2 > 0.9$ ), however there are observably better fits for the pseudo-second order model. Iron(II) will not be mentioned throughout this section of the discussion, as the slow desorption towards equilibrium generated difficulty to model.

The reasonable fits to the film diffusion kinetic model and the very close estimations of the experimental equilibrium adsorptions lead to the assumption of film diffusion determined rates, as opposed to particle diffusion. While the equilibrium adsorption of copper is predicted by this model to be within error of the experimental value, neither lead nor zinc are (both being predicted within  $\sim 10\%$  of experimental values). The macroporous nature of the resin bead, and efficient agitation are likely causes for the prevention of an intra-particulate gradient barrier.

With regards to the Elovich equation, copper will be ignored due to the poor fit. The desorption of lead is much higher than that of zinc, regardless of the fact that the rate of adsorption is much higher than that of lead, again, assumed to be due to the larger ionic radius of lead. The high binding energies of zinc, lead to the assumption of a strong chelating interaction between zinc and IDA preventing desorption. The desorption constants of lead and zinc are similar to that of the desorption constants that were reported for the same resin within an acetate system (Chapter 5).

The variation in fits between pseudo-first and pseudo-second order models leads to the assumption that each adsorption process follows a pseudo-second order reaction. The kinetics of this process follow the trend  $\text{Cu} > \text{Pb} = \text{Zn}$ . This

heavy reliance on the pseudo-second order kinetic model can be rationalised by a competition between the equilibrium of the complex formation within each species and the adsorption to the resin surface. This is reiterated for lead by the heterogeneous nature of its binding to this functionality. Both copper, and zinc, while not displaying the multiple species within solution, do display high stability constant for the complex that is maintained within solution at this pH and citrate concentration.

While the half-lives for copper and lead are similar to that observed within the acetate system (lead being slightly larger), zinc displays a half-life nearly half that of the acetate system. Counter to this, initial rates of both lead and copper are an order of magnitude higher within the citric acid system, while zinc remains the same (Chapter 5). In the case of the iminodiacetic acid functionality, copper is very hindered, displaying a half-life an order of magnitude longer with respect to the same commercially available resin<sup>[182]</sup>. Previous studies of carboxylic acid complexing agents has shown that lead behaves in a kinetically similar fashion towards both carboxylic acid and IDA functionalise resin (Chapter 5), leading to the assumption that there is a hindrance of this species towards the IDA functionality, displaying a much slower half-life than a weak acid resin in the absence of a complexant<sup>[172]</sup>. With comparisons to strong acid resins displaying adsorption half-lives an order of magnitude lower<sup>[221]</sup>, the selectivity of this system becomes the attractive and interesting feature.

## 7.5 Conclusions

The adsorption of copper, iron(II), lead and zinc by MTS9301 from citric acid media has been studied with regards to citrate concentration, metal abundance and time. Solution phase speciation was modelled in order to determine the influence of citrate complexes on extraction phenomena. Data obtained from the multi-metal isotherm and kinetic studies were fit to common isotherm and kinetic

models as well as an isotherm model derived in an attempt to better describe a system containing desorption/competition.

It was determined that the most effective concentration of citric acid for the adsorption of metals from solution was  $0.1 \text{ mol L}^{-1}$ . This allowed for the maximum amount of copper, lead and zinc to be removed, while suppression of iron(II) adsorption was maintained at a reasonable level. Above this concentration, suppression of lead and zinc began to climb, and below this concentration iron(II) suppression decreased, followed by an increase in suppression of lead and zinc due to difficulties in maintaining post-contact pH.

MTS9301 maintained relatively average capacities for copper, lead and zinc within this media, especially considering the multi-metal media. Iron(II) capacity, however, dwindled markedly with a low equilibrium adsorption that decreased further with an increase in total metal abundance. While the total effectiveness of the resin was decreased within this media, modelled capacities for individual metals did not vary markedly from those observed within the acetate system. Kinetics, on the other hand were altered by citrate, with desorption of iron(II) leading to a two stage kinetic process, and the rates of copper, lead and zinc adsorption improving overall.

This study has shown that citric acid media is a viable media for the RIP system proposed for the removal of metals from acid leached sewage sludge. While there are definitely stronger interactions between citrate moieties and metals than within other weak acid media, the ability for MTS9301 for recovery of copper, lead and zinc was maintained, while simultaneously reducing interference by iron within a real system. With implications for both this process and the broader hydrometallurgical field, citrate has been determined as suitable weak acid, complexing lixiviant of metals.



# Chapter 8

## Conclusive Remarks and Further Work

### 8.1 Recycling Sewage Sludge

Phosphate, as a resource, is of underrated importance to the global population. This resource creates the foundation to which every agricultural process is based upon; without it there would be no crop growth, no livestock and therefore, no food<sup>[3]</sup>. Being the precious nutrient it is, a global deficit would be an alarming prospect.

Currently, the phosphate reserves are sitting at a predicted lifetime of between 30 and 400 years<sup>[4,7]</sup>, this is assuming population growth and consumption continue to grow at the predicted rate. The time limits vary from source to source depending on the reserves that have been included within the models<sup>[4,7]</sup>, with the lower quality reserves being profitable (from an environmental and safety perspective), as many heavy metals, including in some cases radionuclides, are incorporated into the phosphate mineral matrix<sup>[222]</sup>. These numbers are extremely alarming and, although there may be new natural reserves waiting to be discovered, the time limit will only be extended, not completely avoided.

With this in consideration, the recycling of ingested phosphate (through the usage of sewage sludge) becomes appealing. Sewage sludge can contain up to 44% of the phosphate that is contained within commercially available fertilisers<sup>[15]</sup>, which is an extremely high number considering that it is thought of as waste in many regions. The reuse of this phosphate source is already reasonably common, with the utilisation of almost 80% of all sewage sludge for amendment of agricultural soil within the UK (Figure 8.1)<sup>[16]</sup>. This agricultural use of sludge is limited, however, in season and crop application<sup>[16]</sup>, and in many cases not the most environmentally conscious practice.

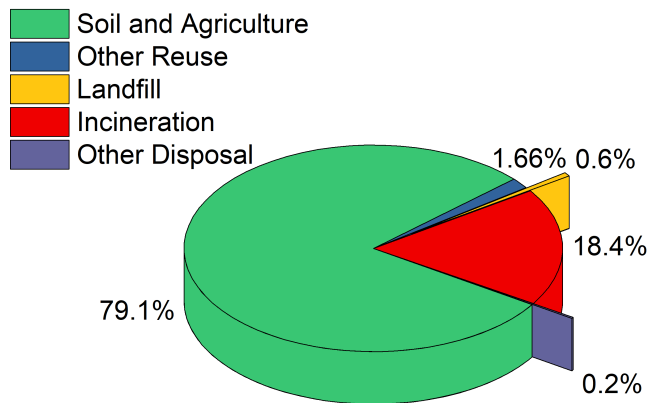


**Figure 8.1:** Proportion of final routes for disposal or reuse of sewage sludge within the UK<sup>[16]</sup>

Due to source combination of waste water streams, such as industrial waste waters, domestic waste waters and storm water, particularly in older infrastructure, the concentration of metals within sewage sludge can reach alarming highs. Many metals such as copper, lead and zinc (as well as nickel, chromium, arsenic and cadmium) can be high enough to render the sewage sludge unfit for application or at least raise concern for accumulation<sup>[34]</sup>. This inclusion of heavy metals into sewage sludge has led to guidelines on sludge

usage, and is also a cause for the application limits stated previously.

There is a large disparity between the guidelines that are imposed upon sewage sludge and those that are imposed upon fertilisers; which are far more stringent<sup>[23,24]</sup> (Figure 8.2). This means that the application of sewage sludge as a phosphate source replacement can actually be detrimental to crop growing land. These disparities in regulation that lead to the requirement of both crop and temporal limitations regarding sludge application<sup>[25]</sup> are not imposed upon mineral phosphate based fertilisers, perhaps with the removal of heavy metals from sludge, its value as a fertiliser could be increased.

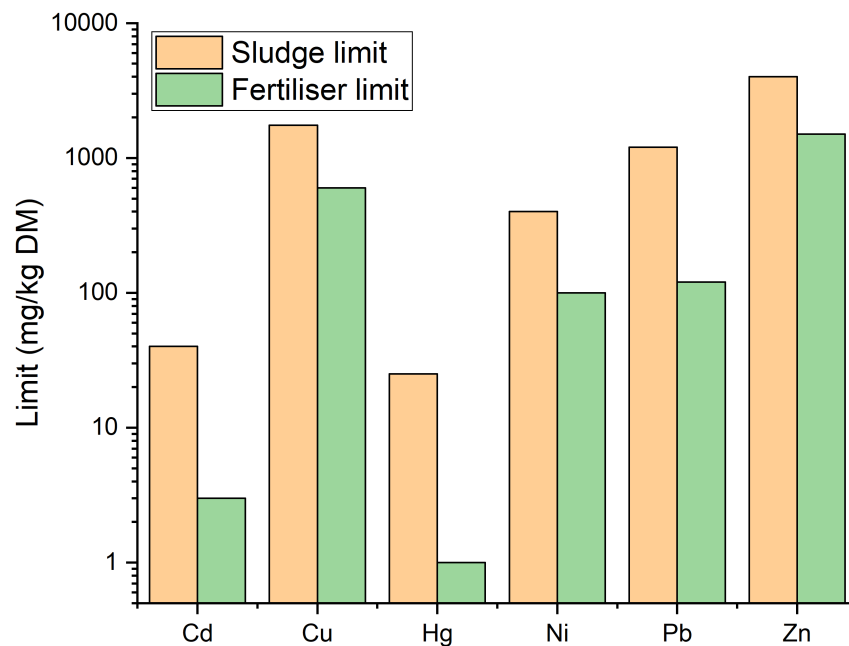


**Figure 8.2:** Permissible limits of heavy metals within sludge intended for agricultural application and fertilisers based upon mineral phosphates<sup>[23,24,223]</sup>

Despite the argument that many of these metals are also micro-nutrients, and that soil deficiencies within crop-growing regions are increasing<sup>[45,224]</sup>, there is currently no real effort towards the control of the metallic concentrations within sludge intended for farming application, with the focus, instead, being on immobilisation<sup>[16,35]</sup>. This becomes an issue as, while metals are beneficial to both crop growth and human health, there is an extremely fine line between

a deficiency and an excess of many of these metals. Figure 8.3 displays a comparison between limits of micro-nutrient deficiency, guideline soil limits, sludge concentrations and levels of micro-nutrients that can lead to plant toxicity. It can be seen how quickly accumulation of excessive micro-nutrients is not only an issue with sewage sludge, there is also this concern leading to plant toxicity with regards to micro-nutrient amended soils<sup>[35,45]</sup>. The deleterious effects of accumulations of micro-nutrients within soils can lead to toxicity within crop growth for decades after the excess becomes obvious<sup>[45]</sup>.

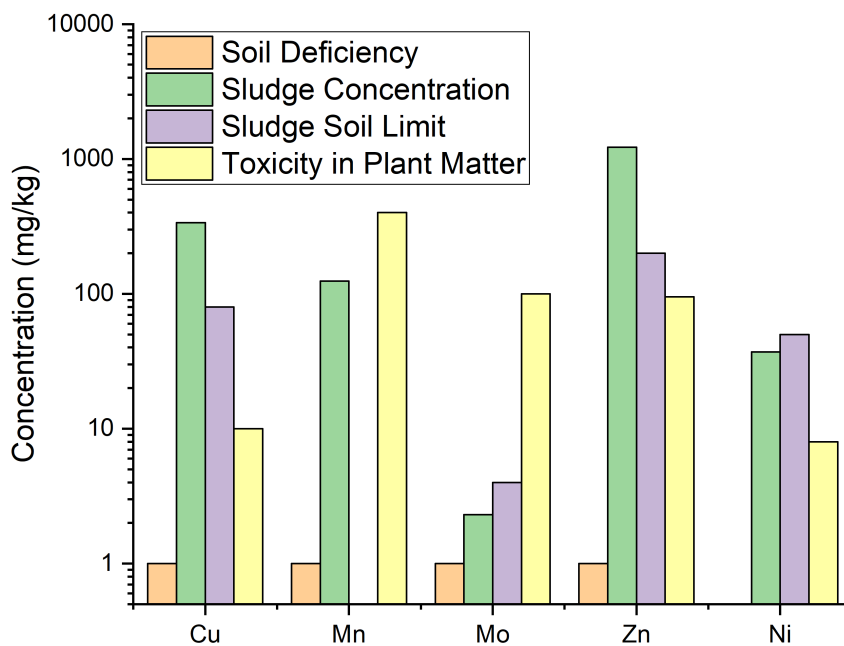


**Figure 8.3:** A comparison of the concentration of metals that constitute a deficiency in micro-nutrients<sup>[225]</sup>, concentration of metals within sludge (Cu, Zn and Mo were referenced Inglezakis, *et al.* 2014<sup>[34]</sup>, while a lack of data required Mn and Mo to be sourced from Vriens, *et al.* 2017<sup>[33]</sup>), limits of metals within soils for sludge application<sup>[23]</sup> and levels that lead to toxicity within plant matter<sup>[45]</sup>.

The high concentration of metals within sewage sludge, although limiting for the agricultural utilisation, open up the opportunity for a stockpile of raw metals, generating the potential for a secondary income stream. Toxic metals such as cadmium, copper, lead, nickel and zinc, these contain value within their own right<sup>[40–42]</sup>. While base metals do not carry the highest of value propositions, the waste water input unlocks a further far more valuable proposition - precious

metals<sup>[33]</sup>.

**Table 8.1:** Values of specified precious metals attainable from sewage sludge.

Metal	Value (£.t <sup>-1</sup> )	Sludge (£.t sludge <sup>-1</sup> )	Reference
Cadmium	30539	0.24	[40]
Cerium	3139	2.68	[40]
Cobalt	25780	1.11	[41]
Copper	5190	0.30	[41]
Lead	1370	0.17	[41]
Neodinium	49091	1.01	[40]
Titanium	3696	0.86	[42]
Zinc	1860	0.29	[41]
Precious Metal	Value	Sludge (£.t sludge <sup>-1</sup> )	Reference
Gold	£1923.4.t oz <sup>-1</sup>	123.80	[41]
Paladium	£1876.49.t oz <sup>-1</sup>	59.49	[41]
Platinum	£681.45.t oz <sup>-1</sup>	48.20	[41]
Rhodium	£733.85.t oz <sup>-1</sup>	237.09	[42]
Ruthenium	£14.78.t oz <sup>-1</sup>	1.94	[40]
Silver	£19.32.t oz <sup>-1</sup>	65.23	[41]

With the decay of catalytic converters within every car exhaust system, heavily trafficked areas exhibit high concentrations of platinum group metals (PGM, Pt, Rh, Rd, Pd) within roadside dirt, itself being a sought after resource<sup>[43]</sup>. Being some of the most valuable elements on the periodic table, PGM can be valued between £14.78 to £1876.49.t oz<sup>-1</sup><sup>[40-42]</sup>. Couple this with the high concentrations of gold and silver also found within sewage sludge (in some cases rivalling that of low quality ore<sup>[33]</sup>) and the economical picture is starting to build up quite remarkably.

Much of the work surrounding the removal of metals from sewage sludge has been focused on metals as a waste material, with a multitude of studies utilising either bioleaching and chemical leaching methods<sup>[61-72,78,79]</sup>, in many cases mobilising close to 100% of metals from immobile phases. The downfall is,

however, that all of these previous studies propose a solid-liquid separation stage as a final solution, and as dewatered sludge generally has a moisture content of  $\sim 40\text{-}80\%$ <sup>[14]</sup>, a large fraction of the now mobile metallic species will remain entrained within the solid residue. Despite the later immobilisation of metals by sludge neutralisation, these fractions will still remain more mobile than the original sulphide speciation; which is where ion exchange and the current body of work gains significance.

With a wealth of information surrounding the removal of metals from immobile phases within sewage sludge already existing within the literature, there is only one thing necessary to complete the process for the recycling of phosphate from sewage sludge - that is the effective extraction of metals from sewage sludge leachate slurry. Utilising RIP technology, it is possible to add a solid phase extractant directly to the sludge, mitigating the issues that arise for the current hypothesis of a solid-liquid separations stage<sup>[86-92]</sup>. This could not only be hypothesised to be better, environmentally, than the direct addition of sludge, but it would also create the potential for controlled addition of micro-nutrients and allow for a potential secondary income via sales of base and precious metals (Figure 8.4).

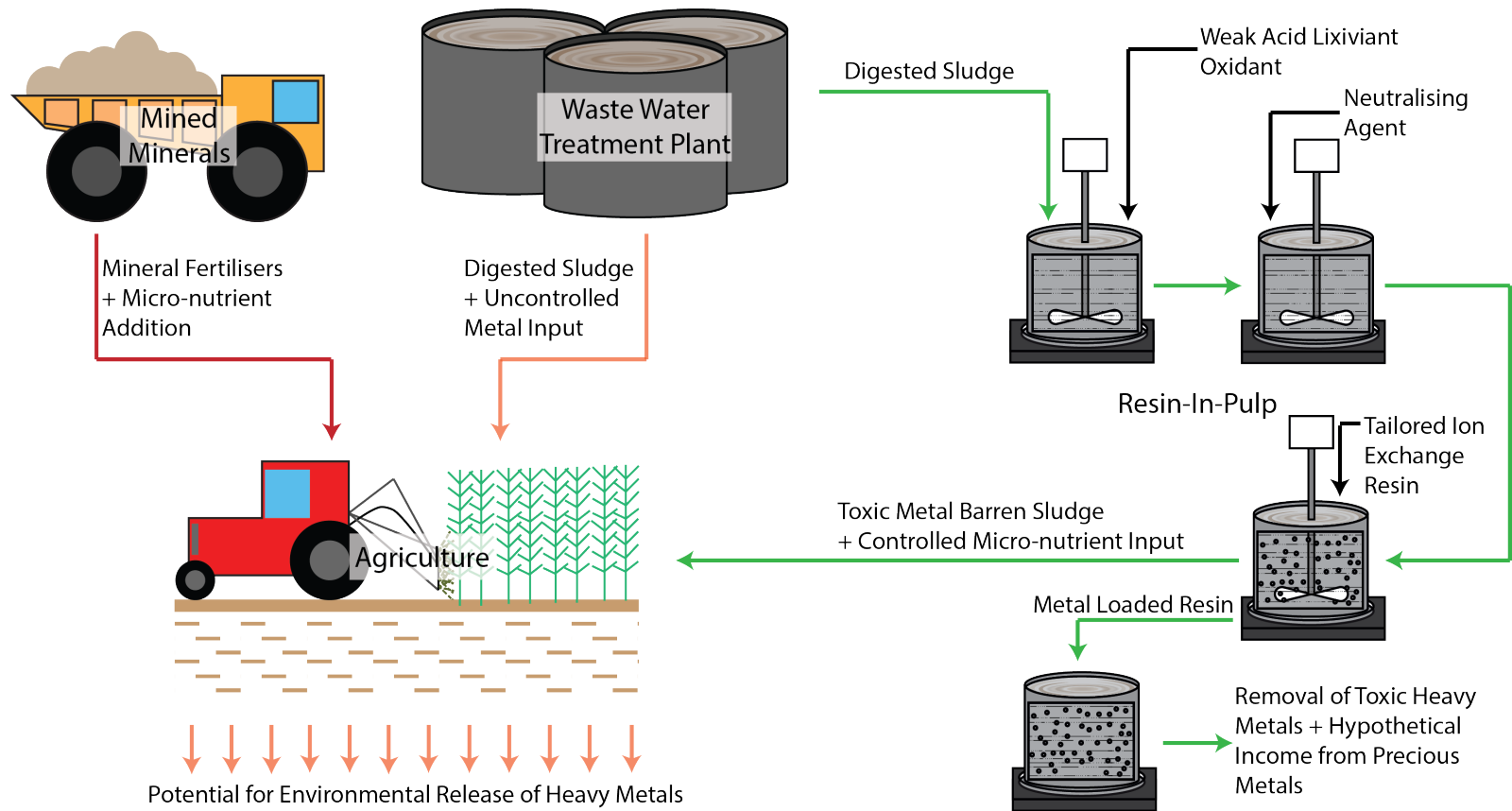


**Figure 8.4:** A summary where the process derived throughout this thesis fits into the supplementation and replacement of mineral fertilisers. Arrows in red represent nutrients sourced from commercial fertilisers, arrows in orange represent nutrients sourced directly from digested sewage sludge and arrows in green represents the RIP process from this thesis.

The aim of this body of work is to answer the question "can the use of weak acids as a lixiviant be used within a RIP process for the removal and recovery of copper, lead and zinc as an alternative to solid-liquid separation?" This work has been focused on the usage of weak, complexing acids as a method of stabilisation of metals within solution, preventing precipitation of the focus species, understanding the nature of commercially available ion exchange resins within these media and their applicability to system with a high concentration of organic solid matter. With the success of weak acid leaching on sewage sludge<sup>[69,71,78,79]</sup>, the potential for weak acids to add a layer of selectivity upon the ion exchange resin functionality<sup>[118,119,124,135]</sup> and the lack of understanding within this field, the majority of the work conducted surrounded gaining an in depth understanding of the ion exchange processes within weak acid media, the mechanistic details and performance of these otherwise well understood phenomena.

Within this body of work, two broad studies have screened a selection of ion exchange functionalities within weak acid media, gaining an understanding of the effect solution phase conditions can display upon commercially available resins<sup>[119,135]</sup>. Acetic acid, citric acid and lactic acid were compared against each other, determining the potential selectivity of each resin within complexing media (summarised within Figure 8.5), determining that acetic acid had the least effect overall on the pH dependence of the ion exchange resin, however this led to the least selectivity within unsaturated conditions. An understanding of selectivity between functionalities and media is crucial to elucidate a path forward for the extraction of target metals within media that saturated in problematic species; this was presented within both acetic (Chapter 4<sup>[124]</sup> and Chapter 5) and citric acid (Chapter 7) systems generating knowledge for scavenging metals within sewage sludge and hydrometallurgy in general.



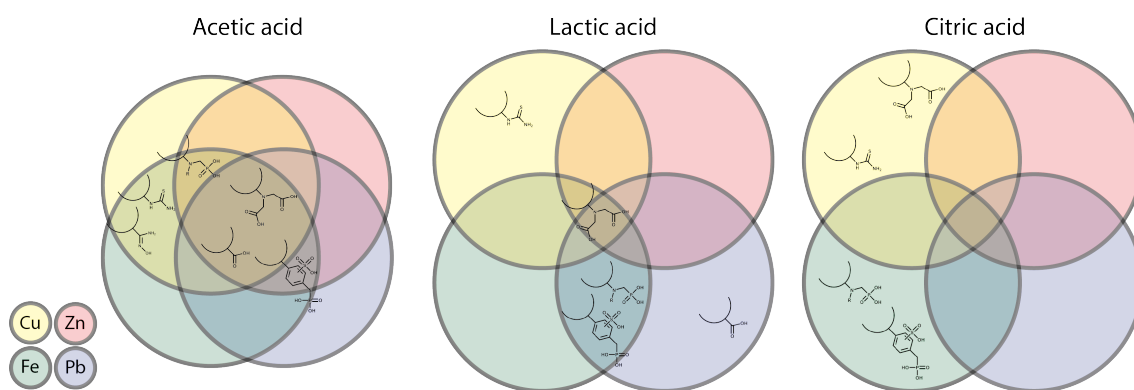


**Figure 8.5:** Venn diagrams summarising the selective nature of each functionality determined from the resin screening study within acetic, lactic and citric acid media. Reproduced from Bezzina *et al.* 2019<sup>[119]</sup>.

With an understanding of the ion exchange behaviour within weak acid established through experimentation and an understanding of the leaching behaviour gathered from literature sources<sup>[69,71,78,79]</sup>, a lab-scale RIP process on a simulated sludge was undertaken. Increasing the complexity from clean, simulated PLS to a more realistic leachate slurry (inclusive of organic matter and phosphate) led to many downfalls in comparison to the clean PLS counterpart study; such as inefficient leaching stages, precipitation of target species and competitive extraction of contaminant species within the leachate slurry. With all the pitfalls, this led to maximum recoveries of 39% copper, 38% lead and 54% zinc, this is representative of a simple, single stage extraction process, and the process has been proved to be possible.

While the recoveries are not 100%, the total number of applications of sludge to a field would be increased by this value and this process has proved (extraction-wise) competitive with the solid-liquid separation phase. Furthermore, metals have been rendered in a commercially attainable form, on the surface of an easily elutable resin and the application of multiple stages could be utilised to control the concentration of micro-nutrients, again, increasing the value of this material as a fertiliser. The economics, on the other hand, were not favourable for the unoptimised process; with the most profitable case returning a net deficit (before consideration of cheaper alternative reagents and reuse of the resin) was -£1576.

This is to be expected, however, when attempting an economical assessment prior to the implementation of more economical reagents and a linear scaling from bench experiments.

Understanding the bench-scale nature of this proof-of-concept, it is assumed that with optimisation, economic selection of reactants and the addition of income gathered by the potential extraction of precious metals, this process could be quite profitable<sup>[33,194]</sup>. The potential economic gain of the extraction of metals from sewage sludge, however, is not the sole draw and is most certainly not the reason that this research was conducted (hence the decided copper, lead and zinc for extraction within this work). Anthropological, environmental and sustainability issues surrounding phosphate as a raw material should still be the main driving factor, so the economic appeal of the process may well be only used to attract commercial interest and investment; made paramount when this cost is compared to the dramatic fluctuation in the cost of raw phosphate<sup>[217]</sup> and social issues that this can cause<sup>[226]</sup>. In summary, with the looming shortages in phosphate reserves, potential environmental issues with the direct application of digested sludge in agriculture and the potential economic gain with process optimisation, there is the urgent need for the exploration of every resource that is available to human kind.

## 8.2 Future Work

### Engineering the Process

With the experimental success of this work in comparison to the solid-liquid separation stages hypothesised; issues with regards to competing species and the effects that solids and complexants within sludge have on the entire ion exchange process have been determined. These issues are combined with the uneconomical nature of the process generated, the perceived issues and some actions that could achieve a higher technical readiness level, are listed as follows:

- Contaminant species are orders of magnitude higher than the focus metals within sewage sludge.
  - A clean PLS study is required on the effect of concentration of iron, calcium and humic and other strong complexing acids on extraction of the target metals
  - A clean PLS study on the pH, ORP and complexing acid reliance on haematite and cuprousferrite precipitation will give further details on the operational conditions
- With all studies on RIP processes, the effect of solids on the kinetics or the capacity of an ion exchange resin is unknown or unreported.
  - Controlled studies must be undertaken, creating a matrix of solids content vs kinetic and isotherm parameters to understand the effect that an increase in solids has on the diffusion and equilibrium of ion exchange adsorption
- Many questions have been risen about the cost and the disposal of the organic acids required in this study.
  - Studies must be conducted into the removal of organic acids from the liquid effluent product of this process

- Estimates on the recoverability of these acids through distillation processes and techno-economic assessments of these processes should be conducted
- With the current negative attention that microplastics have within the environmental setting, and the percentage of resins below the stated size range, the possibility of microplastic release is quite high.
  - Novel adsorbent materials, such as extruded polymers, could be functionalised, to create a strand or woven adsorbent material further simplifying the separation
  - With the thermo-plastic nature of PVC, utilising this substrate for the extruded polymer backbone could allow for an easily substituted chloride group as well as providing a cheap, simple source from recycled plastic materials.
- With the unfavourable economics of this process, optimisations and reevaluations are required.
  - Similar studies should be conducted using sulphuric acid as an economic alternative to nitric acid within the acidification stage, and utilising ozone to replace hydrogen peroxide within the oxidation stage of the metal sulphides
  - With the increasing interest in more environmentally friendly and economic thiourea leaches of precious metals from low quality ores<sup>[227]</sup>, this should be included into the RIP process for the extraction of more economically focused metals from sewage sludge.
- With the knowledge of the effect that contaminants and solids can have on the RIP process, the next stage is to understand how this will perform within a realistic scenario on the small scale.

- Conduct RIP experiments on real sewage sludge with parameters determined from within this thesis
- With the RIP experiment conducted, a techno-economic assessment is required to understand the feasibility of base metals removal

### **Fundamental Ion Exchange Study**

The use of complexing agents and their effect on ion exchange extractants is highly understudied. This work has created a lot of questions regarding the effect of a complexing agent with a similar functional group to that of an adsorbent matrix has on the performance of this species and therefore the equilibrium between solid adsorbed species. This knowledge is not only of great benefit to the extraction of metals from sewage sludge but to the broader the research and industry surrounding the extraction of value from wastes such as waste electronic equipment, industrial sludge, landfill, etc. and in a world that is swiftly approaching shortages in many essential minerals, this is gaining in relevance. With this, many questions come to mind for a greater understanding of ion exchangers as scavenger species:

- Can complexing lixiviants be utilised to generate a more selective ion exchange process?
- How is each of these processes impacted by ionic strength?
- With the ineffective nature of the desorption modified Langmuir model, is there a possibility for the enhancement of this model?



# Bibliography

- [1] UNDESA, “World population prospects: The 2012 revision, highlights and advance tables,” Tech. Rep. Working Paper No. ESA/P/WP.228., United Nations, Department of Economic and Social Affairs, Population Division (2013), 2013.
- [2] United Nations, “World population prospects 2019: Highlights,” tech. rep., United Nations, 2019.
- [3] M. Roser and E. Ortiz-Ospina, “World population growth,” *Our World in Data*, 2017.
- [4] D. Cordell, J. Drangert, and S. White, “The story of phosphorus: global food security and food for thought,” *Global environmental change*, 2009.
- [5] D. Cordell, S. White, and T. Prior, “Securing phosphorus: food for thought, and food for the future,” *The Conversation*, 09 2011.
- [6] FAO, “World fertilizer trends and outlook to 2022,” summary report, Food and Agriculture Organization of the United Nations, 2019.
- [7] P. Wan, S. Davidsson, S. Johansson, and M. Höök, “Phosphate rock production and depletion: Regional disaggregated modeling and global implications,” *Resources, Conservation and Recycling*, vol. 93, pp. 178–187, 2014.
- [8] E.C., “Critical raw materials,” 2017.

- [9] U. G. Survey, "Mineral commodity summaries 2019," tech. rep., U.S. Department of the Interior, 2019.
- [10] G. Reta, X. Dong, Z. Li, B. Su, X. Hu, H. Bo, D. Yu, H. Wan, J. Liu, Y. Li, G. Xu, K. Wang, and S. Xu, "Environmental impact of phosphate mining and beneficiation: review," *Int. J. Hydro.*, vol. 2, no. 4, pp. 424–431, 2018.
- [11] F. Faridullah, M. Umar, A. Alam, M. Amjad Sabir, and D. Khan, "Assessment of heavy metals concentration in phosphate rock deposits, hazara basin, lesser himalaya pakistan," *Geosci. J.*, vol. 21, pp. 743–752, 2017.
- [12] Sabiha-Javied, T. Mehmood, M. Chaudhry, M. Tufail, and N. Irfan, "Heavy metal pollution from phosphate rock used for the production of fertilizer in pakistan," *Microchem. J.*, vol. 91, no. 1, pp. 94–99, 2009.
- [13] A. Modaihsh and A. MS, "Heavy metals content of commercial inorganic fertilizers marketed in the kingdom of saudi arabia," *Precision Agriculture*, 1999.
- [14] Metcalf, Eddy, G. Tchobanoglous, F. L. Burton, V. T. Chow, R. Eliassen, and R. K. Linsley, *Wastewater Engineering: Treatment Disposal Reuse*. Wastewater Engineering, McGraw-Hill Book Company, second ed., 1991.
- [15] J. Spångberg, P. Tidåker, and H. Jönsson, "Environmental impact of recycling nutrients in human excreta to agriculture compared with enhanced wastewater treatment," *Sci Total Environ*, vol. 493, pp. 209–219, 2014.
- [16] DEFRA, "Waste water treatment in the united kingdom - 2012," 2012.
- [17] D. Fytili and A. Zabaniotou, "Utilization of sewage sludge in EU application of old and new methodsA review," *Renew Sustain Energy Rev*, vol. 12, no. 1, pp. 116–140, 2008.



- [18] S. Ishii and T. Boyer, "Life cycle comparison of centralized wastewater treatment and urine source separation with struvite precipitation: Focus on urine nutrient management," *Water Res*, vol. 79, pp. 88–103, 2015.
- [19] K. Suzuki, Y. Tanaka, K. Kuroda, D. Hanajima, Y. Fukumoto, and T. Yasuda, "The technology of phosphorous removal and recovery from swine wastewater by struvite crystallization reaction," *JARQ*, vol. 40, no. 4, pp. 341 – 349, 2006.
- [20] Y. Ueno and M. Fujii, "Three Years Experience of Operating and Selling Recovered Struvite from Full-Scale Plant," *Environ. Technol.*, vol. 22, no. 11, pp. 1373–1381, 2001.
- [21] H. Weigand, M. Bertau, W. Hübner, F. Bohndick, and A. Bruckert, "RecoPhos: full-scale fertilizer production from sewage sludge ash," *Waste Management*, vol. 33, no. 3, pp. 540–544, 2013.
- [22] juris GmbH,  
"German fertilizer ordinance (verordnung über das inverkehrbringen von düngemitteln, bodenhilfsstoffen, kultursubstraten und pflanzenhilfsmitteln (düngemittelverordnung - dümv)),", tech. rep., Bundesministeriums der Justiz und für Verbraucherschutz, 2012.
- [23] EC, *Council Directive on the protection of the environment, and in particular of the soil, when sewage sludge is used in agriculture [82/278/EEC]*. The Council of the European Communities, 1986.
- [24] T. E. Parliament and the Council of the European Union, eds., *Regulation (EU) 2019/ Of the European Parliament and of the Council of laying down rules on the making available on the market of EU fertilising products and amending Regulations (EC) No 1069/2009 and (EC) No 1107/2009 and repealing Regulation (EC) 2003/2003*, EU, 2019.
- [25] DEFRA, "Code of Practice for Agriculture Use of Sewage Sludge," 2006.

- [26] A. J. G. Geoffrey M. Gadd, "Microorganisms and heavy metal toxicity," *Microbial Ecology*, vol. 4, pp. 303–317, Dec. 1977.
- [27] R. Stevens, "Targeted national sewage sludge survey sampling and analysis technical report," tech. rep., United States Environmental Protection Agency, 2009.
- [28] P. Hsiau and S. Lo, "Extractabilities of heavy metals in chemically-fixed sewage sludges," *J. Haz. Mat.s*, vol. 58, no. 1-3, pp. 73 – 82, 1998.
- [29] Z. Liu, G. Qian, Y. Sun, R. Xu, J. Zhou, and Y. Xu, "Speciation evolutions of heavy metals during the sewage sludge incineration in a laboratory scale incinerator," *Energy Fuels*, vol. 24, no. 4, pp. 2470–2478, 2010.
- [30] D. de la Varga, D. Díaz, M. A. Ruiz, and I. Soto, "Heavy metal removal in an uasb-cw system treating municipal wastewater," *Chemosphere*, vol. 93, no. 7, pp. 1317 – 1323, 2013.
- [31] F. Fu and Q. Wang, "Removal of heavy metal ions from wastewaters: A review," *J. Environ. Manage.*, vol. 92, no. 2, pp. 407 – 418, 2011.
- [32] K. Kolecka and H. Obarska-Pempkowiak, "Potential fertilising properties of sewage sludge treated in the sludge treatment reed beds (strb)," *Water Sci. Technol.*, vol. 68, no. 6, pp. 1412 – 1418, 2013.
- [33] B. Vriens, A. Voegelin, S. Hug, R. Kaegi, L. Winkel, A. Buser, and M. Berg, "Quantification of element fluxes in wastewaters: A nationwide survey in switzerland," *Environ Sci Technology*, vol. 51, pp. 10943 – 10953, 2017.
- [34] V. J. Inglezakis, A. A. Zorpas, A. Karagiannidis, P. Samaras, I. Voukkali, and S. Sklari, "European Union Legislation on Sewage Sludge Management," *Fresenius Environ. Bull.*, vol. 23, no. 2a, pp. 635–639, 2014.
- [35] S. R. Smith, *Agricultural Recycling of Sewage Sludge and the Environment*. CAB International, 1996.

- [36] M. M. Marchioretto, *Heavy metals removal from anaerobically digested sludge*. PhD thesis, Wageningen University, 2003.
- [37] R. Singh and M. Agrawal, "Potential benefits and risks of land application of sewage sludge," *Waste Manage*, vol. 28, no. 2, pp. 347–358, 2008.
- [38] N. A. Kruse, L. DeRose, R. Korenowsky, J. R. Bowman, D. Lopez, K. Johnson, and E. Rankin, "The role of remediation, natural alkalinity sources and physical stream parameters in stream recovery," *J. Environ. Manage.*, vol. 128, pp. 1000–1011, 2013.
- [39] EEA, "Municipal waste management across european countries," tech. rep., European Environment Agency, 2018.
- [40] Mineralprices, "mineralprices.com," tech. rep., 2020.
- [41] LME, "London metal exchange," tech. rep., HKEX Group, Oct. 2019.
- [42] Metalary, "Metalary.com," tech. rep., 2020.
- [43] H. Prichard, J. Sampson, and M. Jackson, "A further discussion of the factors controlling the distribution of pt, pd, rh and au in road dust, gullies, road sweeper and gully flusher sediment in the city of sheffield, UK," *Sci Total Environ*, vol. 407, no. 5, pp. 1715–1725, 2009.
- [44] H. D. Robinson, K. Knox, R. Formby, and B. D. Bone, "Testing of residues from incineration of municipal solid waste," tech. rep., Environment Agency, 2004.
- [45] U. C. Gupta, K. WU, and S. LIANG, "Micronutrients in Soils, Crops, and Livestock," *Earth Science Frontiers*, vol. 15, no. 5, pp. 110–125, 2008.
- [46] R. J. Coppinger and A. M. Diamond, "Selenium deficiency and human disease," *Selenium*, pp. 219–233, 2001.

- [47] B. G. Survey, "The advanced soil geochemical atlas of England and Wales," *The Advanced Soil Geochemical Atlas of England and Wales*, pp. 70–74, 2012.
- [48] T. Schütte, C. Niewersch, T. Wintgens, and S. Yüce, "Phosphorus recovery from sewage sludge by nanofiltration in diafiltration mode," *Journal of Membrane Science*, vol. 480, pp. 74–82, 2015.
- [49] G. Al-Enezi, M. F. Hamoda, and N. Fawzi, "Ion exchange extraction of heavy metals from wastewater sludges," *J. Environ. Sci. Health., Part A*, vol. 39, no. 2, pp. 455 – 464, 2004.
- [50] P. Ghasemzadeh and A. Bostani, "The removal of lead and nickel from the composted municipal waste and sewage sludge using nanoscale zero-valent iron fixed on quartz," *Ecotoxicol. Environ. Saf*, vol. 145, pp. 483 – 489, 2017.
- [51] M. Fuerhacker, T. M. Haile, D. Kogelnig, A. Stojanovic, and B. Keppler, "Application of ionic liquids for the removal of heavy metals from wastewater and activated sludge," *Water Sci. Technol.*, vol. 65, no. 10, pp. 1765 – 1773, 2012.
- [52] A. Latawiec and B. Reid, "Sequential extraction of polycyclic aromatic hydrocarbons using subcritical water," *Chemosphere*, vol. 78, no. 8, pp. 1042–1048, 2010.
- [53] E. Yabalak and M. Gizir, "Subcritical and supercritical fluid extraction of heavy metals from sand and sewage sludge," *J Serb Chem Soc*, vol. 78, no. 7, pp. 1013–1022, 2013.
- [54] G. Peng, G. Tian, J. Liu, Q. Bao, and L. Zang, "Removal of heavy metals from sewage sludge with a combination of bioleaching and electrokinetic remediation technology," *Desalination*, vol. 271, no. 1-3, pp. 100–104, 2011.

- [55] D. Pei, C. Xiao, Q. Hu, and J. Tang, "Electrokinetic Gathering and Removal of Heavy Metals from Sewage Sludge by Ethylenediamine Chelation," *Procedia Environ. Sci.*, vol. 31, pp. 725–734, 2016.
- [56] H. Lei, K. Chen, Y. Li, H. Li, Q. Yu, X. Zhang, and C. Yao, "Electrokinetic recovery of copper, nickel, and zinc from wastewater sludge: Effects of electrical potentials," *Environ. Eng. Sci.*, vol. 29, no. 6, pp. 472–478, 2012.
- [57] Y. Xu, C. Zhang, M. Zhao, H. Rong, K. Zhang, and Q. Chen, "Comparison of bioleaching and electrokinetic remediation processes for removal of heavy metals from wastewater treatment sludge," *Chemosphere*, vol. 168, pp. 1152–1157, 2017.
- [58] S. Filho, P. J. Castagno, and K. R. L. Elicker, "Electroremediation of heavy metals in sewage sludge," *ABEQ*, vol. 31, no. 2, pp. 365 – 371, 2014.
- [59] C. Adam, G. Kley, and F.-G. Simon, "Thermal Treatment of Municipal Sewage Sludge Aiming at Marketable {P-Fertilisers}," *Mater Trans*, vol. 48, no. 12, pp. 3056–3061, 2007.
- [60] H. Herzel, O. Krüger, and C. Adam, "Thermochemical treatment of sewage sludge ash for p-fertilizer production," *BAM*, 2015.
- [61] A. Lombardi and O. Garcia, "An evaluation into the potential of biological processing for the removal of metals from sewage sludges," *Crit Rev Microbiol*, vol. 25, no. 4, pp. 275–288, 2008.
- [62] A. Lombardi, O. Garcia, and A. Mozeto, "Bioleaching of metals from anaerobic sewage sludge: effects of total solids, leaching microorganisms, and energy source," *J Environ Sci Heal Part*, vol. 36, no. 5, pp. 793–806, 2001.
- [63] J. Blais, R. Tyagi, and J. Auclair, "Comparison of acid and microbial leaching for metal removal from municipal sludge," *Wat. Sci. Tech.*, vol. 26, no. 1-2, pp. 197 – 206, 1992.

- [64] J. F. Blais, J. C. Auclair, and R. D. Tyagi, "Cooperation between two thiobacillus strains for heavy-metal removal from municipal sludge," *Can. J. Microbiol.*, vol. 38, no. 3, pp. 181–187, 1992.
- [65] Y.-M. Wen, H.-Y. Lin, Q.-P. Wang, and Z.-L. Chen, "Bioleaching of heavy metals from sewage sludge using acidithiobacillus thiooxidans," *2nd International Symposium on Aqua Science, Water Resource and Low Carbon Energy : Sanya, Hainan, China*, vol. 1251, pp. 189 – 192, 2010.
- [66] F. Y. R. Tyagi, and K. Narasiah, "Simultaneous sewage sludge digestion and metal leaching: effect of aeration," *Process Biochem*, vol. 36, no. 3, pp. 263–273, 2000.
- [67] R. Tyagi, J. Blais, N. Meunier, and H. Benmoussa, "Simultaneous sewage sludge digestion and metal leachingEffect of sludge solids concentration," *Water Research*, vol. 31, no. 1, pp. 105–118, 1997.
- [68] H. Benmoussa, R. D. Tyagi, and P. G. C. Campbell, "Simultaneous sewage sludge digestion and metal leaching using an internal loop reactor," *Water Res*, vol. 31, no. 10, pp. 2638–2654, 1997.
- [69] D. del Mundo Dacera and S. Babel, "Use of citric acid for heavy metals extraction from contaminated sewage sludge for land application," *Water Sci. Technol.*, vol. 54, no. 9, pp. 129 – 135, 2006.
- [70] S. Yoshizaki and T. Tomida, "Principle and process of heavy metal removal from sewage sludge," *Environmental Science and Technology*, vol. 34, no. 8, pp. 1572–1575, 2000.
- [71] Z. wei Wang, "Removal of heavy metals in municipal sludge by using acetic acid-h<sub>2</sub>o<sub>2</sub>- ferrite way," *3rd International Conference on Bioinformatics and Biomedical Engineering*, pp. 6316 – 6319, 2009.
- [72] Y. Zhu, G. Zeng, P. Zhang, C. Zhang, M. Ren, J. Zhang, and M. Chen, "Feasibility of bioleaching combined with fenton-like reaction to remove

- heavy metals from sewage sludge,” *Bioresour. Technol.*, vol. 142, pp. 530 – 534, 2013.
- [73] M. Couillard and D. Chartier, “Removal of metals from aerobic sludges by biological solubilisation in batch reactors,” *J. Biotechnol.*, 1991.
- [74] M. Stylianou, D. Kollia, K. Haralambous, V. Inglezakis, K. Moustakas, and M. Loizidou, “Effect of acid treatment on the removal of heavy metals from sewage sludge,” *Desalination*, vol. 215, no. 1-3, pp. 73–81, 2007.
- [75] M. miao Ren, X. zhong Yuan, Y. Zhu, H. jun Huang, G. ming Zeng, H. Li, M. Chen, H. Wang, C. ya Chen, and N. bo Lin, “Effect of different surfactants on removal efficiency of heavy metals in sewage sludge treated by a novel method combining bio-acidification with Fenton oxidation,” *J. Cent. South Univ.*, vol. 21, no. 12, pp. 4623–4629, 2014.
- [76] T. Sreekrishnan and R. Tyagi, “A comparative study of the cost of leaching out heavy metals from sewage sludges,” *Process Biochem*, vol. 31, no. 1, pp. 31–41, 1996.
- [77] R. L. Jenkins, B. J. Scheybeler, M. L. Smith, R. Baird, M. P. Lo, and R. T. Haug, “Metals removal and recovery from municipal sludge,” *Water Pollution Control Federation*, vol. 53, pp. 25–32, Jan. 1981.
- [78] B. Pérez-Cid, C. Silva, and C. Boia, “Application of leaching tests for the assessment of available heavy metals from domestic and industrial sludges,” *Int. J. Environ. Anal. Chem.*, vol. 82, no. 10, pp. 21 – 732, 2002.
- [79] C. Bloomfield and G. Pruden, “The effects of aerobic and anaerobic incubation on the extractabilities of heavy metals in digested sewage sludge,” *Environ. Pollut.*, vol. 8, no. 3, pp. 217 – 232, 1975.
- [80] S. E. Gaber, M. S. Rizk, and M. M. Yehia, “Extraction of certain heavy metals from sewage sludge using different types of acids,” *Biokemistri*, vol. 23, no. 1, pp. 41 – 48, 2011.

- [81] E. Zaleckas, V. Paulauskas, N. Sabiene, and G. Kusliene, "Copper and zinc removal from sewage sludge using different organic acids," in *Rural Development*, 2009.
- [82] A. Azhdarpoor, R. Hoseini, and M. Dehghani, "Leaching Zn, Cd, Pb, and Cu from Wastewater Sludge Using Fenton Process," *Heal. Sci Surveill. Sys*, vol. 3, no. 4, pp. 163–169, 2015.
- [83] R. Burgos-Castillo, M. Sillanpää, E. Brillas, and I. Sirés, "Removal of metals and phosphorus recovery from urban anaerobically digested sludge by electro-Fenton treatment," *Sci. Total Environ.*, vol. 644, no. 2018, pp. 173–182, 2018.
- [84] X. Gu, J. Wong, and R. Tyagi, "11 - bioleaching of heavy metals from sewage sludge for land application," in *Current Developments in Biotechnology and Bioengineering* (J. W.-C. Wong, R. D. Tyagi, and A. Pandey, eds.), pp. 241 – 265, Elsevier, 2017.
- [85] L. Strande, M. Ronteltap, and D. Brdjanovic, *Faecal Sludge Management: Systems Approach for Implementation and Operation*. IWA Publishing, 2014.
- [86] M. Z. Mubarak and P. S. Irianto, "Improving Gold Recovery from Artificial {Preg-Robbing} Ore by Pre-treatment using Blinding Agent and Resin-in-Leach," *J Eng Technological Sci*, vol. 48, no. 3, pp. 276–287, 2016.
- [87] F. Mendes, "Resin-in-leach process to recover nickel and/or cobalt in ore leaching pulps," *US Patent 7*, 2011.
- [88] M. Nicol and Z. Zainol, "The development of a resin-in-pulp process for the recovery of nickel and cobalt from laterite leach slurries," *Int J Miner Process*, vol. 72, no. 1-4, pp. 407–415, 2003.
- [89] K. Mirjalili and M. Roshani, "Resin-in-pulp method for uranium recovery



- from leached pulp of low grade uranium ore,” *Hydrometallurgy*, vol. 85, no. 2-4, pp. 103–109, 2007.
- [90] T. Sreenivas and K. Rajan, “Studies on the separation of dissolved uranium from alkaline carbonate leach slurries by resin-in-pulp process,” *Sep Purif Technol*, vol. 112, pp. 54–60, 2013.
- [91] T. Udayar, M. H. Kotze, and V. Yahorava, “Recovery of uranium from dense slurries via resin-in-pulp,” *The Southern African Institute of Mining and Metallurgy 6th Southern African Base Metals Conference*, pp. 49 – 64, 2011.
- [92] Y. Choi and S. Chefai, “Co-current and counter current resin-in-leach in gold leaching processes,” {US} *Patent 8*, 2014.
- [93] D. Kulikowska, B. K. Klik, Z. M. Gusiatin, and R. Jabłoński, “Sewage sludge can provide a washing agent for remediation of soil from a metallurgical area,” *Catena*, vol. 173, no. June 2018, pp. 22–28, 2019.
- [94] J. T. Novak, G. L. Goodman, A. Pariroo, and J.-C. Huang, “The blinding of sludges during filtration,” *J. WPCF*, vol. 60, no. 2, pp. 206 – 214, 1988.
- [95] J. D. Eye and T. K. Basu, “Use of fly ash in wastewater treatment and sludge conditioning,” *J. WPCF*, vol. 42, no. 5, 1970.
- [96] R. F. Nelson and B. D. Brattlof, “Sludge pressure filtration with fly-ash addition,” *J. WPCF*, vol. 51, no. 5, pp. 1024 – 1031, 1979.
- [97] J. T. Christ, Y. Zevi, J. F. McCarthy, J. A. Throop, and T. S. Steenhuis, “Transport and retention mechanisms of colloids in partially saturated porous media,” *VZJ*, vol. 4, no. 1, pp. 184 – 195, 2005.
- [98] A. Q. Jaradat, S. J. Grimberg, and T. M. Holsen, “Colloid transport through natural filter material,” *J. Environ. Eng.*, vol. 135, no. 7, pp. 544 – 550, 2009.

- [99] I. Alinnor, "Adsorption of heavy metal ions from aqueous solution by fly ash," *Fuel*, vol. 86, no. 5-6, pp. 853–857, 2007.
- [100] P. D. Johnson, P. Girinathannair, K. N. Ohlinger, S. Ritchie, L. Teuber, and J. Kirby, "Enhanced removal of heavy metals in primary treatment using coagulation and flocculation," *Water Environ. Res.*, vol. 80, no. 5, pp. 472–479, 2008.
- [101] J. I. Houghton, J. E. Burgess, and T. Stephenson, "Off-line particle size analysis of digested sludge," *Water Research*, vol. 36, no. 18, pp. 4643 – 4647, 2002.
- [102] P. Littlejohn and J. Vaughan, "Recovery of nickel and cobalt from laterite leach tailings through resin-in-pulp scavenging and selective ammoniacal elution," *Miner. Eng.*, vol. 54, pp. 14–20, 2013.
- [103] F. Habashi, *Textbook of Hydrometallurgy*. Laval University, Quebec City, Canada: Métallurgie Extractive Québec, second ed., 1999.
- [104] I. Puigdomenech, "HYDRA: Hydrochemical Equilibrium-Constant Database (data retrieval to create input files for MEDUSA)." [www.kemi.kth.se/medusa](http://www.kemi.kth.se/medusa), Aug. 2009.
- [105] A. Chagnes, G. Cote, C. Ekberg, M. Nilsson, and T. Retegan, *WEEE recycling: Research, development, and policies*. Elsevier, 2016.
- [106] C. E. Harland, *Ion Exchange: Theory and Practice*. Royal Society of Chemistry Paperback, second ed., 1994.
- [107] F. G. Helfferich, *Ion Exchange*, vol. 1962. McGraw-Hill, New York, 1962.
- [108] Z.-Z. Wang, H.-D. Duan, X. Meng, Y.-F. Zhang, and H.-M. Qi, "Adsorption of lead(ii) from aqueous solution by two modified porous chelating resins based on (3-mercaptopropyl) trimethoxysilane," *Macromolecular Research*, vol. 24, no. 9, pp. 757–766, 2016.

- [109] S. Edebalı and E. Pehlivan, "Evaluation of chelate and cation exchange resins to remove copper ions," *Powder Technol.*, vol. 301, pp. 520–525, 2016.
- [110] W. A. Trochimczuk, "New ion-exchange/coordination resins with carboxylate and phosphate functional groups," *Eur. Polym. J.*, vol. 35, no. 9, pp. 1457–1464, 1999.
- [111] X.-C. Yin, X. Liu, J.-C. Fan, J.-J. Wu, J.-L. Men, and G.-S. Zheng, "Preparation of gel resins and removal of copper and lead from water," *J. Appl. Polym. Sci.*, vol. 134, no. 7, 2017.
- [112] A. Dąbrowski, Z. Hubicki, P. Podkościelny, and E. Robens, "Selective removal of the heavy metal ions from waters and industrial wastewaters by ion-exchange method," *Chemosphere*, vol. 56, no. 2, pp. 91–106, 2004.
- [113] K. Srinivasa-Rao, P. K. Dash, D. Sarangi, G. Roy-Chaudhury, and V. N. Misra, "Treatment of wastewater containing pb and fe using ion-exchange techniques," *J. Chem. Technol. Biotechnol.*, vol. 80, no. 8, pp. 892–898, 2005.
- [114] L. M. Ferreira, J. M. Loureiro, and A. E. Rodrigues, "Sorption of metals by an amidoxime chelating resin. part i: Equilibrium," *Sep. Sci. Technol.*, vol. 33, no. 11, pp. 1585–1604, 1998.
- [115] F. Mendes and A. Martins, "Selective sorption of nickel and cobalt from sulphate solutions using chelating resins," *Int. J. Miner. Process*, vol. 74, no. 1-4, pp. 359 – 371, 2004.
- [116] D. Kolodynska, "Application of a new generation of complexing agents in removal of heavy metal ions from different wastes," 2013.
- [117] E. Gîlc, A. Micneanu, and P. Ilea, "Removal of zinc ions as zinc chloride complexes from strongly acidic aqueous solutions by ionic exchange," *Central European Journal of Chemistry*, vol. 12, no. 8, pp. 821–828, 2014.

- [118] J. P. Bezzina, M. D. Ogden, E. M. Moon, and K. L. Soldenhoff, "REE behavior and sorption on weak acid resins from buffered media," *J. Ind. Eng. Chem.*, vol. 59, pp. 440–455, 2018.
- [119] J. P. Bezzina, L. R. Ruder, R. Dawson, and M. D. Ogden, "Ion exchange removal of Cu(II), Fe(II), Pb(II) and Zn(II) from acid extracted sewage sludge Resin screening in weak acid media," *Water Res.*, vol. 158, pp. 257–267, 2019.
- [120] Z. Hubicki, M. Leszczyńska, B. Łodyga, and A. Łodyga, "Recovery of palladium(II) from chloride and chloride-nitrate solutions using ion-exchange resins with S-donor atoms," *Desalination*, vol. 207, no. 1-3, pp. 80–86, 2007.
- [121] B. McKevitt and D. Dreisinger, "A comparison of various ion exchange resins for the removal of ferric ions from copper electrowinning electrolyte solutions Part I: Electrolytes Containing No Other Impurities," *Hydrometallurgy*, vol. 98, no. 1-2, p. 116, 2009.
- [122] V. S. Soldatov, V. M. Zelenkovskii, and L. A. Orlovskaya, "Sorption of bivalent ions by a fibrous chelating ion exchanger and the structure of sorption complexes," *Reactive and Functional Polymers*, vol. 71, no. 1, pp. 49–61, 2011.
- [123] K. S. Rao, P. K. Dash, D. Sarangi, G. R. Chaudhury, and V. N. Misra, "Treatment of wastewater containing Pb and Fe using ion-exchange techniques," *J. Chem. Technol. Biotechnol.*, vol. 80, no. 8, pp. 892–898, 2005.
- [124] J. P. Bezzina, T. Robshaw, R. Dawson, and M. D. Ogden, "Single metal isotherm study of the ion exchange removal of Cu(II), Fe(II), Pb(II) and Zn(II) from synthetic acetic acid leachate," *Chem Eng J*, vol. 394, p. 124862, 2020.

- [125] P. Gans, A. Sabatini, and A. Vacca, *Hyperquad Simulation and Speciation*. Protonic Software, 4.0.31 ed., 2009.
- [126] A. E. Martell, R. M. Smith, and R. J. Motekaitis, *NIST Critically Selected Stability Constants of Metal Complexes*. NIST Standard Reference Data, 8.0 ed., 2004.
- [127] Perkin Elmer, Inc., *The Analytical Methods for Atomic Absorption Spectroscopy*, 1996.
- [128] D. Harris, *Quantitative Chemical Analysis*. W. H. Freeman, 2010.
- [129] Brookfield, *Brookfield Digital Viscometer Model DV-E - Operating Instructions*.
- [130] A. L. Riley, S. E. Pepper, A. J. Canner, S. F. Brown, and M. D. Ogden, "Metal recovery from jarosite waste A resin screening study," *Separation Science and Technology (Philadelphia)*, vol. 53, no. 1, pp. 22–35, 2018.
- [131] R. Raghavan and C. Bhatt, "Comparative study of certain ion-exchange resins for application in copper-bearing process solutions," *Hydrometallurgy*, vol. 50, no. 2, pp. 169 – 183, 1998.
- [132] R. Molinari, P. Argurio, T. Poerio, and G. Gullone, "Selective separation of copper(ii) and nickel(ii) from aqueous systems by polymer assisted ultrafiltration," *Desalination*, vol. 200, no. 1, pp. 728 – 730, 2006. Euromembrane 2006.
- [133] C. P. Mane and M. A. Anuse, "Extraction behaviour of 2-octylaminopyridine towards lead(ii) from succinate media and its separation from other toxic metals," *Journal of Hazardous Materials*, vol. 152, no. 3, pp. 1146 – 1154, 2008.
- [134] C. Simpson and S. Laurie, "Ion exchange studies on zinc-rich waste liquors," *Hydrometallurgy*, vol. 51, no. 3, pp. 335 – 344, 1999.

- [135] J. P. Bezzina, J. T. M. Amphlett, and M. D. Ogden, "Extraction of Heavy Metals from Simulant Citrate Leachate of Sewage Sludge by Ion Exchange," *Journal of Ion Exchange*, vol. 29, no. 3, pp. 1–7, 2018.
- [136] P. L. Brown and C. Ekberg, *Hydrolysis of Metal Ions*. Wiley-VCH, 2016.
- [137] J. E. Gorman and F. M. Clydesdale, "Thermodynamic and Kinetic Stability Constants of Selected Carboxylic Acids and Iron," *Journal of Food Science*, vol. 49, pp. 500–503, 1984.
- [138] T. B. Field, J. L. McCourt, and W. a. E. McBryde, "Composition and Stability of Iron and Copper Citrate Complexes in Aqueous-Solution," *Canadian Journal of Chemistry-Revue Canadienne De Chimie*, vol. 52, no. 17, pp. 3119–3124, 1974.
- [139] H. Kalka, "Aqion: Manual (selected topics)." <http://www.aqion.de/site/98>, 2015.
- [140] S. Aktas and M. H. Morcali, "Gold uptake from dilute chloride solutions by a Lewatit TP 214 and activated rice husk," *International Journal of Mineral Processing*, vol. 101, no. 1-4, pp. 63–70, 2011.
- [141] M. H. Morcali, B. Zeytuncu, and O. Yucel, "Comparison of the adsorption by rice hulls and Lewatit TP 214 of platinum from chloroplatinic solution," *Journal of the Serbian Chemical Society*, vol. 78, no. 6, pp. 811–826, 2013.
- [142] D. Kołodyńska and Z. Hubicki, "FT-IR / PAS Studies of Cu ( II ) EDTA Complexes Sorption on the Chelating Ion Exchangers," *Ind. Eng. Chem. Res*, vol. 116, no. 3, pp. 340–343, 2009.
- [143] C. J. Doona and D. M. Stanbury, "Equilibrium and Redox Kinetics of Copper(II)-Thiourea Complexes," *Inorganic Chemistry*, vol. 35, no. 11, pp. 3210–3216, 1996.

- [144] S. Krzewska, H. Podsiadły, and L. Pajdowski, "Studies on the reaction of copper(II) with thioureaIII," *J. Inorg. Nucl. Chem.*, vol. 42, no. 1, pp. 89–94, 1980.
- [145] A. Rosenheim and V. J. Meyer, "ber die thiokarbamidverbindungen zweiwertiger metallsalze," *Zeitschrift fr anorganische Chemie*, vol. 49, no. 1, pp. 13–27, 1906.
- [146] R. Chiariza, E. P. Horwitz, S. D. Alexandrators, and M. J. Gula, "Diphonix® Resin: A Review of Its Properties and Applications," *Separation Science and Technology*, vol. 32, no. 1-4, pp. 1–35, 1997.
- [147] M. Pesavento, R. Biesuz, M. Gallorini, and A. Profumo, "Sorption mechanism of Trace Amounts of Divalent Metal ions on a Chelating Resin Containing Iminodiacetate Groups," *Analytical Chemistry*, vol. 65, no. 18, pp. 2522–2527, 1993.
- [148] J. L. Cortina, N. Miralles, M. Aguilar, and A. M. Sastre, "Distribution studies of Zn ( II ), Cu ( II ) and Cd ( II ) with Levextrel resins containing ( Lewatit TP807 ')," *Hydrometallurgy*, vol. 40, no. 94, pp. 195–206, 1996.
- [149] I. Puigdomenech, "MEDUSA: Make Equilibrium Diagrams Using Sophisticated Algorithms." [www.kemi.kth.se/medusa](http://www.kemi.kth.se/medusa), Dec. 2010.
- [150] E. Pehlivan and T. Altun, "Ion-exchange of Pb<sup>2+</sup>, Cu<sup>2+</sup>, Zn<sup>2+</sup>, Cd<sup>2+</sup>, and Ni<sup>2+</sup> ions from aqueous solution by Lewatit CNP 80," *J. Hazard. Mater.*, vol. 140, no. 1-2, pp. 299–307, 2007.
- [151] Y. S. Ho, J. F. Porter, and G. McKay, "Equilibrium isotherm studies for the sorption of divalent metal ions onto peat: Copper, nickel and lead single component systems," *Water. Air. Soil Pollut.*, vol. 141, no. 1-4, pp. 1–33, 2002.

- [152] K. Y. Foo and B. H. Hameed, "Insights into the modeling of adsorption isotherm systems," *Chem. Eng. J.*, vol. 156, no. 1, pp. 2–10, 2010.
- [153] J. Dai, F. L. Ren, and C. Y. Tao, "Adsorption behavior of Fe(II) and Fe(III) ions on thiourea cross-linked chitosan with Fe(III) as template," *Molecules*, vol. 17, no. 4, pp. 4388–4399, 2012.
- [154] A. Dada, A. O. Olalekan, "Langmuir, Freundlich, Temkin and DubininRadushkevich Isotherms Studies of Equilibrium Sorption of Zn 2+ Unto Phosphoric Acid Modified Rice Husk," *IOSR J. Appl. Chem.*, vol. 3, no. 1, pp. 38–45, 2012.
- [155] E. Voudrias, K. Fytianos, and E. Bozani, "Sorption-desorption isotherms of dyes from aqueous solutions and wastewaters with different sorbent materials," *Global NEST Journal*, vol. 4, no. 1, pp. 75–83, 2002.
- [156] C.-S. Chiou, G.-B. Hong, and H.-W. Chen, "Adsorption Behavior of Recyclable Magnetites with N-Components for Adsorption of Copper Ion," *J. Nanosci. Nanotechnol.*, vol. 18, no. 3, pp. 2241–2248, 2017.
- [157] Z. Zhang, J. Peng, C. Srinivasakannan, Z. Zhang, L. Zhang, Y. Fernández, and J. Menéndez, "Leaching zinc from spent catalyst: Process optimization using response surface methodology," *J Hazard Mater*, vol. 176, no. 1-3, pp. 1113–1117, 2010.
- [158] D. Balarak, F. Mostafapour, H. Azarpira, and A. Joghataei, "Langmuir, Freundlich, Temkin and Dubininradushkevich Isotherms Studies of Equilibrium Sorption of Ampicilin unto Montmorillonite Nanoparticles," *J. Pharm. Res. Int.*, vol. 20, no. 2, pp. 1–9, 2017.
- [159] A. M. Ghaedi, M. Ghaedi, A. Vafaei, N. Irvani, M. Keshavarz, M. Rad, I. Tyagi, S. Agarwal, and V. K. Gupta, "Adsorption of copper (II) using modified activated carbon prepared from Pomegranate wood: Optimization



- by bee algorithm and response surface methodology,” *J. Mol. Liq.*, vol. 206, pp. 195–206, 2015.
- [160] C. Theivarasu, S. Mylsamy, and N. Sivakumar, “Cocoa Shell as Adsorbent for the Removal of Methylene Blue from Aqueous Solution : Kinetic and Equilibrium Study,” *Universal Journal of Environmental Research and Technology*, vol. 1, pp. 70–78, 2011.
- [161] D. Mutavdžić Pavlović, L. Čurković, I. Grčić, I. Šimić, and J. Župan, “Isotherm, kinetic, and thermodynamic study of ciprofloxacin sorption on sediments,” *Environ. Sci. Pollut. Res.*, vol. 24, no. 11, pp. 10091–10106, 2017.
- [162] F. Liu, L. Li, P. Ling, X. Jing, C. Li, A. Li, and X. You, “Interaction mechanism of aqueous heavy metals onto a newly synthesized IDA-chelating resin : Isotherms , thermodynamics and kinetics,” *Chem. Eng. J.*, vol. 173, no. 1, pp. 106–114, 2011.
- [163] L.-c. Lin and R.-s. Juang, “Ion-exchange equilibria of Cu ( II ) and Zn ( II ) from aqueous solutions with Chelex 100 and Amberlite IRC 748 resins,” *Chemical Engineering Journal*, vol. 112, no. 1-3, pp. 211–218, 2005.
- [164] P. Bulai, C. Balan, C. Scripcariu, and M. Macoveanu, “Equilibrium and kinetic studies of copper (II) removal on purolite S930 resin,” *Environ. Eng. Manag. J.*, vol. 8, no. 5, pp. 1103–1109, 2009.
- [165] L. Fu, C. Shuang, F. Liu, A. Li, Y. Li, Y. Zhou, and H. Song, “Rapid removal of copper with magnetic poly-acrylic weak acid resin: Quantitative role of bead radius on ion exchange,” *J. Hazard. Mater.*, vol. 272, pp. 102–111, 2014.
- [166] P. Ling, F. Liu, L. Li, X. Jing, B. Yin, K. Chen, and A. Li, “Adsorption of divalent heavy metal ions onto IDA-chelating resins: Simulation of

physicochemical structures and elucidation of interaction mechanisms,” *Talanta*, vol. 81, no. 1-2, pp. 424–432, 2010.

- [167] A. R. Kaveeshwar, M. Sanders, S. K. Ponnusamy, D. Depan, and R. Subramaniam, “Chitosan as a biosorbent for adsorption of iron (II) from fracking wastewater,” *Polym. Adv. Technol.*, vol. 29, no. 2, pp. 961–969, 2018.
- [168] F. Liu, X. Luo, X. Lin, L. Liang, and Y. Chen, “Removal of copper and lead from aqueous solution by carboxylic acid functionalized deacetylated konjac glucomannan,” *J. Hazard. Mater.*, vol. 171, no. 1-3, pp. 802–808, 2009.
- [169] L. Li, F. Liu, X. Jing, P. Ling, and A. Li, “Displacement mechanism of binary competitive adsorption for aqueous divalent metal ions onto a novel IDA-chelating resin: Isotherm and kinetic modeling,” *Water Res.*, vol. 45, no. 3, pp. 1177–1188, 2011.
- [170] N. Wang, X. Xu, H. Li, J. Zhai, L. Yuan, K. Zhang, and H. Yu, “Preparation and application of a xanthate-modified thiourea chitosan sponge for the removal of Pb(II) from aqueous solutions,” *Ind. Eng. Chem. Res.*, vol. 55, no. 17, pp. 4960–4968, 2016.
- [171] C. hua XIONG and C. ping YAO, “Adsorption behavior of gel-type weak acid resin (110-H) for Pb<sup>2+</sup>,” *Trans. Nonferrous Met. Soc. China (English Ed.)*, vol. 18, no. 5, pp. 1290–1294, 2008.
- [172] I. Vergili, G. Soltobaeva, Y. Kaya, Z. B. Gönder, S. Çavuş, and G. Gürda, “Study of the removal of Pb(II) using a weak acidic cation resin: Kinetics, thermodynamics, equilibrium, and breakthrough curves,” *Industrial and Engineering Chemistry Research*, vol. 52, no. 26, pp. 9227–9238, 2013.
- [173] E. G. Vieira, I. V. Soares, N. C. Da Silva, S. D. Perujo, D. R. Do Carmo, and N. L. Dias Filho, “Synthesis and characterization of 3-[(thiourea)-propyl]-

- functionalized silica gel and its application in adsorption and catalysis," *New J. Chem.*, vol. 37, no. 7, pp. 1933–1943, 2013.
- [174] R. D. Johnson and F. H. Arnold, "The temkin isotherm describes heterogeneous protein adsorption," *Biochim. Biophys. Acta (BBA)/Protein Struct. Mol.*, vol. 1247, no. 2, pp. 293–297, 1995.
- [175] S. Vasiliu, I. Bunia, S. Racovita, and V. Neagu, "Adsorption of cefotaxime sodium salt on polymer coated ion exchange resin microparticles: Kinetics, equilibrium and thermodynamic studies," *Carbohydr. Polym.*, vol. 85, no. 2, pp. 376–387, 2011.
- [176] S. K. Yong, N. Bolan, E. Lombi, and W. Skinner, "Synthesis and characterization of thiolated chitosan beads for removal of Cu(II) and Cd(II) from wastewater," *Water. Air. Soil Pollut.*, vol. 224, no. 12, 2013.
- [177] A. S. Franca, L. S. Oliveira, and M. E. Ferreira, "Kinetics and equilibrium studies of methylene blue adsorption by spent coffee grounds," *Desalination*, vol. 249, no. 1, pp. 267–272, 2009.
- [178] S. Akhtar and R. Qadeer, "Active carbon as an adsorbent for lead ions," *Adsorpt. Sci. Technol.*, vol. 15, no. 10, pp. 815–824, 1997.
- [179] K. Hollmann, A. Oppermann, M. Witte, S. Li, M. Amen, U. Flörke, H. Egold, G. Henkel, and S. Herres-pawlis, "Copper (I) Complexes with Thiourea Derivatives as Ligands: Revealing Secrets of Their Bonding Scheme," *Eur. J. Inorg. Chem.*, vol. 1, no. 9, pp. 1266–1279, 2017.
- [180] X. Zuo, "Preparation and evaluation of novel thiourea/chitosan composite beads for copper(ii) removal in aqueous solutions," *Ind. Eng. Chem. Res.*, vol. 53, no. 3, pp. 1249–1255, 2014.
- [181] J. Gao, F. Liu, P. Ling, J. Lei, L. Li, C. Li, and A. Li, "High efficient removal of Cu(II) by a chelating resin from strong acidic solutions: Complex formation and DFT certification," *Chem. Eng. J.*, vol. 222, pp. 240–247, 2013.

- [182] I. Bleotu, S.-A. Dorneanu, M. Mureseanu, E. Gilca, and P. Ilea, "Selective Removal of Cu (II) from Diluted Aqueous Media by an Iminodiacetic Acid Functionalized Resin," *Rev. Chim. -Bucharest-*, vol. 66, no. 6, pp. 797–802, 2015.
- [183] H. A. Panahi, N. Mehmandost, E. Moniri, and I. Y. Galaev, "Iminodiacetic acid-containing polymer brushes grafted onto silica gel for preconcentration and determination of copper(II) in environmental samples," *J. Appl. Polym. Sci.*, vol. 126, no. 2, pp. 480–489, 2012.
- [184] J. Wang, X. Ma, G. Fang, M. Pan, X. Ye, and S. Wang, "Preparation of iminodiacetic acid functionalized multi-walled carbon nanotubes and its application as sorbent for separation and preconcentration of heavy metal ions," *J. Hazard. Mater.*, vol. 186, no. 2-3, pp. 1985–1992, 2011.
- [185] Y. A. Skorik, "Carboxyethylated polyaminostyrene for selective copper removal," *Polym. Bull.*, vol. 68, no. 4, pp. 1065–1078, 2012.
- [186] X. Liang, Y. Xu, L. Wang, Y. Sun, D. Lin, Y. Sun, X. Qin, and Q. Wan, "Sorption of Pb<sup>2+</sup> on mercapto functionalized sepiolite," *Chemosphere*, vol. 90, no. 2, pp. 548–555, 2013.
- [187] G. E. Sharaf El-Deen and S. E. Sharaf El-Deen, "Kinetic and isotherm studies for adsorption of Pb(II) from aqueous solution onto coconut shell activated carbon," *Desalin. Water Treat.*, vol. 57, no. 59, pp. 28910–28931, 2016.
- [188] P. Lodeiro, J. L. Barriada, R. Herrero, and M. E. Sastre de Vicente, "The marine macroalga *Cystoseira baccata* as biosorbent for cadmium(II) and lead(II) removal: Kinetic and equilibrium studies," *Environ. Pollut.*, vol. 142, no. 2, pp. 264–273, 2006.
- [189] A. Murugesan, T. Vidhyadevi, S. S. Kalaivani, M. P. Premkumar, L. Ravikumar, and S. Sivanesan, "Kinetic and thermodynamic studies

- on the removal of  $Zn^{2+}$  and  $Ni^{2+}$  from their aqueous solution using poly(phenylthiourea)imine,” *Chem. Eng. J.*, vol. 197, pp. 368–378, 2012.
- [190] O. Abdelwahab, N. K. Amin, and E. S. El-Ashtouky, “Removal of zinc ions from aqueous solution using a cation exchange resin,” *Chem. Eng. Res. Des.*, vol. 91, no. 1, pp. 165–173, 2013.
- [191] N. Z. Misak, “Langmuir isotherm and its application in ion-exchange reactions,” *React. Polym.*, vol. 21, no. 1-2, pp. 53–64, 1993.
- [192] S. J. Allen and P. A. Brown, “Isotherm analyses for single component and multicomponent metal sorption onto lignite,” *J. Chem. Technol. Biotechnol.*, vol. 62, no. 1, pp. 17–24, 1995.
- [193] K. K. Choy, J. F. Porter, and G. McKay, “Langmuir isotherm models applied to the multicomponent sorption of acid dyes from effluent onto activated carbon,” *J. Chem. Eng. Data*, vol. 45, no. 4, pp. 575–584, 2000.
- [194] P. Westerhoff, S. Lee, Y. Yang, G. W. Gordon, K. Hristovski, R. U. Halden, and P. Herckes, “Characterization, Recovery Opportunities, and Valuation of Metals in Municipal Sludges from {U.S.} Wastewater Treatment Plants Nationwide,” *Environ. Sci. Technol.*, vol. 49, no. 16, pp. 9479–9488, 2015.
- [195] T. Tarawou and E. Young, “Intraparticle and Liquid film Diffusion Studies on the Adsorption of  $Cu^{2+}$  and  $Pb^{2+}$  Ions from Aqueous Solution using Powdered Cocoa Pod ( *Theobroma cacao* ),” *Int. Res. J. Eng. Technol.*, vol. 2, no. 8, pp. 236–243, 2015.
- [196] G. E. Boyd, A. W. Adamson, and L. S. Myers Jr., “The Exchange Adsorption of Ions from Aqueous Solutions by Organic Zeolites. II. Kinetics,” *Kinet. Ion. Exch. Adsorpt. Process.*, vol. 69, pp. 2836–2848, 1948.
- [197] X. Yi, Z. Xu, Y. Liu, X. Guo, M. Ou, and X. Xu, “Highly efficient removal of uranium(VI) from wastewater by polyacrylic acid hydrogels,” *RSC Adv.*, vol. 7, no. 11, pp. 6278–6287, 2017.

- [198] M. T. Amin, A. A. Alazba, and M. Shafiq, "Adsorptive removal of reactive black 5 from wastewater using bentonite clay: Isotherms, kinetics and thermodynamics," *Sustain.*, vol. 7, no. 11, pp. 15302–15318, 2015.
- [199] C. Aharoni and F. C. Tompkins, "Kinetics of Adsorption and Desorption and the Elovich Equation," *Adv. Catal.*, vol. 21, no. C, pp. 1–49, 1970.
- [200] F. C. Wu, R. L. Tseng, and R. S. Juang, "Characteristics of Elovich equation used for the analysis of adsorption kinetics in dye-chitosan systems," *Chem. Eng. J.*, vol. 150, no. 2-3, pp. 366–373, 2009.
- [201] Y. S. Ho, "Review of second-order models for adsorption systems," *J. Hazard. Mater.*, vol. 136, no. 3, pp. 681–689, 2006.
- [202] R. L. Tseng, F. C. Wu, and R. S. Juang, "Characteristics and applications of the Lagergren's first-order equation for adsorption kinetics," *J. Taiwan Inst. Chem. Eng.*, vol. 41, no. 6, pp. 661–669, 2010.
- [203] Y. Ho and G. McKay, "Application of Kinetic Models to the Sorption of Copper(II) on to Peat," *Adsorpt. Sci. Technol.*, vol. 20, no. 8, pp. 797–815, 2002.
- [204] S. Çavuş, G. Yaar, Y. Kaya, Z. B. Gönder, G. Gürda, and . Vergili, "Synthesis and characterization of gel beads based on ethyleneglycol dimethacrylate and 2-acrylamido-2-methyl-1-propane sulfonic acid: Removal of Fe(II), Cu(II), Zn(II), and Ni(II) from metal finishing wastewater," *Process Saf. Environ. Prot.*, vol. 103, pp. 227–236, 2016.
- [205] S. Benkhatou, A. Djelad, M. Sassi, M. Bouchekara, and A. Bengueddach, "Lead(II) removal from aqueous solutions by organic thiourea derivatives intercalated magadiite," *Desalin. Water Treat.*, vol. 57, no. 20, pp. 9383–9395, 2016.
- [206] E. Hong, A. M. Yeneneh, T. K. Sen, H. M. Ang, and A. Kayaalp, "A comprehensive review on rheological studies of sludge from various

- sections of municipal wastewater treatment plants for enhancement of process performance,” *Advances in Colloid and Interface Science*, vol. 257, pp. 19–30, 2018.
- [207] J. T. Radford, C. Underdown, K. Velkushanova, A. Byrne, D. P. K. Smith, R. A. Fenner, J. Pietrovito, and A. Whitesell, “Faecal sludge simulants to aid the development of desludging technologies,” *Journal of Water, Sanitation and Hygiene for Development*, vol. 5, no. 3, p. 456, 2015.
- [208] J. Baudez, P. Ginisty, C. Peuchot, and L. Spinosa, “The preparation of synthetic sludge for lab testing,” *Wat. Sci. Tech.*, vol. 56, no. 9, p. 67, 2007.
- [209] K. Wignarajah and E. Litwiller, “Simulated human feces for testing human waste processing technologies in space systems,” tech. rep., SAE International, 400 Commonwealth Drive, Warrendale PA 15096-0001 U.S.A, 2006.
- [210] Pollution Research Group, “Selection of synthetic sludge simulant for the bill and melinda gates foundation’s reinvent the toilet fair,” tech. rep., University of KwaZulu-Natal, 2014.
- [211] G. Guibaud, P. Dollet, N. T. C. Dagot, and A. Baudu, “Characterisation of the evolution of activated sludges using rheological measurements,” *Process Biochem.*, vol. 39, no. 11, pp. 1803 – 1810, 2004.
- [212] F. Markis, J.-C. Baudez, R. Parthasarathy, P. Slatter, and N. Eshtiaghi, “Predicting the apparent viscosity and yield stress of mixtures of primary, secondary and anaerobically digested sewage sludge: Simulating anaerobic digesters,” *Water Res.*, vol. 100, pp. 568 – 579, 2016.
- [213] V. Lotito, L. Spinosa, G. Mininni, and R. Antonacci, “The rheology of sewage sludge at different steps of treatment,” *Water Sci Technol*, vol. 36, no. 11, pp. 79–85, 1997.

- [214] G. Moeller and L. G. Terres, "Rheological characterization of primary and secondary sludges treated by both aerobic and anaerobic digestion," *Bioresour. Technol.*, vol. 61, no. 3, pp. 207 – 211, 1997.
- [215] alibaba, "alibaba.com," tech. rep., 2020.
- [216] Acros Organics, "fischersci.com," tech. rep., Fisherscientific, 2020.
- [217] indexmundi, "indexmundi.com," tech. rep., 2020.
- [218] W. Astuti, T. Hirajima, K. Sasaki, and N. Okibe, "Comparison of effectiveness of citric acid and other acids in leaching of low-grade indonesian saprolitic ores," *Minerals Engineering*, vol. 85, pp. 1 – 16, 2016.
- [219] C. Aharoni and M. Ungarish, "Kinetics of Activated Chemisorption. Part 1. - The Non-Elovichian Part of the Isotherm," *J. Chem. Soc. Faraday Transactions 1 Phys. Chem. Condens. Phases*, vol. 72, pp. 400–408, 1976.
- [220] F. C. Wu, R. L. Tseng, S. C. Huang, and R. S. Juang, "Characteristics of pseudo-second-order kinetic model for liquid-phase adsorption: A mini-review," *Chem. Eng. J.*, vol. 151, no. 1-3, pp. 1–9, 2009.
- [221] B. Alyüz and S. Veli, "Kinetics and equilibrium studies for the removal of nickel and zinc from aqueous solutions by ion exchange resins," *J Hazard Mater*, vol. 167, no. 1-3, pp. 482–488, 2009.
- [222] L. Scholten and C. Timmermans, "Natural radioactivity in phosphate fertilizers," *Fert Res*, vol. 43, no. 1-3, pp. 103–107, 1996.
- [223] H. Hudcová, J. Vymazal, and M. Rozkošný, "Present restrictions of sewage sludge application in agriculture within the European Union," *Soil and Water Research*, vol. 14, no. 2, pp. 104–120, 2019.
- [224] B. G. Survey, "The advanced soil geochemical atlas of England and Wales," *The Advanced Soil Geochemical Atlas of England and Wales*, pp. 70–74, 2012.



- [225] R. H. McKenzie, "Micronutrient Requirements of Crops," Tech. Rep. C, Alberta Agriculture, Food and Rural Development, 1992.
- [226] D. Adam, "Food prices rises threaten global security - un," *The Guardian*, 04 2008.
- [227] C. R. Adams, C. P. Porter, T. J. Robshaw, J. P. Bezzina, V. R. Shields, R. Bruce, and M. D. Ogden, "An alternative to cyanide leaching of waste activated carbon ash for gold and silver recovery via synergistic dual-lixiviant treatment," *Journal of Industrial and Engineering Chemistry*, vol. 92, pp. 120–130, 2020.
- [228] P. Gans, A. Sabatini, and A. Vacca, "Hyperquad Simulation and Speciation," 2009.
- [229] R. K. Sinnott and G. Towler, *Chemical Engineering Design*. Elsevier, fifth edition ed., 2009.
- [230] J. M. Coulson, J. R. Backhurst, J. F. Richardson, J. H. Harker, and R. P. Chhabra, *Chemical Engineering: Fluid Flow, Heat Transfer and Mass Transfer*, vol. 1. Elsevier, sixth edition ed., 1999.
- [231] S. M. Shaikh, M. S. Nasser, I. Hussein, A. Benamor, S. A. Onaizi, and H. Qiblawey, "Influence of polyelectrolytes and other polymer complexes on the flocculation and rheological behaviors of clay minerals: A comprehensive review," *Sep. Purif. Tech.*, vol. 187, pp. 137 – 161, 2017.



## **Appendix A**

**Ion exchange removal of Cu(II),  
Fe(II), Pb(II) and Zn(II) from acid  
extracted sewage sludge - Resin  
screening in weak acid media:  
Supplementary Information**

## **A.1 Resin characteristics**

This appendix contains the supplementary information accepted publication by Water Research on 20/04/2019 alongside the paper Ion exchange removal of Cu(II), Fe(II), Pb(II) and Zn(II) from acid extracted sewage sludge - Resin screening in weak acid media. DOI:[doi.org/10.1016/j.watres.2019.04.042](https://doi.org/10.1016/j.watres.2019.04.042)

The manufacturer's information for each of the resins tested is given in Table A.1

**Table A.1:** Physical and chemical characteristics of the resins tested throughout this study, as obtained from suppliers' information data sheets (PS = polystyrene, PA = polyacrylic, DVB = divinylbenzene). All are spherical beads.

Name	TP214	MTS9100	MTS9570	MTS9301	MTS9501	C107E
Manufacturer	Lanxess	Purolite	Purolite	Purolite	Purolite	Purolite
Functionality	Thiourea	Amidoxime	Phosphonic + sulfonic acid	Iminodiacetic acid	Amino phosphonic acid	Carboxylic acid
Commercial equivalent	Puromet MTS9140	Duolite ES346	n/a	Chelex 100 Lewatit TP208	Amberlite IRC747	Dowex MAC-3
Matrix	PS-DVB	PA-DVB	PA-DVB	PS-DVB	PS-DVB	PA-DVB
Size ( $\mu\text{m}$ )	550	330 -1200	550 -750	425 -1000	425 -800	300 -1600
Capacity	1.0 eq.L <sup>-1</sup>	40 g.L <sup>-1</sup> Cu <sup>2+</sup>	18 g.L <sup>-1</sup> Fe <sup>3+</sup>	50 g.L <sup>-1</sup> Cu <sup>2+</sup>	24 g.L <sup>-1</sup> Ca <sup>2+</sup>	3.6 eq.L <sup>-1</sup>
Water retention (wt%)	43-48	52-60	55-70	52-60	55-65	53-58
Ionic form shipped	Freebase	Freebase	H <sup>+</sup>	Na <sup>+</sup>	Na <sup>+</sup>	H <sup>+</sup>
Cost			> £30L <sup>-1</sup>	≈ £10L <sup>-1</sup>	≈ £10L <sup>-1</sup>	

## A.2 Separation factors

**Table A.2:** TP214 separation factors of copper, iron, lead and zinc from acetate media at 20 °C after 24hr of contact time.

pH	Cu			Fe			Pb			Zn		
	Fe	Pb	Zn	Cu	Pb	Zn	Cu	Fe	Zn	Cu	Fe	Pb
3.74	36.4	17.2	119	0.027	0.473	3.25	2.11	0.0580	6.88	0.307	0.00844	0.145
3.97	0.20	20.6	101	4.81	99.2	488	0.0101	0.0485	4.92	0.00205	0.00986	0.203
4.25	0.14	27.3	109	7.11	195	755	0.00514	0.0366	3.99	0.00129	0.00918	0.251
4.51	0.15	36.4	106	6.79	247	721	0.00404	0.0275	2.92	0.00139	0.00942	0.343
4.74	4.99	41.1	94.0	0.200	8.24	18.8	0.121	0.0243	2.29	0.0531	0.0106	0.437
4.91	7.99	50.3	105	0.125	6.30	13.1	0.159	0.0199	2.09	0.0761	0.00952	0.479
5.04	24.4	48.3	95.2	0.0409	1.98	3.89	0.506	0.0207	1.97	0.257	0.0105	0.508
5.22	45.9	57.1	96.1	0.0218	1.24	2.09	0.804	0.0175	1.68	0.478	0.0104	0.594
5.51	42.2	54.9	102	0.0237	1.30	2.42	0.769	0.0182	1.86	0.413	0.00978	0.537
5.73	171	50.2	103	0.00584	0.293	0.601	3.41	0.0199	2.05	1.66	0.00972	0.488

**Table A.3:** MTS9100 separation factors of copper, iron, lead and zinc from acetate media at 20 °C after 24hr of contact time.

	Cu			Fe			Pb			Zn		
pH	Fe	Pb	Zn	Cu	Pb	Zn	Cu	Fe	Zn	Cu	Fe	Pb
3.74	4.19	8.59	53.1	0.239	2.05	12.7	0.116	0.488	6.18	0.0188	0.0789	0.162
3.97	3.51	8.35	58.1	0.285	2.38	16.6	0.120	0.420	6.96	0.0172	0.0604	0.144
4.25	3.00	7.98	62.0	0.333	2.66	20.7	0.125	0.376	7.77	0.0161	0.0484	0.129
4.51	2.90	8.24	59.6	0.345	2.84	20.6	0.121	0.352	7.23	0.0168	0.0486	0.138
4.74	1.95	8.16	48.4	0.513	4.19	24.9	0.122	0.239	5.93	0.0206	0.0402	0.169
4.91	1.18	7.56	42.0	0.845	6.39	35.5	0.132	0.157	5.55	0.0238	0.0282	0.180
5.04	1.02	7.28	38.9	0.983	7.16	38.2	0.137	0.140	5.34	0.0257	0.0262	0.187
5.22	0.773	8.01	40.8	1.29	10.4	52.7	0.125	0.0965	5.09	0.0245	0.0190	0.197
5.51	3.92	7.34	33.0	0.255	1.87	8.42	0.136	0.534	4.49	0.0303	0.119	0.222
5.73	6.59	7.25	28.1	0.152	1.10	4.26	0.138	0.910	3.88	0.356	0.235	0.258

**Table A.4:** MTS9570 separation factors of copper, iron, lead and zinc from acetate media at 20 °C after 24hr of contact time.

	Cu			Fe			Pb			Zn		
pH	Fe	Pb	Zn	Cu	Pb	Zn	Cu	Fe	Zn	Cu	Fe	Pb
2.84	0.0172	0.105	1.31	58.0	6.09	76.2	9.52	0.164	12.5	0.761	0.0131	0.0799
3.71	0.0186	0.152	0.562	53.7	8.19	30.2	6.56	0.122	3.69	1.78	0.0331	0.271
4.02	0.0163	0.151	0.368	61.5	9.27	22.7	6.63	0.108	2.44	2.72	0.0441	0.409
4.34	0.01614	0.124	0.232	62.0	7.67	14.4	8.07	0.130	1.87	4.31	0.0696	0.534
4.50	0.0143	0.106	0.190	70.1	7.46	13.3	9.40	0.134	1.78	5.26	0.0751	0.560
4.70	0.0118	0.101	0.151	85.1	8.56	12.8	9.94	0.117	1.50	6.63	0.0780	0.667
4.75	0.0144	0.0921	0.146	69.4	6.39	10.1	10.9	0.157	1.59	6.84	0.0986	0.630
4.99	0.0129	0.0850	0.118	77.9	6.61	9.14	11.8	0.151	1.38	8.50	0.109	0.723
5.22	0.0164	0.0778	0.0978	60.8	4.74	5.95	12.8	0.211	1.26	10.2	0.168	0.796
5.42	0.0178	0.0714	0.0922	56.3	4.02	5.19	14.0	0.249	1.29	10.8	0.193	0.774



**Table A.5:** MTS9301 separation factors of copper, iron, lead and zinc from acetate media at 20 °C after 24hr of contact time.

pH	Cu			Fe			Pb			Zn		
	Fe	Pb	Zn	Cu	Pb	Zn	Cu	Fe	Zn	Cu	Fe	Pb
3.26	49.1	30.5	40.9	0.0204	0.623	0.834	0.0327	1.61	1.34	0.0244	1.20	0.746
3.62	15.7	27.3	18.7	0.0636	1.74	1.19	0.0366	0.575	0.685	0.0535	0.841	1.46
3.99	6.38	21.3	9.25	0.157	3.33	1.45	0.0470	0.300	0.435	0.108	0.689	2.30
4.30	4.82	19.3	7.40	0.208	4.01	1.54	0.0517	0.249	0.383	0.135	0.650	2.61
4.55	17.7	71.3	23.0	0.0565	4.03	1.30	0.0140	0.248	0.322	0.0436	0.771	3.11
4.70	2.87	10.1	2.95	0.349	3.51	1.03	0.0994	0.285	0.293	0.339	0.973	3.41
4.85	2.78	7.69	2.20	0.360	2.77	0.791	0.130	0.361	0.286	0.455	1.26	3.50
4.95	9.10	9.18	2.34	0.110	1.01	0.257	0.109	0.991	0.254	0.428	3.90	3.93
5.12	13.2	6.80	1.50	0.0760	0.516	0.114	0.147	1.94	0.221	0.667	8.79	4.53
5.32	4.69	7.78	3.34	0.213	1.66	0.713	0.129	0.602	0.429	0.299	1.40	2.33

**Table A.6:** MTS9501 separation factors of copper, iron, lead and zinc from acetate media at 20 °C after 24hr of contact time.

pH	Cu			Fe			Pb			Zn		
	Fe	Pb	Zn	Cu	Pb	Zn	Cu	Fe	Zn	Cu	Fe	Pb
3.67	0.0651	18.6	9.19	15.4	285	141	0.0538	0.00350	0.494	0.109	0.00709	2.02
4.03	0.0750	16.3	5.88	13.3	216.9	78.4	0.0615	0.00461	0.361	0.170	0.0128	2.77
4.32	0.124	13.4	4.50	8.06	108	36.3	0.0744	0.00923	0.335	0.222	0.0276	2.99
4.54	0.0969	13.3	3.89	10.3	137	40.2	0.0754	0.00730	0.293	0.257	0.0249	3.41
4.75	0.0374	12.1	3.57	26.8	323	95.6	0.0828	0.00309	0.296	0.280	0.0105	3.38
4.92	0.0359	11.8	3.26	27.9	329	90.9	0.0848	0.00304	0.276	0.307	0.0110	3.62
5.02	0.0296	12.5	3.31	33.8	423	112	0.0798	0.00236	0.264	0.302	0.00895	3.79
5.19	0.0163	10.9	2.97	61.5	673	183	0.0914	0.00149	0.271	0.337	0.00548	3.68
5.37	0.116	8.161	3.28	8.59	70.1	28.2	0.123	0.0143	0.402	0.305	0.0355	2.49
5.71	4.32	5.83	2.60	0.232	1.35	0.602	0.171	0.740	0.446	0.385	1.66	2.24

**Table A.7:** C107E separation factors of copper, iron, lead and zinc from acetate media at 20 °C after 24hr of contact time.

pH	Cu			Fe			Pb			Zn		
	Fe	Pb	Zn	Cu	Pb	Zn	Cu	Fe	Zn	Cu	Fe	Pb
3.74	0.00767	0.508	8.25	130	66.3	1080	1.97	0.0151	16.2	0.121	0.000929	0.0616
3.97	0.00776	0.632	8.11	129	81.5	1050	1.58	0.0123	12.8	0.123	0.000956	0.0779
4.25	0.0141	0.752	7.95	71.0	53.4	565	1.33	0.0187	10.6	0.126	0.00177	0.0946
4.51	0.748	0.815	7.72	1.34	1.09	10.3	1.23	0.0918	9.47	0.130	0.0969	0.106
4.74	2.07	1.13	8.29	0.482	0.544	4.00	0.887	1.84	7.35	0.121	0.250	0.136
4.91	8.06	1.27	7.19	0.124	0.158	0.892	0.787	6.34	5.65	0.139	1.12	0.177
5.04	18.1	1.60	8.46	0.0552	0.0886	0.467	0.623	11.3	5.27	0.118	2.14	0.190
5.22	24.9	1.95	8.06	0.0401	0.0782	0.324	0.513	12.8	4.14	0.124	3.09	0.242
5.51	70.0	3.34	8.48	0.0143	0.0477	0.121	0.299	21.0	2.54	0.118	8.25	0.394
5.73	138	5.11	10.5	0.00726	0.0371	0.0759	0.196	27.0	2.05	0.0956	13.2	0.489

**Table A.8:** TP214 separation factors of copper, iron, lead and zinc from lactate media at 20 °C after 24hr of contact time.

pH	Cu			Fe			Pb			Zn		
	Fe	Pb	Zn	Cu	Pb	Zn	Cu	Fe	Zn	Cu	Fe	Pb
2.98	6690	174	2740	0.000149	0.026	0.409	0.00576	38.5	15.8	0.000365	2.44	0.063
3.14	8830	235	2840	0.000113	0.0264	0.322	0.00428	37.8	12.2	0.000352	3.11	0.0822
3.37	4790	247	3530	0.000209	0.0515	0.737	0.00405	19.4	14.3	0.000283	1.36	0.0698
3.55	8180	319	3490	0.000122	0.0390	0.426	0.00313	25.6	10.9	0.000287	2.35	0.0915
3.83	454	375	3270	0.000220	0.083	0.721	0.00267	12.1	8.73	0.000306	1.39	0.115
4.00	6260	528	3960	0.000160	0.0843	0.633	0.00189	11.9	7.50	0.000252	1.58	0.133
4.24	3850	680	4750	0.000260	0.177	1.24	0.00147	5.66	6.99	0.000210	0.809	0.143
4.51	6350	896	5350	0.000157	0.141	0.842	0.00112	7.09	5.97	0.000187	1.19	0.167
4.740	5920	909	7320	0.000169	0.154	1.24	0.00110	6.51	8.06	0.000137	0.808	0.124
4.85	7710	1220	9370	0.000130	0.158	1.22	0.000823	6.35	7.71	0.000107	0.823	0.130

**Table A.9:** MTS9100 separation factors of copper, iron, lead and zinc from lactate media at 20 °C after 24hr of contact time.

pH	Cu			Fe			Pb			Zn		
	Fe	Pb	Zn	Cu	Pb	Zn	Cu	Fe	Zn	Cu	Fe	Pb
2.60	0.338	1.23	0.408	2.96	3.65	1.21	0.812	0.274	0.331	2.45	0.828	3.02
2.81	0.417	1.07	0.356	2.40	2.56	0.853	0.936	0.391	0.333	2.811	1.17	3.00
2.96	0.574	1.05	0.543	1.74	1.83	0.946	0.952	0.547	0.517	1.84	1.0574	1.93
3.12	0.713	0.920	0.451	1.40	1.29	0.633	1.09	0.776	0.491	2.22	1.58	2.04
3.43	0.660	0.834	0.551	1.52	1.26	0.836	1.20	0.791	0.661	1.82	1.20	1.51
3.67	0.875	0.510	0.520	1.14	0.583	0.594	1.96	1.72	1.02	1.92	1.68	0.981
3.85	1.28	0.660	0.987	0.780	0.515	0.770	1.51	1.94	1.50	1.01	1.30	0.670
4.10	1.20	0.489	0.878	0.835	0.408	0.733	2.05	2.45	1.80	1.14	1.36	0.556
4.28	2.19	0.406	1.68	0.456	0.185	0.764	2.46	5.40	4.13	0.596	1.31	0.242
4.39	1.85	0.472	2.28	0.540	0.255	1.23	2.12	3.92	4.83	0.438	0.811	0.207

**Table A.10:** MTS9570 separation factors of copper, iron, lead and zinc from lactate media at 20 °C after 24hr of contact time.

pH	Cu			Fe			Pb			Zn		
	Fe	Pb	Zn	Cu	Pb	Zn	Cu	Fe	Zn	Cu	Fe	Pb
2.53	0.000966	0.0578	0.291	1030	59.8	301	17.3	0.0167	5.03	3.44	0.00332	0.199
2.7	0.000743	0.0314	0.242	1350	42.2	325	31.9	0.0237	7.71	4.14	0.00307	0.13
3.06	0.00103	0.0227	0.182	969	22	176	44	0.0454	7.99	5.51	0.00568	0.125
3.35	0.00049	0.00626	0.0664	2040	12.8	136	160	0.0783	10.6	15.1	0.00738	0.0942
3.66	-0.00087	-0.00752	-0.0951	-1150	8.64	109	-133	0.116	12.7	-10.5	0.00915	0.079
3.81	0.000668	0.00476	0.0595	1500	7.12	89	210	0.14	12.5	16.8	0.0112	0.0799
4.01	0.00196	0.00395	0.145	511	2.02	74.3	253	0.496	36.8	6.87	0.0135	0.0271
4.19	0.00177	0.00713	0.109	565	4.03	61.8	140	0.248	15.3	9.14	0.0162	0.0652
4.35	-0.00146	-0.00483	-0.0754	-684	3.3	51.6	-207	0.303	15.6	-13.3	0.0194	0.064
4.51	0.00197	0.00557	0.0888	506	2.82	45	180	0.355	16	11.3	0.0222	0.0626

**Table A.11:** MTS9301 separation factors of copper, iron, lead and zinc from lactate media at 20 °C after 24hr of contact time.

pH	Cu			Fe			Pb			Zn		
	Fe	Pb	Zn	Cu	Pb	Zn	Cu	Fe	Zn	Cu	Fe	Pb
2.75	7.32	18	54.1	0.137	2.46	7.39	0.0554	0.406	3	0.0185	0.135	0.333
3.01	7.1	12.1	43.9	0.141	1.7	6.18	0.0828	0.588	3.64	0.0228	0.162	0.275
3.31	10	8.34	37.1	0.0997	0.832	3.7	0.12	1.2	4.45	0.0269	0.27	0.225
3.51	11.7	7.53	30.9	0.0852	0.642	2.63	0.133	1.56	4.1	0.0324	0.38	0.244
3.73	14.2	6.49	27.7	0.0704	0.457	1.95	0.154	2.19	4.27	0.0361	0.513	0.234
3.93	18.1	7.77	23	0.0551	0.428	1.27	0.129	2.34	2.96	0.0436	0.79	0.338
4.14	21.3	8.51	20.6	0.047	0.4	0.967	0.118	2.5	2.42	0.0486	1.03	0.414
4.29	21.3	11.7	16.3	0.0469	0.55	0.764	0.0852	1.82	1.39	0.0614	1.31	0.721
4.43	18.6	10.1	11.5	0.0537	0.545	0.62	0.0986	1.84	1.14	0.0866	1.61	0.879
4.52	21.2	10.9	11.2	0.0471	0.515	0.528	0.0914	1.94	1.02	0.0892	1.89	0.976

**Table A.12:** MTS9501 separation factors of copper, iron, lead and zinc from lactate media at 20 °C after 24hr of contact time.

pH	Cu			Fe			Pb			Zn		
	Fe	Pb	Zn	Cu	Pb	Zn	Cu	Fe	Zn	Cu	Fe	Pb
2.96	0.00103	0.279	0.623	970	270	604	3.59	0.0037	2.23	1.61	0.00166	0.448
3.2	0.00159	0.266	0.657	629	168	413	3.75	0.00597	2.47	1.52	0.00242	0.405
3.48	0.00171	0.262	0.678	584	153	396	3.81	0.00652	2.58	1.48	0.00253	0.387
3.72	0.002	0.251	0.764	499	125	381	3.98	0.00797	3.04	1.31	0.00262	0.329
3.97	0.00191	0.279	0.9	524	146	472	3.59	0.00685	3.23	1.11	0.00212	0.31
4.19	0.00212	0.287	0.94	471	135	443	3.48	0.00739	3.27	1.06	0.00226	0.306
4.37	0.0037	0.302	1.04	270	81.5	280	3.31	0.0123	3.44	0.965	0.00357	0.291
4.58	0.00509	0.331	1.11	197	65.1	218	3.02	0.0154	3.36	0.9	0.00458	0.298
4.77	0.00913	0.376	1.21	110	41.2	133	2.66	0.0243	3.22	0.826	0.00755	0.311
4.88	0.00879	0.422	1.32	114	48	150	2.37	0.0208	3.12	0.76	0.00668	0.321



**Table A.13:** C107E separation factors of copper, iron, lead and zinc from lactate media at 20 °C after 24hr of contact time.

pH	Cu			Fe			Pb			Zn		
	Fe	Pb	Zn	Cu	Pb	Zn	Cu	Fe	Zn	Cu	Fe	Pb
2.77	0.148	0.379	1.13	6.77	2.57	7.67	2.64	0.39	2.99	0.883	0.13	0.335
3.04	0.247	0.203	1.5	4.04	0.82	6.08	4.93	1.22	7.41	0.665	0.165	0.135
3.22	0.264	0.0927	0.525	3.79	0.351	1.99	10.8	2.85	5.66	1.91	0.503	0.177
3.53	0.551	0.0563	0.578	1.81	0.102	1.05	17.7	9.79	10.3	1.73	0.954	0.0975
3.75	-2.76	0.0288	0.578	-0.363	-0.0105	-0.21	34.7	-95.6	20.1	1.73	-4.77	0.0499
3.9	-0.302	-0.00591	-0.122	-3.31	0.0195	0.403	-169	51.2	20.6	-8.21	2.48	0.0485
4.12	1.81	0.0326	0.725	0.553	0.018	0.401	30.7	55.5	22.3	1.38	2.5	0.0449
4.26	19	0.0401	2.06	0.0527	0.00211	0.108	24.9	473	51.3	0.486	9.23	0.0195
4.46	12.4	0.0335	1.43	0.0804	0.00269	0.115	29.9	371	42.8	0.698	8.67	0.0234
4.61	2.28	0.0404	1.74	0.439	0.0178	0.765	24.7	56.3	43.1	0.574	1.31	0.0232

**Table A.14:** TP214 separation factors of copper, iron, lead and zinc from citrate media at 20 °C after 24hr of contact time.

pH	Cu			Fe			Pb			Zn		
	Fe	Pb	Zn	Cu	Pb	Zn	Cu	Fe	Zn	Cu	Fe	Pb
2.27	163	58.5	817	0.00612	0.358	5	0.0171	2.79	14	0.00122	0.2	0.0716
2.73	202	84.6	1050	0.00494	0.418	5.21	0.0118	2.39	12.5	0.000948	0.192	0.0802
3.39	584	183	1420	0.00171	0.313	2.43	0.00547	3.2	7.77	0.000705	0.412	0.129
3.89	786	377	2490	0.00127	0.48	3.17	0.00265	2.08	6.61	0.000401	0.315	0.151
4.51	477	321	854	0.0021	0.672	1.79	0.00312	1.49	2.66	0.00117	0.559	0.376
5.08	80.5	87.7	218	0.0124	1.09	2.7	0.0114	0.919	2.48	0.00459	0.37	0.403
5.69	39.2	52.6	57.8	0.0255	1.34	1.47	0.019	0.746	1.1	0.0173	0.679	0.91
6.23	34.8	50	50.6	0.0288	1.44	1.46	0.02	0.695	1.01	0.0198	0.687	0.988
6.93	23.9	33	31.1	0.0418	1.38	1.3	0.0303	0.725	0.942	0.0322	0.77	1.06
7.29	23.2	25.5	29	0.0432	1.1	1.25	0.0393	0.91	1.14	0.0345	0.799	0.878

**Table A.15:** MTS9100 separation factors of copper, iron, lead and zinc from citrate media at 20 °C after 24hr of contact time.

pH	Cu			Fe			Pb			Zn		
	Fe	Pb	Zn	Cu	Pb	Zn	Cu	Fe	Zn	Cu	Fe	Pb
2.11	0.18	2.28	2.29	5.55	12.7	12.7	0.0789	0.438	1	0.0786	0.436	0.995
2.77	1.35	2.26	2.9	0.742	1.67	2.15	0.597	0.443	1.29	0.464	0.345	0.777
3.34	6.01	1.57	1.81	0.166	0.261	0.301	3.84	0.638	1.15	3.32	0.553	0.867
3.96	22.9	0.814	1.12	0.0437	0.0356	0.0491	28.1	1.23	1.38	20.4	0.89	0.725
4.51	2.14	0.466	0.692	0.467	0.218	0.324	4.6	2.15	1.49	3.09	1.44	0.673
5.07	1.28	0.468	0.595	0.781	0.366	0.465	2.73	2.14	1.27	2.15	1.68	0.787
5.66	1.34	0.713	0.739	0.745	0.531	0.55	1.88	1.4	1.04	1.82	1.35	0.965
6.15	1	0.693	1.63	0.999	0.693	1.63	1.44	1.44	2.35	0.614	0.613	0.425
6.33	1.52	0.761	1.9	0.657	0.5	1.25	2	1.31	2.5	0.8	0.526	0.4
6.43	1.75	0.742	2.97	0.573	0.425	1.7	2.35	1.35	4	0.588	0.337	0.25

**Table A.16:** MTS9570 separation factors of copper, iron, lead and zinc from citrate media at 20 °C after 24hr of contact time.

pH	Cu			Fe			Pb			Zn		
	Fe	Pb	Zn	Cu	Pb	Zn	Cu	Fe	Zn	Cu	Fe	Pb
1.87	0.00123	0.173	0.384	815	141	313	5.78	0.00709	2.22	2.6	0.00319	0.45
2.59	0.00365	0.0595	0.206	274	16.3	56.3	16.8	0.0614	3.46	4.86	0.0177	0.289
3.23	0.00433	0.0259	0.121	231	6	27.9	38.5	0.167	4.65	8.29	0.0358	0.215
3.84	0.0118	0.0228	0.117	84.4	1.92	9.89	43.9	0.52	5.14	8.54	0.101	0.195
4.41	0.00238	0.0023	0.00997	420	0.964	4.18	435	1.04	4.34	100	0.239	0.23
4.98	0.0265	0.0143	0.0422	37.8	0.538	1.6	70.2	1.86	2.96	23.7	0.627	0.337
5.55	0.187	0.0627	0.138	5.36	0.336	0.741	15.9	2.98	2.21	7.22	1.35	0.453
5.98	0.151	0.0373	0.158	6.61	0.247	1.05	26.8	4.06	4.25	6.31	0.954	0.235
6.27	0.0398	0.00745	0.0315	25.1	0.187	0.792	134	5.35	4.23	31.7	1.26	0.236
6.38	0.404	0.0627	0.249	2.48	0.155	0.617	16	6.45	3.98	4.01	1.62	0.251

**Table A.17:** MTS9301 separation factors of copper, iron, lead and zinc from citrate media at 20 °C after 24hr of contact time.

pH	Cu			Fe			Pb			Zn		
	Fe	Pb	Zn	Cu	Pb	Zn	Cu	Fe	Zn	Cu	Fe	Pb
1.44	14.4	76.5	91	0.0694	5.31	6.32	0.0131	0.188	1.19	0.011	0.158	0.841
2.13	80.5	94.1	45.2	0.0124	1.17	0.561	0.0106	0.856	0.48	0.0221	1.78	2.08
2.76	270	21.9	22.5	0.00371	0.081	0.0835	0.0457	12.3	1.03	0.0444	12	0.971
3.38	451	25.7	15.7	0.00222	0.0569	0.0347	0.039	17.6	0.61	0.0639	28.8	1.64
3.94	542	37.4	12.1	0.00185	0.069	0.0224	0.0268	14.5	0.325	0.0823	44.6	3.08
4.51	627	48.1	10.1	0.0016	0.0768	0.0161	0.0208	13	0.209	0.0991	62.1	4.77
5.05	708	56.2	9.6	0.00141	0.0794	0.0136	0.0178	12.6	0.171	0.104	73.7	5.85
5.53	672	42.7	6.65	0.00149	0.0636	0.00989	0.0234	15.7	0.156	0.15	101	6.42
5.73	540	35.2	5.07	0.00185	0.0652	0.0094	0.0284	15.3	0.144	0.197	106	6.94
5.82	654	37.9	5.24	0.00153	0.0579	0.00801	0.0264	17.3	0.138	0.191	125	7.23

**Table A.18:** MTS9501 separation factors of copper, iron, lead and zinc from citrate media at 20 °C after 24hr of contact time.

pH	Cu			Fe			Pb			Zn		
	Fe	Pb	Zn	Cu	Pb	Zn	Cu	Fe	Zn	Cu	Fe	Pb
2.15	0.00292	0.501	0.433	343	172	148	2	0.00583	0.864	2.31	0.00674	1.16
2.76	0.0159	0.369	0.34	63	23.3	21.4	2.71	0.043	0.919	2.95	0.0468	1.09
3.38	0.000294	0.348	0.341	3410	1190	1160	2.87	0.000843	0.979	2.93	0.000861	1.02
3.97	0.00455	0.418	0.433	220	91.9	95.2	2.39	0.0109	1.04	2.31	0.0105	0.965
4.55	0.0124	0.687	0.814	80.7	55.4	65.6	1.46	0.0181	1.19	1.23	0.0152	0.844
5.12	0.0188	0.883	0.994	53.3	47.1	53	1.13	0.0212	1.13	1.01	0.0189	0.889
5.71	0.0267	1.1	1.27	37.5	41.2	47.7	0.909	0.0242	1.16	0.787	0.021	0.865
6.3	0.0521	1.09	1.52	19.2	20.9	29.2	0.917	0.0478	1.4	0.656	0.0342	0.715
6.54	0.0883	1.02	1.44	11.3	11.6	16.3	0.98	0.0866	1.41	0.696	0.0615	0.711
6.7	0.131	0.995	1.41	7.63	7.59	10.8	1	0.132	1.42	0.709	0.0929	0.705

**Table A.19:** C107E separation factors of copper, iron, lead and zinc from citrate media at 20 °C after 24hr of contact time.

pH	Cu			Fe			Pb			Zn		
	Fe	Pb	Zn	Cu	Pb	Zn	Cu	Fe	Zn	Cu	Fe	Pb
2.21	0.25	0.494	2.55	4.01	1.98	10.2	0.505	2.03	5.17	0.0977	0.392	0.193
2.8	0.234	0.218	0.784	4.28	0.934	3.35	1.07	4.58	3.59	0.298	1.28	0.278
3.34	0.184	0.142	0.591	5.45	0.772	3.22	1.3	7.06	4.17	0.311	1.69	0.24
3.95	0.168	0.124	0.831	5.96	0.737	4.95	1.36	8.08	6.72	0.202	1.2	0.149
4.44	0.502	0.0176	0.319	1.99	0.0351	0.636	28.5	56.8	18.1	1.57	3.13	0.0552
5.02	-0.517	0.0853	0.611	-1.93	-0.165	-1.18	-6.07	11.7	7.17	-0.846	1.64	0.139
5.45	0.0663	-0.0179	-0.145	15.1	-0.27	-2.19	-3.7	-55.8	8.11	-0.456	-6.88	0.123
5.87	0.594	-0.0328	-1.8	1.68	-0.0552	-3.03	-18.1	-30.5	54.9	-0.33	-0.556	0.0182
5.99	-1.6	-0.0778	1.46	-0.626	0.0487	-0.916	20.5	-12.9	-18.8	-1.09	0.683	-0.0531
6.05	-1	0.0122	-0.471	-1	-0.0122	0.471	-82	81.9	-38.6	2.12	-2.12	-0.0259

### A.3 Solution-phase speciation

The speciation of metals and complexes within solution will be very pH dependent due pH dependence of conjugate base concentration of the weak acids. With a higher concentration of conjugate base leading to the potential for more complexation and even dimerization of complexes, in order to explain extraction trends observed, the speciation of metals in solution was modelled. All speciation data used for the modelling is included within Tables A.20 - A.28. As suggested by the difference in in proton concentration, each metal transitions between free metal to metal-anion complex as the pH approaches the  $pK_a$  of the acids, due to the higher available concentration of conjugate base. Generally speaking, the more bound moieties in the complex (mono-, bis-, tris-), the higher the stability constant. The referencing of species in tables is [1] Brown and Ekberg (2016), [2] Martell, *et al.* (2009), [3] Gorman and Clydesdale (1984) and [4] Field, *et al.* (1974).

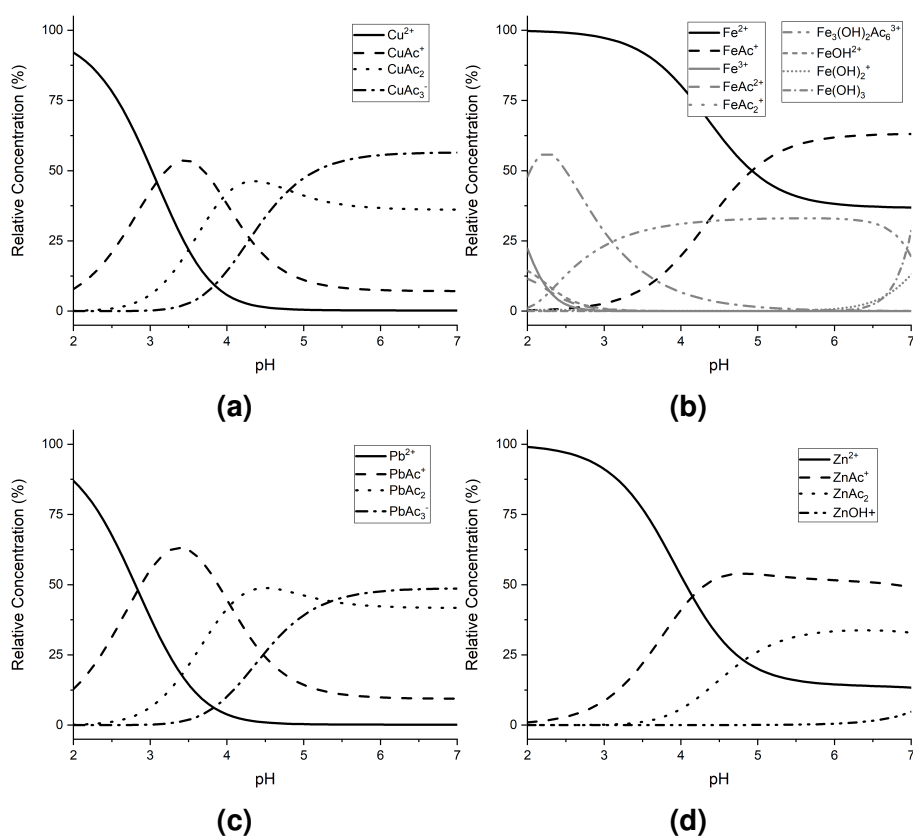
**Table A.20:** Stability constants for solid phase hydrolysis products of each metal at 0.0 M ionic strength [1].

Metal	Species	$\log K_{sp}$	Metal	Species	$\log K_{sp}$	Metal	Species	$\log K_{sp}$
Copper(II)	CuO	7.90	Iron(II)	Fe <sub>3</sub> O <sub>4</sub>	12.02	Zinc	ZnO	11
	CuO	8.68	Iron(III)	FeO(OH)	0.3		Zn(OH) <sub>2</sub>	12
				Fe <sub>2</sub> O <sub>3</sub>	-0.1	Lead(II)	PbO	12.6



**Table A.21:** Stability constants for solution phase hydrolysis products of each metal at 0.0 M ionic strength [1].

Metal	Species	$\log\beta$	Metal	Species	$\log\beta$	Metal	Species	$\log\beta$
Copper(II)	$\text{CuOH}^+$	-7.53	Iron(II)	$\text{FeOH}^+$	-9.32	Zinc	$\text{ZnOH}^+$	-9
	$\text{Cu(OH)}_2$	-16.22		$\text{Fe(OH)}_2$	-20.6		$\text{Zn(OH)}_2$	-17.8
	$\text{Cu(OH)}_3^-$	-26.59		$\text{Fe(OH)}_3^-$	-32.6		$\text{Zn(OH)}_3^-$	-28.4
	$\text{Cu}_2(\text{OH})_3^{3+}$	-6.4	Iron(III)	$\text{FeOH}^{2+}$	-2.19	$\text{Zn(OH)}_4^{2-}$	-40.5	
$\text{Cu}_2(\text{OH})_2^{2+}$	-10.43	$\text{Fe(OH)}_2^+$		-5.7	$\text{Zn}_2\text{OH}^{3+}$	-8.7		
$\text{Cu}_3(\text{OH})_4^{2+}$	-21.10	$\text{Fe(OH)}_3$		-12.4	Lead	$\text{PbOH}^+$	-7.46	
		$\text{Fe(OH)}_4^-$	-22	$\text{Pb(OH)}_2$		-16.9		
		$\text{Fe}_2(\text{OH})_2^{4+}$	-2.91	$\text{Pb(OH)}_3^-$		-28		
		$\text{Fe}_3(\text{OH})_4^{5+}$	-6.3	$\text{Pb}_3(\text{OH})_4^{2+}$		-23.7		
				$\text{Pb}_4(\text{OH})_4^{4+}$		-20.3		
				$\text{Pb}_6(\text{OH})_8^{4+}$	-43.2			

**Figure A.1:** Solution speciation of  $\text{Cu}^{2+}$  (a),  $\text{Fe}^{2+}$  and  $\text{Fe}^{3+}$  (b),  $\text{Pb}^{2+}$  (c) and  $\text{Zn}^{2+}$  (d) in acetic acid, calculated by the HySS software<sup>[125]</sup> with stability constants attained from the NIST database<sup>[126]</sup>.

**Table A.22:** Stability constants for copper acetate species at 0.1 M ionic strength [2]. [L] = complexing acid, [M] = metal, [H] = proton, [OH] = hydroxide.

Ion	Species	$\log\beta$
Acetate <sup>-</sup>	[HL]	4.56
Cu <sup>2+</sup>	[ML]	1.79
	[ML <sub>2</sub> ]	2.80
	[ML <sub>3</sub> ]	3.30

**Table A.23:** Stability constants for iron(II) acetate species at 3.0 M ionic strength [2]. [L] = complexing acid, [M] = metal, [H] = proton, [OH] = hydroxide.

Ion	Species	$\log\beta$
Acetate <sup>-</sup>	[HL]	4.78
Fe <sup>2+</sup>	[ML]	0.54

**Table A.24:** Stability constants for metal acetate species at 1.0 M ionic strength [2]. [L] = complexing acid, [M] = metal, [H] = proton, [OH] = hydroxide.

Ion	Species	$\log\beta$	Ion	Species	$\log\beta$
Acetate <sup>-</sup>	[HL]	4.58	Pb <sup>2+</sup>	[ML]	2.05
Fe <sup>3+</sup>	[ML]	2.8		[ML <sub>2</sub> ]	3.00
	[ML <sub>2</sub> ]	6.5		[ML <sub>3</sub> ]	3.37
	[M <sub>3</sub> (OH) <sub>2</sub> L <sub>6</sub> ]	20	Zn <sup>2+</sup>	[ML]	0.87
				[ML <sub>2</sub> ]	1

**Table A.25:** Stability constants for metal lactate species at 1.0 M ionic strength [2]. [L] = complexing acid, [M] = metal, [H] = proton, [OH] = hydroxide.

Ion	Species	$\log\beta$	Ion	Species	$\log\beta$	Ion	Species	$\log\beta$
Lactate <sup>-</sup>	[HL]	3.59	Pb <sup>2+</sup>	[ML]	1.99	Zn <sup>2+</sup>	[ML]	1.86
Cu <sup>2+</sup>	[ML]	2.47		[ML <sub>2</sub> ]	2.88		[ML <sub>2</sub> ]	2.6
	[ML <sub>2</sub> ]	4.08		[ML <sub>3</sub> ]	3.50		[ML <sub>3</sub> ]	3.4
	[ML <sub>3</sub> ]	4.70						

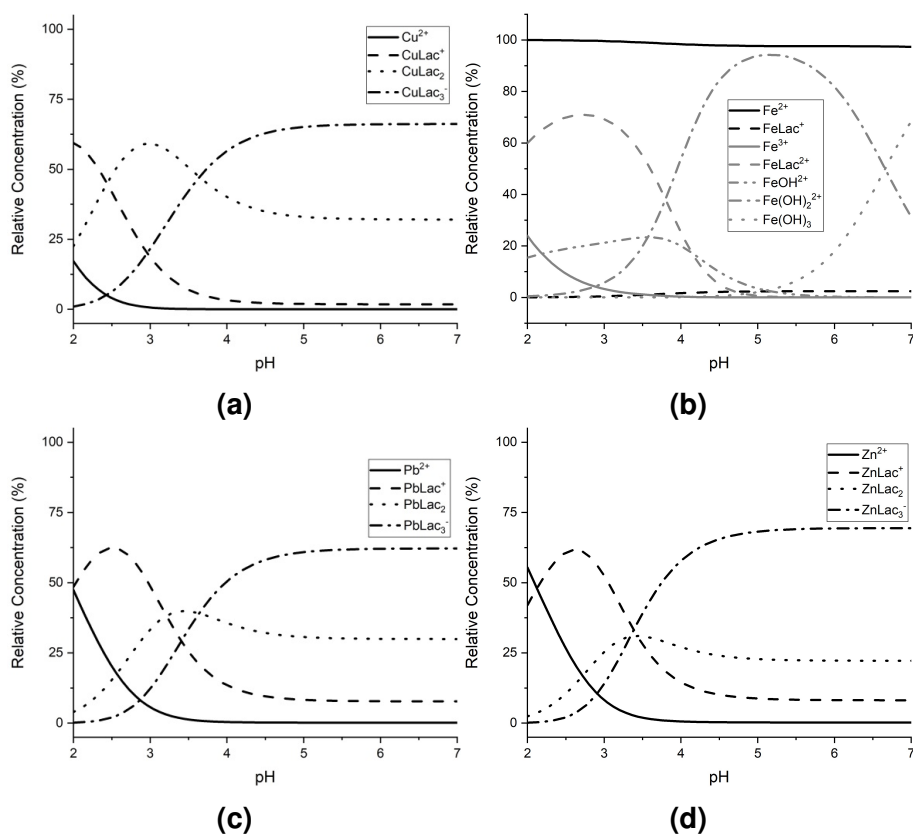


**Figure A.2:** Solution speciation of  $\text{Cu}^{2+}$  (a),  $\text{Fe}^{2+}$  and  $\text{Fe}^{3+}$  (b),  $\text{Pb}^{2+}$  (c) and  $\text{Zn}^{2+}$  (d) in lactic acid, calculated by the HySS software (Gans, *et al.*, 2009) with stability constants attained from the NIST database (Martell, *et al.*, 2009), apart from  $\text{Fe}^{2+}$  and  $\text{Fe}^{3+}$ , that were gathered from Gorman and Clydesdale (1984).

**Table A.26:** Stability constants for metal lactate species at 0.1 M ionic strength [2,3]. [L] = complexing acid, [M] = metal, [H] = proton, [OH] = hydroxide.

Ion	Species	$\log \beta$
Lactate <sup>-</sup>	[HL]	3.67
Fe <sup>2+</sup>	[ML]	-1.30
Fe <sup>3+</sup>	[ML]	2.38

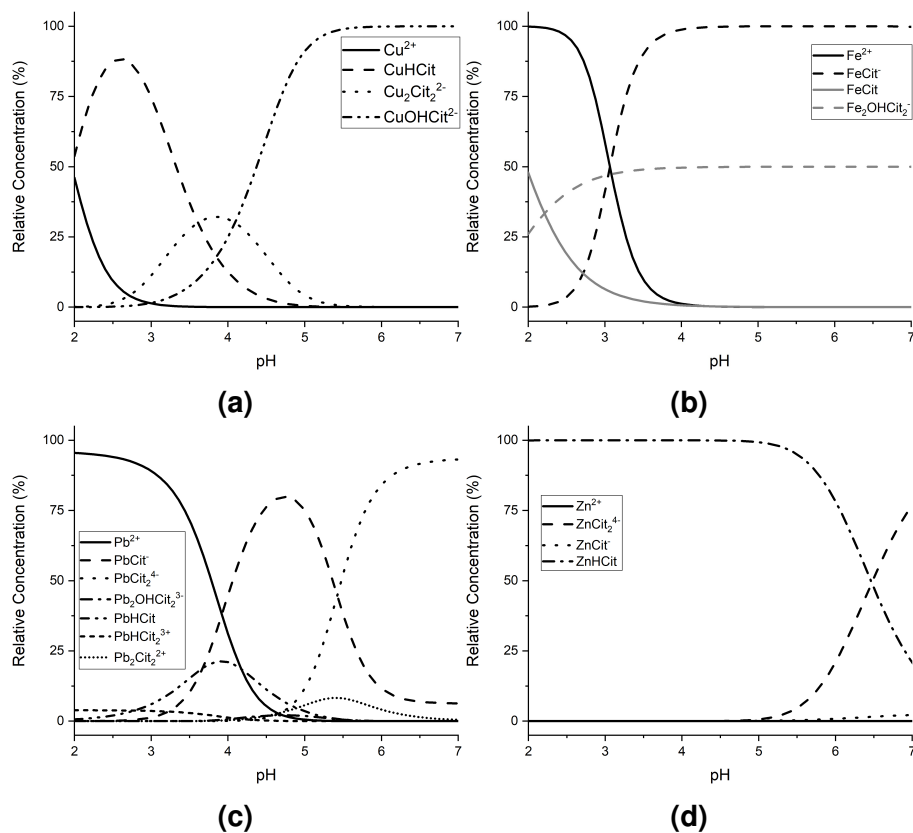


**Figure A.3:** Solution speciation of  $\text{Cu}^{2+}$  (a),  $\text{Fe}^{2+}$  and  $\text{Fe}^{3+}$  (b),  $\text{Pb}^{2+}$  (c) and  $\text{Zn}^{2+}$  (d) in citric acid, calculated by the HySS software (Gans, *et al.*, 2009) with stability constants attained from the NIST database (Martell, *et al.*, 2009), apart from  $\text{Cu}^{2+}$ ,  $\text{Fe}^{2+}$  and  $\text{Fe}^{3+}$ , that were gathered from Field, *et al.*(1974).

**Table A.27:** Stability constants for metal citrate species at 0.1 M [2,4]. [L] = complexing acid, [M] = metal, [H] = proton, [OH] = hydroxide.

Ion	Species	$\log\beta$	Ion	Species	$\log\beta$	Ion	Species	$\log\beta$
$\text{Citrate}^-$	[HL]	5.64	$\text{Fe}^{2+}$	[MHL]	8.62	$\text{Zn}^{2+}$	[ML]	4.93
	[HL <sub>2</sub> ]	9.99		[ML]	4.80		[ML <sub>2</sub> ]	6.8
	[HL <sub>3</sub> ]	12.89		[MHL <sub>2</sub> ]	11.81		[MHL]	12.91
$\text{Cu}^{2+}$	[MHL]	9.31	$\text{Fe}^{3+}$	[MHL]	12.38		[MH <sub>2</sub> L]	11.19
	[M <sub>2</sub> L <sub>2</sub> ]	14.72		[ML]	11.21	[M <sub>2</sub> (OHL) <sub>2</sub> ]	-2.85	
	[MOHL]	1.61		[M <sub>2</sub> OHL <sub>2</sub> ]	8.60			





## **Appendix B**

# **Single Metal Isotherm Study of the Ion Exchange Removal of Cu(II), Fe(II), Pb(II) and Zn(II) from Synthetic Acetic Acid Leachate: Supplementary Information**

## Resin Characteristics

This appendix contains the supplementary information accepted publication by Chemical Engineering Journal on 21/03/2020 alongside the paper Single Metal Isotherm Study of the Ion Exchange Removal of Cu(II), Fe(II), Pb(II) and Zn(II) from Synthetic Acetic Acid Leachate. DOI: 10.1016/j.cej.2020.124862

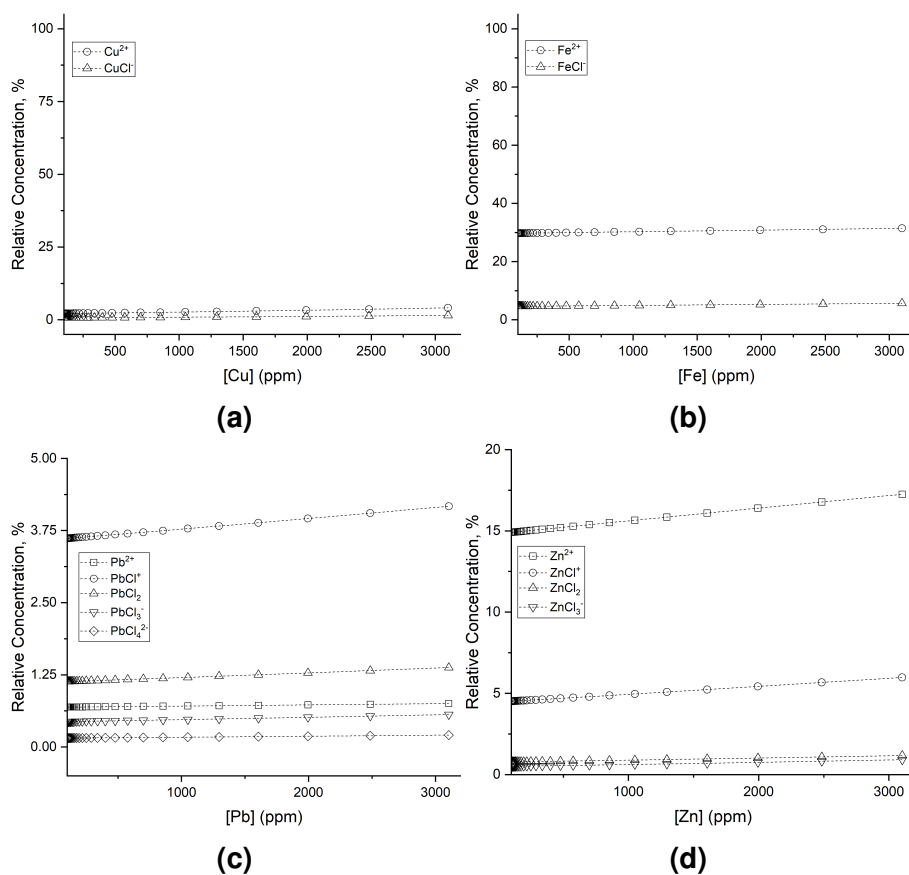
**Table B.1:** Physical and chemical characteristics of the resins tested throughout this study, as obtained from suppliers information data sheets (PS = polystyrene, PA = polyacrylic, DVB = divinylbenzene). All are spherical beads.

Name	TP214	MTS9301	C107E
Manufacturer	Lanxess	Purolite	Purolite
Functionality	Thiourea	Iminodiacetic acid	Carboxylic acid
Commercial equivalent	Puromet	Lanxess	Dowex
Matrix	PS-DVB	PS-DVB	PA-DVB
Size ( $\mu\text{m}$ )	550	800-1300	300-1600
Capacity	1.0 eq.L <sup>-1</sup>	1.57 eq.L <sup>-1</sup>	3.6 eq.L <sup>-1</sup>
Water retention (wt%)	43-48	52-60	53-58
Specific gravity (g.mL <sup>-1</sup> )	1.1	1.18	1.17
Ionic form shipped	Freebase	Na <sup>+</sup>	H <sup>+</sup>

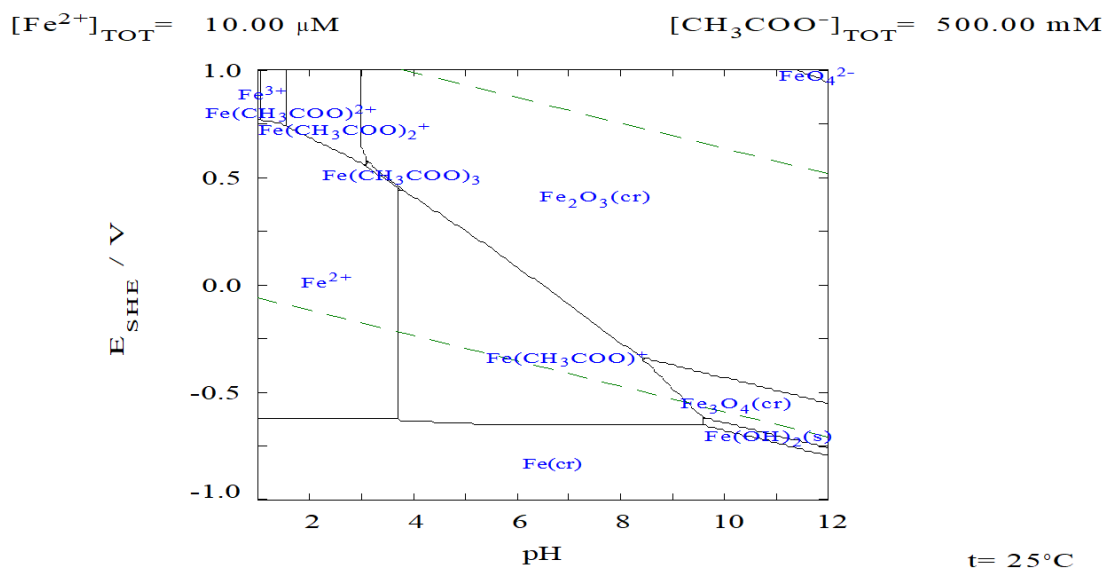
## Modelling of the Metal Speciation

Figure B.1 displays the solution phase Phreeqc modelling of copper (Figure B.1a), iron(II) (Figure B.1b), lead (Figure B.1c) and zinc (Figure B.1d) single metal solutions. Each solution was modelled with 0.5 M NaCl and acetic acid at pH 4.5. Models were conducted at concentrations between 100 ppm to 3000 ppm in order to mimic the solution conditions of each isotherm experiment. In each case, ionic forms are labelled within the legend, however complex formation is not predicted, therefore the remainder of metal ions from the total is assumed to be bound within complexes, as predicted by HySS modelling within previous work<sup>[119]</sup>. Solution phase copper(II) and iron(II) remain within the 2+ oxidation





**Figure B.1:** Phreeqc modelling of each metal in solution at concentration ranges of 100 ppm to 3000 ppm (single metal solutions) generated in Aqion<sup>[139]</sup>; 0.5 M NaCl; 0.5 M acetic acid; pH 4.5.



**Figure B.2:** Predominance diagram created using the HYDRA<sup>[104]</sup> and Medusa<sup>[149]</sup> software, modelled at  $25^\circ\text{C}$ .

states throughout all of these single metal experiments. All metals maintain a high proportion of the relative abundance in acetate complexes, with the largest non-complexed metal being iron(II) with  $\sim 30\%$  of its speciation being in the  $\text{Fe}^{2+}$  species. Figure B.2 contains a predominance diagram of iron within a system containing 0.5 M acetate, this shows that towards pH 4.5, the precipitation of  $\text{Fe}_2\text{O}_3$  becomes more likely with an increase in ORP beyond  $\sim 250\text{mV}$ . While this shows a high likelihood of  $\text{Fe}_2\text{O}_3$  precipitation, as there was no ORP control, there was no observable precipitation, therefore it is assumed that majority of iron remained in solution and within the 2+ oxidation state.

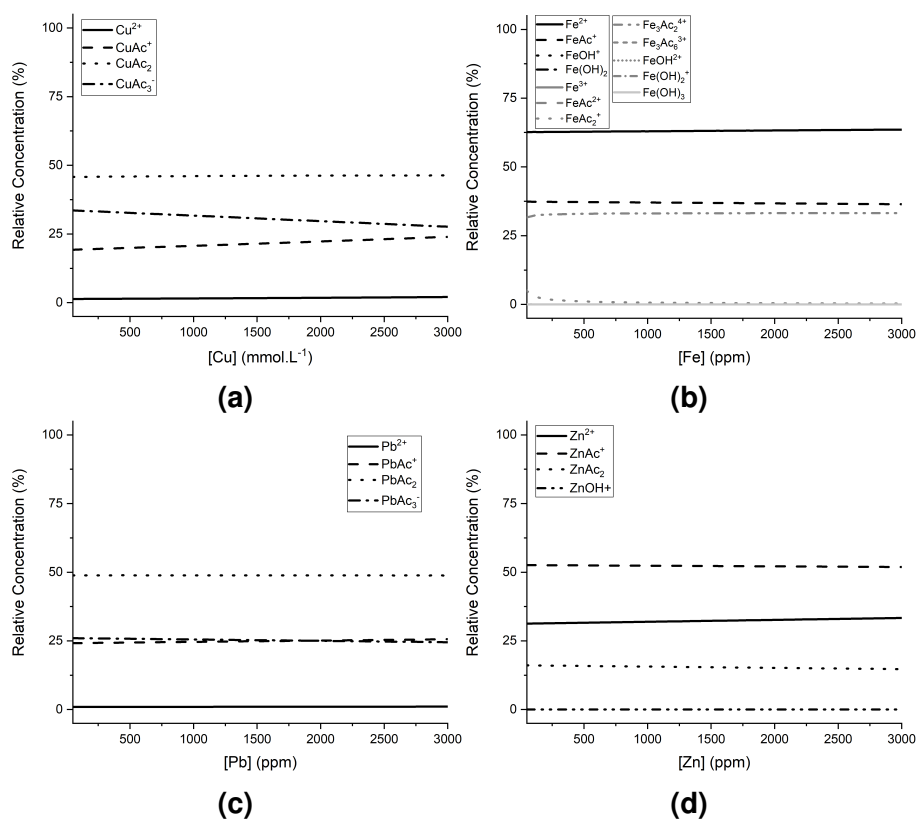
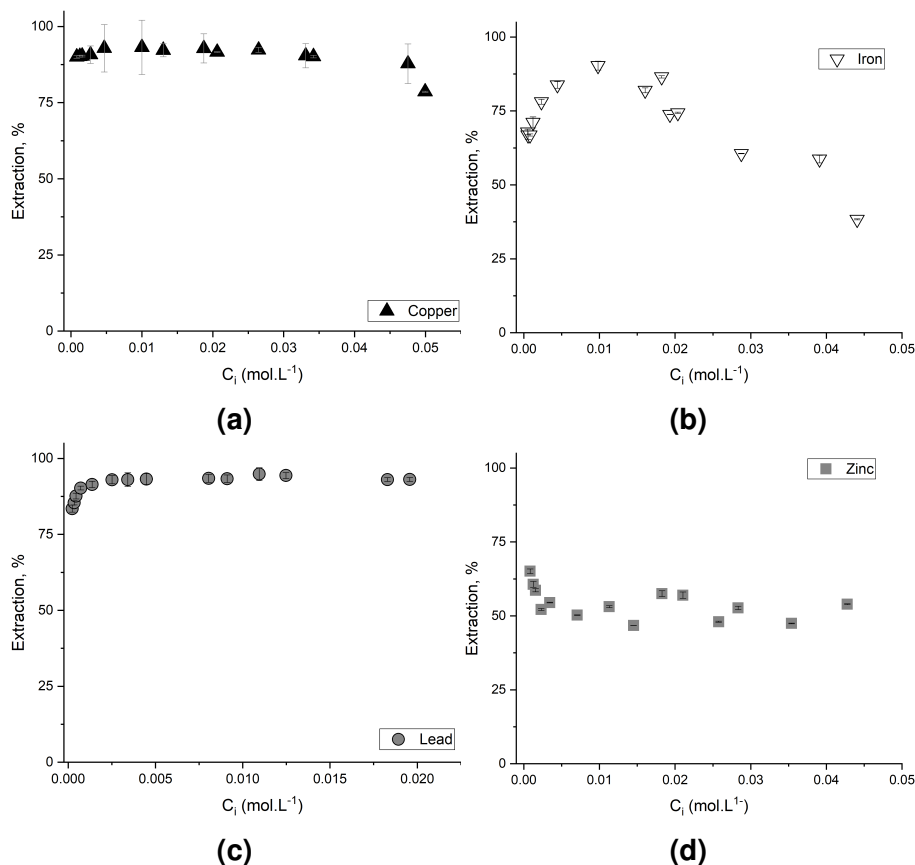


**Figure B.3:** Speciation modelling of each metal in solution at concentration ranges of 100 ppm to 3000 ppm (single metal solutions) using the HySS software<sup>[228]</sup>; 0.5 M acetic acid; pH 4.5.

Figure B.3 displays the modelled speciation of each metal across the concentration range studied within this paper. Overall, the change in relative concentration of each species of metals changes fairly insignificantly. Copper complexes  $\text{CuAc}^+$  and  $\text{CuAc}_3^-$  display the largest amount of deviation with

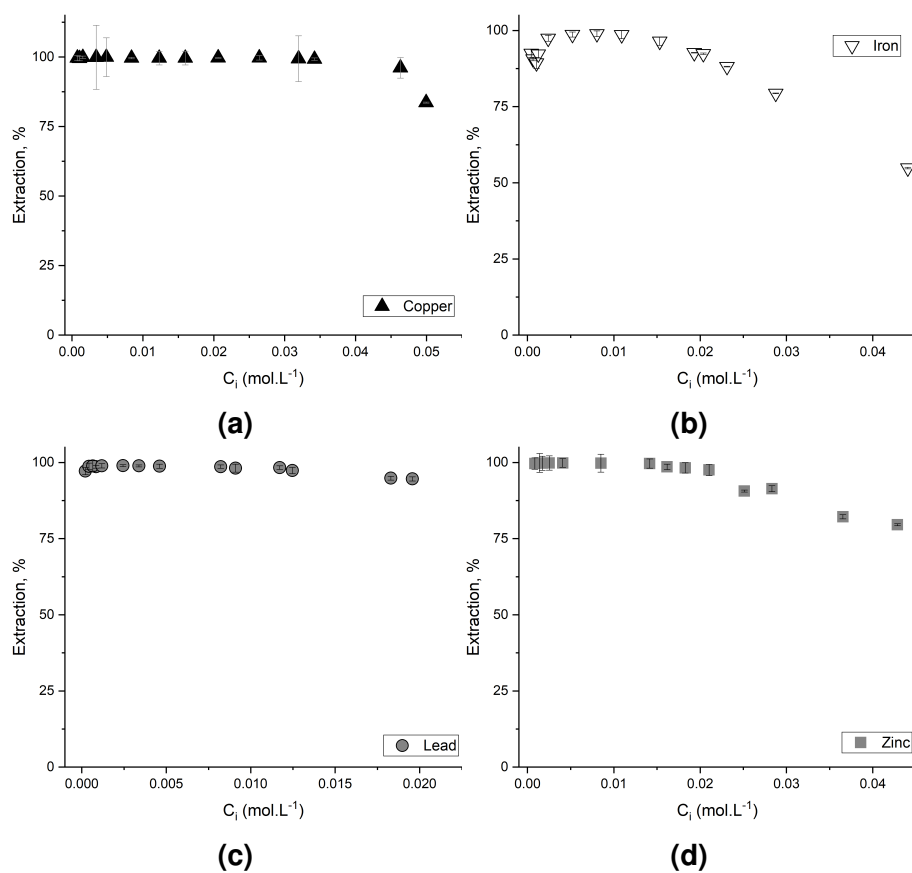
concentration, from  $\sim 30\%$  and  $\sim 20\%$ , respectively at the lowest concentrations to both reaching  $\sim 25\%$  towards the higher molar concentrations.

## Supplementary Extraction Data



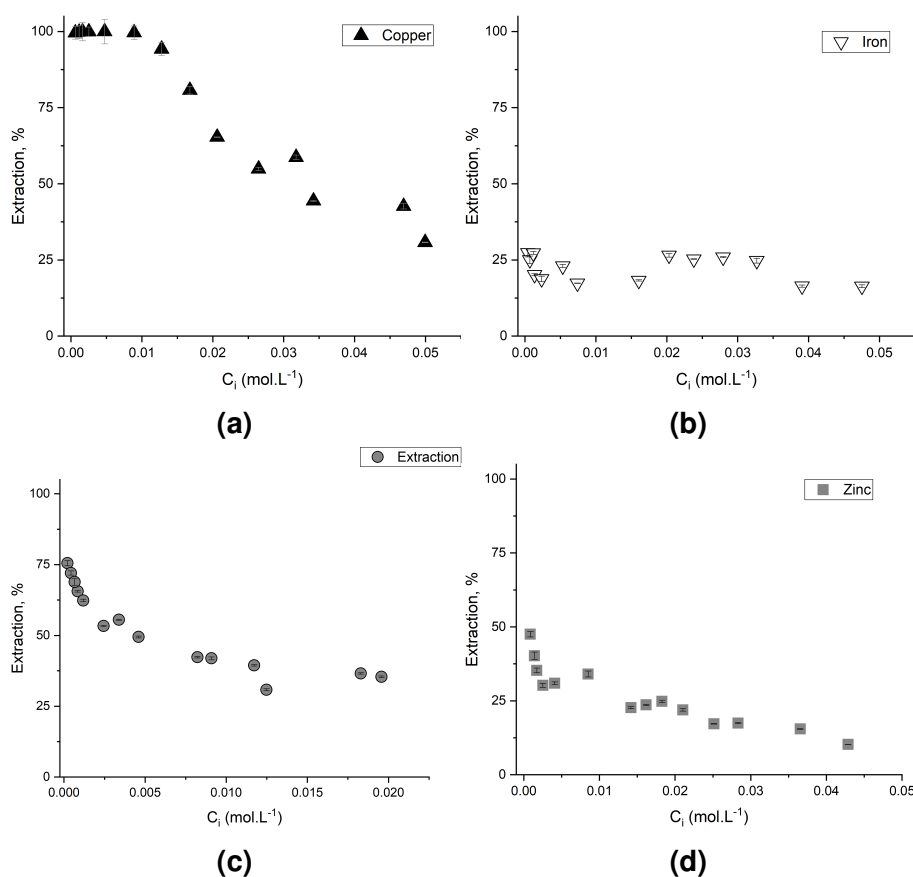
**Figure B.4:** Extraction % as a function of initial concentration in  $\text{mol.L}^{-1}$  for copper (a), iron (b), lead (c) and zinc (d) by C107E (initial concentrations 25 ppm to 3000 ppm; temperature  $20^\circ\text{C}$ ;  $0.5\text{ M NaCl}$ ;  $0.5\text{ M acetic acid}$ ;  $2\text{ ml wet settled resin}$ ;  $50\text{ ml solution}$ ).

Figure B.4 displays the percentage extraction of copper (a), iron (b), lead (c) and zinc (d). Both lead and copper maintain high extraction % throughout the entire concentration range, with saturation of copper being potentially displayed beyond  $0.05\text{ mol.L}^{-1}$ . Iron increases extraction % until an initial concentration of  $0.01\text{ mol.L}^{-1}$  where it begins to decrease, and zinc maintains  $\sim 50\%$  extraction beyond  $\sim 0.005\text{ mol.L}^{-1}$ .



**Figure B.5:** Extraction % as a function of initial concentration in mol L<sup>-1</sup> for copper (a), iron (b), lead (c) and zinc (d) by MTS9301 (initial concentrations 25 ppm to 3000 ppm; temperature 20 °C; 0.5 M NaCl; 0.5 M acetic acid; 2 ml wet settled resin; 50 ml solution).

The extraction percentage of copper (a), iron (b), lead (c) and zinc (d) as a function of initial concentration is displayed within Figure B.5. Initially, all metals are extracted to high extent, with all metals achieving  $>85\%$  extraction. Lead is not abundant in concentrations high enough to saturate the resin, however copper extraction, again, decreases beyond  $\sim 0.05 \text{ mol g}^{-1}$ , while iron began to decrease to a lowest measured extraction of  $\sim 55\%$  from  $0.015 \text{ mol L}^{-1}$  and zing began to decrease to  $\sim 75\%$  from an initial concentration of  $\sim 0.02 \text{ mol L}^{-1}$ .



**Figure B.6:** Extraction % as a function of initial concentration in  $\text{mol L}^{-1}$  for copper (a), iron (b), lead (c) and zinc (d) by TP214 (initial concentrations 25 ppm to 3000 ppm; temperature  $20^\circ\text{C}$ ;  $0.5 \text{ M NaCl}$ ;  $0.5 \text{ M acetic acid}$ ;  $2 \text{ ml wet settled resin}$ ;  $50 \text{ ml solution}$ ).

Of all three resins, TP214 displays the lowest extraction % for all metals, these are displayed as a function of initial concentration in Figure B.6. Iron extraction does not exceed 30% by TP214, while initially lead and zinc extraction is 75% and 50%, with these decreasing as initial concentration increases. Copper extraction

is initially at 100%, however beyond  $0.01 \text{ mol L}^{-1}$  initial concentration, this begins to decrease, to 25% by  $\sim 0.05 \text{ mol L}^{-1}$ .

## B.1 Comparison of Isotherm Parameters to IR, solution phase complex $\Delta H$ and $\Delta S$ and Electronegativity

**Table B.2:** Summary of the trends found by comparison of the isotherm data of C107E, MTS9301 and TP214 and the ionic radius, average  $\Delta H$  of complex formation, average  $\Delta S$  of complex formation and electronegativity.

Variable	C107E				MTS9301				TP214			
	IR	$\Delta H$	$\Delta S$	EN	IR	$\Delta H$	$\Delta S$	EN	IR	$\Delta H$	$\Delta S$	EN
$q_m$	N	N	N	Y	Y	N	N	N	N	N	N	N
$a_L$	N	N	N	N	N	N	N	N	N	N	N	N
$b_F$	N	N	N	Y	N	N	N	N	N	N	N	N
$\Delta E$	N	N	N	Y	N	N	N	N	N	N	N	N

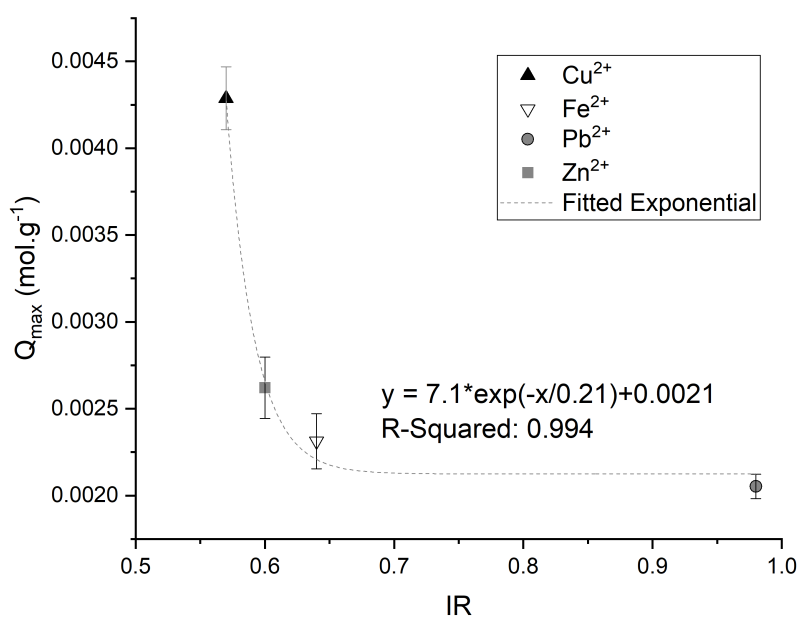


**Figure B.7:** Comparison of the Langmuir determined MTS9301  $Q_{\max}$  as a function of the ionic radius of each metal.

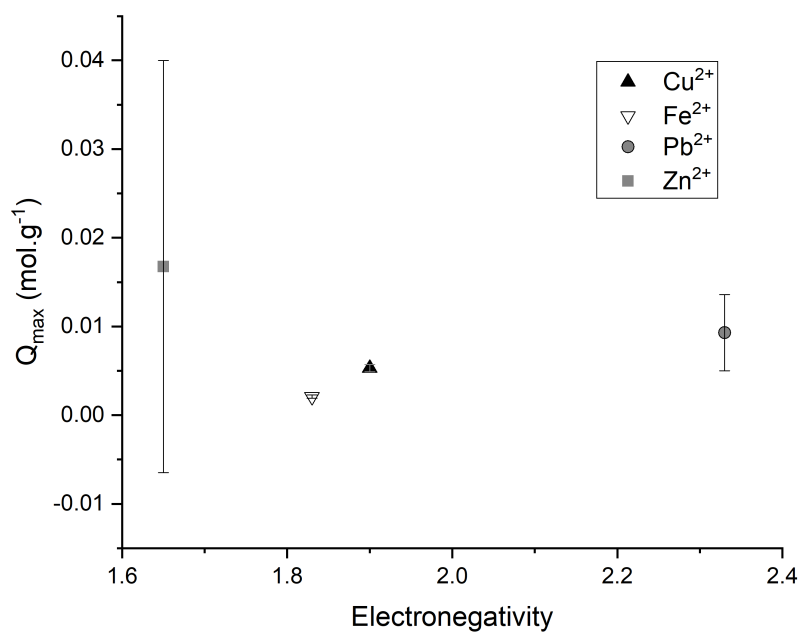


**Figure B.8:** Comparison of the Langmuir determined C107E  $Q_{\max}$  as a function of the electronegativity of each metal.

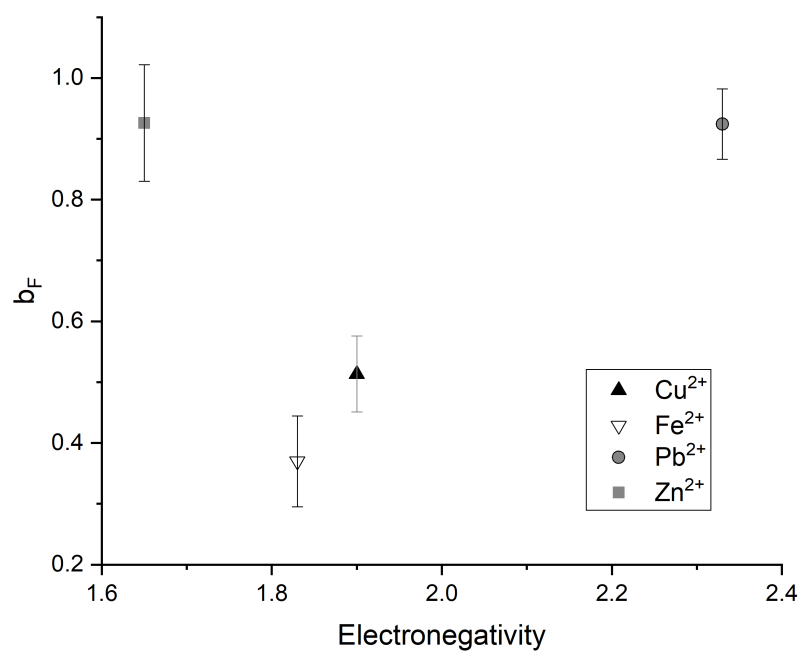


**Figure B.9:** Comparison of the Freundlich determined C107E  $b_F$  as a function of the electronegativity of each metal.

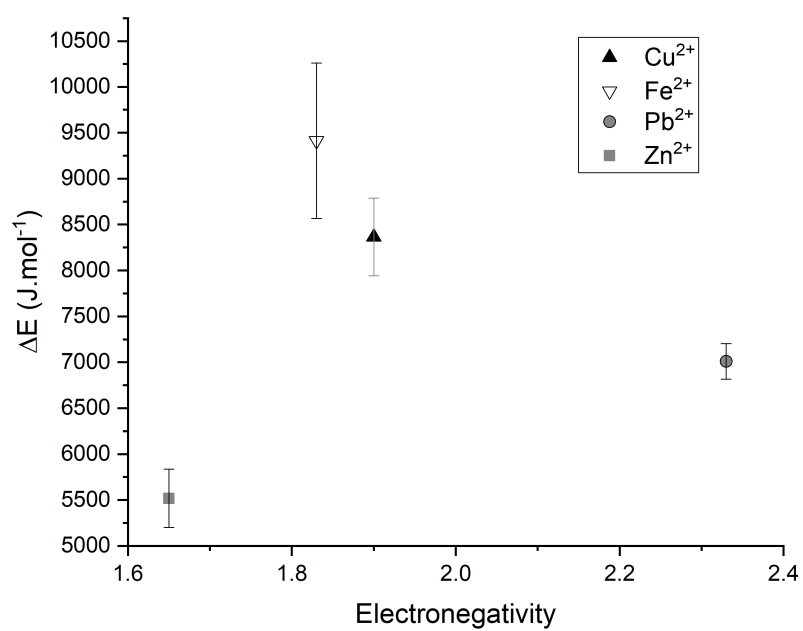


**Figure B.10:** Comparison of the D-R determined C107E free energy of adsorption as a function of the electronegativity of each metal.



Figures B.7-B.10 describe the relationships between the isotherm parameters and physiochemical parameters that have observable trends, as stated in Table B.2. No trend is seen with  $Q_{max}$  of  $a_L$  for either resin, apart from with the MTS9301  $Q_{max}$ , where there seems to be an almost exponential trend, increasing with decreasing IR (fitting the exponential to an  $r^2$  of 0.994). C107E displays a trend that follows an increase in electronegativity, decreasing binding intensity and free energy of adsorption.



# Appendix C

## Multi-metal System Supplementary Data

### C.1 Multi-metal Isotherm Extraction Percentages

Figures C.1 - C.3 display the isotherm data reanalysed to report the percentage extraction per mole of metal dissolved in solution for C107E, MTS9301 and TP214. Both lead and copper display increasing adsorption of metal to the resin surface throughout the experiment, however the percentage of metal extracted from solution decreases substantially as the moles of metal in the initial solution increases from both copper and lead displaying 95% extraction, to 50 and 60% extraction, respectively. Iron(II) displayed 98% until contact with  $\sim 0.0945$ mmol where it displays a steep decrease till 15% removal from solution towards the largest volume of solution added. Zinc displays a similar decrease to iron(II), however with an initial extraction of only 73% and a decrease to 17%.

MTS9301 displays 99% extraction of copper until 0.51mmol of copper are in solution, dropping to 92% by the largest volume of solution added (Figure C.2). All other metals display a reverse sigmoidal curve, plateauing at 99-100% extraction before dropping sharply due to competition. Lead displays the first drop in extraction at 0.089mmol of dissolved metal, dropping to a low of 11% extraction,

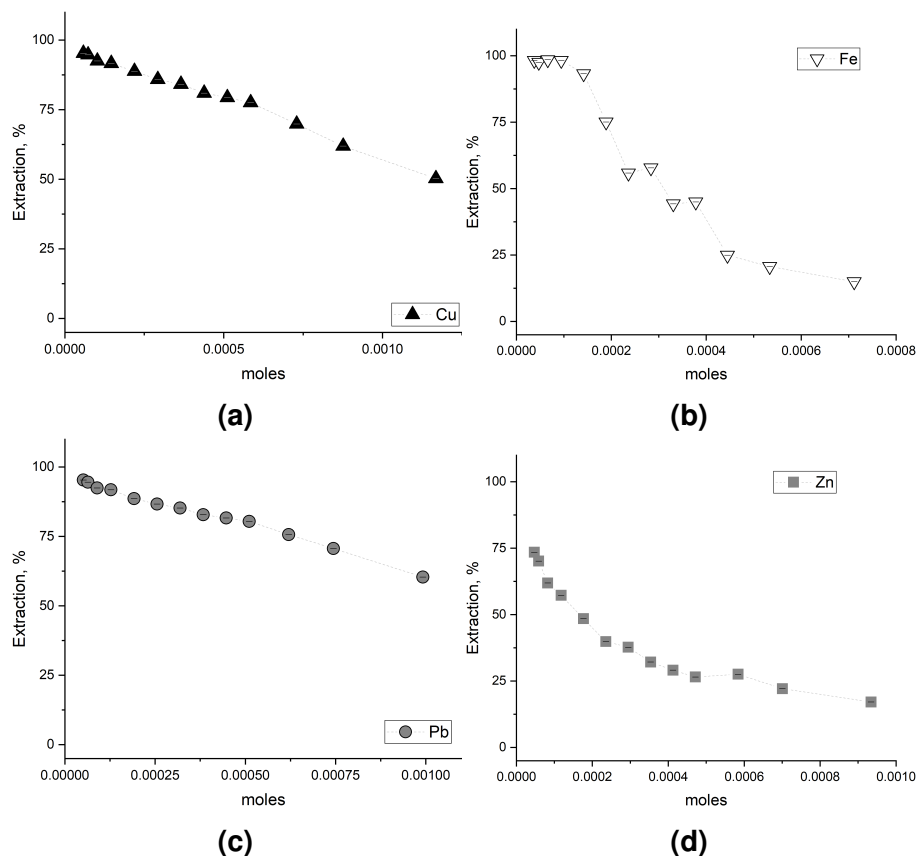


**Figure C.1:** Extraction percentage of copper (a), iron (b), lead (c) and zinc (d) by C107E as a function of total number of moles in contact with in acetic acid media (initial concentration  $200\text{mmol L}^{-1}$ ; temperature  $21^\circ\text{C}$ ;  $0.5\text{M NaCl}$ ;  $0.5\text{M}$  acetic acid;  $2\text{ml}$  wet settled resin;  $20\text{-}400\text{ml}$  solution).

zinc then follows at  $0.24\text{mmol}$ , falling to  $24\%$  extraction and finally iron(II) drops at  $0.28\text{mmol}$ , falling to  $36\%$  extraction.

Similarly to MTS9301, very high % extraction of copper is apparent throughout the entire volume range studied in this experiment (Figure C.3). Neither iron(II), lead nor zinc reach  $100\%$  extraction towards the lower volumes of solutions added. The largest extraction was lead with  $75\%$ , then zinc at  $48\%$  and iron(II) at  $26\%$ , decreasing to  $11$ ,  $15$  and  $9\%$ , respectively.

## C.2 Multi-metal Kinetic Extraction Percentages

Figures C.4 - C.6 display the kinetic data reanalysed to report the percentage extraction as a function of time for C107E, MTS9301 and TP214. Similarly to the

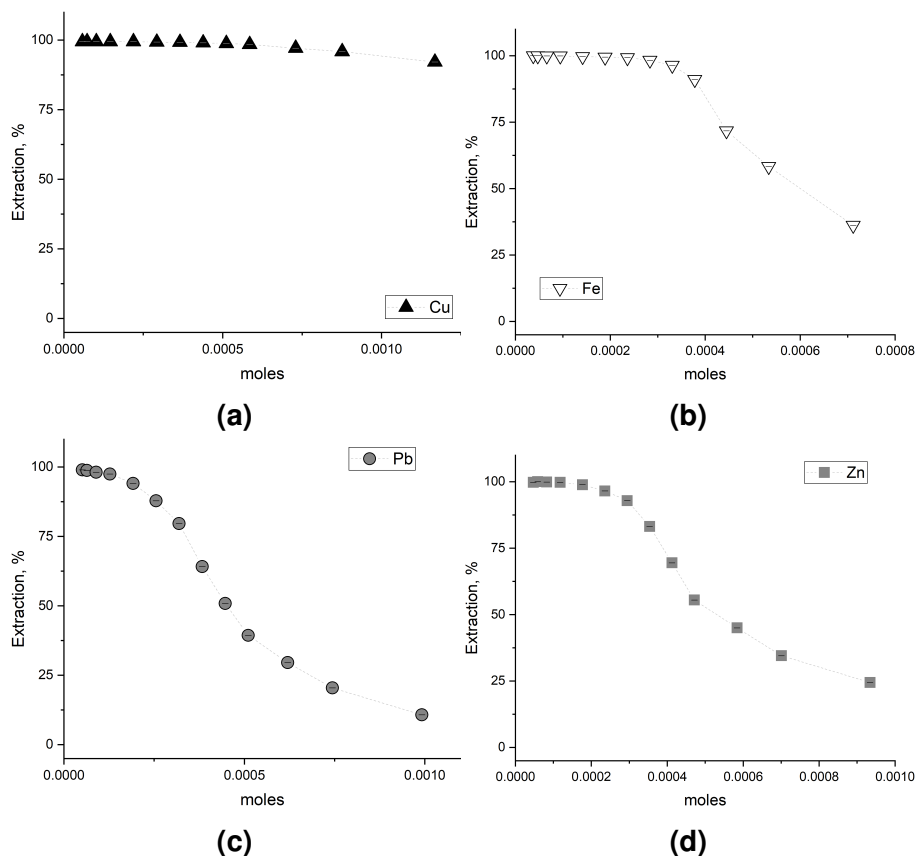


**Figure C.2:** Extraction percentage of copper (a), iron (b), lead (c) and zinc (d) by MTS9301 as a function of total number of moles in contact with in acetic acid media (initial concentration  $200\text{mmol L}^{-1}$ ; temperature  $21^\circ\text{C}$ ;  $0.5\text{M NaCl}$ ;  $0.5\text{M}$  acetic acid;  $2\text{ml}$  wet settled resin;  $20\text{-}400\text{ml}$  solution).

mixed metal isotherms, both lead and copper display high levels of extraction, reaching  $>80\%$  by the end of the  $24\text{h}$  contact with C107E (Figure C.4). Zinc and iron(II) display far lower extractions with a maximum extraction of  $41$  and  $25\%$ , respectively.

MTS9301 displays a high affinity to all metals within this study (Figure C.5). Iron(II) is extracted to the highest %, in this case, with  $98\%$  extraction followed by copper at  $96\%$ . Copper, iron(II) and zinc all reach  $>90\%$  extraction, while lead remains behind at  $87\%$ .

TP214 achieves  $90\%$  extraction for copper within the acetic acid medium (Figure C.6). Second to copper is lead, which achieves  $23\%$  extraction at  $80\text{min}$  before decreasing to an extraction of  $15\%$ . Neither iron(II) nor zinc breached  $10\%$

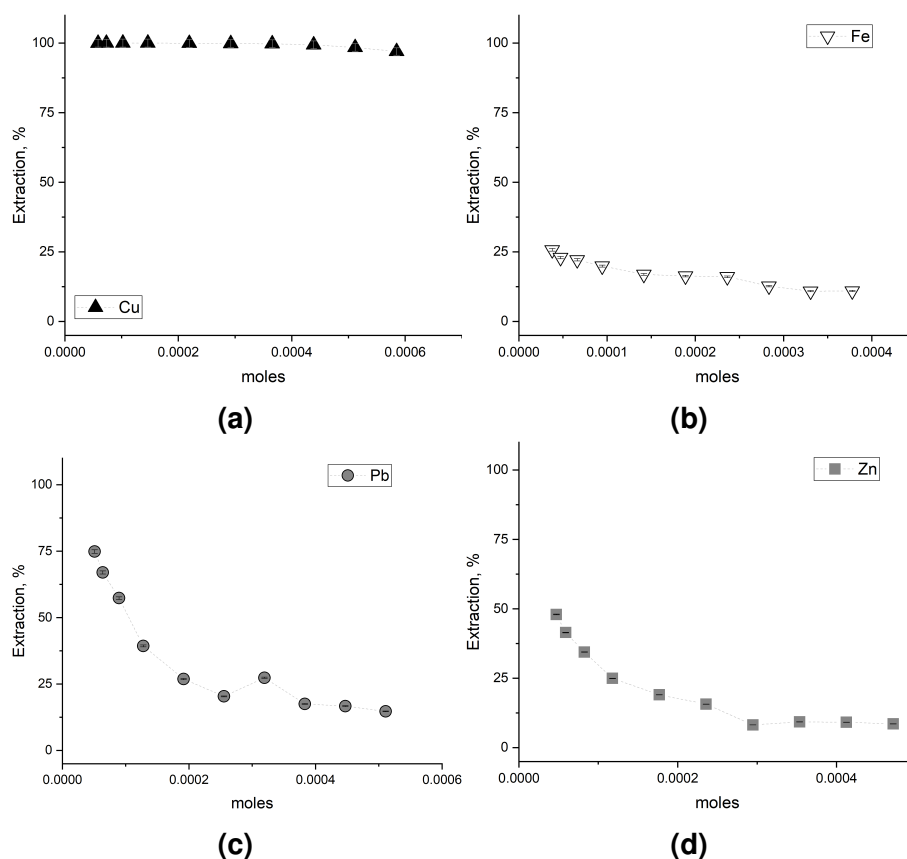


**Figure C.3:** Extraction percentage of copper (a), iron (b), lead (c) and zinc (d) by TP214 as a function of total number of moles in contact with in acetic acid media (initial concentration  $200\text{mmol L}^{-1}$ ; temperature  $21^\circ\text{C}$ ;  $0.5\text{M NaCl}$ ;  $0.5\text{M}$  acetic acid;  $2\text{ml}$  wet settled resin;  $20\text{-}400\text{ml}$  solution).

extraction.

### C.3 Correlation with Physical/Chemical Parameters

**Comparison of Multi-metal Isotherm Parameters to IR, solution phase complex  $\Delta H$  and  $\Delta S$  and Electronegativity**

**Comparison of Kinetic Parameters to IR, solution phase complex  $\Delta H$  and  $\Delta S$  and Electronegativity**

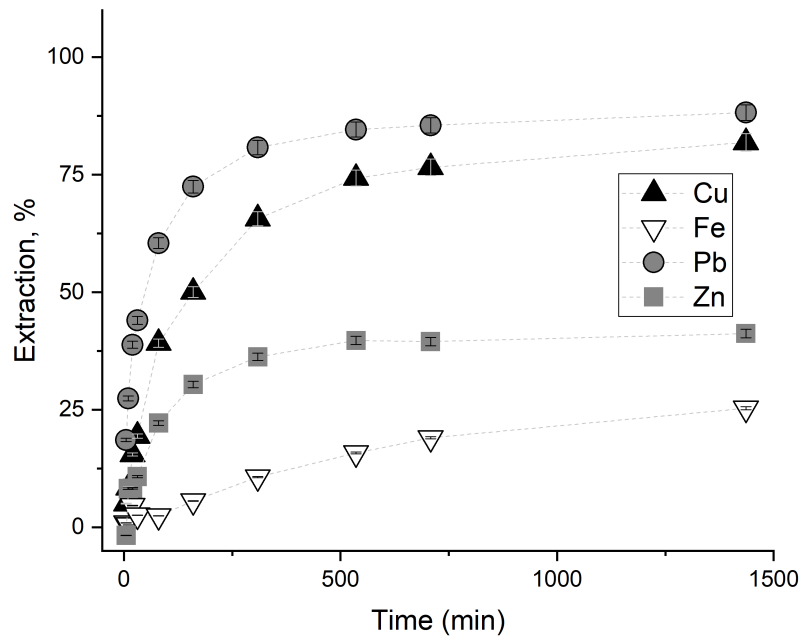


**Figure C.4:** Extraction percentage of copper, iron, lead and zinc by C107E as a function of time (initial concentration 200ppm; temperature 21°C; 0.5M NaCl; 0.5M acetic acid; 10ml wet settled resin; 500ml solution).

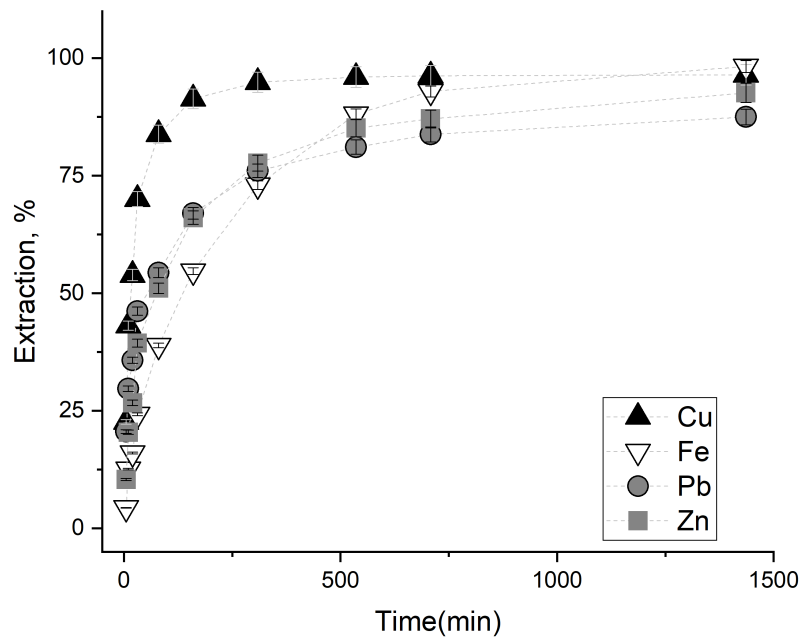


**Figure C.5:** Extraction percentage of copper, iron, lead and zinc by MTS9301 as a function of time (initial concentration 200ppm; temperature 21°C; 0.5M NaCl; 0.5M acetic acid; 10ml wet settled resin; 500ml solution).

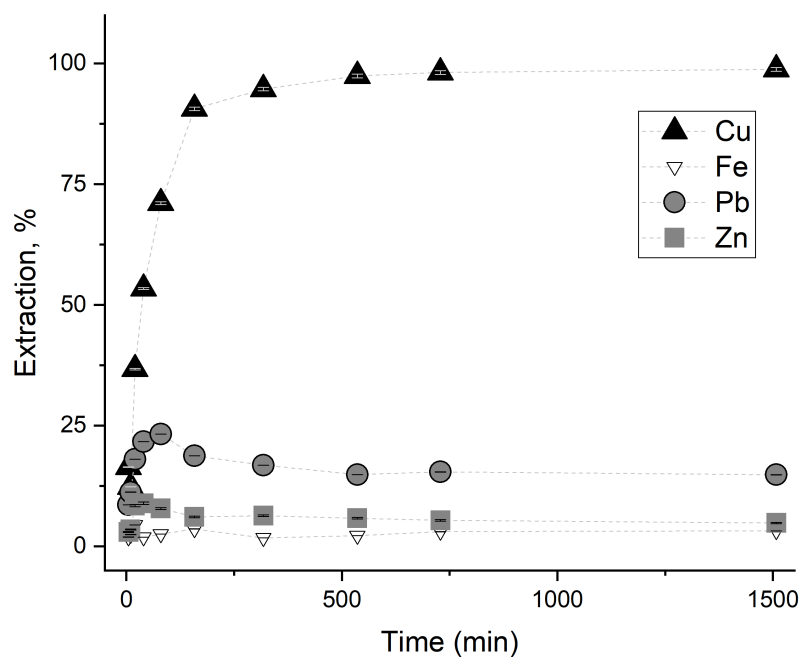


**Figure C.6:** Extraction percentage of copper, iron, lead and zinc by TP214 as a function of time (initial concentration 200ppm; temperature 21°C; 0.5M NaCl; 0.5M acetic acid; 10ml wet settled resin; 500ml solution).

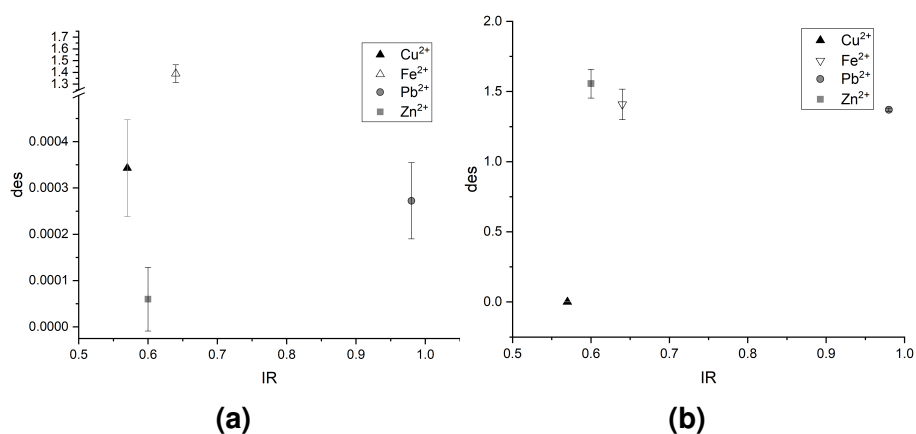


**Figure C.7:** Plot of the *des* constant derived from the desorption-modified Langmuir isotherm model as a function of the IR of each metal for each resin. Figures a and b are the *des* values for C107E and MTS9301, respectively.



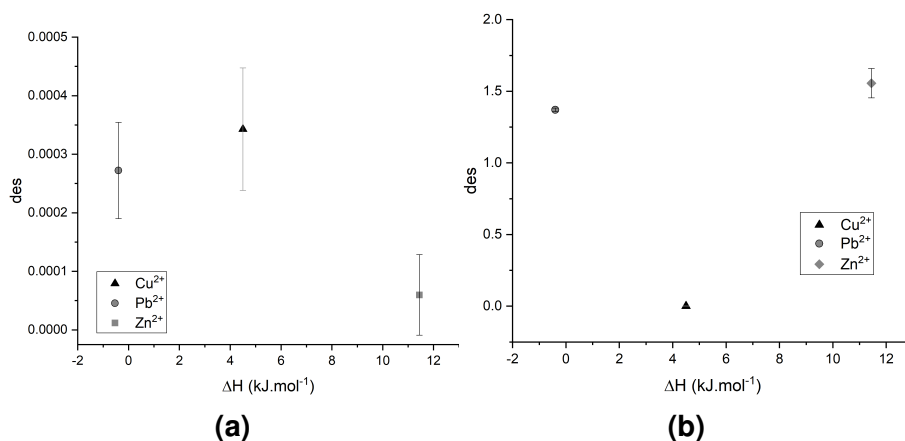


**Figure C.8:** Plot of the  $des$  constant derived from the desorption-modified Langmuir isotherm model as a function of the the average solution  $\Delta H$  for each metal-acetate species of each metal for each resin. Figures a and b are the  $des$  values for C107E and MTS9301, respectively.

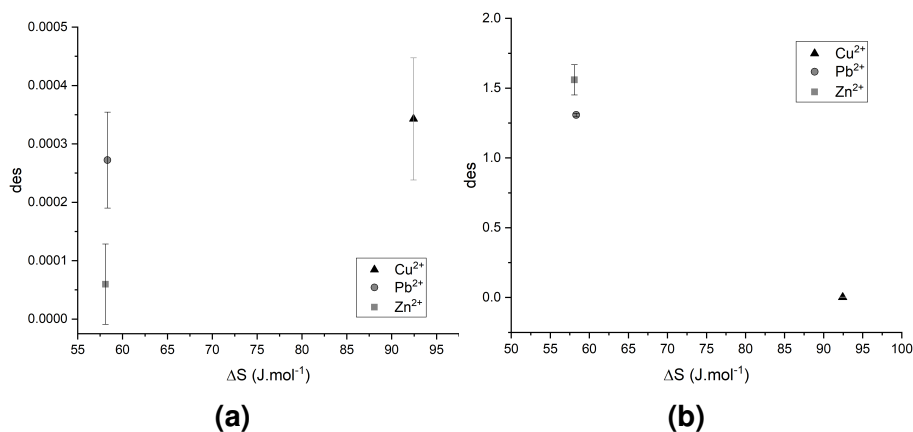


**Figure C.9:** Plot of the  $des$  constant derived from the desorption-modified Langmuir isotherm model as a function of the the average solution  $\Delta S$  for each metal-acetate species of each metal for each resin. Figures a and b are the  $des$  values for C107E and MTS9301, respectively.

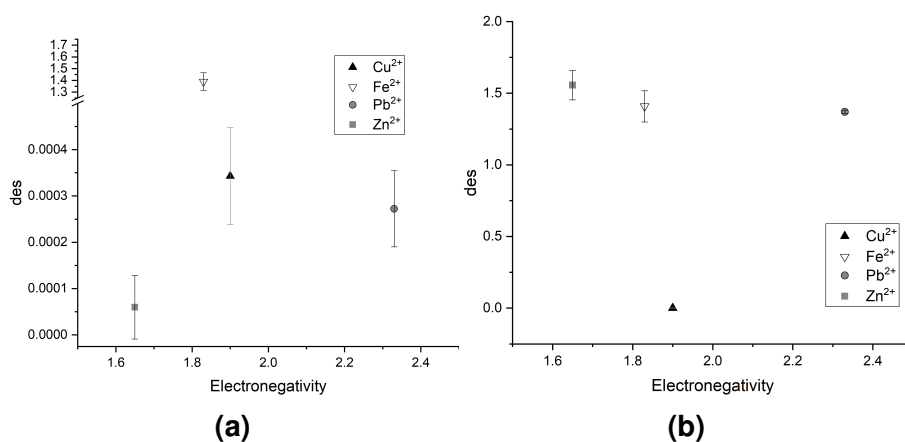


**Figure C.10:** Plot of the  $des$  constant derived from the desorption-modified Langmuir isotherm model as a function of the electronegativity of each metal for each resin. Figures a and b are the  $des$  values for C107E and MTS9301, respectively.

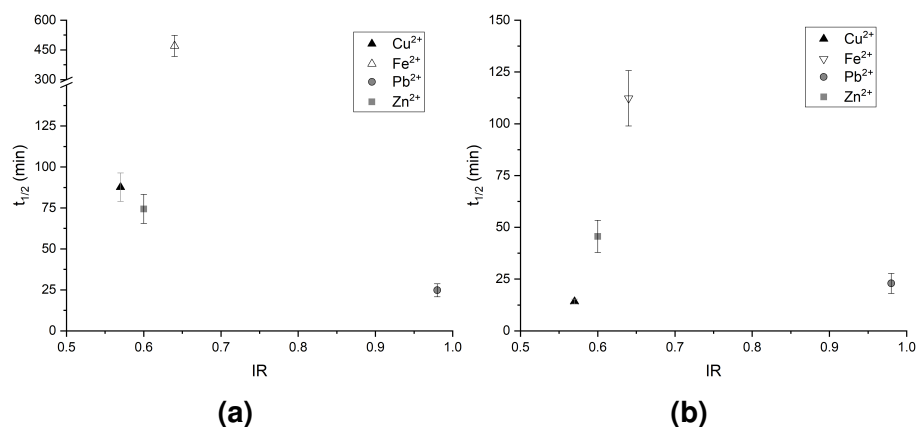


**Figure C.11:** Plot of the half-lives derived from the Lagergren Pseudo-First Order kinetic model as a function of the IR of each metal for each resin. Figures a and b are the half-life values for C107E and MTS9301, respectively.

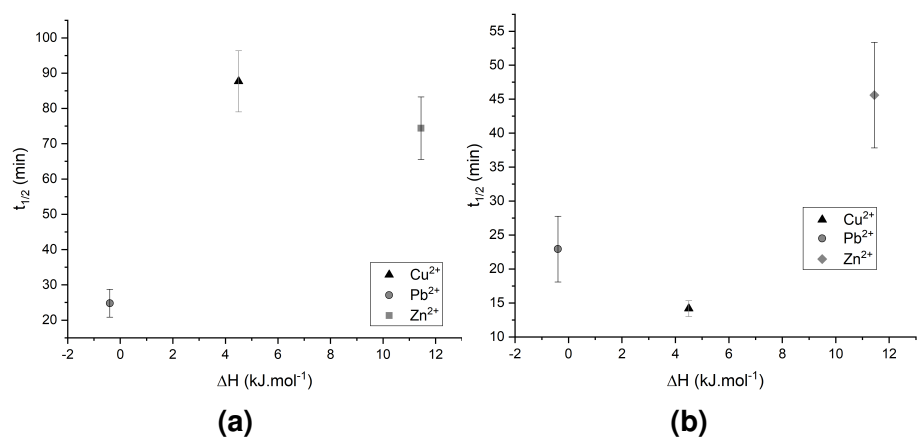


**Figure C.12:** Plot of the half-lives derived from the Lagergren Pseudo-First Order kinetic model as a function of the average solution  $\Delta H$  for each metal-acetate species for each resin. Figures a and b are the half-life values for C107E and MTS9301, respectively.

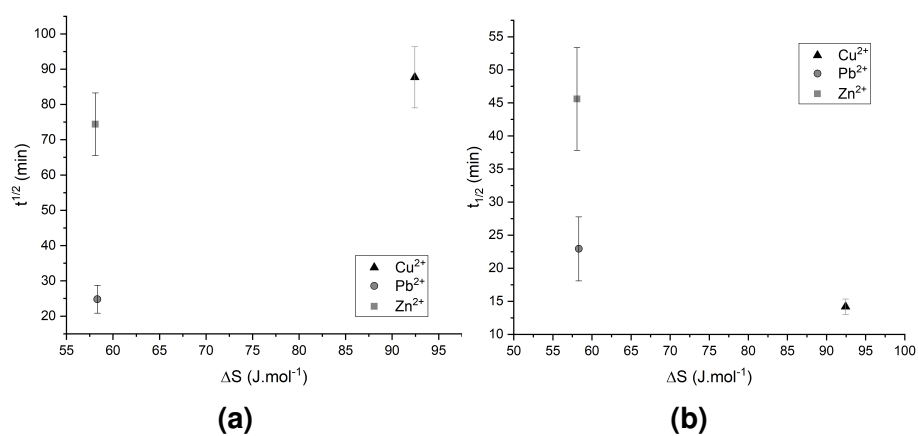


**Figure C.13:** Plot of the half-lives derived from the Lagergren Pseudo-First Order kinetic model as a function of the average solution  $\Delta S$  for each metal-acetate species for each resin. Figures a and b are the half-life values for C107E and MTS9301, respectively.

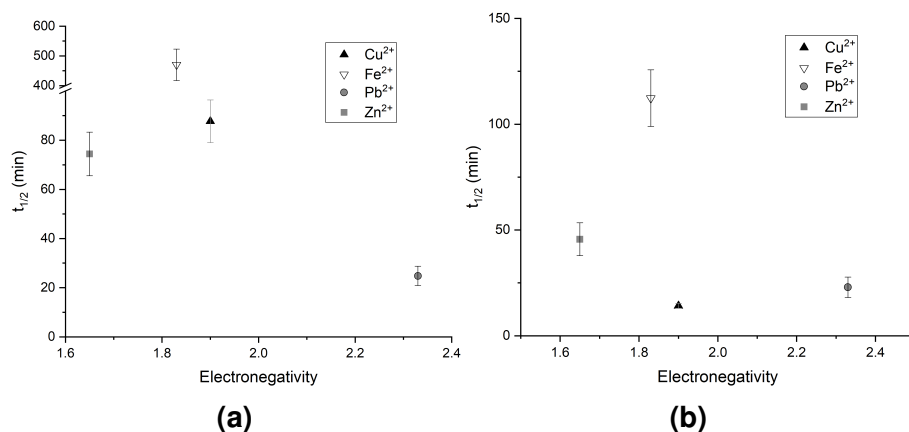


**Figure C.14:** Plot of the half-lives derived from the Lagergren Pseudo-First Order kinetic model as a function of the electronegativity of each metal for each resin. Figures a and b are the half-life values for C107E and MTS9301, respectively.

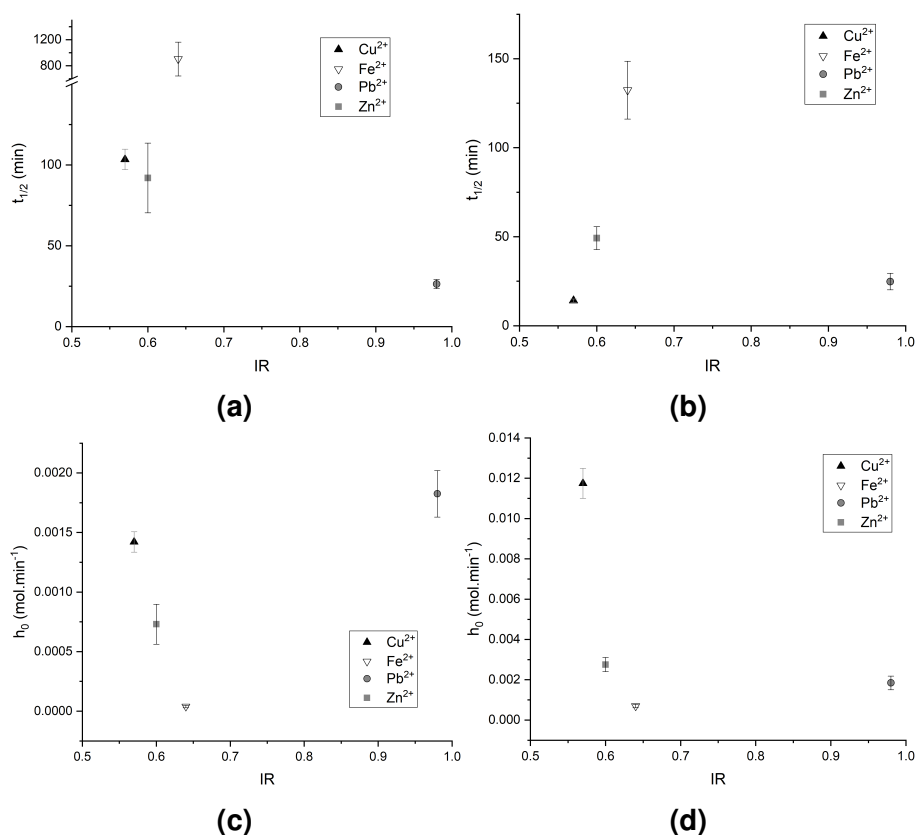


**Figure C.15:** Plot of the pseudo-second order half-life and initial rate of reaction derived by the pseudo-second order kinetic model as a function of IR for each metal and each resin. Figures a and b are the values of  $t_{1/2}$  while c and d are the values of  $h_0$  for C107E and MTS9301, respectively.

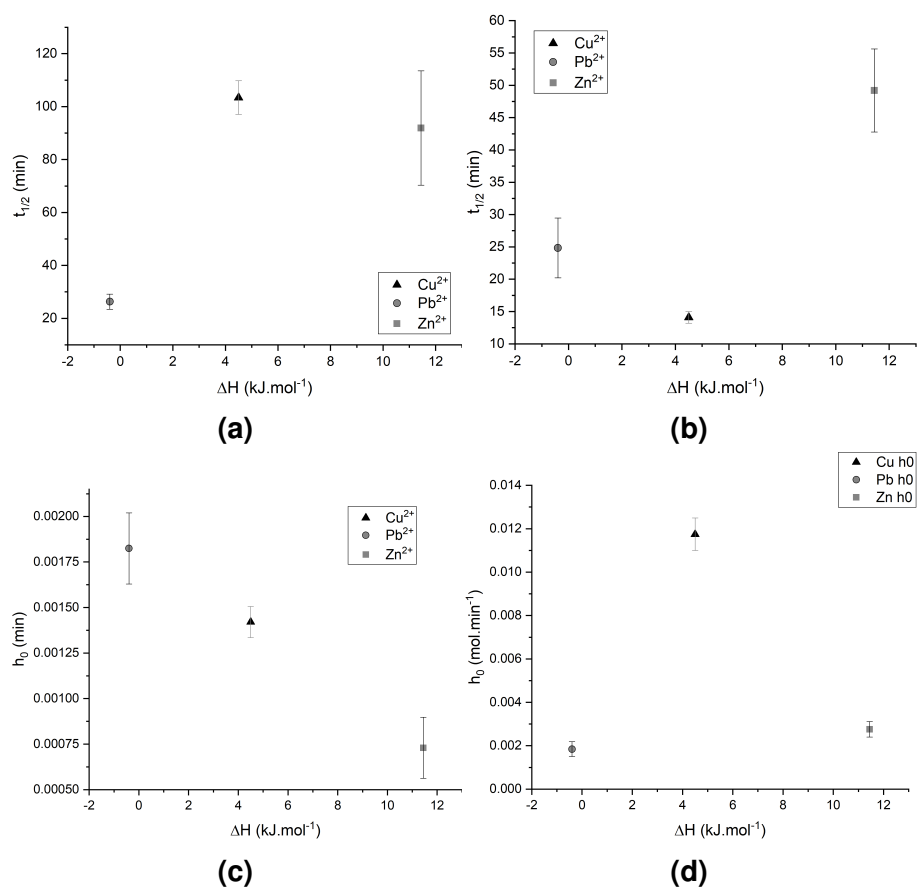


**Figure C.16:** Plot of the pseudo-second order half-life and initial rate of reaction derived by the pseudo-second order kinetic model as a function of the average solution  $\Delta H$  for each metal-acetate species and each resin. Figures a and b are the values of  $t_{1/2}$  while c and d are the values of  $h_0$  for C107E and MTS9301, respectively.

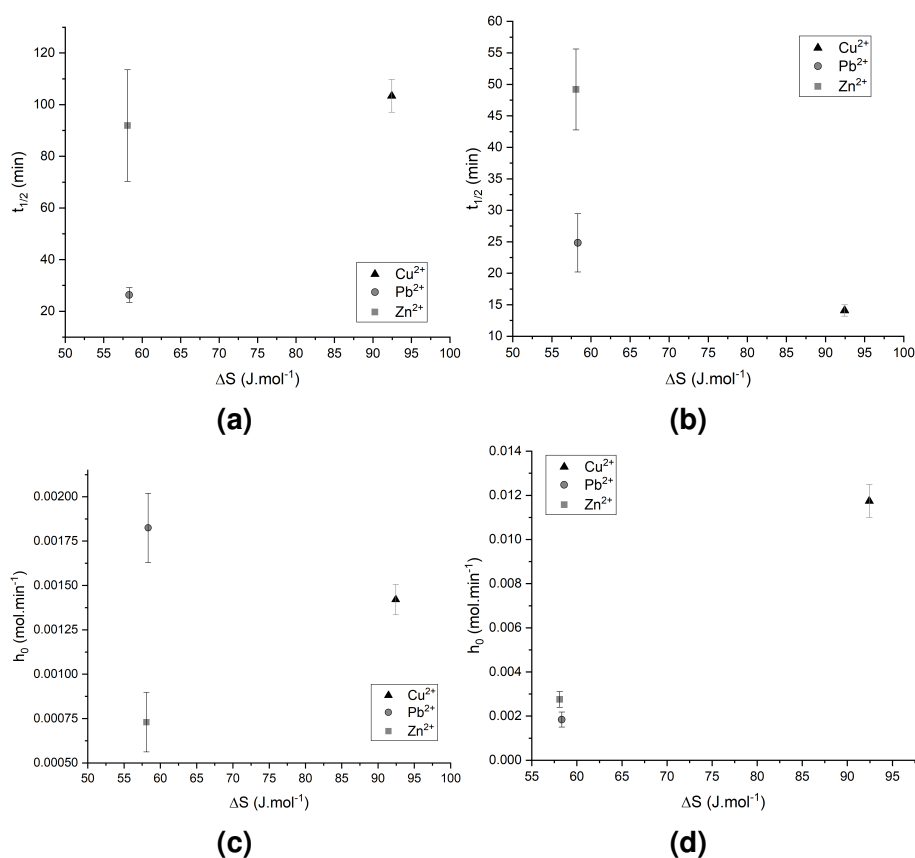


**Figure C.17:** Plot of the pseudo-second order half-life and initial rate of reaction derived by the pseudo-second order kinetic model as a function of the average solution  $\Delta S$  for each metal-acetate species and each resin. Figures a and b are the values of  $t_{\frac{1}{2}}$  while c and d are the values of  $h_0$  for C107E and MTS9301, respectively.

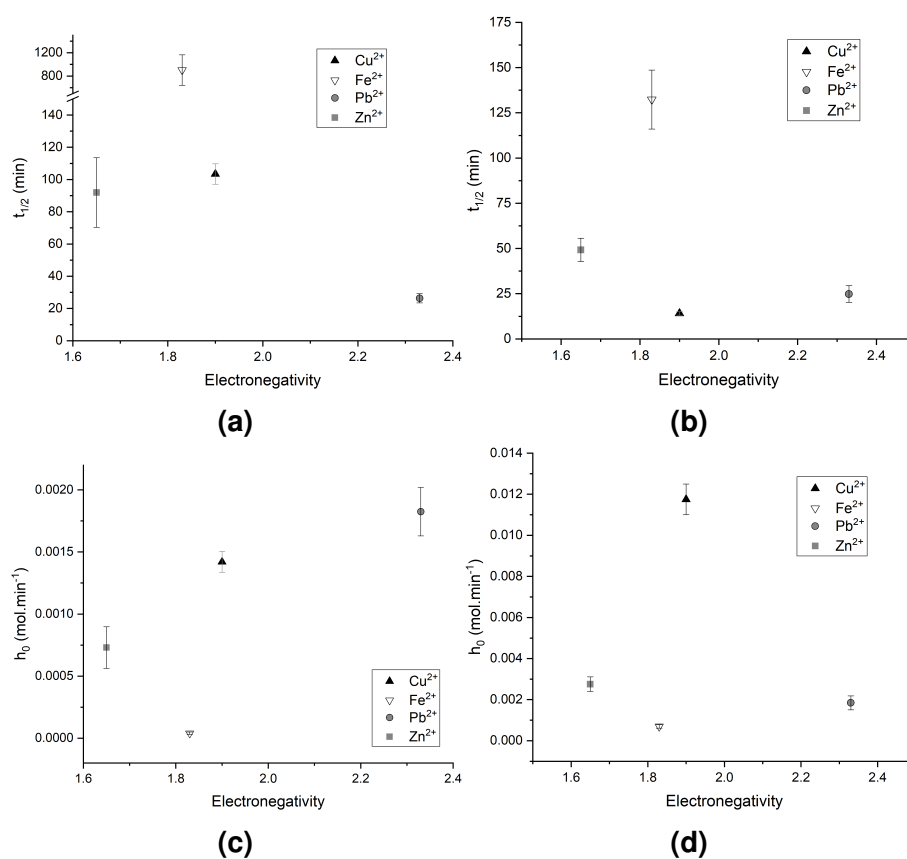


**Figure C.18:** Plot of the pseudo-second order half-life and initial rate of reaction derived by the pseudo-second order kinetic model as a function of the electronegativity of each metal and each resin. Figures a and b are the values of  $t_{1/2}$  while c and d are the values of  $h_0$  for C107E and MTS9301, respectively.

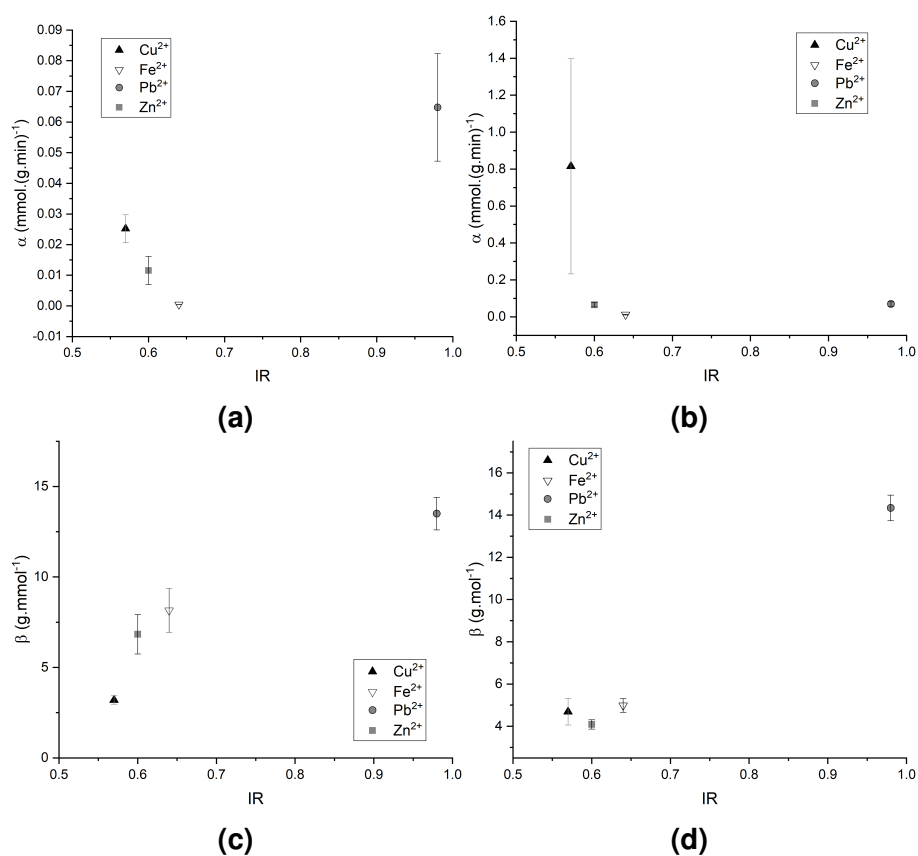


**Figure C.19:** Plot of the adsorption and desorption rate derived from the Elovich model as a function of the ionic radius of each metal and each resin. Figures a and b are the values of  $\alpha$  while c and d are the values of  $\beta$  for C107E and MTS9301, respectively.

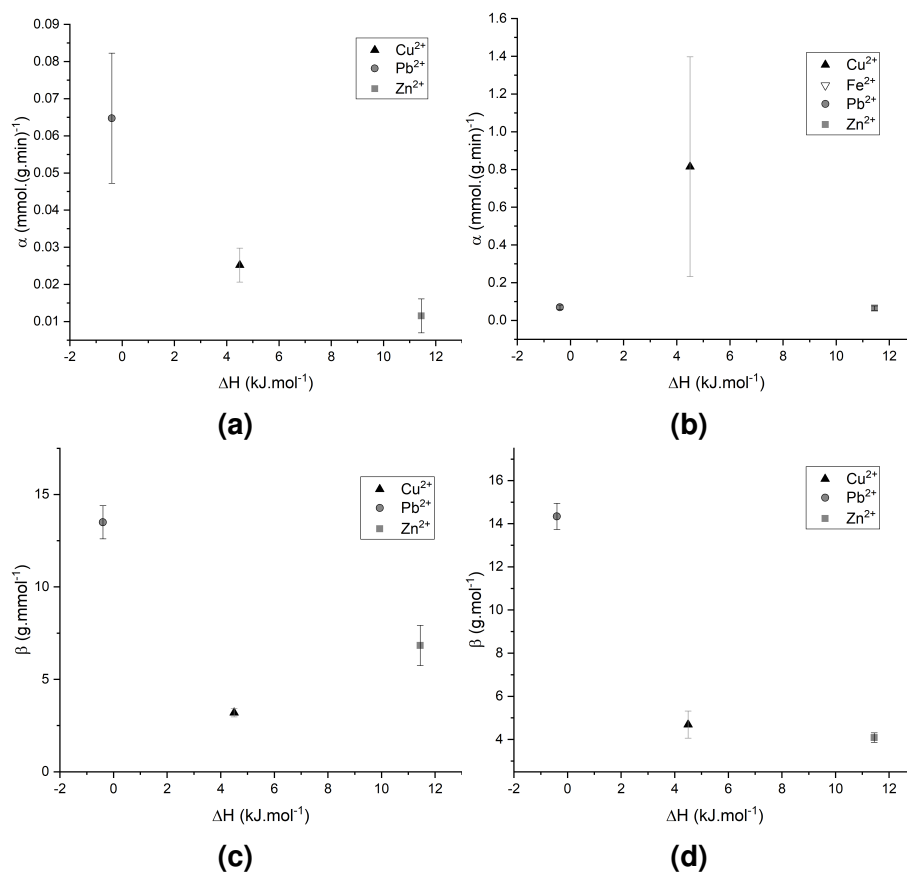


**Figure C.20:** Plot of the adsorption and desorption rate derived from the Elovich model as a function of the average solution  $\Delta H$  for each metal-acetate species and each resin. Figures a and b are the values of  $\alpha$  while c and d are the values of  $\beta$  for C107E and MTS9301, respectively.



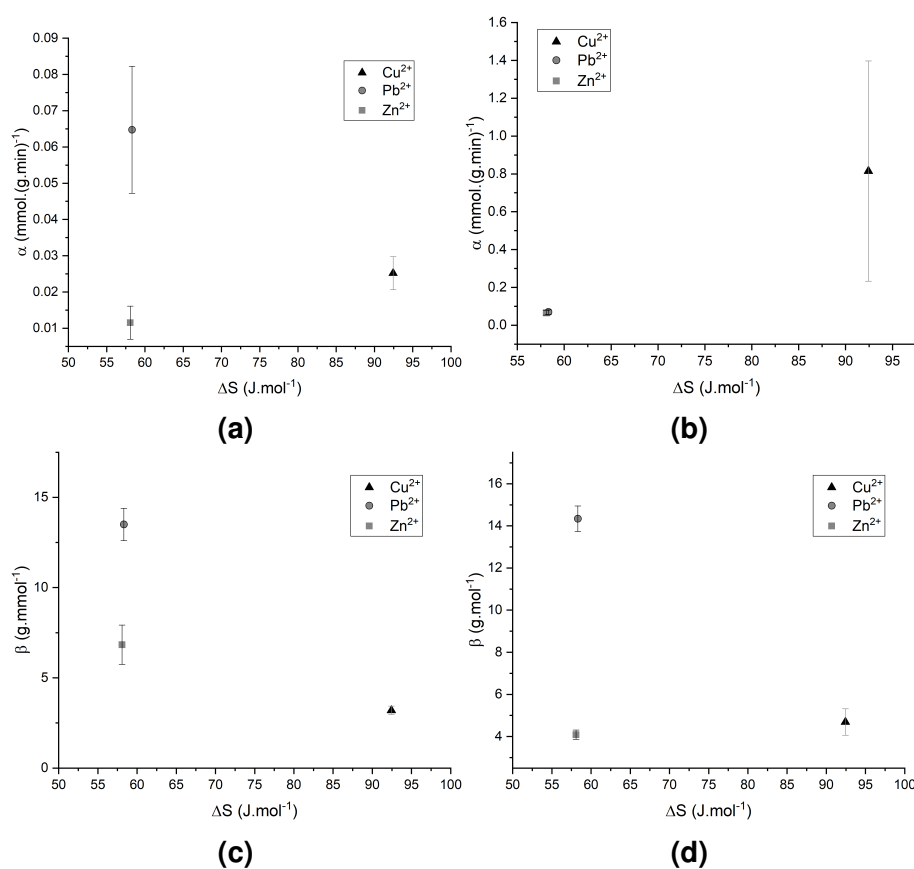


**Figure C.21:** Plot of the adsorption and desorption rate derived from the Elovich model as a function of the average solution  $\Delta S$  for each metal-acetate species and each resin. Figures a and b are the values of  $\alpha$  while c and d are the values of  $\beta$  for C107E and MTS9301, respectively.

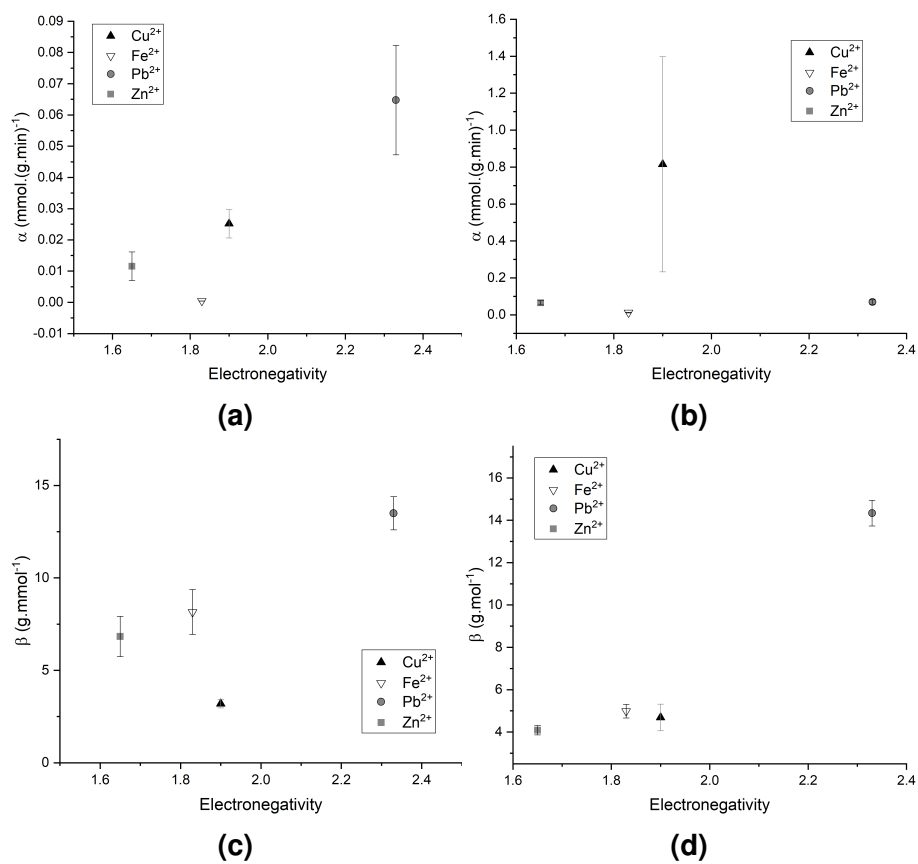


**Figure C.22:** Plot of the adsorption and desorption rate derived from the Elovich model as a function of the electronegativity of each metal and each resin. Figures a and b are the values of  $\alpha$  while c and d are the values of  $\beta$  for C107E and MTS9301, respectively.

# Appendix D

## Simulated Process Supplementary Data

### D.1 Literary Properties of Sludge

Due to anaerobic digested sludge being one of the most common sludge<sup>[14]</sup>, and due to the large water consumption required to leach incinerated or dewatered sludge, anaerobic sludge will be the targeted input to this process and will be the sludge simulated. Table D.1 reports an average general chemical make-up of digested sewage sludge<sup>[14]</sup>. Generally speaking digested sludge contains a high concentration of organic matter with very little solids content..

**Table D.1:** Characteristics of digested sludges<sup>[14]</sup>

Characteristic	Range
Total dry solids %	6.0-12.0
Volatile solids % of TS	30-60
Grease and fats % of TS	5.0-20.0
Cellulose % of TS	8.0-15
Protein % of TS	15-20
Phosphorus % of TS	1.5-4.0
Nitrogen % of TS	1.6-6.0
Silica (SiO <sub>2</sub> ) % of TS	10.0-20.0

The % of VOC within digested sludge can reach up to 60% of the total solids content (Table D.1), while silica can be as high as 20%. Within this study, the chemical characteristics of the simulant chosen will focus on the VOC, due to the fact that the organic matter within sewage sludge has the potential for adsorption of leached metallic ions<sup>[93]</sup>. This creates issues with preg-robbing and poor sludge filterability<sup>[86]</sup>. While this describes chemical characteristics of sewage sludge, the requirement of this simulant will be mostly physical. Particle size and viscosity content will be the most important factors determining the applicability of this simulant in question.

While moisture content will be an important physical parameter, it is one parameter that is easily modified; the two physical parameters that this simulant must mimic are particle size and viscosity. Particle size must be comparable to that of digested sludge due to the operational considerations with regards to separation of resin from sludge, especially considering sieving is the most likely separation technique. Viscosity must be similar to that of digested sewage sludge, first and foremost, because this will dictate how resin beads are capable of

dispersing through the slurry. The second reason for the importance of viscosity is the latter design of a process, as viscosity will be the single determinant of the agitation method and the pumping method<sup>[229,230]</sup>.

## D.2 Anaerobically Digested Esholt Sludge

Figure D.1 displays a simplified schematic of the Esholt Wastewater Treatment Plant, with the sample point of the digested sludge labelled. Figure D.2 is a spreadsheet provided with the sludge, outlining an analysis of the composition of the sludge.

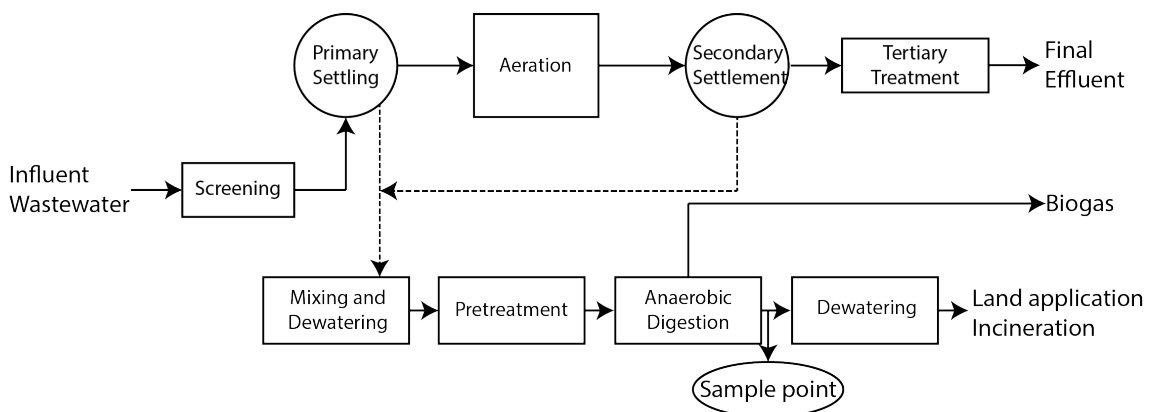


**Figure D.1:** A simplified schematic of the Esholt Wastewater Treatment Plant

**Figure D.2: Analysis of the Esholtsludge**



ANALYSIS SERVICES DIRECT  
 NRM LABORATORIES  
 COOPERS BRIDGE  
 BRAZIERS LANE  
 BRACKNELL  
 BERKS

**R600**

Please quote above code for all enquiries

DEPT OF ANIMAL-PLANT SCIENCES  
 ALFRED DENNY BUILDING  
 UNIVERSITY OF SHEFFIELD

CAKE

Reference : IRENE JOHNSON

**CAKE (Metric Units)**

Sample Reference : ESHOLT CAKE NOV17

Sample Matrix : CAKE

The sample submitted was of adequate size to complete all analysis requested.

The sample will be kept as the dry ground sample for at least 1 month.

Laboratory References	
Report Number	82741
Sample Number	86853

Date Received	24-NOV-2017
Date Reported	28-NOV-2017

**ANALYTICAL RESULTS**

Determinand on a DM basis unless otherwise indicated	Units	Result	Amount per fresh tonne	Amount applied at an equivalent total Nitrogen application of 250 kg N/ha	Units
pH 1:6 [Fresh]		7.70			
Oven Dry Matter	%	25.7	257.00	3828	kg DM
Total Nitrogen	% w/w	6.53	16.78	250	kg N
Ammonium Nitrogen	mg/kg	8217	2.11	31.46	kg NH4-N
Nitrate Nitrogen	mg/kg	<10	< 0.01		kg NO3-N
Total Phosphorus (P)	% w/w	2.63	15.48	230.58	kg P2O5
Total Potassium (K)	% w/w	0.106	0.33	4.87	kg K2O
Total Magnesium (Mg)	% w/w	0.287	1.22	18.24	kg MgO
Total Sulphur (S)	% w/w	1.06	6.81	101.45	kg SO3
Total Copper (Cu)	mg/kg	225	0.06	0.86	kg Cu
Total Zinc (Zn)	mg/kg	603	0.15	2.31	kg Zn
Total Sodium (Na)	% w/w	0.070	0.24	3.61	kg Na2O
Total Calcium (Ca)	mg/kg	24803	6.37	94.96	kg Ca
Equivalent field application rate		—	1.00	14.90	tonnes/ha

The above equivalent field application rate for total nitrogen of 250 kg/ha has been provided purely for guidance purposes only. Organic manures should be used in accordance with the Defra Code of Good Agricultural Practice and where required within the specific regulatory guidance for the spreading of that material to land. To get the most benefit from your organic manures it is recommended that you follow the principles as set out in Defra's Fertiliser Manual (RB209) or as directed by a FACTS qualified adviser.

Released by .....Darren Whitbread.....

Date .....28/11/17.....

**NRM** Coopers Bridge, Braziers Lane, Bracknell, Berkshire RG42 6NS  
 Tel: +44 (0) 1344 886338 Fax: +44 (0) 1344 890972 Email: enquiries@nrm.uk.com www.nrm.uk.com

NRM Laboratories is a division of Cawood Scientific Ltd, Coopers Bridge, Braziers Lane, Bracknell, Berkshire RG42 6NS Registered Number: 05655711

## D.3 Simulant Sludge Rheology

Sewage sludges are reported to behave as non-Newtonian fluids, described by either the Bingham Plastic Model<sup>[211,213]</sup>, Ostwald (or Power-Law) Model<sup>[209,213,214]</sup> or the Herschel-Bulkley Model<sup>[206]</sup>. Although the rheology of sludge differs markedly between sources it commonly fits the characteristics of a shear thinning fluid<sup>[206]</sup> (shear stress decreases with increasing shear rate) and the sludge becomes more Newtonian in nature as water content increases/digestion occurs<sup>[206,209,211–214]</sup>.

Newtonian fluids follow a linear relationship between the shear stress,  $\tau$  (Pa), and the shear rate,  $\gamma$  ( $\text{s}^{-1}$ ), following the law:

$$\tau = k\gamma \quad (\text{D.1})$$

where  $k$  is the viscosity of the given fluid (Pa.S), and the fluid behaves perfectly Newtonian. As sludge drifts from this Newtonian fluid model (solids content increases<sup>[213]</sup>), variations are required upon this Newtonian model in order to describe their relationship between shear stress and rate. Plastic fluids are such that display little to no flow with low shear rate, displaying more Newtonian flow behaviour once the shear stress breaches a yield-stress. Non-Newtonian plastic fluids, described by the Bingham Plastic model:

$$\tau = \tau_y + k\gamma \quad (\text{D.2})$$

incur a yield stress,  $\tau_y$  (Pa), required to initiate flow, following a linear relationship between shear stress and shear rate, otherwise. In this situation,  $k$  is, once again, the viscosity (Pa.S), directly comparable to that of the Newtonian model. Pseudo-plastic fluids, do not follow these linear trends, decreasing in relative shear stress with shear rate.

**Table D.2:** Bingham Plastic Model parameters.

	$\tau_y$ (Pa)	k (Pa.s)	$r^2$
5% Solids	0.005±0.005	0.009±0.003	0.943 - 0.958
10% Solids	0.0121±0.0005	0.0268±0.0001	0.841 - 0.936
20% Solids	0.039±0.002	0.122±0.006	0.891 - 0.936
Esholt Sludge	0.0065±0.0006	0.0074±0.0003	0.810 - 0.935

The constants obtained from the plastic model are included within Table D.2. This model is a poor descriptor of the data. While comparison of this modelled data will be tentative, it does show an increase in viscosity index with increased solids content of the simulant. From 5% to 20% the viscosity index increases from 0.009±0.003 through to 0.122±0.006 Pa.s. Following this increase is the increase in yield stress, increasing from 0.005±0.005 to 0.039±0.002 Pa from 5-20%. The values obtained by the Esholt sludge are similar to that of the 5% solids simulant sludge, with 0.0065±0.0006 Pa yield stress and 0.0074±0.0003 Pa.s viscosity constant, while being described to a lesser extent.

Sewage sludge is most commonly described as a pseudo-plastic fluid; pseudo-plastic, or shear-thinning fluids are fluids which display a decrease in viscosity with an increase in shear rate. There are two common pseudo-plastic models used for the description of sewage sludge, these are the Otswald model and the Herschel-Bulkley model. The Otswald model<sup>[213,214,231]</sup> can be described by:

$$\tau = k\dot{\gamma}^n \quad (\text{D.3})$$

Where  $k$  is the fluid flow consistency (Pa.S <sup>$n$</sup> ) and is dictated by  $n$ , which is the flow-behaviour index<sup>[231]</sup>. With  $n > 1$  indicating a shear thickening fluid,  $n < 1$  indicating a shear thinning or pseudoplastic fluid, and as  $n$  approaches 1 the fluid becomes more plastic or Newtonian.



**Table D.3:** Power-Law Model parameters.

	k (Pa.S <sup>n</sup> )	n	r <sup>2</sup>
5% Solids	0.012±0.003	0.36±0.04	0.979 - 0.996
10% Solids	0.0409±0.0007	0.298±0.006	0.976 - 0.990
20% Solids	0.17±0.01	0.336±0.003	0.980 - 0.997
Esholt Sludge	0.0143±0.0007	0.19±0.01	0.961 - 0.981

Data obtained from fitting of the Pseudoplastic (Otswald/Power-law) viscosity model are displayed in Table D.3. All sludges fit reasonably well to the power law model, with the lowest r<sup>2</sup> being observed by the Esholt sludge sample, with 0.961 being the lower value, however the highest of the three measurements was 0.981. The consistency index (k, Pa.s<sup>n</sup>) of the three simulants increases with increasing solids, from 0.12±0.003 to 0.17±0.01 Pa.s<sup>n</sup>, with that of the digested sludge being similar to the 5% solids simulant. The simulant rheological constant throughout these experiments, does not significantly change, all of the values returned are within error of each other, however, the Esholt sludge returned values more than 25% lower for this rheological constant, being far more shear thinning..

The Herschel-Bulkley<sup>[231]</sup> model can be described in a similar fashion to the Otswald model, however it also incorporates a variable to describe the yield stress of a fluid:

$$\tau = \tau_y + k\gamma^n \quad (\text{D.4})$$

where, again, k is the fluid flow consistency (Pa.S<sup>n</sup>), also dependent on the flow-behaviour index (*n*), however the yield stress  $\tau$  is given, similarly to the Bingham model.

The variables obtained by fitting of all sludges to the Herschel-Bulkley Model are included in Table D.4. This model fits similarly to that of the power law, with

**Table D.4:** Herschel-Bulkley Model parameters.

	$\tau_y$ (Pa)	k (Pa.S <sup>n</sup> )	n	r <sup>2</sup>
5% water	0.0008±0.0005	0.011±0.004	0.43±0.02	0.987 - 0.996
10% water	-0.001±0.006	0.042±0.006	0.29±0.08	0.980 - 0.990
20% water	0.00±0.02	0.17±0.03	0.33±0.07	0.983 - 0.998
Esholt Sludge	0.000±0.005	0.015±0.006	0.5±0.1	0.964 - 0.985

the maximum r<sup>2</sup> of all fits being >0.98, and the lowest r<sup>2</sup> being that of Esholt sludge, with 0.964. With error inclusive, the yield stress in each case (including the Esholt sludge) was negligible.. The consistency index of the simulant sludge, again, increased with an increase in solids content. In this case the rheological constant remained similar between 10 and 20% solids, while increasing at 5% solids content, being comparable between the Esholt sludge and the 5% solids content simulant.

## D.4 Leaching Conditions

**Table D.5:** Measured parameters of the leach consisting of 3% H<sub>2</sub>O<sub>2</sub>.

Hour	Temp (°C)	pH	HNO <sub>3</sub> added (g)	ORP (mV)
0:00	23	1.03	4.224	585
0:27	21	1.03	0.2049	581
0:49	20	1.05		583
1:20	20	1.09		586
1:39	20	1.11		584
2:37	20	1.11		589
4:09	20	1.09		593
5:43	20	1.14		595
7:33	19	1.18		595
23:38	20	1.11		598

**Table D.6:** Measured parameters of the leach consisting of 6% H<sub>2</sub>O<sub>2</sub>.

Hour	Temp (°C)	pH	HNO <sub>3</sub> added (g)	ORP (mV)
0:00	21	1.02	4.196	584
0:33	21	1.02	0.196	584
1:13	21	1.04		589
1:36	21	1.06		590
1:57	21	1.04		591
2:40	21	1.04		592
4:21	21	1.08		595
5:52	20	1.08		595
7:49	20	1.10		596
23:34	16	0.98		598

**Table D.7:** Measured parameters of the leach consisting of 9% H<sub>2</sub>O<sub>2</sub>, also used for system 1.

Hour	Temp (°C)	pH	HNO <sub>3</sub> added (g)	1M NaOH (g)	ORP (mV)
0:00	23	1.03	6.038		601
0:28	22	1.05			589
0:50	22	1.06			591
1:45	21	1.10			595
2:45	21	1.03			597
4:23	20	1.06			600
5:37	20	1.06			603
7:51	21	1.03			604
23:57	22	0.97			605
24:20	22	4.50		48.031	399

**Table D.8:** Measured parameters of the leach consisting of 3% H<sub>2</sub>O<sub>2</sub> increased after ~4h to 9%.

Hour	Temp (°C)	pH	HNO <sub>3</sub> added (g)	ORP 3% (mV)	ORP 9% (mV)
0:00	23	0.98	8.25	586	
0:30	21	0.98	0.124	579	
0:55	20	1.02		584	
1:47	20	1.04		588	
2:46	20	1.04	0.092	590	
3:52	20	0.93		588	600
4:30	20	0.96			602
5:00	20	0.84			604
5:39	19	0.82			602
6:53	20	0.80			601
7:58	21	0.80			599
8:51	20	0.96			600
10:02	20	0.82			605
24:27	20	0.91			607

**Table D.9:** Measured parameters of the leach consisting of 9% H<sub>2</sub>O<sub>2</sub>, also used for system 2.

Hour	Temp (°C)	pH	HNO <sub>3</sub> added (g)	1M NaOH (g)	ORP (mV)
0:00	19	1.01	6.038		608
0:26	19	1.01			597
0:55	20	1.01			595
2:03	20	1.05			593
2:51	20	0.93			599
4:20	20	0.90			595
6:04	20	0.90			593
7:59	20	0.88			592
23:50	20	0.99			594
24:11	20	4.50		50.641	403

# Appendix E

## Citric Acid System Supplementary Data

### E.1 Citrate Concentration Dependence Data

Figure E.1 displays the citrate concentration dependence of uptake for each metal, recalculated as a percentage extraction. Copper maintains close to 100% extraction throughout the entire range of citrate concentrations within this study. Iron increases from <10% to close to 100% by  $0.01\text{ mol L}^{-1}$ . Both lead and zinc increase to close to 100% extraction by  $0.05\text{ mol L}^{-1}$  (lead displays a much more pronounced increase, from  $\sim 50\%$ ), while both metals decrease to  $\sim 80\%$  once the citrate concentration decreases to  $0.01\text{ mol L}^{-1}$ .

The percentage abundance of each species from citrate concentrations of  $0.0005$  to  $0.55\text{ mol L}^{-1}$ , relative to the total available concentration of that species, is displayed for each citrate, copper, iron(II), lead and zinc within Figure E.2. Due to the small amount of citrate available for complexation, prior to  $0.1\text{ mol L}^{-1}$  citrate there is an equilibrium shift, causing solution phase speciation to change. Copper maintains a  $\text{CuOHCit}^{2-}$  with citrate from  $0.005\text{ mol L}^{-1}$ . Iron(II) forms 100%  $\text{FeCit}^-$  with a concentration of citrate  $\sim 0.01\text{ mol L}^{-1}$  before transitioning to  $\text{FeHCit}_2^{3-}$ , forming  $\sim 50\%$  of each species at  $0.1\text{ mol L}^{-1}$  citrate. Lead forms a

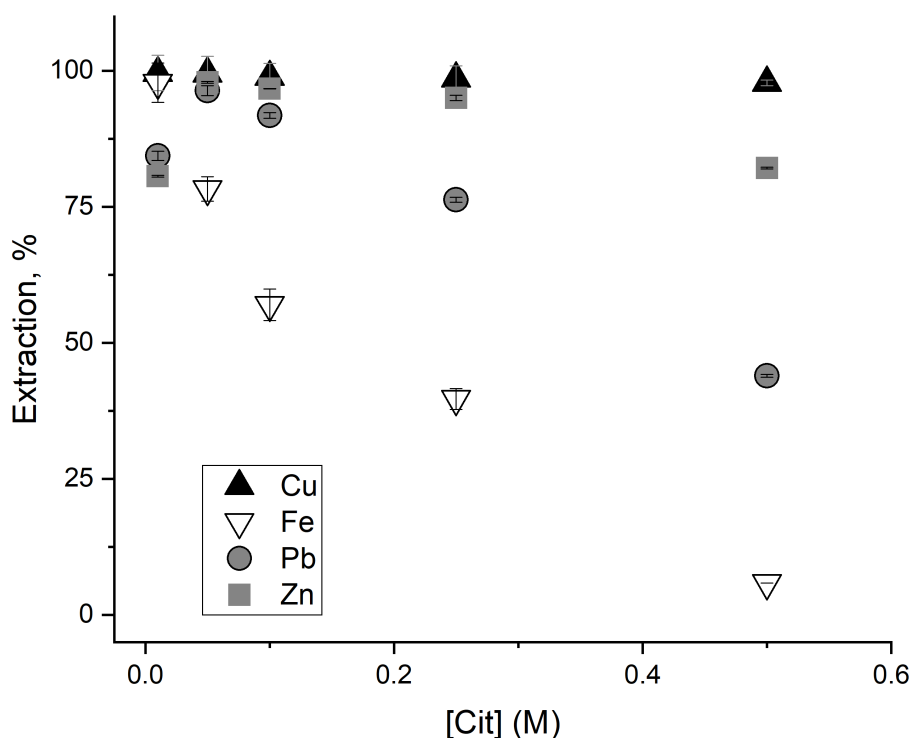


**Figure E.1:** Citrate acid concentration dependent extraction percentage of copper (a), iron(II) (b), lead (c) and zinc (d) by MTS9301 (initial concentration 200ppm; temperature 21°C; 0.5mol L<sup>-1</sup> NaCl; 0.01-0.5mol L<sup>-1</sup> citric acid; 2ml wet settled resin; 50ml solution; 24h).

majority PbCit<sup>-</sup> by 0.01mol L<sup>-1</sup>, before forming PbCit<sub>2</sub><sup>4-</sup> by 0.1mol L<sup>-1</sup> citrate, also forming ~50% of each species at 0.1mol L<sup>-1</sup> citrate. Zinc forms 100% ZnCit<sup>-</sup> at 0.01mol L<sup>-1</sup> citrate, and transitions to ZnCit<sub>2</sub><sup>4-</sup> by 0.1mol L<sup>-1</sup>.

The post-contact pH of each of the citric acid concentration dependence experiments is displayed in Figure E.3. This data shows a distinct decrease in post-contact pH with a decrease in citric acid concentration. This corresponds to an increase in total percentage of metals extracted (Figure E.1).

The pH dependence of citrate species for copper, iron(II), lead and zinc calculated at 0.1mol L<sup>-1</sup>, are displayed in E.4. Between pH 2.5 and 3.5, copper is predicted to be a majority of CuHCit, transitioning first to a copper-citrate dimer at pH 4, then COHCit<sup>3-</sup> from pH 4.5. Iron(II) becomes majority FeHCit from pH ~3 till pH 4, where it is FeCit<sup>-</sup> before becoming FeHCit<sub>2</sub><sup>-3</sup> from pH 4.5, then FeCit<sup>-</sup> from pH 6. The speciation of lead is more complicated than iron(II) and

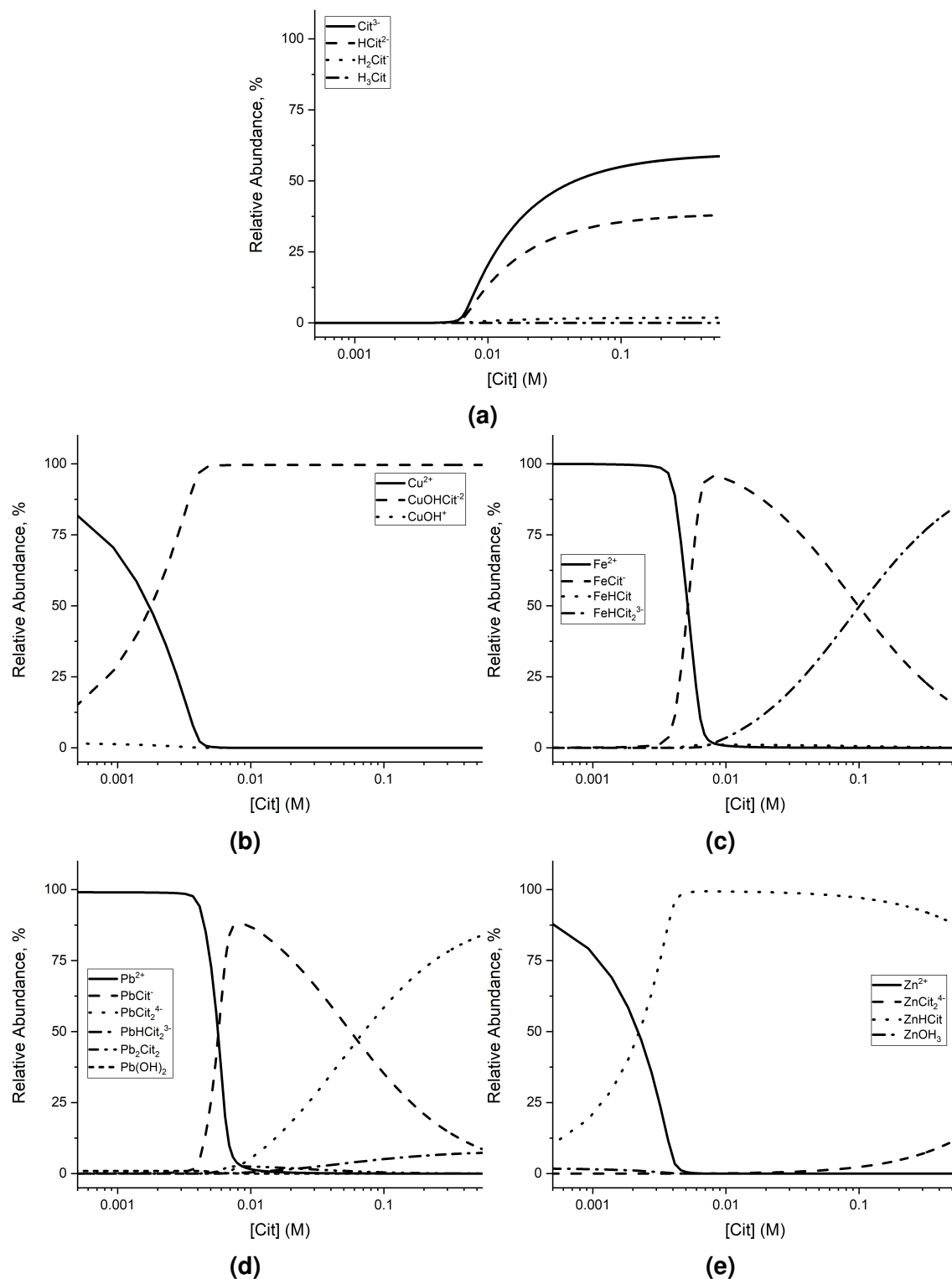
copper, with multiple species occurring in tandem with the PbCit species that occur from pH 4. Zinc displays the only calculated speciation with a singular dominant species throughout the entire pH range, ZnHCit.

## E.2 Extraction Percentages in Isotherm Data

Figure E.5 displays the dependence of extraction percentage on total metallic concentration within a multi-metal isotherm. Copper maintains the highest extraction percentage, with  $>90\%$  until  $\sim 0.6\text{mmol}$  present within solution. Lead and zinc behave similarly, with both initially displaying  $\sim 100\%$  extraction, before plummeting, lead decreasing earlier than zinc but less pronounced. Lead reaches  $\sim 25\%$  extraction at  $\sim 0.5\text{mmol}$ , which is similar to zinc. Iron(II) displays the poorest performance, with an initial extraction of  $>80\%$ , that rapidly decreases to a negligible amount by  $0.4\text{mmol}$ .

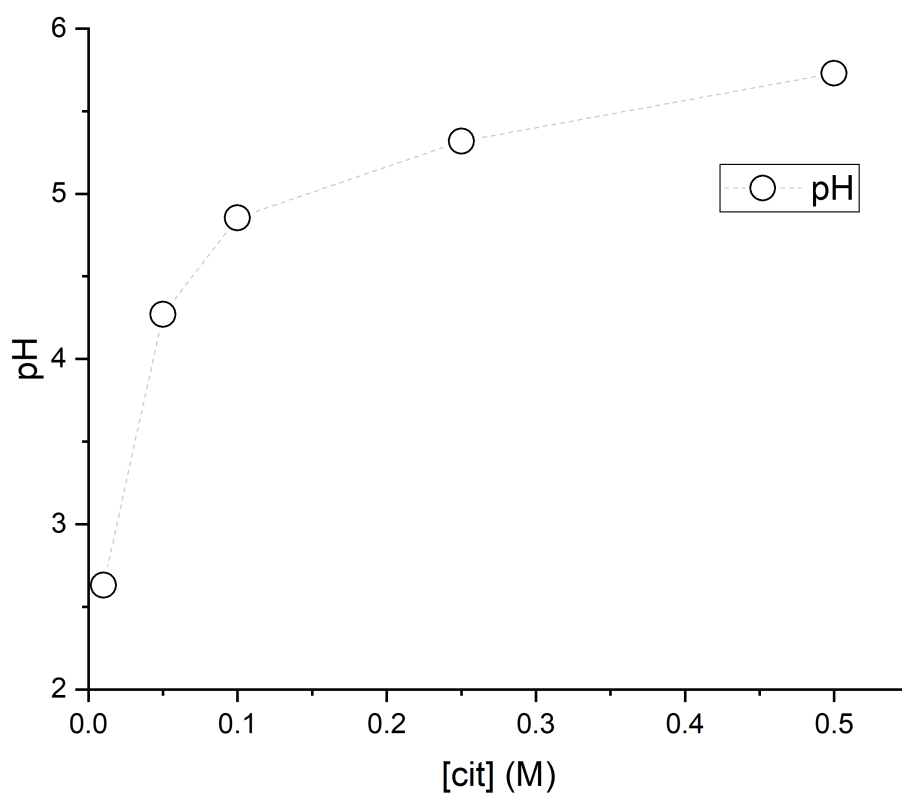
## E.3 Extraction Percentages in Kinetic Data

Figure E.6 displays the kinetic data displayed in Figure 7.3 reanalysed to display extraction percentages as a function of time. Copper reaches  $99\%$  by  $700\text{min}$ , while both lead and zinc reach  $90\%$  by  $1500\text{min}$  (and maintain this extraction beyond). Iron(II) reaches a maximum extraction of  $29\%$  at  $300\text{min}$  before desorption occurs, and the extraction decreases to  $14\%$  by  $3000\text{min}$ .



**Figure E.2:** Speciation of citrate, copper, iron(II), lead and zinc as a function of citric acid concentration, relative to total concentration of each species (Modelled at pH 5.75 by HySS software suite, using stability constants provided within Bezzina *et al.* (2019)<sup>[119]</sup>).





**Figure E.3:** Citrate acid concentration dependence of the post-contact pH for each mixed metal experiment performed (initial concentration 200ppm; temperature 21°C; 0.5mol L<sup>-1</sup> NaCl; 0.01-0.5mol L<sup>-1</sup> citric acid; 2ml wet settled resin; 50ml solution; 24h).

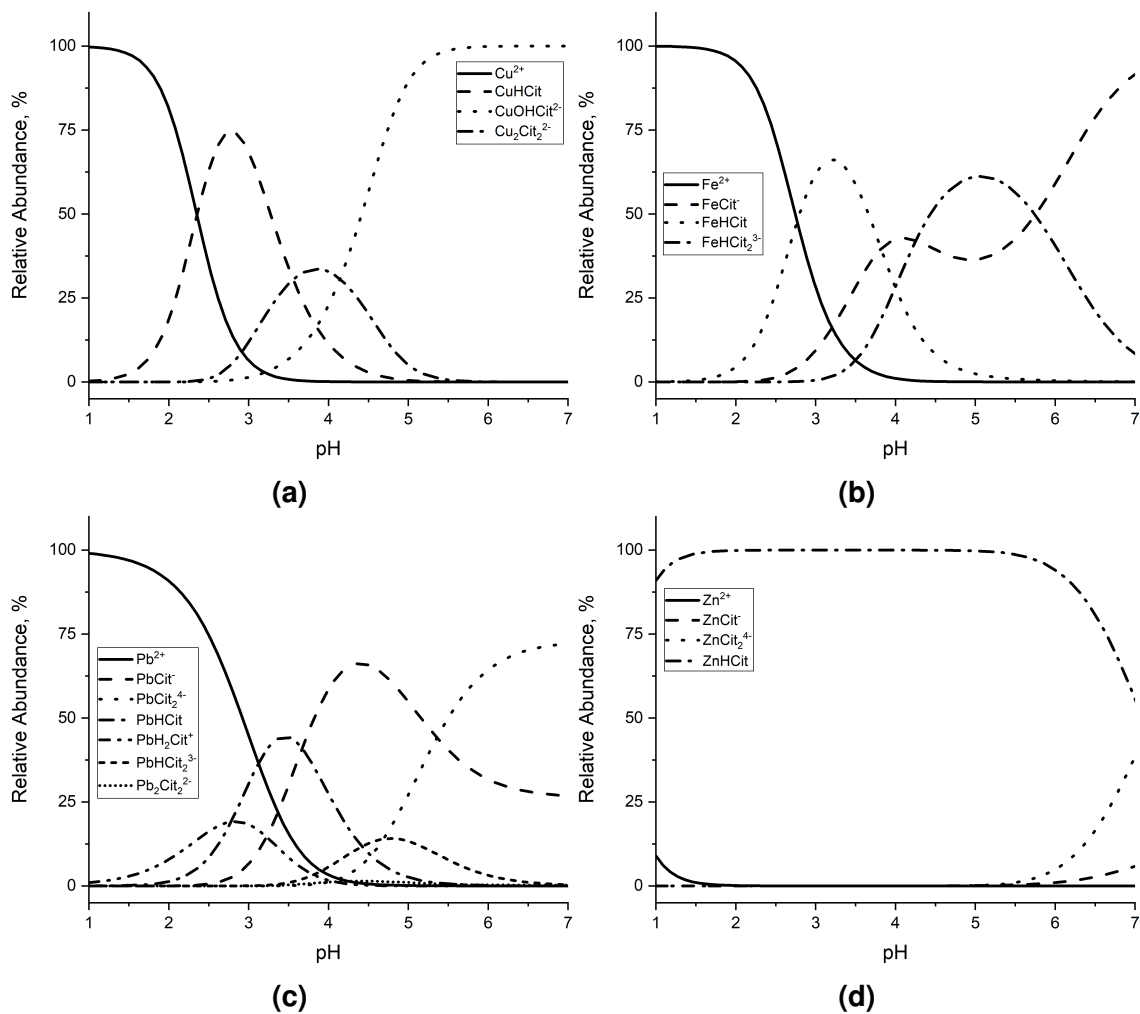


**Figure E.4:** Speciation of citrate, copper, iron(II), lead and zinc as a function of citric acid concentration, relative to total concentration of each species (Modelled at pH 5.75 by HySS software suite, using stability constants provided within Bezzina *et al.* (2019)<sup>[119]</sup>).

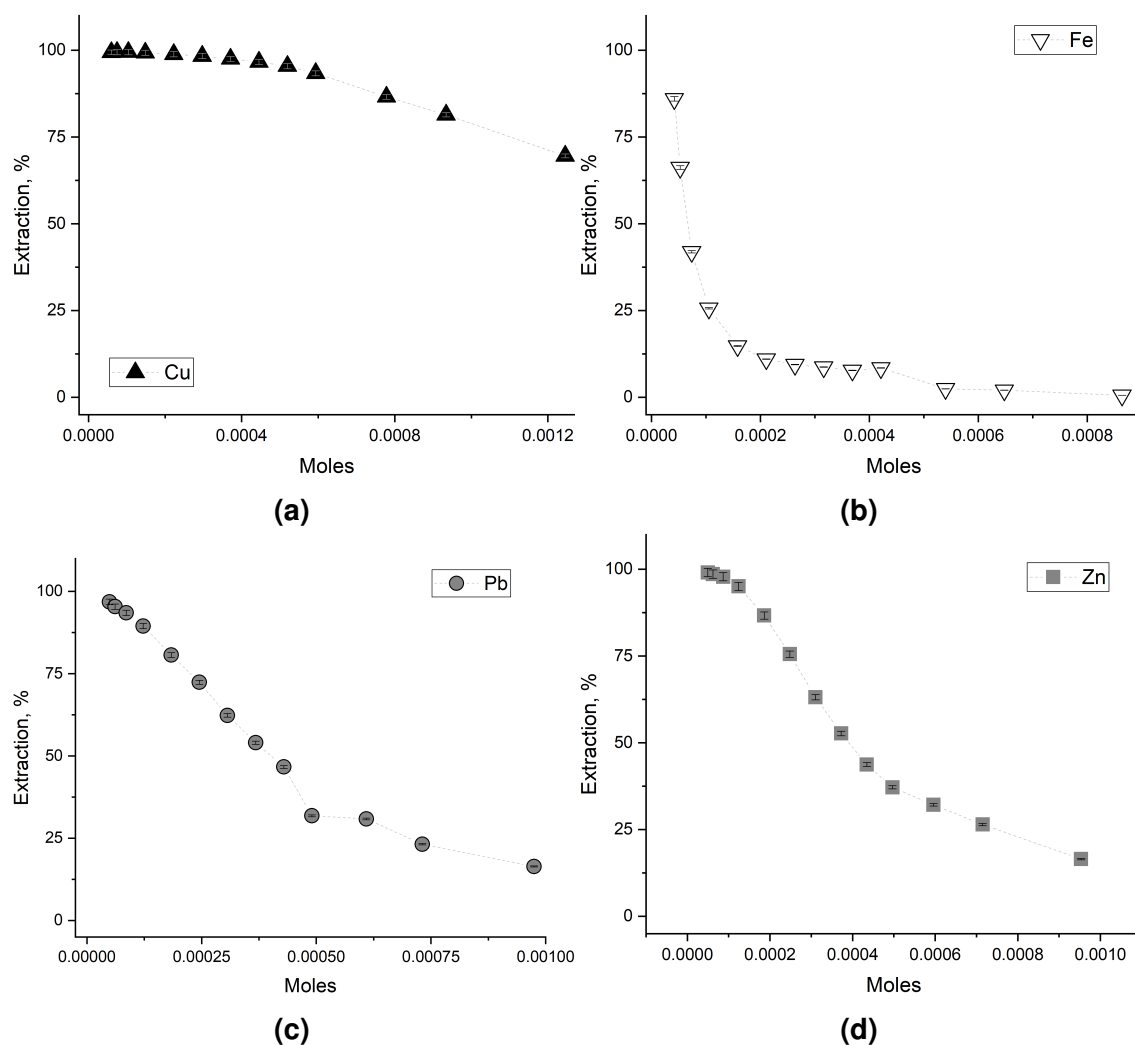


**Figure E.5:** Concentration dependent extraction percentage of copper (a), iron (b), lead (c) and zinc (d) by MTS9301 in citric acid media as a function of total  $\text{mmol L}^{-1}$  in initial solution (initial concentration  $200\text{mmol L}^{-1}$ ; temperature  $21^\circ\text{C}$ ;  $0.5\text{mol L}^{-1}$  NaCl;  $0.1\text{mol L}^{-1}$  citric acid; 2ml wet settled resin; 25-400ml solution; 24h).

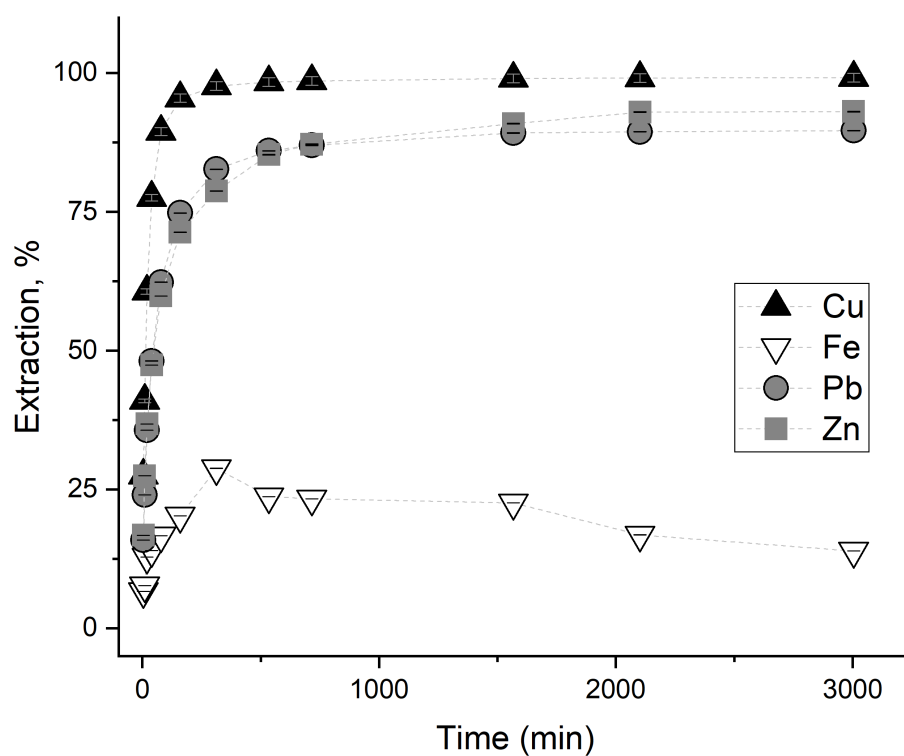


**Figure E.6:** Time dependent extraction percentage of copper (a), iron(II) (b), lead (c) and zinc (d) by MTS9301 in citric acid media (initial concentration 200ppm; temperature 21°C; 0.5mol L<sup>-1</sup> NaCl; 0.1mol L<sup>-1</sup> citric acid; 10ml wet settled resin; 500ml solution).